An Investigation into the molecular mechanisms of complement terminal pathway induced inflammation.

David John Walters

A thesis submitted to Cardiff University in candidature for the degree of Doctor of Philosophy

December 2018

DECLARATION

This work has not been submitted in substance for any other degree or award at this or any other university or place of learning, nor is being submitted concurrently in candidature for any degree or other award.

Signed …… (candidate) Date ……

STATEMENT 1

This thesis is being submitted in partial fulfillment of the requirements for the degree of ……(insert MCh, MD, MPhil, PhD etc, as appropriate)

Signed …… (candidate) Date ……

STATEMENT 2

This thesis is the result of my own independent work/investigation, except where otherwise stated.

Other sources are acknowledged by explicit references. The views expressed are my own.

Signed …… (candidate) Date ……

STATEMENT 3

I hereby give consent for my thesis, if accepted, to be available for photocopying and for inter-library loan, and for the title and summary to be made available to outside organisations.

Signed …… (candidate) Date ……

STATEMENT 4: PREVIOUSLY APPROVED BAR ON ACCESS

I hereby give consent for my thesis, if accepted, to be available for photocopying and for inter-library loans **after expiry of a bar on access previously approved by the Academic Standards & Quality Committee.**

Signed …… (candidate) Date ……

Acknowledgements:

First and foremost, I would like to thank my supervisors Professors Paul Morgan and Kathy Triantafilou for their patience, direction and invaluable advice over the course of the project. A special thank you is required for Dr Tim Hughes whose constant enthusiasm was essential for both technical direction and moral support over the years, as well as Martha Triantafilou for her help throughout the project. Also, thanks is due to the BBSRC and GSK for providing the funding for this CASE studentship.

I'd also like to thank all members of the BPM group, both past and present, who have made the lab a place that I have felt welcome and supported throughout. Special thanks is due to Dina and Lana, who's incredible support and organisational skills made things run as smoothly as a PhD can. I'd also like to thank Wiola and Matt for their direct input and collaboration with parts of the work and technical insight in to their respective topics. Outside of the BPM group, James and Cleo deserve a thank you for moral support, input on experiments and listening to me constantly moan!

The teams at GSK in both the C3 DPU and the catalyst also helped massively in my secondments to the labs, with Eva, Darren and Robin being crucial in organising the placements and assisting in planning and performing experiments respectively, which I hugely appreciate.

Finally, all my friends and family, especially my parents, deserve special credit for supporting me through the PhD, in both the good and bad times. Without all of you, I'd never have got to the point of writing this!

Contents:

List of abbreviations used:

AA- Amino acid

ACPA- Anti-Citrullinated Protein Antibody

ACR20 – American college of rheumatology 20 test

ADP – Adenosine Diphosphate

aHUS – Atypical hemolytic ureamic syndrome

AMD – Age related macular degeneration

AMP – Adenosine Monophosphate

AP – Alternative pathway

APB – Alternative pathway buffer

ASC – Associated Speck like protein

ATP – Adenosine Triphosphate

BMDM – Bone marrow derived monocytes

Bp – Base pair

BSA – Bovine serum albumin

C3aR – C3a receptor

C5aR – C5a receptor

Ca^{2+} - Calcium ion

CAIA- Collagen antibody induced arthritis

cAMP – Cyclic AMP

CAPS- Cryopyrin associated periodic syndrome

CARD – Caspase activation and recruitment domain

CC – Cholesterol Crystals

CFD – Complement fixing diluent

CRD – Carbohydrate recognition domain

CRP – C-reactive protein

CV – Column Volumes

CVF – Cobra Venom Factor

DAF – Delay accelerating factor

DAMPS – Damage associated molecular patterns

DMARD – Disease modifying anti-rheumatic drug

DMSO – Dimethyl Sulphoxide

DNA – Deoxyribose Nucleic Acid

ECL-Enhanced chemiluminescence

ECM – Extracellular matrix

EDTA – Ethylene diamine tetra-acetic acid

EGF – Epidermal Growth factor

EGTA – Ethylene glycol-bis (ß-aminoethyl ether) tetra-acetic acid

ELISA – Enzyme linked immunosorbent assay

ER – Endoplasmic Reticulum

Fab – Fragment antigen binding

FACS – Fluorescence activated cell sorter

FB – Factor B

FC – Fragment crystallisable

FD – Factor D

FH – Factor H

FITC – Fluorescein Isothiocyanate

FLS – Fibroblast like synoviocyte

GAG – Glycosaminoglycan

GPCR – G protein coupled receptor

GPI- Glycosylphosphatidylinositol

gRNA- guide RNA

GSDM D – Gasdermin D

HAE – Hereditary Angioedema

HLA – Human Leukocyte Antigen

IFN - Interferon

IgG – Immunoglobulin G

IgM – Immunoglobulin M

IL-18 – Interleukin 18

IL-1ß – Interleukin 1 beta

IL-6 – Interleukin 6

IP3 – Inositol triphosphate

K^+ - Potassium ion

kb - Kilobase

kDa – Kilodalton

KO – Knockout

LDH – Lactate Dehydrogenase

LPS – Lipopolysaccharide

LRR – Leucine rich domain

mAb – Monoclonal antibody

MAC- Membrane attack complex

MASP – Mannose associated serine protease

MBL – Mannose Binding Lectin

MCP – Membrane co-factor protein

Mg^{2+} - Magnesium ion

MiRNA – Micro RNA

mRNA – messenger ribonucleic acid

MSU – Monosodium Urate

MTX - Methotrexate

MVB- Multi-Vesicular body

MW – Molecular weight

Na^+ - Sodium ion

NACHT – Nucleotide binding and oligomerisation domain

NLR- Nod Like receptor

NLRP3 – Nod Like receptor protein 3

NMR – Nuclear magnetic resonance

NS – Non-significant

OA – Osteoarthritis

P2XR – P2X receptor

PAGE – Polyacrylamide gel electrophoresis

PAM – Protospacer adjacent motif

PAMPS – Pathogen associated molecular patterns

PBMC – Peripheral blood mononuclear cell

PBS – Phosphate buffered saline

PE – Phycoerythrin

PFA – Paraformaldehyde

PLC – Phospholipase C

PNH – Paroxysmal Nocturnal Haemoglobinuria

PYD – Pyrin domain

RA – Rheumatoid Arthritis

RBC – Red blood cell

RCA – Regulators of complement activation

RF- Rheumatoid factor

RL – Reactive lysis

RLR – Rig-like receptor

RNS – Reactive nitrile species

ROS – Reactive oxygen species

RT- Reverse transcriptase

RYR – Ryanodine receptor

SCR – Short consensus repeat

SDS – Sodium Dodecyl Sulphate

SEM – Standard error of the mean

SLE – Systemic Lupus Erythematosus

sMAC- Soluble MAC

SNP – Single nucleotide polymorphism

TCC – Terminal complement components

TED – Thioester domain

TLR – Toll like receptor

TMB- 3,3',5,5'-Tetramethylbenzidine

TNFα – Tumour necrosis factor alpha

TRIS – Tris (Hydroxymethyl) methylamine

UV- Ultra Violet

WT – Wild type

List of figures:

List of Tables:

Abstract:

The complement system is a bastion of the innate immune system which mediates opsonic, inflammatory and lytic responses to pathogenic activating stimuli, culminating in the formation of the membrane attack complex (MAC) (Sarma and Ward 2011). MAC deposition on non-nucleated or bacterial cell membranes results in chemiosmotic flux; subsequently inducing cell swelling and rupture (Morgan 2000). However, sublytic MAC formation may occur on nucleated self-cells, inducing the release of inflammatory cytokines, including IL-1β (Tegla *et al* 2011; Ricklin, Reis and Lambris 2016). IL-1β proteolytic maturation and secretion requires activation of inflammasomes, with the NLRP3 inflammasome being demonstrated as the central mediator of MAC induced IL-1β secretion in a range of cell types (Triantafilou *et al* 2013; Laudisi *et al* 2013; Suresh *et al* 2016). However, the cellular mechanisms linking MAC deposition and NLRP3 activation are poorly defined, with a range of activation mechanisms proposed.

In the work described in this thesis I investigated the mechanisms linking sublytic MAC to NLRP3 activation in monocytic and synovial cell lines to delineate conserved cell signalling pathways involved in NLRP3 activation, as well as investigating the broader interactions of NLRP3 with the complement system.

Firstly, classical and reactive lysis systems of complement activation were established and validated to generate sublytic membrane attack on cells for study of the interaction with NLRP3. Within these experiments, interesting observations surrounding the role of CD59 in the regulation of C3b, as well as the role of C5 depletion or inhibition on C3b deposition were made. LPS primed THP-1 monocytes were used as a model for NLRP3 activation by sublytic MAC. In concordance with the published literature and studies by our group, both primary and secondary Ca^{2+}flux and ROS production had roles in MAC mediated IL-1β secretion (Triantafilou *et al* 2013). However, extracellular KCl was demonstrated to be a non-specific inhibitor of IL-1β release as the addition of NaCl to the stimulation media demonstrated inhibition of NLRP3 activation in the same manner as KCl in this system. To further explore pharmacological manipulation of sublytic MAC mediated activation, inhibitors of a range of known MAC activated kinases were used to identify signalling pathways linking sublytic MAC and NLRP3 activation. Only an AKT inhibitor, Perifosine,

induced statistically significant changes in MAC mediated IL-1β release; however, this was shown to be through the activation of cell death and stress pathways such as JNK rather than attributable to its effects on AKT signalling. Subsequent simultaneous inhibition of JNK and ERK signalling significantly inhibited both IL-1β secretion and Caspase-1 activation in response to sublytic MAC. MAC-induced activation of NLRP3 and the induction of IL-1β release was also subsequently demonstrated using purified components in the reactive lysis system; cells exposed to sublytic MAC via reactive lysis were subjected to RNA-Seq analysis, providing preliminary evidence of transcriptomic changes with implications for inflammatory cell signalling in response to MAC.

Finally, NLRP3 expression was knocked out using the CRISPR/CAS9 system in SW 982 synoviocytes, to investigate interactions between NLRP3 expression and MAC mediated responses. NLRP3 -/- cells were protected from MAC mediated cell death, a consequence of increased CD59 expression on the cell surface.

Collectively, this thesis improves understanding of the mechanisms linking complement and NLR inflammasomes, highlighting novel cell signalling pathways linking the two systems and providing evidence that NLRP3 modulates MAC sensitivity by regulating CD59 localisation within the cell.

Chapter 1 – Introduction:

The innate immune system is a fundamental cornerstone of the body's ability to rapidly react and respond to the multitudes of potentially harmful stimuli, whether self-derived or from exogenous pathogens, encountered in everyday life (Holers and Banda 2018). One of the crucial effectors for the innate immune system is the complement system. The complement system comprises of a proteolytic cascade generating a range of effector molecules as a front-line response to pathogens and altered self-cells, which is kept in check by an array of cell surface and fluid phase regulators (Sarma and Ward 2011).

Activation of the complement system induces the production of opsonic fragments, anaphylatoxins and membranolytic agents; therefore, it is unsurprising that the complement system can exert a highly potent pro-inflammatory, pro-necrotic and opsonic effect (Rus *et al* 2006). Subsequently, the aberrant activation and dysregulation of complement can result in a range of pathological conditions. These range from well-characterised diseases where complement dysregulation is the key factor such as paroxysmal nocturnal haemoglobinuria (PNH) and atypical haemolytic uremic syndrome (aHUS), to other conditions where insidious roles for the pro-inflammatory effects of complement are becoming increasingly elucidated, including cardiovascular disease and atherosclerosis, Alzheimer's disease and neurodegenerative conditions and rheumatoid arthritis (RA) (Caroll and Sim 2011).

Complement activation in RA is well documented, with studies highlighting complement activation as a central driver of RA inflammation in both *in vitro* and *in vivo* models (Low and Moore 2005). The cause of complement activation in the RA joint is unclear; however, a range of possible complement activators are generated in disease progression. Potential activators include rheumatoid factor (RF), anti-citrullinated protein antibody (ACPA) and other immune complexes, CRP deposition or cartilage components such as fibromodulin, which have all been demonstrated to activate classical or alternative pathways (Ballanti *et al* 2011).

Nevertheless, the cell signalling mechanisms enabling complement activation to drive the inflammatory state in the resident joint synoviocytes and infiltrating monocytes are unclear, with the intracellular cascades activated by C5a and sublytic membrane attack complex (MAC) being largely undefined in these cell types. Furthermore, the interaction between the complement cascade and the intracellular "danger sensing" machinery of the NLRP3 inflammasome may be pathological in RA, with the inflammasome activation product IL-1β already being targeted, albeit with limited efficacy, in the disease (Mertens and Singh 2009; Triantafilou *et al* 2013). Therefore, in this thesis I set out to elucidate the mechanisms linking complement and the activation of the NLRP3 inflammasome in synoviocytes and monocytic cell line models, to identify cell signalling pathways for the mediation of complement mediated NLRP3 activation and potentially highlight new therapeutic targets for RA in the future.

1.1 – Background to the complement system

The discovery of the heat labile bactericidal properties of serum by early immunologists such as Bordet and initiated our understanding of this innate immune pathway (Buchner 1895; Bordet 1898). The function of innate immunity within the overall immunological landscape is to, alongside the adaptive immune response, protect the host from pathogenic infection. From Bordet's simple observation, our understanding of complement has developed to encompass a system of overlapping, synergistic and antagonistic pathways mediating the effects of complement in both health and disease (Ogundele 2001).

The complement system consists of over 30 components and regulators which make up around 15% of the protein content of blood plasma. Complement proteins circulate as zymogens until induced to activate through conformational change or proteolytic cleavage, or in the case of C3, through spontaneous hydrolysis (Dunkelberger 2009). The historical interpretation of this pathway as merely "complementing" the more defined humoral response upon the recognition of pathogens is becoming increasingly challenged. The recent elucidation of the wide-reaching roles of complement signalling in lipid metabolism, coagulation and synaptic development highlight complement and result in it becoming increasingly viewed as a central homeostatic mechanism (Amara 2008; Stephen 2012;

Guavreau *et al* 2013). The complement components are predominantly synthesised hepatically and released into the circulation; however, localised extrahepatic synthesis can occur in many organs and tissues, including the epithelia of the GI tract, skin fibroblasts, the eye and most significantly in monocytes and mononuclear cells to act as a rapid response to injury (Noris and Remuzzi 2013). The recent discovery of intracellular activities of complement opens a range of roles for complement in cellular homeostasis, which will undoubtedly be explored and diversify in the coming years (Arbore, Kemper and Kolev 2017).

Despite the seeming complexity underlying the cascade with the large number of proteins and regulators involved, the primary role of the system is to recognise and eliminate pathogens or altered self-cells. This is managed in several ways, including the induction of inflammation and recruitment of immune cells through the anaphylatoxins and MAC, MAC mediated cell lysis or opsonisation through C3b products (Chen, Daha and Kallenberg 2010). The importance and potency of the responses induced by the complement system are further demonstrated by the range of pathophysiological conditions with which ectopic complement activity is associated, including Alzheimer's disease, cancer, type II diabetes and rheumatoid arthritis (Holers *et al* 2014; Reis *et al* 2017; King and Blom 2017). These common, chronic conditions are becoming causes of increasing financial and medical strain in the aging western population, consequently, the understanding and potential management of the roles of complement signalling in these conditions is hugely significant in the development of therapeutics and potentially mitigating their impact upon society (Holers 2014).

1.2 – Complement activation pathways

The complement system consists of three established activation pathways, classical, lectin and alternative pathways. All three activation pathways converge on a common terminal pathway. Although the active products are the same, the activating ligands, activation complexes and regulation are unique to each pathway, allowing fine detail and regulation of key steps within the cascade to modulate activity (reviewed in Sarma and Ward 2011). A schematic overview of the complete complement system can be seen in Figure 1.1 a, and a schematic of complement activation pathways in Figure 1.1 b.

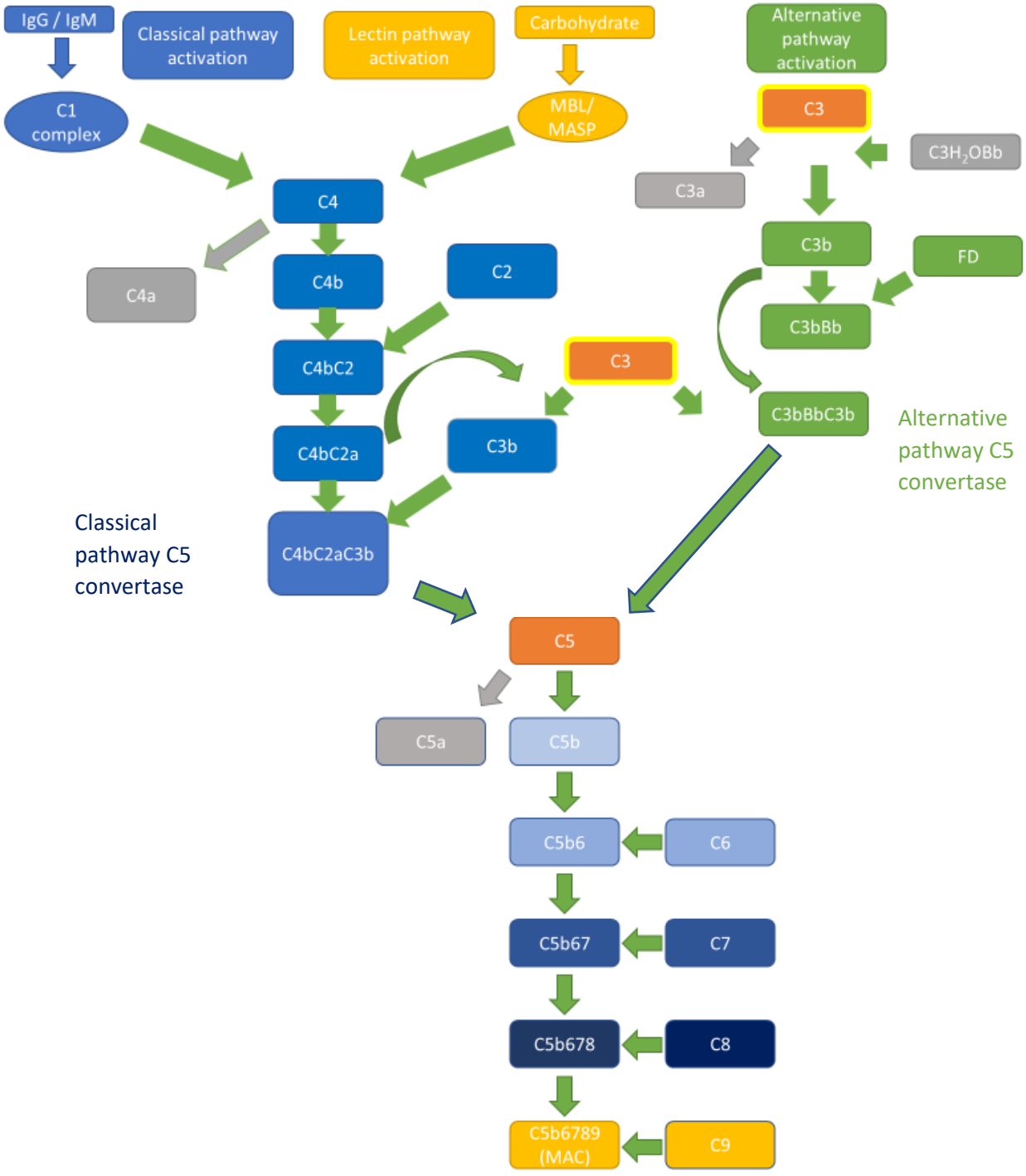

Figure 1.1. Schematic of complement cascade. Activation pathways triggered in response to agonists converge at the C3 convertase, which subsequently binds C3b to alter the convertase affinity to C5. C5 convertase activity allows C5 cleavage in to C5a and C5b, with the latter forming the nidus of the forming MAC complex. Subsequent C6, C7, C8 and C9 binding results in MAC formation on the cell surface.

1.2.1 The classical pathway – C1q binding and activation

Classical activation acts as an interface between innate and adaptive immunity by interaction of C1q with immunoglobulins (multiple IgG molecules or a single IgM) to initiate activation (Duncan and Winter 1988). C1q binding to immunoglobulin Fc regions is dependent on either IgM deformation from planar to a staple-like shape on ligand binding or proximity of multiple ligand-bound IgG molecules (reviewed in Sarma and Ward 2011). IgG-mediated C1q activation has been shown to be optimal with six IgG molecules in close proximity and in a specific array formation on the target surface, suggesting IgM is a more efficient classical pathway activator (Diebolder *et a*l 2014). However, C1q is also capable of interacting with and becoming activated by an array of other molecules including LPS, apoptotic cells and CRP, causing complement-based responses to a range of PAMPS and DAMPS (Gal *et al* 2009).

The C1 complex consists of a single C1q associated with a $C1r_2/C1s_2$ tetramer, with a combined molecular mass of 790 kDa. C1q itself is a 460 kDa collagenous protein formed from 18 homologous polypeptide chains (6 A, 6 B and 6 C chains), which form the C1q "stalk" region and the 6 arms culminating in globular head regions resembling a bouquet structure (Figure 1.2) (Arlaud 2002). The structure is highly dependent on interchain disulphide bond formation from conserved Cysteine residues to generate the A-B and C-C chain subunits of the molecule, whilst further conserved Cysteine residues are believed to contribute to intrachain bridge forming (Kishore and Reid 2000). Activation of the C1q complex is dependent on the presence of Ca^{2+} to allow interaction of K61 from the B chain or K58 of the C chain of the collagen like stem region of C1q with a shallow groove on the $C1r_2$ /$C1s_2$ complex to allow oligomerisation (Girija *et al* 2013).

The interaction of the globular C1q heads with activators induces a conformational change within C1q which transposes into activation of C1r via association of the collagen-binding domain with the protease. This occurs via an intermediate structure in a similar mechanism to Trypsin-mediated cleavage before the auto-proteolysis of C1r, yielding the functional protease form (Gaboriaud 2014). Upon activation, a single C1r subunit within the highly flexible tetramer can cause subsequent proteolysis of both C1s zymogens within the complex, to yield a fully active C1 complex (Major *et al* 2010).

The C1s proteases in turn induce the cleavage of C4 and C2 to generate the focal point of the various complement pathways, the C3 convertase (C4bC2a in the classical pathway). This is possible due to the high flexibility of the C1 complex around the C1r/s proteolytic domains, allowing them to swing out of the complex upon activation and instigate the initial cleavage of C4 (Wallis *et al* 2010).

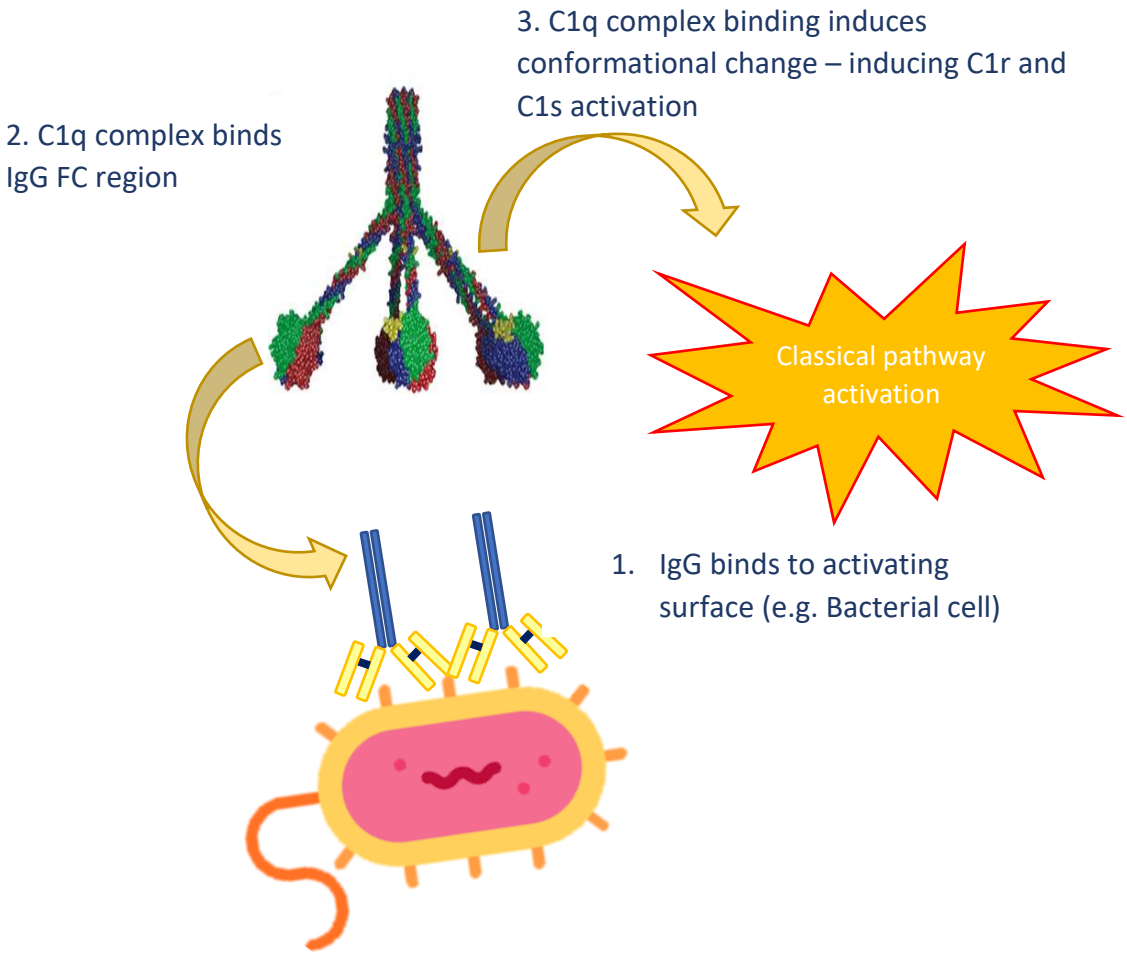

Figure 1.2. The intricate heterotrimeric structure of C1q with the collagen-like stalk region forming into the six globular heads required for IgG and pathogen recognition (Image edited from Gaboriaud et al 2012). Upon binding, the C1q complex undergoes conformational change to a permissive state for C1r and C1s activation.

1.2.2 C1q signalling and non-complement roles

Alongside the traditional role of C1q as the mediator of C1 complex target recognition and activation, a range of non-complement mediated roles are becoming elucidated. These include important functions in angiogenesis in neonates of relevance to preeclampsia, and roles in cell adherence and apoptosis in prostate cancer; these activities have been attributed to its cytokine-like structure and apparent evolution from a TNF-α precursor (Ghebriwet *et al* 2012). Importantly, in the context of this project, C1q has distinct roles in the induction and regulation of inflammation. C1q deposition in Drusen deposits, the pathological hallmark of AMD, was demonstrated to have a pro-inflammatory effect through activation of NLRP3 and the induction of IL-1ß and IL-18 secretion; however, the mechanism of which remains unclear but seems to involve phagolysosomal destabilisation through endocytosis of the C1 complex (Doyle *et al* 2012). However, other groups have demonstrated a role for C1q in the inhibition of NLRP3 activation in macrophages, primed macrophages exhibiting a decrease in pro-IL-1β and Caspase-1 cleavage in response to extracellular ATP when exposed to C1q-opsonised apoptotic lymphocytes, alongside a decrease in IFN and IL-27 responses suggesting a global anti-inflammatory effect (Benoit *et al* 2012).

1.2.3 C4 activation and classical pathway convertase formation

Upon C4 cleavage the smaller C4a fragment is released, allowing it to act as an anaphylatoxin alongside C3a and C5a. Although C4a is the weakest of the complement anaphylatoxins, indeed it has been suggested to have no biological activity, it has also been postulated that there is cross talk and interaction between these inflammatory mediators. This was demonstrated by testing the effects of C4a on C5a induced neointima formation in mice with arterial injury - mice receiving C4a alongside C5a showed significantly inhibited neointima formation as well as inhibition of the expression of various proinflammatory molecules such as TNFα and IL-6 (Zhao 2014). The recent demonstration that C4a binds the receptors PAR1 and PAR4 suggests a biological significance of the molecule, with a capacity to induce ERK signalling and Ca^{2+} mobilisation as well as affecting endothelial permeability (Lambris, Ricklin and Wang 2017).

The larger fragment, C4b becomes anchored to the target cell surface through its reactive thioester group, which becomes exposed upon cleavage, allowing it to remain fixed adjacent the C1 complex. C2 binds fixed C4b and is presented for C1s cleavage, releasing a fragment C2b while the enzymatic fragment C2a remain bound to form the classical C3 convertase, C4bC2a (Mathern and Heeger 2015).

1.2.4 The Lectin Pathway

The second activation pathway of the complement cascade is the Lectin Pathway (LP) which is comparable, although not completely analogous, to the classical pathway. Mannan binding lectin (MBL) is a member of the Collectin family of proteins (alongside SP-A and SP-D) encoded on a gene cluster on the long arm of chromosome 10 in humans and is the prototypical activator of the Lectin pathway (Ip *et al* 2000). The structure of the MBL monomer comprises a cysteine rich N terminal domain, multiple collagen repeats and a C terminal "neck" domain which orientates the six globular recognition heads in to the correct geometry. However, *In vivo*, MBL associates into different oligomeric states, including dimers, trimers and hexamers (Turner 1998).

A second, less well characterised group of activators of the lectin pathway are the multimeric lectin Ficolin family, consisting of three members (H, L and M Ficolin) which are highly homologous to MBL, demonstrated in Figure 1.3. Ficolins recognise acetylated moieties on the cell surface including N-acetyl-Glucosamine and N-acetyl-Galactosamine - allowing recognition of a range of pathogens including *Escherichia coli, Staphylococcus aureus* and *Salmonella typhimurium* (Matsushita 2013). Furthermore, the recognition of human cytokeratin, exposed after endothelial oxidative stress, demonstrates a potential mechanism of recognition of "altered self" cells and a route for activation of complement in response to oxidative stress and ischaemia (Osthoff *et al* 2018).

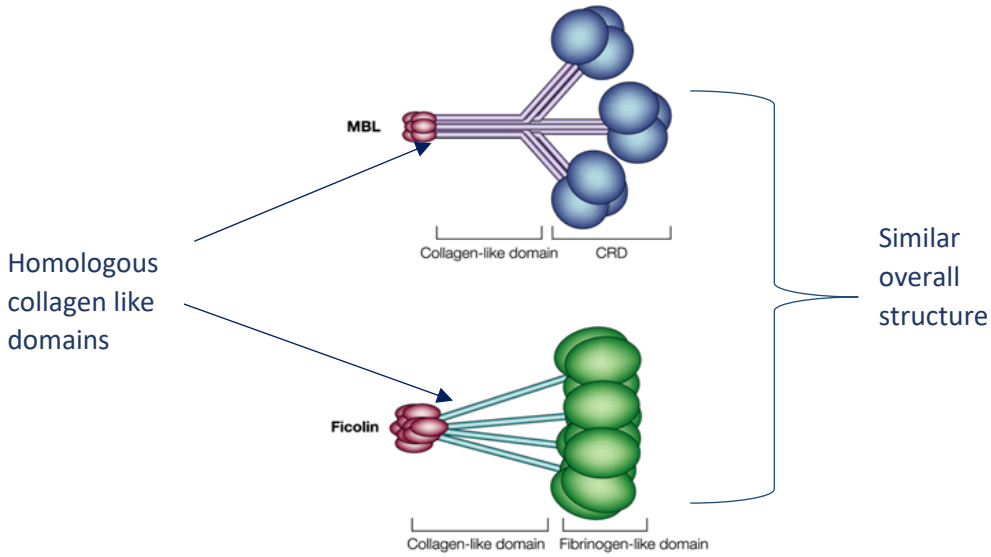

Figure 1.3 – Comparative schematic structures of MBL (Top) and Ficolins (Bottom), which highlights their structural similarity to C1q shown previously (Image edited from Matsushita and Fujita 2002)

MBL is synthesised in hepatocytes before secretion into plasma, where it can induce complement activation via interactions with a range of pathogens. These can include both gram negative and gram-positive bacteria, viruses, parasites and yeasts - alongside the fundamentally important property of distinguishing healthy self from apoptotic/necrotic and non-self-cells (Takahashi 2005). Upon infection, serum levels of MBL increase 2-3-fold, indicating that it is an important acute phase response protein (Dommet, Klein and Turner 2006). The process of target recognition by MBL is dependent on the geometry and spatial orientation of carbohydrate binding domains on the target cell surface, and the differences in composition and orientation between these and the arrangement of glycoproteins on a human cell allow specificity of MBL targeting (Takahashi 2005).

Upon activation via binding to correctly orientated carbohydrate residues on the cell surface, MBL oligomerisation is fundamental to activity, with the carbohydrate recognition domains (CRDs) forming high avidity, polyvalent interactions with the ligands and providing a platform for the interactions required for MASP activation (Laursen 2012). Three forms of MASP's are present in the MBL immunocomplexes, MASP1 - 3 alongside a further truncated form of MASP2 known as sMAP. Of the associated MASPs, MASP-2 has been highlighted as the central

(and possibly only necessary) form for activation (Takahashi 2008). The roles of MASP-1 / 3 seem to be more subsidiary and supportive or regulating to the activity of MASP-2.

1.2.5 The alternative pathway

The final activation pathway of the complement system, known as the alternative pathway (AP), is fundamentally different from the homologous classical / Lectin pathways. The labelling of the AP as a distinct pathway is something of a misnomer because it is in fact the central complement amplification loop. The AP operates via a distinctly separate mechanism to create a differently constituted, but functionally identical C3 convertase. It should be noted that whilst most molecules within the Classical/ Lectin pathways have homologues or domains of similar function, the alternative pathway has three unique components in the forms of Factor B (FB) Factor D (FD) and Properdin (FP).

In contrast to the other pathways which require specific antibody: protein/carbohydrate: protein interactions to induce pathway activation, the AP undergoes a low rate of continuous activation equalling roughly 1% of total C3 / hour, termed "tickover" (Thurman 2006). The "tickover" theory of C3 activation in the alternative pathway originated in the 1970's; slow, spontaneous hydrolysis of C3 in the fluid phase by nucleophilic attack of water to yield $C3H_2O$ (Lachmann and Nichol 1973; Pangburn *et al* 1981; Daha 2013). This attack creates a more open structure in the C3d region which in turn facilitates the interaction of $C3H_20$ with factor B (FB) (Winters 2005). FB bound to $C3H_20$ is cleaved by the serum protease factor D (FD) to yield the fluid-phase convertase $C3H_20Bb$.

FB is a 93 kDa glycoprotein which binds C3b in the presence of Mg^{2+} and is then cleaved by FD (Lambris and Muller-Eberhard 1984). FB binding to C3b induces an open conformation, exposing the scissile loop in FB that FD cleaves, releasing the Ba fragment from the complex (Forneris *et al* 2010). Bb bound to immobilised C3b comprises the amplification loop C3 convertase (C3bBb).

FD is a small (25 kDa) single domain chymotrypsin-like protease that circulates in a self-inhibited form via its loop domain that disrupts the catalytic triad of the protease. This causes an increased distance between catalytic residues by forming a salt bridge with Asp 177 of the S1 substrate binding pocket, the displacement of which upon enzyme activation is crucial for catalytic activity (Forneris *et al* 2010). Plasma concentrations of FD are the lowest of any complement component, indicating its importance in the regulation and activation of the AP, maintained by a high rate of turnover within the blood (Katschke *et al* 2012).

The C3 convertase (C3bBb) is stabilised by properdin, a 53 kDa, highly positively charged molecule synthesised in a range of cell types (unlike most complement factors which are predominantly hepatocyte synthesised) which *in vivo* oligomerises into dimers, trimers and tetramers by head to tail association of the monomer units (Agarwal 2010). Properdin was the first, and for a long time only, established positive regulator of complement activation, prior to the recent discovery of FHR1 acting as a competitor for FH binding to the C3 convertase and therefore reducing delay acceleration factor activity (Reuter *et al* 2010). Properdin functions by forming a curving vertex around the C3 convertase via interactions with both C3b and Bb that displaces the C3b thioester domain (TED), thus occluding the binding sites of convertase inhibitors, resulting in an increase in C3bBb half-life up to 10-fold (Alcorlo *et al* 2013). Further roles for properdin in the induction of cell signalling and later stages of complement regulation have been postulated but are still controversial.

Therefore, C3 convertase initiates the amplification loop of the alternative pathway; irrespective of the initial activation pathway, the amplification loop is responsible for around 80-90% of complement effectiveness (Lambris and Ricklin 2016).

1.3 - Regulation of complement activation

1.3.1 Regulation of Classical pathway activation

The initial stages of complement activation are regulated by C1 inhibitor (C1-Inh), a potent down-regulator of complement activation and inflammatory processes in the blood (Beinrohr 2007). The 105 kDa protein is present in plasma at around 0.24 g/L, indicative of an important and widespread role (Caliezi *et a*l 2000). C1-Inh, a member of the Serpin family of inhibitors of cysteine and serine proteases, functions via a non-competitive mechanism by acting as a pseudo substrate for the enzyme, locking the active site in an intermediate, non-functional state (Patston *et al* 1991). This binding causes changes within the Serpin structure that irreversibly inactivate the enzyme and expose clearance and degradation epitopes that facilitate complex removal (Cugno 2009).

The effects of C1-Inh deficiencies, which manifest in the condition Hereditary angioedema (HAE), highlight the importance of early stage regulation of complement. HAE is caused by an autosomal dominant mutation within the C1-Inh gene, which results in serious symptoms, predominantly in recurrent swelling of the skin (angioedema), occasionally involving mucosa of the upper airways or bowels, which can be life threatening (Gower *et al* 2011). The administration of recombinant or purified C1-Inh for the treatment of HAE is a mainstay of prophylactic treatment alongside attenuated androgens. The role of C1-Inh in HAE is independent of its complement regulatory function; loss of regulation of coagulation by C1-Inh, specifically activation of FXII and the subsequent release of Bradykinin, drives the condition (Gower *et al* 2011).

1.3.2 Regulation of the C3 convertases

The C3 convertases C4bC2a and C3bBb are labile and decay with time; nevertheless, there are several proteins in plasma and on cell surfaces that function to further regulate the convertases. The key regulator is Factor I (FI), a heterodimeric, heavily glycosylated serine protease present in plasma in an inactive zymogen form at relatively high concentrations (~35 µg/ml) (Alba-Dominguez *et al* 2012). FI, in the presence of appropriate cofactors, cleaves C3b or C4b to inactive forms (iC3b, iC4b and smaller fragments) that are incapable of forming convertase. Inactivation of C3b prevents a spiralling of the positive feedback loop within the alternative pathway and hence C3 depletion through uncontrolled activation. The degradation products of FI mediated C3b/C4b cleavage have specific roles in the modulation of phagocytosis and induction of the acquired immune response (Roversi *et al* 2011). A schematic of the sequential proteolytic cleavage of C3 into subsequent fragments is shown in Figure 1.4.

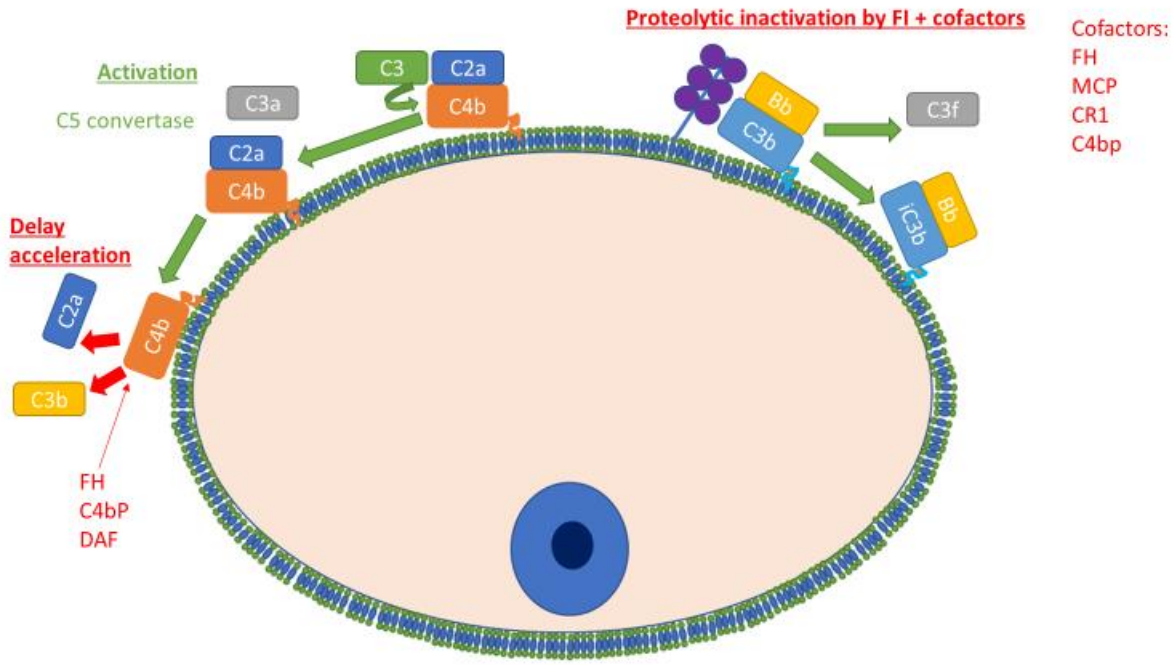

Figure 1.4. The roles of FI / FH as cofactors in the proteolytic degradation of C3b to inactive C3 products as well as mediating delay accelerating activity of the alternative pathway C3 convertase, increasing Bb dissociation rates and thus inhibiting the amplification of the AP.

For AP regulation FI is highly dependent on factor H (FH) as co-factor; FH also regulates by accelerating the decay of AP convertases. FH plasma concentrations are relatively high, up to 300 μg/ml, highlighting its importance; FH deficiency in man and mouse leads to spontaneous, complete C3 consumption (Schreiber *et al* 1978; Fakhouri *et al* 2010). Beyond FH total deficiency, a diverse range of single nucleotide polymorphisms (SNPs) in FH can incur different levels of activity. The most well characterised FH polymorphism is Y402H, a strong genetic risk factor for AMD. Despite the large genetic load of Y402H risk for AMD, the mechanism was unclear. The polymorphism does not alter FH affinity for C3bBb or affect AP convertase regulation; however, Y402H mutation may alter interactions with CRP, sulphated glycosaminoglycans and other cell surface proteins, reducing FH association with the membrane (Hageman *et al* 2005). This was subsequently demonstrated to be important for FH binding to Bruch's membrane via Heparin sulphate, with a different region of FH being implicated in binding to the differently sulphated GAG's in the kidney, suggesting the mechanism by which Y402H confers AMD risk (Clark *et al* 2013).

The observation that the complement polymorphisms has been further explored beyond Y402H, with the array of SNPs in an individual cumulatively strongly affecting complement activity. This concept of an individual's array of complement SNPs conferring a higher or lower level of complement activity generated the complotype hypothesis. The complotype concept suggests the range of common polymorphisms in any individual affect the overall activity of the system and may predispose the individual to complement mediated disease or increased susceptibility of infection, depending on the balance of the SNPs. The combinations of common SNPs in complement AP components generate up to a 6-fold difference in haemolytic activity, demonstrating that individual small changes in activity may cumulatively have profound effects (Harris *et al* 2012).

FH therefore acts as something of a "reverse recognition" marker by binding to and protecting cells expressing self-epitopes (polyanionic molecules such as sialic acid and glycosaminoglycans) but not foreign cells lacking the required recognition markers (Ferreira *et al* 2010). Furthermore, FH recognises markers of apoptosis such as DNA and the cytoplasmic phospholipid annexin II. The binding of FH in this instance regulates complement activation and C3b deposition resulting in opsonisation by phagocytes whilst preventing

excessive inflammatory responses or the release of intracellular autoantigens in the surrounding environment (Trouw *et al* 2007). The involvement of FH in self-recognition is highlighted by the presence of autoantibodies against FH in a range of rheumatic diseases including RA, SLE and aHUS – although the mechanism by which FH is aberrantly recognised in these conditions is unclear (Zadura *et al* 2012).

1.3.3 Membrane bound C3 convertase regulation

On cell surfaces, C3 convertases are controlled by two proteins working in tandem, CD55 and CD46. CD55 (decay accelerating factor/DAF) is formed of four short consensus repeats (SCRs) followed by a short, heavily glycosylated stalk region and a GPI anchor (Weller and Wang 1994). Binding of CD55 to the C3bBb or C4b2a convertase leads to accelerated decay by displacing the enzymatic component (Harris *et al* 2007). CD46 (membrane cofactor protein; MCP) is a ubiquitous membrane bound glycoprotein regulator present on all nucleated cells, with multiple roles in the co-ordination of innate and adaptive immune responses (Yamamoto *et al* 2013). CD46 also has an important role in modulation of inflammation, importantly in the context of this work, through priming of NLRP3 and induction of changes in cell metabolism (Arbore and Kemper 2016). In complement regulation, CD46 acts as a cofactor for FI cleavage of C3b and C4b, thus irreversibly inactivating the C3 convertase.

The C3 convertase generated either by the classical/lectin (C4b2a) or the alternative (C3bBb) pathways acts as a focal point of the complement pathway, uniting the three activation mechanisms and inducing a common downstream response. It should be noted however that the alternative pathway has the unique ability to self-amplify in a positive feedback loop, C3 convertase generating more C3b which may be deposited on the target cell surface via its thioester bond, leading to further FB binding and convertase generation. This amplification is crucial for all activation pathways, with C3b generated from a CP convertase capable of forming an AP convertase to allow signal propagation, with amplification dependent on the balance between activation and inhibition (Lachmann 2009).

1.3.4 C3b, opsonisation and cell signalling

C3b and its degradation products iC3b, C3c and C3dg also have crucial roles as opsonins to facilitate phagocytosis of bacteria or dysfunctional host cells, with all C3 derived ligands and receptors shown in Figure 1.5. Although phagocytes are capable of PAMP and DAMP recognition directly, the diversity and effectiveness of the phagocytic response can be modulated by the presence of opsonins. C3 products, as well as other complement proteins such as C1q, have been shown to activate macrophages in vitro (Ezekowitz *et al* 1985; Bobak *et al* 1988). Interestingly, the interactions of C3b with membrane acceptors is selective for non-self surfaces, dictated by factors such as the position of primary hydroxyl groups on sugars and specific residues on proteins as points of interaction (Sahu 2001). This selectivity focusses C3b deposition onto bacterial, altered or immune complex coated surfaces, therefore limiting downstream "collateral damage" to healthy cells. The recognition of C3b and its degradation products is mediated by members of three gene super families; the regulators of complement activation (RCA) family short consensus repeat (SCR) module-containing CR1 and CR2, the β_2-integrin family members CR3 and CR4 and the immunoglobulin-like receptor family member CRIg (Campange *et al* 2007).

SCR-containing receptors CR1 and CR2 recognise both C3b and C4b through distinct sites each comprising three SCR repeats. The expression level of CR1 (also known as CD35) was found to be crucial for erythrocyte mediated immune complex clearance to the liver and spleen where hepatic / splenic macrophages strip the complexes from erythrocytes and elicit an immune response through antigen presentation (Krych-Goldberg and Atkinson 2001) (Liszewski *et al* 2015). Monocyte/macrophage binding of C3 fragments involves initial interaction with CR1 followed by crosstalk with CR3 to induce the phagocytic process. The exact interactions of the receptors and the intracellular morphological remodelling machinery required for pathogen uptake remains unclear (Rittig *et al* 1998).

CR3 is also the predominant regulator of phagocytic uptake of cholesterol crystals (CCs) in the atherosclerosis model, where CR3 expression on granulocytes and monocytes was increased by C5a and correlated strongly with inflammasome activation and cytokine production,

demonstrating the importance of the phagocytic response in the mediation of inflammation (Samstad *et al* 2014).

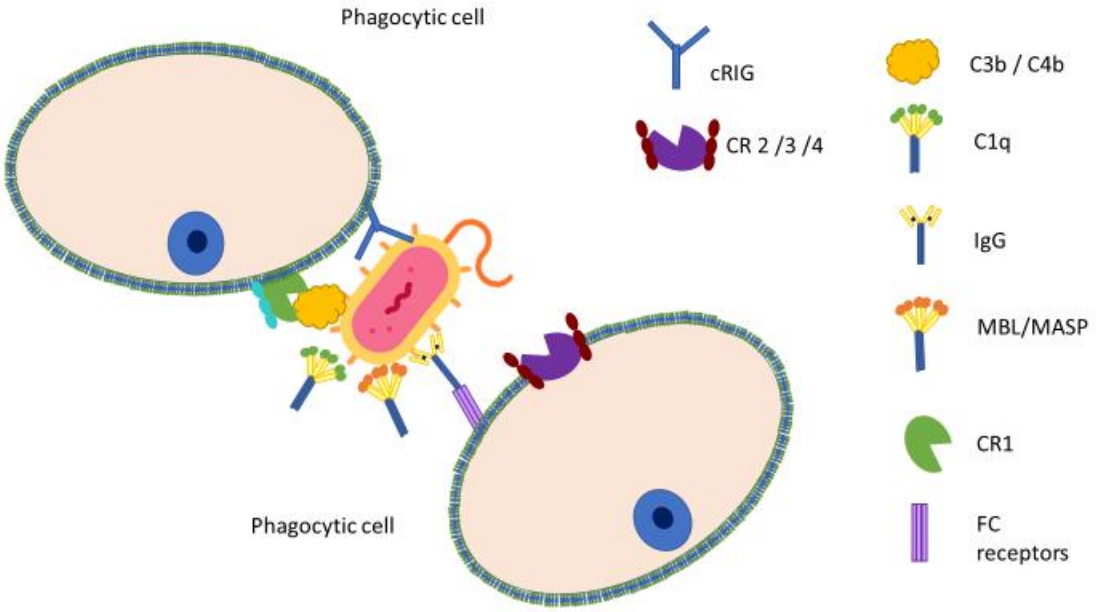

Figure 1.5 – The array of complement activation products and receptors mediating opsonisation and phagocytosis (Figure based on image in Dunkelberger and Song 2010)

1.3.5 C3a and C5a function

From the central C3 convertase the first potent anaphylatoxin is generated, C3a. The anaphylatoxins C3a and C5a are strikingly similar molecules with similar polypeptide chain lengths, high sequence homology, similar charge and a core structure based on four helix bundles, and therefore, will be addressed together (Nettesheim *et al* 1988). The subtle differences between the anaphylatoxin structures are highlighted in Figure 1.6. C3a and C5a induce potent effects, including inducing tachycardia, neutrophil mobilization, monocyte cytokine secretion, altered microvasculature permeability and vasodilation, smooth muscle contraction and mast cell degranulation (Verschoor *et al* 2016). These effects are mediated by their interactions with their respective receptors (C3aR, C5aR1 and C5aR2). The C3aR is highly specific for C3a with a Kd of 1 nm and has limited affinity for C3a-desArg or C5a;

selectivity is highly dependent on the large second extracellular loop and sulphation of Tyr174 (Gao *et al* 2003). C3aR activation triggers downstream intracellular signalling via activation of heterotrimeric G-proteins in a cell dependent manner, with different G-proteins involved in different cell types (Schraufstetter *et al* 2003). These in turn trigger various potent signalling cascades including MAPK, PLC and AKT, leading to cytokine activation and release (Venkatesha *et al* 2005).

C3a/C5a activities are controlled by carboxypeptidases in plasma that inactivate by cleavage of terminal arginine residues (Klos *et al* 2009). The generated C3a-desArg is incapable of interacting with C3aR in any form, although C5a-desArg retains around 10% of its functionality (Campbell *et al* 2002). Although C3a-desArg cannot bind C3aR1, it has been demonstrated to bind C5aR2 and mediate a range of effects within lipid metabolism and intracellular pathways (Kolev and Kemper 2017).

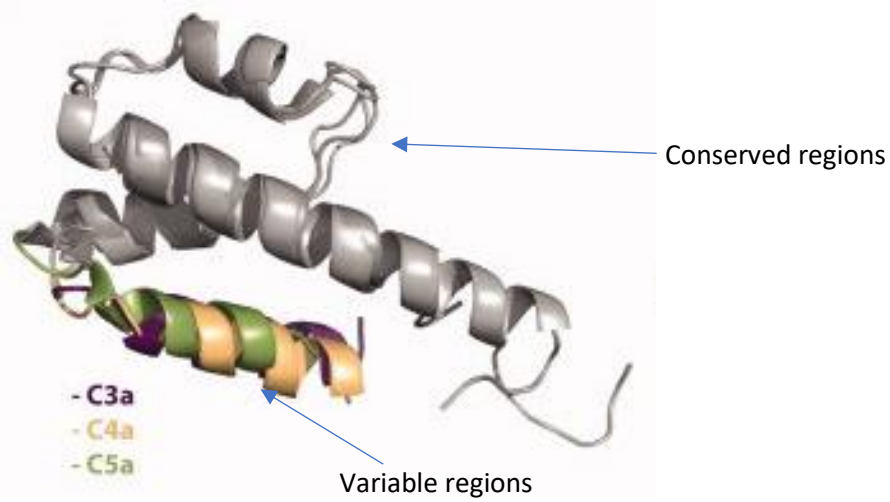

Figure 1.6– Structures of C3a, C4a and C5a highlighting the conserved helical structure between the anaphylatoxins, with the major variation occurring in the α-1 helix as highlighted (Image edited from Bajic et al 2012)

1.3.6 The generation of C5a

The generation of a C5 convertase from any of the activation pathways C3 convertases is dependent on the covalent binding of an additional C3b with the non-catalytic subunit of the convertase to create C5 convertases, C4b2a3b or C3bBbC3b. The additional C3b alters the substrate specificity of the convertase from C3 to C5, allowing C5 cleavage and initiation of the terminal complement pathway (Pangburn and Rawal 2002). The importance of C5 is highlighted by the exceptionally low numbers of C5 deficient individuals within the population, with a pronounced increase in susceptibility to meningococcal infection being a prominent symptom (Arnaout *et al* 2013).

1.3.7 C5a signalling through C5aR1

The effects of C5a binding C5aR1 are far more clearly elucidated than the relatively enigmatic C5aR2. C5aR1 is a classical G protein coupled receptor (GPCR) which mediates its cell signalling effects through $G_{\alpha i}$ and G_{16} subunits (Monk *et al* 2007). C5aR1 was originally reported to only be expressed on leukocyte cell lineages such as neutrophils and monocytes; however, it has now been shown to be expressed on a range of non-immune cells, including fibroblast-like synoviocytes (Yuan *et al* 2003). Activation of the GPCR induces signalling predominantly through Gβ / Gγ subunit translocation in the membrane allowing activation of a range of downstream signalling cascades including cAMP, ERK, PLC and RAS/RAF (Ward 2004). Interestingly, the exact pathways induced vary between cell types, for example, the cAMP response, prominent in neutrophils and hepatocytes, is markedly reduced in dendritic cells and monocytes (Ward 2004; Peng *et al* 2009; Li *et al* 2012; Das *et al* 2014). These differences in cAMP activity between cells can also be demonstrated in other aspects of cell signalling. C5a is classically a highly pro-inflammatory mediator, causing upregulation of IL-8, IL-1 and IL-6 in HUVECs and neutrophils (Shuster *et al* 1997; Monsinjon *et al* 2003); however, in LPS primed monocytes C5aR signalling modulated TLR4 signalling via Gαi/ Raf/MEK/ERK, downregulating the IL-6 and TNFα pro-inflammatory response and inducing IL-10 release, a potent anti-inflammatory cytokine (Seow *et al* 2013). Some of the conserved, central C5aR1 mediated signalling pathways are highlighted in Figure 1.7.

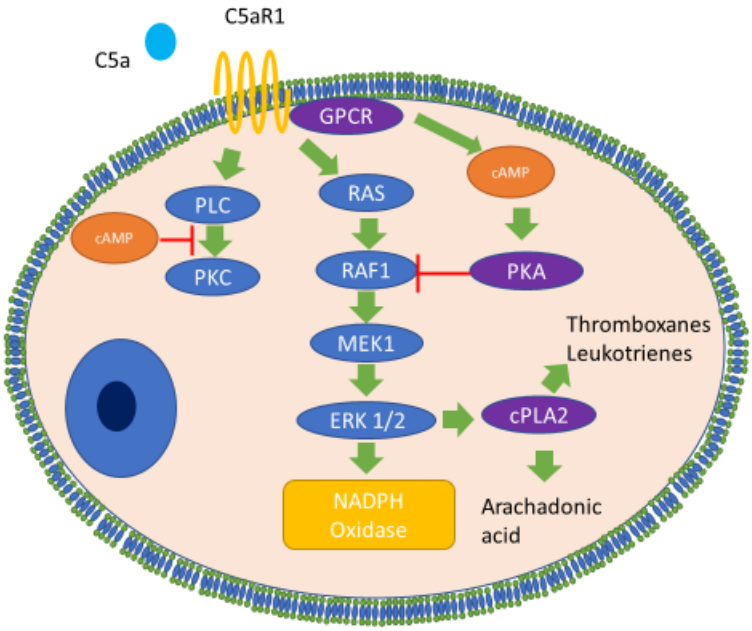

Figure 1.7. Cell signalling transduction in neutrophils induced by C5aR1 GPCR activation, including the synthesis of inflammatory mediators such as Leukotrienes and Thromboxane (Image derived from Ward 2004).

C5a also induces pro-inflammatory effects in non-immune cells, including interactions and synergisms with the Toll like receptor (TLR) family of pattern recognition receptors (PRRs) and the cell danger sensing and inflammatory machinery of the inflammasome. This centrality to a plethora of inflammatory signalling pathways is then mirrored in C5a involvement in a wide range of pathological conditions, for example, atherosclerosis, chronic obstructive pulmonary disease, asthma and allergy, ischaemia / reperfusion injury and RA; hence, targeting of C5aR or modulation of C5a signalling are areas of intense interest in therapeutic development (Lee *et al* 2008).

1.4 – The complement terminal pathway

1.4.1 MAC intermediates and formation

The role of the larger C5 fragment, C5b, is to form the nidus for the terminal complement components to assemble into the lytic membrane attack complex (MAC) pore leading to target cell rupture and death (Nauta *et al* 2002). C5b binds C6 to form C5b6, a stable intermediate complex which can associate with target plasma membranes through hydrophobic interactions (Cooper *et al* 1970; Hu *et al* 1981). C7 can then bind the complex, increasing its lipophilic properties and strengthening association with the membrane (Tschopp, Podack and Muller Eberhard 1982). The interactions of C5b-7 with the membrane only involve the outer lamella of the bilayer; therefore, C5b-7 has no lytic capability.

The binding of C8 to membrane-associated C5b-7 C5b causes a deeper insertion of the complex into the bilayer. C5b-8 complexes act as small, unstable pores that may induce ion flux in some targets (Ramm *et al* 1982; Niculescu and Rus 2001).

The final requirement for effective transmembrane pore formation is binding and polymerisation of multiple C9 molecules; individual C9 molecules sequentially bind, unfold and insert into the membrane, assembling a β–barrel pore resembling the T cell pore former perforin (Hadders *et al* 2012; Arber et al 2013; Bubeck 2014). The mechanism of C9 multimerisation was recently demonstrated, with the TMH1 region acting as an inhibitor of C9 self-assembly in the absence of C5b-8 and upon C5b-8 binding. The TMH1 region is the first region of C9 to traverse the cell membrane, with the subsequent conformational change upon membrane interaction allowing the unidirectional binding of further C9 molecules (Spicer *et al* 2018). Once the MAC is assembled, the large multimeric complex is over 1 MDa in mass and over 10 nm in pore diameter (Tschopp 1984). A schematic of sequential MAC formation is shown in Figure 1.8

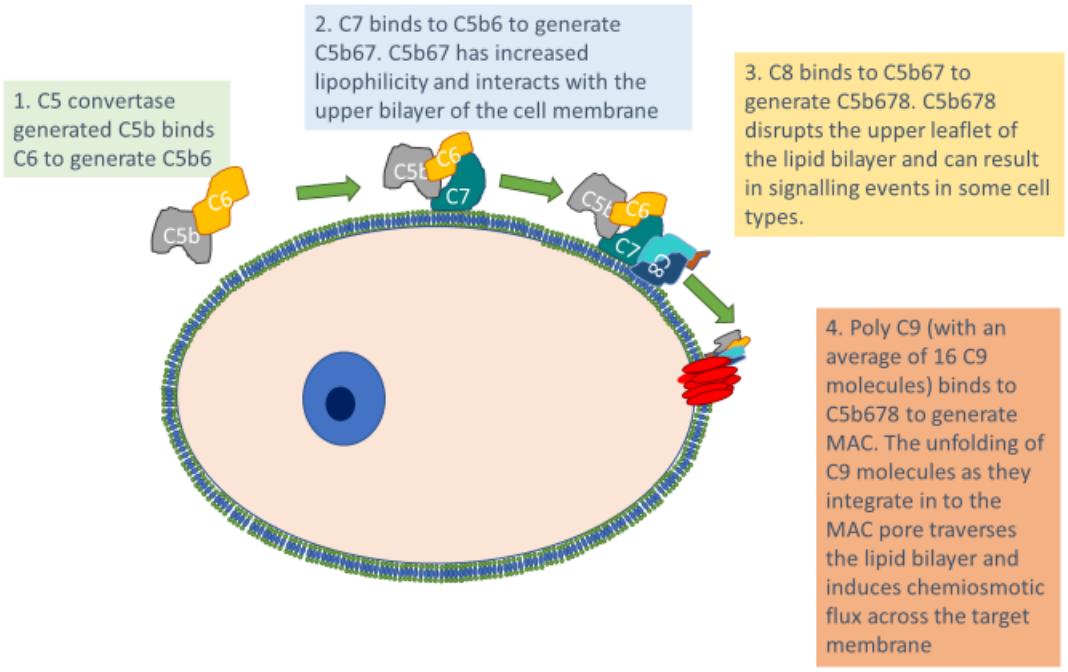

Figure 1.8. Schematic of sequential complement terminal pathway intermediates and subsequent MAC formation on a nucleated cell surface.

1.4.2 MAC structure and lytic effects

The exact structure of MAC pores was long debated; however, recent advances in imaging techniques have generated new MAC structure which provide clarity and insight into function. Utilising cryo-EM of MAC extracted from liposomes has clearly demonstrated an asymmetric pore with a "split washer" appearance, posing interesting new questions relating to MAC structure / function (Menny *et al* 2018*)*.

The MAC transmembrane channel is a non-specific ion channel allowing K^+ efflux, Ca^{2+} influx, osmotic swelling and ultimately cell lysis. Classically, cell death in response to MAC was hypothesised to be mediated through osmotic lysis due to perturbation of the chemiosmotic homeostasis maintained by the intact cell membrane; however, a recent paper hypothesised that bacterial cell death was in fact induced by the build-up of methylglyoxal from glucose metabolism which cannot be detoxified because of the altered biochemical composition of the cytosol (Bloch *et al* 2011).

In contrast, self-cells have a range of mechanisms that protect from MAC induced cell death and consequently do not usually undergo cell lysis in a similar manner to gram negative bacteria due to the regulation of MAC deposition. However, when MAC is deposited to a level which induces cell death in nucleated cells, different mechanisms of killing may occur, including apoptotic and necrotic pathways (Kim *et al* 1987; Bohana-Kashtan *et al* 2004). Necrotic cell death induced by MAC is Ca^{2+} dependent, with loss of AMP, ADP and ATP and loss of inner mitochondrial membrane potential contributing factors (Papadimitrou *et al* 1991). Other potential mechanisms behind MAC mediated nucleated cell death will be discussed later in the context of NLR activation.

1.5 – Regulation of the complement terminal pathway

As mentioned previously, MAC deposition on metabolically active, nucleated cells is predominantly sublytic due to a range of protective mechanisms (Rutkowski *et al* 2010). These mechanisms can be broadly subdivided in to regulation of the preceding complement cascade to reduce MAC formation, regulation of MAC deposition by specific fluid and membrane bound inhibitors, MAC removal through endocytosis or exocytosis, and finally mitigation of the lytic effects of the MAC through normalisation of the induced chemiosmotic gradient (Lakkaraju *et al* 2014). Therefore, the regulation of complement terminal pathway activation is crucial for the protection of self-cells.

1.5.1 – Regulation of MAC formation by CD59

The predominant membrane regulator of the MAC is CD59, a small (around 20 kDa; 77 amino acids), GPI anchored, globular glycoprotein (Kimberley, Sivasankar and Morgan 2007). The glycosylation of the molecule is extensive, with a single N-linked glycosylation site at the Asn 18 which accounts for between 4 and 6 kDa of the molecular mass (Wheeler *et al* 2002). The functional importance of this extensive and heterogenous carbohydrate moiety is unclear, with some studies suggesting an important functional role (Suzuki *et al* 1996), whilst others report no such role (Yu *et al* 1997). The structure of CD59, including the highlighted extensive glycosylation is shown in Figure 1.9.

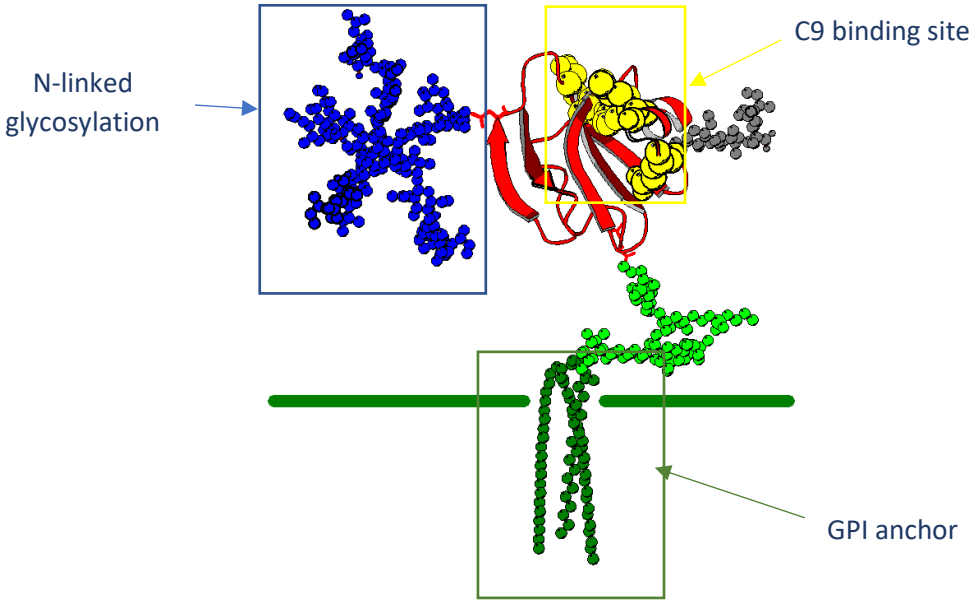

Figure 1.9 – A schematic of CD59 structure which highlights the GPI anchor (Dark green), the extensive N-linked glycosylation (Blue) and the active site residues highlighted in yellow (Image edited from Hill et al 2006).

CD59 inhibits MAC formation by tightly binding to the membrane-bound C5b-8 complex, preventing the subsequent C9 polymerisation and unfolding to form the mature MAC (Meri *et al* 1990). Despite CD59 binding to the C5b-8 complex, a single C9 molecule may still bind but is prevented from unfolding thus preventing further C9 recruitment and MAC pore formation. Binding of CD59 to C5b-8 involves a hydrophobic pocket, highlighted by both mutational and peptide docking assays (Huang *et al* 2006).

The biological significance of CD59 is clear when cases of CD59 deficiency are considered, most notably in the case of PNH. PNH occurs due to a clonal expansion of hematopoietic stem cells with a mutation in the PIGA gene, resulting in the deficiency of the encoded GPI anchor synthesising protein (phosphatidylinositol N-acetylglucosaminyltransferase subunit A), which in turn prevents the effective expression of GPI anchored proteins such as CD55 and CD59. The resulting deficiency of these complement regulators, most notably CD59 as a missense mutation in humans in CD59 alone result in chronic haemolysis and neuropathy, allows dysregulated complement activation on the erythrocyte surface and complement mediated haemolysis (Nevo *et al* 2013; Brodsky 2014; Mevorach 2015). CD59 expression, whilst

ubiquitous, is also subject to modulation. Cell surface levels of CD59 have been demonstrated to be elevated on activated neutrophils in response to formyl like peptide or calcium ionophore A23187, likely due to translocation from cytosolic stores (Okada *et al* 1994). A putative intracellular role for CD59 was demonstrated in the translocation and secretion of insulin from pancreatic β cells, with the loss of CD59 preventing VAMP/syntaxin 2 complexes forming at the cell membrane and limiting exocytic events (Krus *et al* 2014).

A soluble form of CD59 (sCD59) is also found in plasma, released from cells by GPI anchor cleavage. sCD59 was shown to be an effective inhibitor of MAC formation *In Vitro* (Sugita *et al* 1994), but a poor inhibitor *In Vivo* (Lambris *et al* 2012). Despite this sCD59 has been shown to reduce disease in a mouse model of AMD. Mice injected with recombinant sCD59 exhibited reduced choroidal neovascularisation, a hallmark of wet AMD (Bora *et al* 2007).

Alongside its regulatory function, CD59 may also be intrinsically linked to complement induced cell signalling by its GPI anchor. It was demonstrated that when CD59 was bound to or crosslinked through Vaginolysin, CD59 could act as a signalling platform for tyrosine kinases such as SYK, resulting in necroptotic cell signalling (La Rocca *et al* 2015). CD59 crosslinking and signalling may also be reproducible by other CD59 ligands such as MAC, with CD59 binding both C5b8 and C9 in the nascent MAC it is feasible that two CD59 molecules may bind to the same MAC complex. A schematic of a postulated CD59 signalling mechanism is shown in Figure 1.10. Furthermore, MAC deposition induced CD59 clustering in CHO-K1 cells by stabilising homotypic CD59 ectodomain interactions, making cell signalling via CD59 an area of interest in terms of MAC induced cell responses (Suzuki *et al* 2012). Therefore, when trying to dissect apart the mechanisms of sublytic MAC induced cell signalling, the role of CD59 must be considered, especially as previous studies have utilised anti-CD59 antibodies as complement activating and fixing agents – therefore using a system with no anti-CD59 antibody use or CD59 deletion would demonstrate any GPI anchor mediated signalling effects.

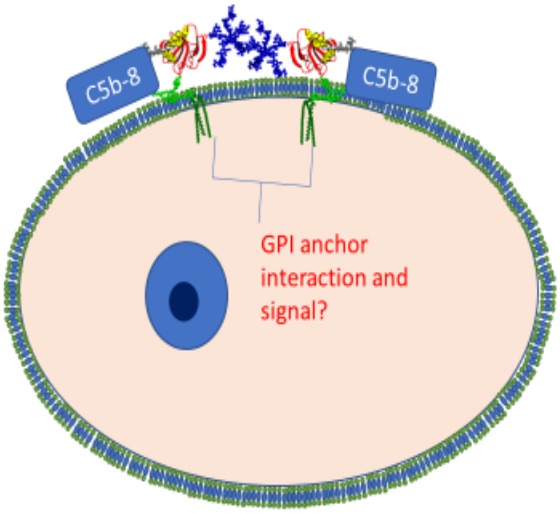

Figure 1.10 - CD59 clustering proposed by Suzuki et al in response to MAC deposition, via stabilisation of homotypic CD59 ectodomain interactions within the lipid raft membrane microenvironment (Image of CD59 sourced from Hill et al 2006, proposed signalling from Suzuki et al 2012)

1.5.2 - Fluid phase regulation of MAC

Fluid phase regulation of MAC formation is medicated by Clusterin and Vitronectin, which both regulate the process at the C5b-7 stage. Binding of Clusterin / Vitronectin to C5b-7 prevents the insertion of the complex in to the membrane but allows the further binding of C8 and C9 to form a soluble MAC complex (sC5b-9). The binding of Clusterin / Vitronectin prevents the soluble MAC from interacting with the cell membrane, subsequently inhibiting lytic capacity (Choi *et al* 1990). The process of inhibition is dependent on recognition of hydrophobic domains in C7 and the β subunits of C8 and C9, the latter dependent on folding of the molecule, with poly-C9 competing with the Clusterin binding site (Tschopp *et al* 1993; Chuahan and Moore 2006).

1.5.3 - Membrane repair and MAC removal

The final mechanism of defence of nucleated cells against MAC is through the removal of MAC from the membrane by endocytosis or membrane shedding followed by repair of the membrane (Campbell and Morgan 1985; Morgan, Dankert and Esser 1987).

The shedding of MAC through exocytosis or ectocytosis has been shown in a range of cell types, including neutrophils and various cell lines (Morgan *et al* 1987; Pilzer and Fishelson 2005). Exocytosis and ectocytosis of MAC occur via different mechanisms; ectosomes form through pinching off regions of the membrane, whereas exosomes require internalisation and sorting into multivesicular bodies (MVBs) before release from the cell; these differential processing pathways are illustrated in Figure 1.11 (Yellon and Davidson 2014).

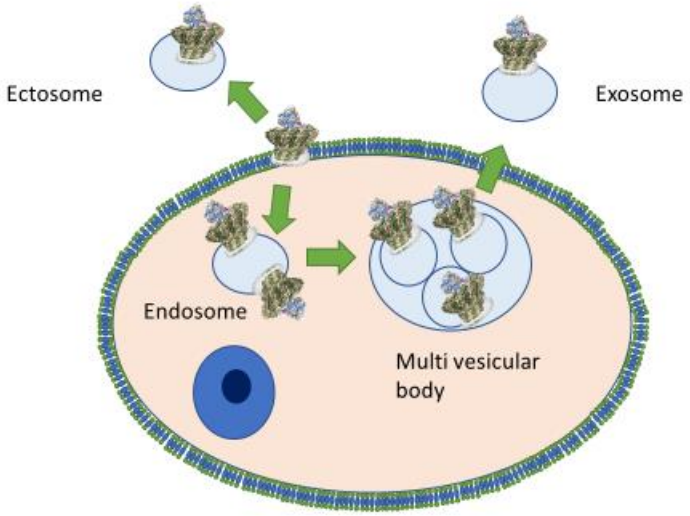

Figure 1.11- Schematic of MAC ectosome, endosome and exosome formation and sorting within multivesicular bodies (CRyo-EM image of the MAC sourced from Menny et al 2018, figure based on Image of MAC internalisation from Pilzer et al 2005)

The initial Ca^{2+} flux induced by the MAC is crucial for signalling MAC expulsion, with chelation of intracellular Ca^{2+} inhibiting the removal of the lesions and increasing cell death (Carney *et al* 1985; Morgan and Campbell 1985). The mechanism by which Ca^{2+} mediates the removal of MAC lesions from the membrane involves kinase activation, with inhibition of ERK being shown to decrease the rate of MAC exocytosis (Pilzer *et al* 2005). Further clues to the mechanism of MAC lesion removal can be discerned from experiments utilising the bacterial pore forming toxin streptolysin. Streptolysin induced Ca^{2+} flux resulted in annexin binding to membrane phospholipids to cause the aggregation and membrane fusions necessary for effective streptolysin pore removal (Babiychuck *et al* 2011).

The endocytosis of MAC lesions is a well-established phenomenon within the field of complement biology, with the internalisation and subsequent exocytosis of MAC lesions shown on neutrophils upon complement attack back in the 1980's (Morgan *et al* 1987). The role of endocytosis in MAC lesion removal may be two-fold. Firstly, allowing the sorting and enrichment of MAC in to MVBs before their subsequent exocytosis, or alternatively allowing the internalised MAC to be degraded or potentially induce intracellular signalling events (De Wit *et al* 2015). Endocytosis of receptor: ligand complexes is a common feature in the mediation of cell signalling, which generally occurs via a Clathrin mediated endocytic pathway (Mbengue *et al* 2016). However, the processes mediating MAC internalisation and endocytosis are controversial, with both conventional Clathrin endocytic pathways and Clathrin-independent mechanisms dependent on lipid rafts containing Caveolin-1 and Dynamin-2 both being implicated (Kerjaschki *et al* 1989; Moskovich *et al* 2012). The latter paper implies that Clathrin has no role in MAC endocytosis, as siRNA knockdown of Clathrin had no effects on MAC endocytosis or cell death; further work is needed to understand this process more clearly.

1.6– Sublytic MAC mediated cell signalling

Due to the defence mechanisms described above, nucleated cells exposed to MAC usually avoid the cytolytic effects suffered by bacteria or aged erythrocytes. However, the disturbances to cellular physiology induced by sublytic MAC cause a range of responses, including the mediate of secretion, degranulation, adherence, aggregation, chemotaxis and proliferation (Morgan 1989; Zhu *et al* 2017).

In an increasing and diverse range of pathologies, deposition of sublytic MAC is implicated as a driver of the inflammation; these include atherosclerosis, cancer, Alzheimer's disease and RA (Lewis *et al* 2010; Pio, Ajona and Lambris 2013; Romero *et al* 2013). Unsurprisingly, given the range of potential effects of sublytic MAC, the mechanisms by which it induces pathologies is diverse. For example, in certain cell types sublytic MAC deposition induces apoptosis, resulting in tissue damage and loss of organ function. In a model of mesangioproliferative glomerulonephritis, sublytic MAC induced glomerular cell apoptosis through activation of Caspase 8 and upregulation of the IRF transcription factor (Liu *et al* 2012). Similarly, in photoreceptor cells, sublytic MAC triggered apoptosis and increased sensitivity to necrotic pathways induced by staurosporine, a broad range kinase inhibitor (Shi *et al* 2015).

In contrast, in other cell types, including aortic smooth muscle, endothelial cells and Schwann cells, sublytic MAC deposition inhibited apoptosis and induced proliferation (Tegla *et al* 2011). The induction of proliferation by sublytic MAC is mediated by several mechanisms, including RAS/RAF and AKT mediated pathways. Some reports suggest that intracellular signalling cascades are activated even before the completion of the MAC pore, with C5b-7 implicated in the activation of membrane phospholipases and cAMP signalling, although the exact mechanism of how the loosely membrane associated C5b-7 induced signalling events was not explored (Carney *et al* 1990). Further anti-apoptotic mechanisms induced by sublytic MAC include the induction of the RAS/RAF, ERK, p38MAPK, JNK and G_i / G_o G-protein activation; these multiple pathways are summarised in Figure 1.12. Anti-apoptotic effects of MAC may correspond to the observed enhancement of cell cycle, involving increased CDK-2 and CDK-4

signalling, whilst reducing p21 cell cycle inhibitor mRNA expression (Rus, Nicolescu and Shin 1996).

Many of these signalling pathways are driven through differential cell type responses to sublytic MAC mediated elevation of intracellular Ca^{2+}, caused by chemiosmotic gradient between the cytosol and the extracellular fluid, which becomes disrupted by the nonspecific MAC pore (Morgan 1989) . The level of elevation, the duration of Ca^{2+} flux and the cell specific signalling machinery mediates the effects Ca^{2+} and may determine which of these contrasting cell fates occurs. Whilst Calcium may activate a raft of associated kinases and signalling pathways, the direct binding of Calcium ions to protein structures can have large effects on pore both structure and function, which may have direct implication on activation of NLRP3 and associated inflammasome components (Yaron *et al* 2015).

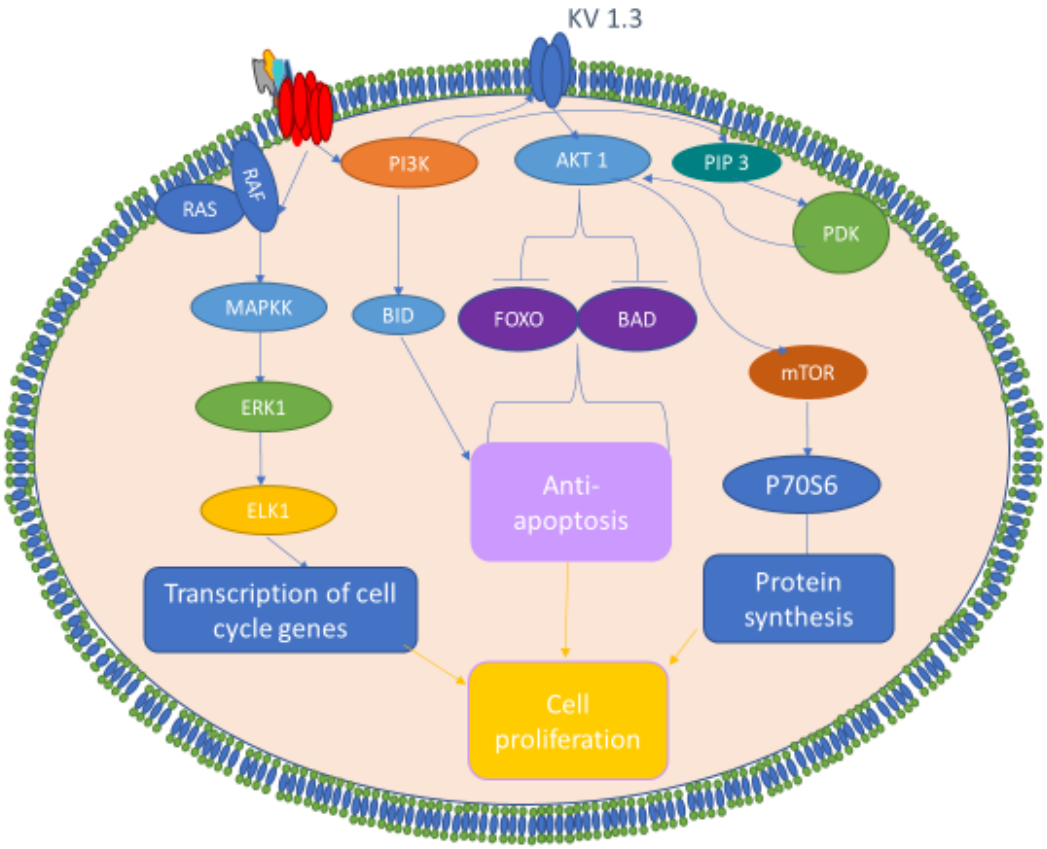

Figure 1.12. Pro-survival signalling pathways activated in different cell types by sublytic MAC. The association of MAC with Giα subunits to drive RAS/RAF is still controversial, however the influx of calcium may also activate MAPK and PLC/IP3 signalling (Image derived from Tegla et al 2011).

The contributions of the pro-inflammatory effects of sublytic MAC and the anaphylatoxins to disease pathology are increasingly implicated in a broad spectrum of diseases. Complement knockout mice show decreased inflammation in models of inflammatory disease, such as collagen antibody-induced rheumatoid arthritis. In this model, clinical severity of this inflammatory autoimmune condition was compared between WT and C3aR -/-, C5aR -/- and C6 -/- mice, with the severity scoring decreasing by 52, 94 and 65% for each respective knockout (Banda *et al* 2012). These data highlight the importance of complement as a pro-inflammatory driver of the innate immune system, in some cases to a pathological level.

The signalling pathways induced by the anaphylatoxins and sublytic MAC are part of the larger, complex network of innate immune system driven signalling pathways. Within this network, complement signalling acts both synergistically and antagonistically with a range of other receptors including Toll like receptors (TLRs), Rig like receptors (RLRs), Nod like receptors (NLRs) and other effectors such as C-reactive protein (CRP). For the signalling impact of complement to be fully appreciated, the interactions with these other mechanisms need to be realised; therefore, anaphylatoxin and sublytic MAC cell signalling will be revisited once these others have been highlighted in the following section. Some of the diverse array of signalling pathways activated by sublytic MAC are shown in Figure 1.13.

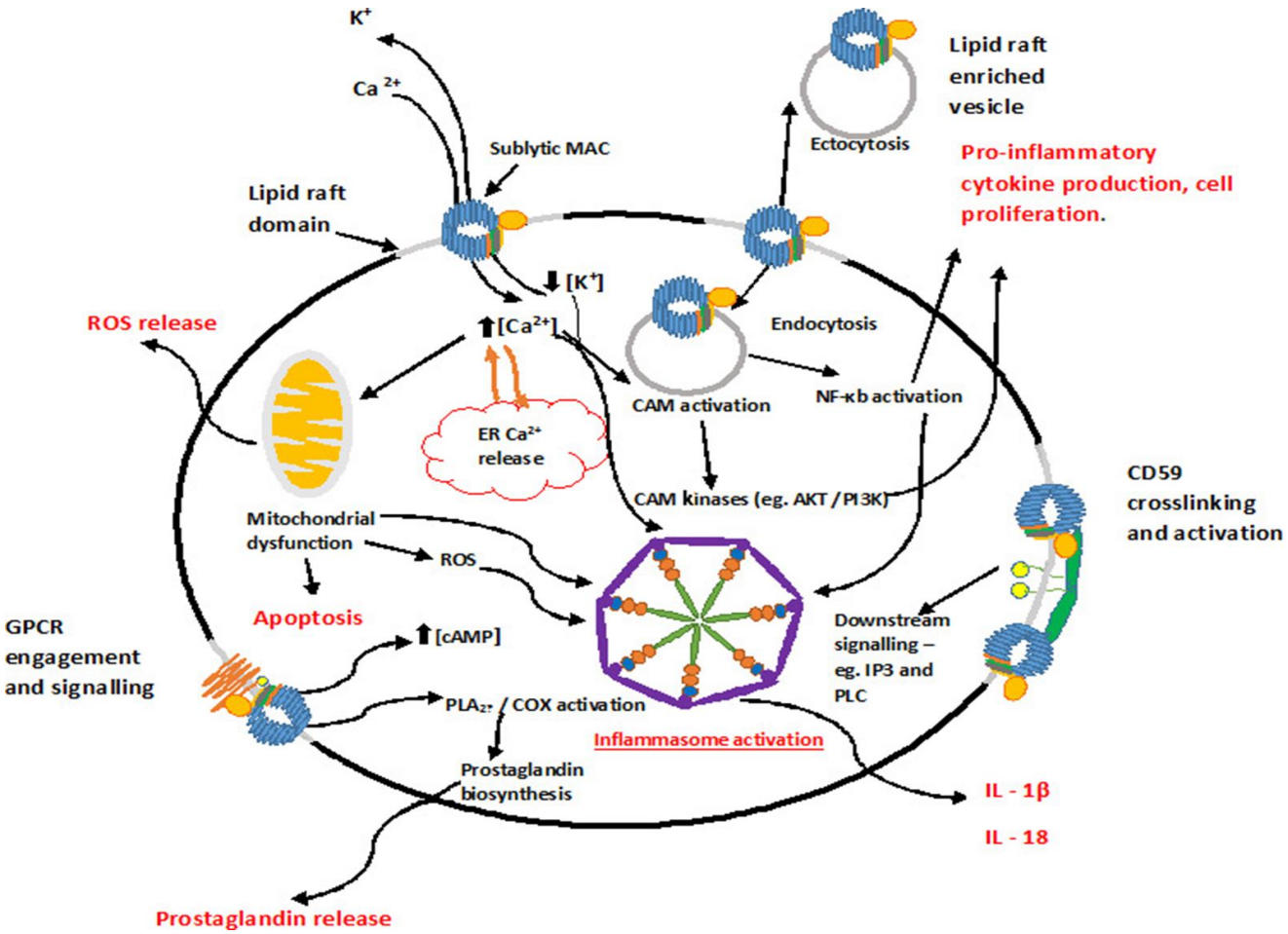

Figure 1.13. Schematic of the range of cellular effects induced by sublytic MAC. Sublytic MAC deposition on the cell can mediate a range of effects through elevation of intracellular Ca^{2+}, induction of cAMP signalling, PLC activation and NF-κB activation. Many of these pathways have implications in inflammasome activation and inflammatory cell signalling. Image sourced from Morgan et al 2016.

1.7 - Nod like Receptors – background, signalling and disease.

Nod like receptors (NLRs) are a versatile family of intracellular receptors with a broad range of functions, ranging from antigen presentation and modulation of inflammation to embryonic development and sensing cellular metabolic changes (Motta *et al* 2015). Evolutionarily, NLRs are well conserved and orthologs are found across much of the animal kingdom (Lange *et al* 2011). The NLR family in humans is diverse, comprising 22 members with specific functions dependent on ligand specificity and effector functions, each determined by individual domains in the molecular tripartite structure. Upon activation the

autoinhibited monomeric inflammasome-forming NLRs oligomerise to form the characteristic pinwheel-shaped active inflammasome structure, leading to cell signalling and cytokine secretion events (Lechtenberg *et al* 2014).

As mentioned, numerous NLRs perform vital roles within the body; however, the most well studied, ubiquitously expressed and pathologically relevant NLR is NLRP3. Dysregulation of NLRP3 can perpetuate chronic inflammation through cytokine maturation and secretion and the induction of pyroptosis and is implicated in classical cryopyrinopathies such as Muckle-Wells syndrome, neonatal-onset multi-system inflammatory disease (NOMID) and more common pathologies such as cardiovascular, metabolic and rheumatic conditions (Tong *et al* 2015; Rheinheimer *et al* 2017; Zhou *et al* 2018). Due to this well documented role of NLRP3 in the perpetuation of aberrant inflammation, it will be my focus experimentally over the course of the project.

1.7.1 – NLR structure and function

NLRs are comprised of a distinct tripartite structure, the Leucine rich repeat region (LRR), the nucleotide binding and oligomerisation domain (NACHT) and N terminal effector domain (normally a pyrin or a Caspase activation and recruitment domain – PYD and CARD respectively) which co-operatively determine both ligand specificity and the presence or absence of a linker between the inflammasome and respective effector Caspase, with NLRP3 structure highlighted in Figure 1.14.

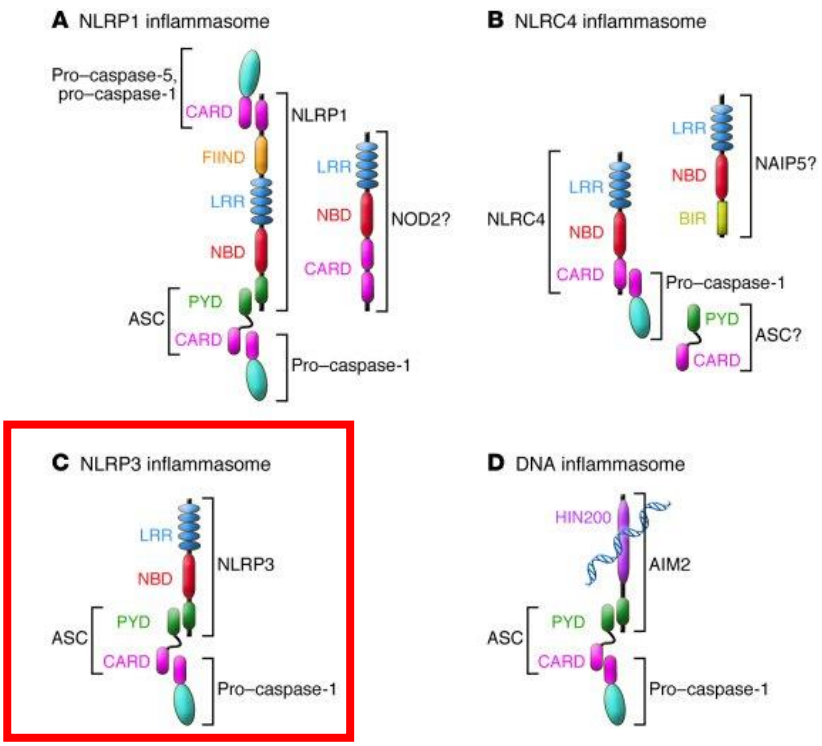

Figure 1.14. Tripartite structures of known inflammasomes with LRR, NACHT and PYD/CARD domains, with NLRP3 highlighted (Image edited from Stutz et al 2009).

1.7.2 - The roles of the LRR in NLRP3 function

The C terminal LRR is functionally responsible for PAMP / DAMP sensing and the specificity of the individual NLRs (He, Hara and Nunez 2015). The LRRs of NLRs and TLRs demonstrate some conserved secondary structural motifs, including a super helical arrangement of short parallel beta strands. The overall topology of LRRs in NLRs is a right-handed helix, as opposed to TLRs that are left handed helix or flat; all contain a highly conserved Leucine repeat (LxxLxLxxNx(x/-)L) where L represents Leucine, N is Asn, Thr, Ser or Cys and X is a non-conserved residue. The general function of the LRR is to mediate homotypic protein-protein interactions, the nature of which in the case of inflammasome activators is still unclear (Kobe and Kajava 2001). However, the SGT-1/HSP70/HSP90 complex is fundamental for inflammasome activation and preferentially interacts with protein LRR regions. This may suggest that this chaperone complex may be intrinsically involved in assisting the protein refolding upon activation, or possibly acting as a linker in a complex with an activating protein such as AKT or MAP3K, which have been shown to associate with the SGT-1 complex when active (Mayor *et al* 2007).

1.7.3 - NACHT function in NLRP3 activation

The second main functional domain within the tripartite inflammasome structure is the central NACHT domain, responsible for the nucleotide binding and oligomerisation of NLRs (Duncan *et al* 2007). Although no 3D structures of the NACHT domains of NLRP proteins have been solved, the structurally and functionally similar NLRC4 and APAF1 NACHT domains have been recently elucidated and may offer new insight into NLRP protein activation and oligomerisation. NLRC4 has been mapped to a resolution of 3.2 Å (minus the CARD) demonstrating that, like APAF-1, NLRC4 monomers exist in an autoinhibited monomeric form with ADP bound to the NACHT domain and the LRR forming a loop spatially binding the nucleotide-binding and HD2 domains (Hu *et al* 2013).

The NACHT of APAF-1 / NLRC4 were shown to contain a central NOD domain with 3 auxiliary helical NAD domains containing 12 conserved motifs relating to nucleotide binding and hydrolysis, including an ATPase specific and catalytic Mg^{2+} binding pocket that enables the

NLRs to associate with the STAND family of AAA+ ATPases (Zhang *et al* 2015). NLRP3 and NLRP12 also exhibit a specific ATPase activity, which has been shown to be necessary for functional inflammasome formation (Maharana *et al* 2015). Often, ATP binding or hydrolysis induces conformational changes in the both the local and overall structures of proteins; therefore, it has been hypothesised that the ATP/ADP bound state of the NLRs may regulate their activity (Duncan *et al* 2007).

Unsurprisingly, due to the plethora of pathophysiological conditions in which inflammasome activation (particularly NLRP3) has been implicated, pharmaceutical modulation of inflammasomes is of intense interest. Notably, a range of vinyl sulphone anti-inflammatory compounds, including Bay 11-7082, which functioned through an unknown mechanism, have been shown to interact directly with the NACHT of NLRP3 (Juliana *et al* 2010).

1.7.4 – The role of the PYD in NLRP3 activation

The final major structural domain of NLRs is the N terminal effector domain which, depending on the NLR, is either a CARD or PYD. Both the NLRP1 and NLRC4 complexes contain the CARD domain, allowing direct interaction between the NLR and its Caspase effector (Lechtenberg *et al* 2014). The inflammasome forming NLRs, including NLRP3, lack a CARD domain and instead interact with the associated Caspase through the linker associated speck like protein (ASC). ASC is a 22 kDa, highly charged protein containing a pyrin domain (PYD) and Caspase activation and recruitment domain (CARD) which was observed to form intracellular specks in response to retinoic acid in HL-60 cells (Masumoto *et al* 1999). Later, it was established that ASC was the central linker in inflammasome formation by binding to the NLR PYD through homotypic interactions, and subsequently with Caspses through the CARD (Liu *et al* 2013).

To date, no crystal structure or mutational analysis of NLR PYD domains have been described; however, NMR spectroscopic techniques have shed some light on a potential mechanism of PYD interactions. Charged regions are present on the PYD of ASC, with helices 1 and 4 being highly negatively charged and 2 and 3 highly positive, allowing PYD/PYD interaction between oppositely charged helices (Liepinsh *et al* 2003). Further, NMR studies on the NLRP12 PYD demonstrate that it forms a tightly packed 6 helical bundle with short loop regions, all

stabilised by a substantial hydrophobic core to give a stable tertiary structure, shown in Figure 1.15 (Pinheiro *et al* 2011). The charge state of the PYD of NLRP3 seems to be crucial for oligomerisation to form an active inflammasome, with the phosphorylation state of Ser5 of crucial importance. The dephosphorylation of Ser5 by protein phosphatase 2 a (PP2a) was demonstrated to be sufficient to induce a permissive state for oligomerisation through allowing charge interactions in the PYD interface (Stutz *et al* 2017).

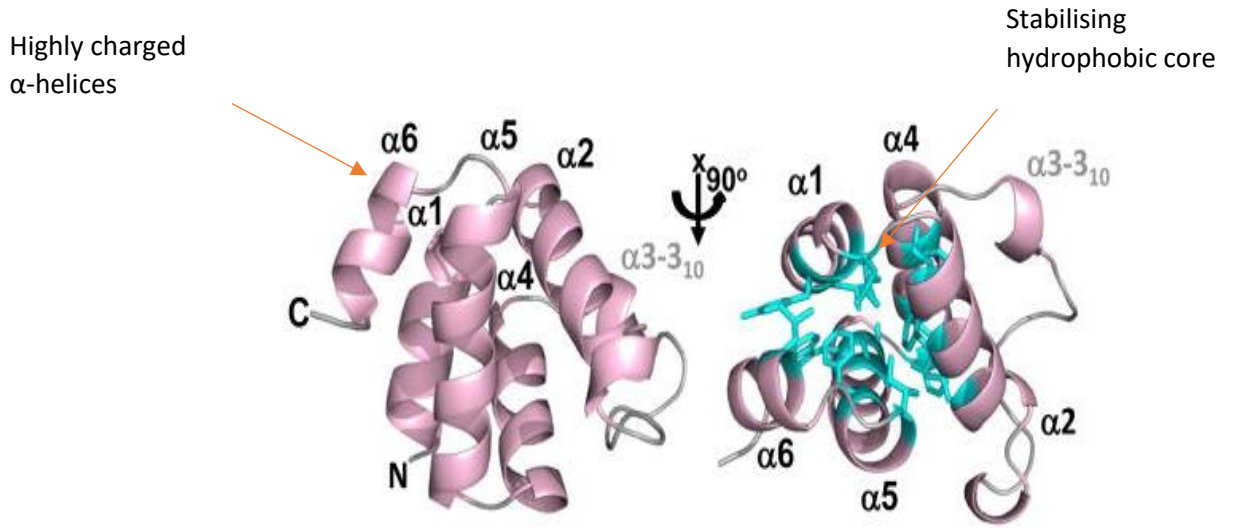

Figure 1.15. A ribbon diagram of the proposed lowest energy conformer of NLRP12 PYD demonstrating the charged α helices thought to be crucial for PYD:PYD interaction (B) The same image rotated through 90˚ and the hydrophobic core residues highlighted in Cyan stick form (C) (Image edited from Pinheiro et al 2011).

1.8– Inflammasome priming – Signal one

To activate the NLRP3 inflammasome, induce oligomerisation and effectively secrete IL-1β and IL-18, a two-step signalling process is generally required with the initial priming step induced by TLR, C5a receptor or cytokine receptor signalling. It was demonstrated that priming, predominantly through NF-κB signalling, was necessary, but not sufficient, to induce NLRP3 activation (Bauernfeind *et al* 2009). It was subsequently demonstrated that NF-κB induced an upregulation of the precursors pro-IL1β/pro-IL18 as well as NLRP3 itself, but not upregulation of the inflammasome components ASC or Caspase-1 (Hornung and Latz 2010).

1.8.1 – Transcriptional priming through TLR4

The prototypical cell signalling for priming of the NLRP3 inflammasome is mediated by TLR4 activation by a range of ligands, including PAMPS such as the bacterial cell wall component lipopolysaccharide (LPS) and DAMPS including HMGB1 (Kim and Jo 2013). TLR4 is a single pass transmembrane receptor comprising a 608 aa extracellular domain, a transmembrane domain and a 187 aa intracellular domain (Kim *et al* 2007). The recognition and interaction of TLR4 with LPS is mediated by MD-2 which undergoes conformational change upon interaction with LPS, permitting phosphate groups on the LPS molecule to induce receptor multimerisation and signal transduction, shown in Figure 1.16 (Park *et al* 2009).

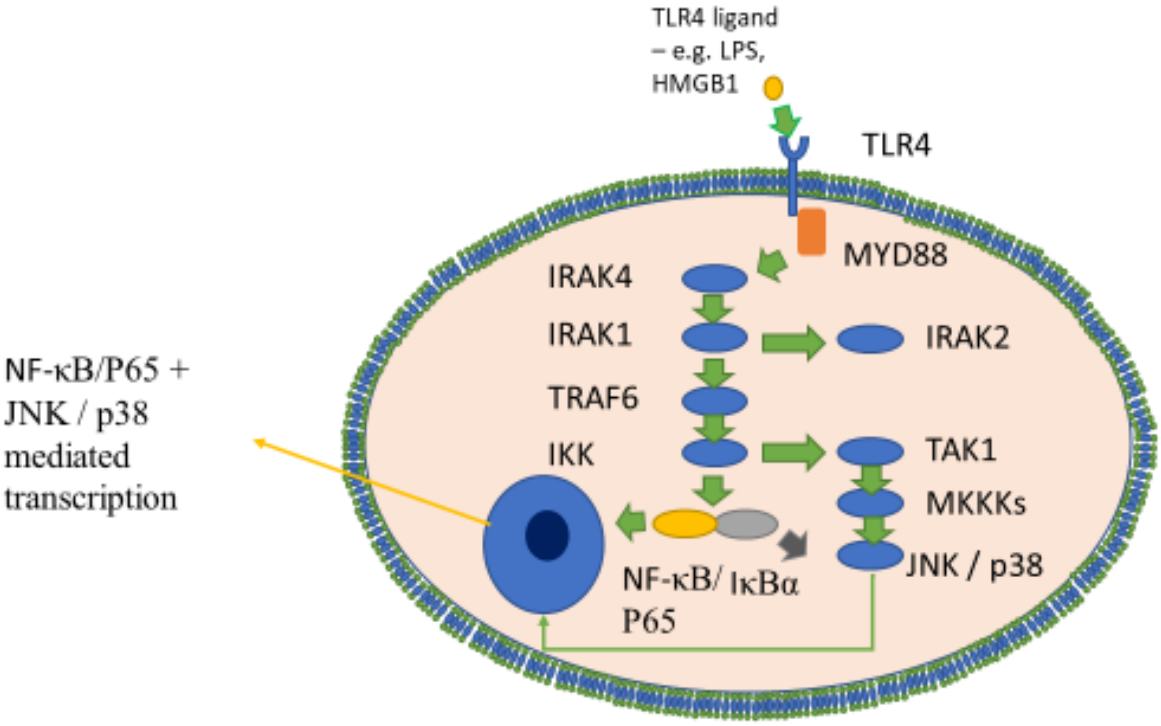

Figure 1.16. The activation of the canonical NF-κB signalling pathway through TLR4. The activation of NF-κB to induce the expression of pro-IL1β, pro-IL18 and NLRP3 is generally necessary for effective inflammasome activation (Image content sourced from Lim and Staudt 2013).

TLR engagement induces the cytoplasmic TIR domain to recruit various signalling adaptors including MYD-88 and/or TRIF/TRAM (Lim and Staudt 2013). Dependent on the signalling adaptor engaged, a range of potential effectors can then be activated, including the IRAK kinase family and the ubiquitin ligases TRAF6 and Pellino 1 (Kawai and Akira 2010). The activation of these pathways then culminates in the engagement of NF-κB, JNK and p38 MAPK signalling pathways to regulate gene transcription (Figure 1.17). The induction of NF-κB signalling through TLR4 activation is via the canonical pathway; IKKβ is activated by phosphorylation and in turn phosphorylates IKKα Ser32 and Ser36, inducing IKKα proteasomal degradation and freeing NF-κB from the inhibitor complex. This then allows NF-κB P50/P65 heterodimer translocation to the nucleus to induce the transcription of a host of pro-inflammatory genes (Hoesel and Schmid 2013).

Alongside the canonical priming mechanism through TLR4 engagement, other mechanisms of priming through TNFαR, C5aR and an autocrine loop through IL-1R signalling also exist, transduced through similar mediators to result in NF-κB mediated NLRP3 priming (He *et al* 2016). These are summarised in Figure 1.17.

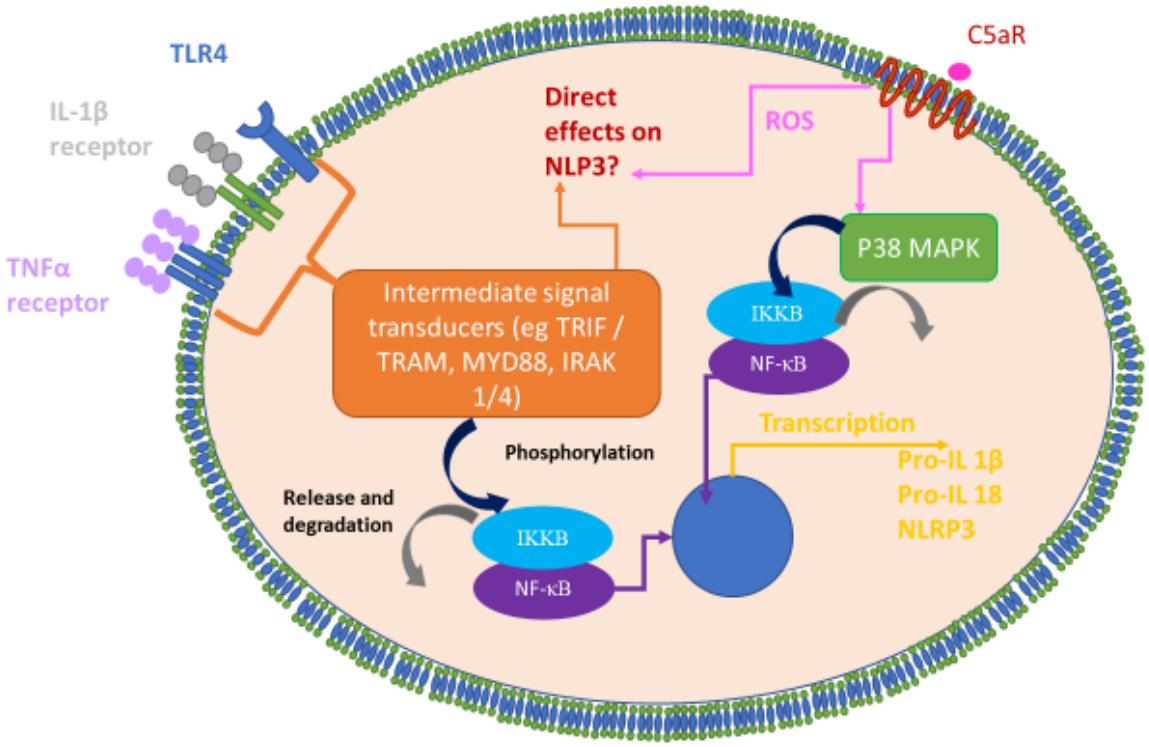

Figure 1.17. Mechanisms of NLRP3 priming. NLRP3 priming occurs via the induction of NF-κB mediated transcription of NLRP3 and Pro-IL1β and Pro-IL18, as well as postulated direct effects on NLRP3 itself via post translational modifications. Alongside canonical TLR4 priming, IL-1R and TNFαR can mediate these effects through IRAK 1/4 , MYD88, FADD, Caspase-8 and TRIF/TRAM related pathways. C5aR has been implicated to directly effect NLRP3 activation through ROS production and priming through P38 MAPK mediated NF-κB activation (Haggadone et al 2016; Groslambert and Py 2018)

1.9- Non-transcriptional priming of NLRP3

The priming signal through the NF-κB signalling pathway was thought to simply induce the transcription of necessary components for inflammasome activation; however, activation of NF-κB also has a direct effect upon NLRP3 through the generation of reactive oxygen species (ROS), which in turn activate the BRCC3 de-ubiquitinase; the resultant de-ubiquitination of NLRP3 may yield a primed state (Juliana *et al* 2012).

Further studies also demonstrate TLR priming is not strictly necessary; for example, simultaneous engagement of TLR4 and NLRP3 induced a strong Caspase-1 response in an IRAK-1 dependent manner in bone marrow derived macrophages (Lin *et al* 2013). A central role for ERK1, ROS and the proteasome in inflammasome activation independent of transcription suggests that the priming step is more complex than just the transcription of inflammasome components (Ghonime *et al* 2014).

The evidence for the involvement of phosphorylation in the priming and activation of the NLRP3 inflammasome also includes a potential role for TAK1 and the MAPK family, with multiple studies highlighting TAK1/JNK and SYK as crucial for release of IL-1β through NLRP3 activation; however, the data indicate a role for these kinases in the induction of ASC speck oligomerisation rather than direct interaction with NLRP3 (Okada *et al* 2014; Patel *et al* 2018). Moreover, TAK1 deficient murine BMDMs demonstrate spontaneous NLRP3 activation in the absence of conventional priming/activation stimuli, mediated through RIPK1 and spontaneous TNF-α autocrine signalling coupled with IKKα/β activation; these cells also demonstrated homeostatic hyperactivation of ERK, traditionally delineated as a downstream activated MAPK of TAK1, demonstrating that non-canonical mechanisms may mediate this effect (Malidreddi *et al* 2018).

1.10 – NLRP3 activation mechanisms – Signal two

The NLRP3 inflammasome, once primed in either a transcription dependent or independent manner, can become activated by a plethora of activating stimuli which break down in to three main categories – intracellular ion fluxes, ROS generation and mitochondrial dysfunction and lysosomal rupture and damage (Zoete *et al* 2014). The effects of these stimuli on the structure and binding partners of NLRP3 are profound; however, how these diverse stimuli elicit the same response is unclear. The diversity of activating stimuli would suggest a conserved set of downstream mediators due to the improbability of NLRP3 directly recognising such diverse signals; however, these mechanisms remain obscure. A schematic illustrating the broad classes of NLRP3 activators is shown in Figure 1.18.

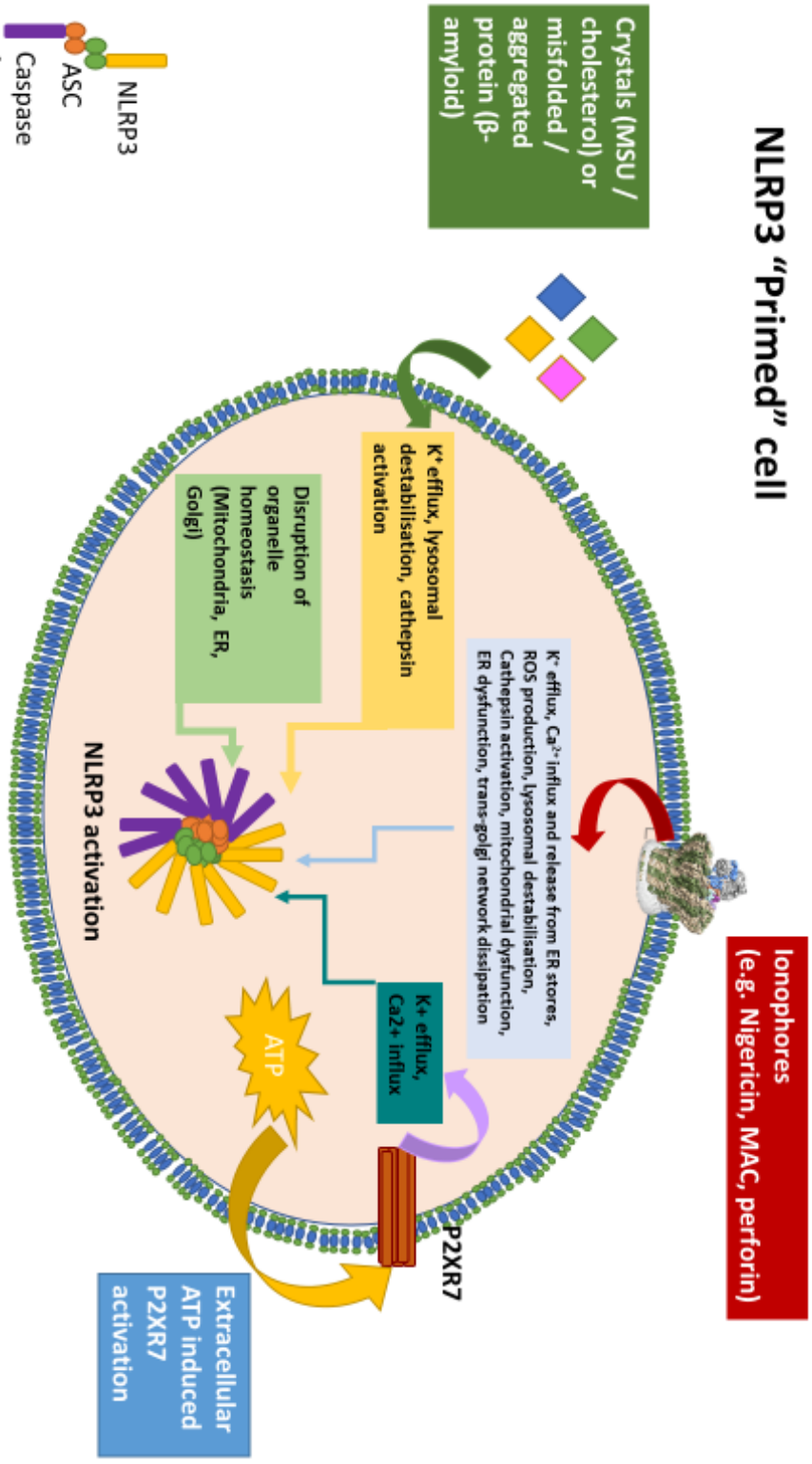

Figure 1.18 – Classes of NLRP3 activators. Broadly, NLRP3 activation is induced through cell membrane disruption through ionophores, frustrated phagocytosis / lysosomal disruption through crystalline substances or aggregated proteins or through extracellular ATP mediating P2XR7 activation. Alongside these external activators, the dysregulation of internal organelle homeostasis (through one of these stimuli or otherwise) may also drive inflammasome activation. The downstream events of these stimuli then broadly divisible in to ionic flux, ROS generation, lysosomal destabilisation and cathepsin release and organelle dysfunction. MAC cryo EM sourced from Menny et al 2018.

A leading hypothesis is that ion flux is a necessary and sufficient signal to induce NLRP3 inflammasome activation; however, the exact nature of the flux, whether it is dependent on potassium efflux, calcium influx, or a combination of both, is still controversial (Chae *et al* 2015; Katsnelson *et al* 2015; Yaron *et al* 2015).

1.10.1 - Potassium efflux as an activator of NLRP3

The hypothesis that potassium efflux is solely responsible for the activation of the NLRP3 inflammasome is supported by the recent report systematically demonstrating that there was no role for Ca^{2+} influx in the activation of NLRP3 (Katsnelson *et al* 2015). It was demonstrated that nigericin-induced Ca^{2+} influx occurred downstream of Caspase-1 activation, likely due to the capacity of Caspase-1 to alter membrane permeability; depletion of Ca^{2+} from the medium, depletion of ER Ca^{2+} stores and Ca^{2+} specific ionophores were all without effect on IL-1β secretion. Furthermore, the group showed that the intracellular Ca^{2+} chelator BAPTA, previously shown to strongly inhibit NLRP3 activation, exerted pleiotropic inhibitory effects, including inhibition of NLRP3 activation in response to Nigericin even in Ca^{2+} depleted medium (Katsnelson *et al* 2015). The exact mechanism by which K^+ efflux activates the inflammasome is as yet unclear. Many other groups have demonstrated NLRP3 inhibitory functions of the K^+ channel inhibitor Glyburide and elevated extracellular K^+ concentrations, making K^+ efflux a strong candidate for NLRP3 activation (Lamkanfi *et al* 2009; Di *et al* 2018).

1.10.2 - Calcium influx as an activation mechanism of NLRP3

Despite the evidence described above, other groups have strongly conflicting data demonstrating a crucial and indispensable role for Ca^{2+} for inflammasome activation (Sutterwala *et al* 2014). For example, the intracellular calcium receptor (CASR) was necessary and sufficient to activate the NLRP3 inflammasome in the presence of elevated cytosolic Ca^{2+} calcium (Lee et al, 2012). Interestingly, they also reported a paradoxical response to increased

extracellular Ca^{2+}, which inhibited NLRP3 activation by extracellular ATP but not flagellin or dsDNA, perhaps beginning to explain some of the discrepancies in the literature.

Some groups have attempted to unify the contrasting theories on the role of ion fluxes in NLRP3 inflammasome activation utilising real time imaging to link the K^+ and Ca^{2+} fluxes, showing that NLRP3 activation is dependent on both ions and proposing a model where K^+ efflux was the regulator for $Ca^{2+,}$ which then in turn induced mitochondrial dysfunction and ROS generation to induce the final activation signal (Yaron *et al* 2015).

1.10.3 - ROS generation, mitochondrial dysfunction and metabolic perturbation as NLRP3 activators

The concept that mitochondria may be intrinsically linked with NLRP3 activation has strong support, with the mitochondria acting as a nexus between Ca^{2+}, ROS and cell metabolism – all of which have been shown to activate or regulate NLRP3 activation. The concept that ROS, predominantly produced by mitochondria, is an activator of the NLRP3 inflammasome is controversial, with studies presenting arguments both for and against the case (Zhou *et al* 2011; Iyer *et al* 2013). Whether ROS act as an activator of NLRP3 or are generated as a consequence of the activation remains unclear, with real time ROS imaging being required to delineate the chronology of events.

Other molecules associated with mitochondria, including Cardiolipin, MAVS, Mitofusins and mitochondrial DNA, have all been shown to act as activators of NLRP3; this, coupled with the demonstration that sphingolipids and other metabolic intermediaries can activate or downregulate the inflammasome, place the NLRP3 inflammasome at a crossroads of immunity, metabolism and cell signalling cascades, aligned with the mitochondria (Camell *et al* 2015; Gurung *et al* 2015). The recent demonstration that NLRP3 translocates to a mitochondrial proximal position upon priming is further evidence of the interactions between mitochondria and NLRP3 (Sutterwala *et al* 2018). The evidence that NLRP3 activation is heavily dependent on the metabolic state of the cell is gradually growing, highlighting a potential immunometabolic axis, the imbalance of which drives the inflammatory state. It has been demonstrated *In vitro* that elevated extracellular glucose (25 mM) induced an

upregulation of NLRP3 and IL-1β in murine podocytes, while NLRP3 or Caspase 1 deficiency ameliorated diabetic nephropathy in mouse models *(*Shahzad *et al* 2015).

1.11 –Pore forming proteins as activators of NLRP3

Whilst the focus of this thesis will be on the potential of the membrane attack complex to activate NLRP3, a range of other pore forming proteins have been demonstrated to be inflammasome activators, including nigericin, haemolysin, perforin and cholesterol dependent cytolysins (Mariathasan *et al* 2006; Chu *et al* 2009; Yao *et al* 2017; Muñoz-Planillo *et al* 2009; Yao *et al* 2017).

Nigericin has been established as a potent NLRP3, first demonstrated to induce mature IL-1β secretion in LPS primed macrophages (Mariathasan *et al* 2006). In contrast to the other pore forming toxins, Nigericin is highly selective for monovalent cations, particularly K^+, with a 45-fold higher affinity for K^+ over Na^+ and limited affinity for divalent cations other than Pb^{2+} (Prabhananda *et al* 1991; Hamidiana *et al* 2004). Therefore, the mechanism by which nigericin drives NLRP3 activation has been strongly associated with the efflux of K^+ from the cell (Katnelson *et al* 2015). Despite this, other groups have suggested that mitochondrial ROS is the predominant activator of NLRP3, as ROS scavengers dose dependently inhibit nigericin mediated NLRP3 activation and mitochondrially derived ROS was shown to drive lysosomal destabilisation, with subsequent NLRP3 activation (Heid *et al* 2013). Although as mentioned, nigericin has limited capacity as a Calcium ionophore, Calcium mobilisation from intracellular ER stores has been demonstrated in response to nigericin, with ablation of ER release through 2-ABP (IP3 receptor antagonist and TRP channel inhibitor), U7312 (Phospholipase C inhibitor) or Xestospongin C (IP3 receptor antagonist) pre-treatment statistically significantly inhibiting Caspase-1 cleavage and IL-1β release (Murakimi *et al* 2012).

The other pore forming proteins demonstrated to activate NLRP3 have less ionic specificity in comparison to nigericin, and therefore can induce primary Ca^{2+} flux across the cell membrane as well as mediating release from endoplasmic stores. Despite this, the staphylococcus derived α-haemolysin has only been demonstrated to activate NLRP3 by a K^+

dependent mechanism, although ROS scavengers or Ca^{2+} modulating agents were not tested (Muñoz-Planillo *et al* 2009; Craven *et al* 2009). Interestingly, elevated extracellular NaCl (130 mM) did not affect α-haemolysin mediated NLRP3 activation, in contrast to data in this thesis for MAC mediated NLRP3 activation (Craven *et al* 2009).

Contrastingly, cholesterol dependent cytolysins (CDLs) have had a demonstrable role for Ca^{2+} in NLRP3 activation, alongside K^+. CDLs mediated NLRP3 activation in murine BMDMs was demonstrated to be at concentrations below a lytic threshold, inhibited by the addition of free extracellular cholesterol and pharmacological inhibitors of Cathepsins, PLA_2, calcium chelators or elevated extracellular K^+ (Chu *et al* 2009). In a similar manner, perforin activation of NLRP3 was also demonstrated to be dependent on both K^+ efflux and Ca^{2+} influx in murine BMDMs, with calcium chelation, inhibition of the release of endoplasmic reticulum calcium stores and elevated extracellular KCl all statistically significantly inhibiting IL-1β secretion.

Therefore, across a range of ionophores (with the exception of haemolysin, where the role of Ca^{2+} was not fully investigated) , both K^+ efflux and Ca^{2+} have been implicated in mediating the activation of NLRP3, even in the case of Nigericin which has limited Ca^{2+} affinity. Further implicated pathways include ROS production and Cathepsin activation, with a summation of the cited literature shown in table 1. MAC mediated activation of NLRP3 will be addressed separately (section 1.18.2), however, MAC has been included in the table for completeness and to allow comparison with the other ionophores.

Ionophore name	Ionophore selectivity	Cell model(s) used	Proposed mechanism(s) of NLRP3 activation	References
Nigericin	$K^+ > Na^+ > Ca^{2+}$	primary murine dendritic cells and bone marrow derived macrophages	K^+ efflux, Ca^{2+} release from intracellular stores, ROS generation	Murakimi *et al* 2012, Katnelson *et al* 2015, Heid *et al 2013*
Haemolysin	Non-specific	THP-1 cells, primary murine bone marrow derived macrophages	K^+ efflux	Craven *et al* 2009, Munoz-Planillo *et al* 2009
Cholesterol dependent cytolysins	Non-specific	Primary murine bone marrow derived macrophages	K^+ efflux, Ca^{2+} influx, Ca^{2+} independent PLA(2), Cathepsin B	Chu *et al* 2009
Perforin	Non-specific	Primary murine bone marrow derived macrophages	K^+ efflux, Ca^{2+} release from intracellular stores (Ca^{2+} total chelation was also inhibitory)	Yao *et al* 2017
Membrane attack complex	Non-specific	A549 lung epithelial cells, Primary human and mouse bone marrow derived macrophages, Primary murine bone marrow derived dendritic cells	Ca^{2+} flux, Ca^{2+} release from intracellular stores, mitochondrial damage, K^+ efflux, ROS production	Triantafilou *et al* 2013, Laudisi *et al* 2013, Suresh *et al* 2016

Table 1: Pore forming proteins known to activate NLRP3. A range of pore forming ionophores have been demonstrated to activate NLRP3 in a range of cell types. Ionophore specificity, proposed mechanisms of NLRP3 activation and cell models used in cited papers.

1.12 - Negative regulation of NLRP3 activation

Due to the potential for aberrant NLRP3 activation to perpetuate chronic inflammation, tight regulation beyond the two-step activation process is required. A range of regulatory mechanisms govern the NLRP3 inflammasome, varying from miRNA transcriptional regulation of components to inhibition of activation of the translated proteins forming the oligomeric complex.

The regulation of the NLRP3 inflammasome by miRNA has been demonstrated by various groups with miRNAs 33, 132 and 9 amongst those implicated as negative NLRP3 regulators (Byeon *et al* 2017; Wang *et al* 2017; Xie *et al* 2018). The former two of these regulated IL-1β and IL-18 expression, whilst miRNA 9 regulated NF-κB through JAK / STAT signalling leading to inflammasome priming in an atherosclerosis model.

Inhibition of NLRP3 assembly pertains directly to the modulation of MAC-mediated activation in primed cells. 5' AMP activated protein kinase (AMPK) signalling is a negative regulator of NLRP3 activation, with AMPK acting as an indirect sensor of the cell metabolic state and becoming activated by elevated AMP:ATP ratios (Richter and Ruderman 2010). The induction of AMPK signalling can regulate NLRP3 through a variety of mechanisms, including the induction of autophagy, mediating mitochondrial plasticity and cell energy homeostasis and managing ER stress responses, all of which are implicated as NLRP3 activators (Cordero *et al* 2018). In a similar manner, cAMP signalling can be an effective inhibitor of NLRP3 activation; cAMP directly binds NLRP3 and inhibits the ATPase NACHT domain, preventing oligomerisation and activation. This is particularly relevant given the ability of MAC to mediate activation of cAMP signalling and the PKA pathway, which may provide an effective "off switch" for MAC mediated NLRP3 activation (Halperin and Weller 1993).

Finally, mechanisms of post translational modification such as ubiquitination and phosphorylation may also regulate the inactivation and dissipation of the NLRP3 inflammasome. The ubiquitinating enzyme FBXL2 mediates the downregulation of NLRP3 through Lys-689 ubiquitination; however, upon LPS stimulation FXBL2 itself becomes ubiquitinated and degraded through action of F-BOX 03, thus the inhibitory effect is removed (Jo *et al* 2017). Phosphorylation can also have inhibitory effects on inflammasome activation.

Phosphorylation of IKKα regulates NLRP3 oligomerisation through secondary ASC phosphorylation and decreased Caspase-1 recruitment. Direct phosphorylation of NLRP3 through PKA phosphorylation of Ser295 can also reduce the ATPase capacity of the NACHT. Interestingly, CAPS associated mutations in NLRP3 localise around Ser295, suggesting hyperactivation and subsequent pathology may be regulated by the region (Mortimer *et al* 2016).

1.13– Inflammasome assembly and effects of IL-1β secretion

As discussed previously, under normal cellular conditions NLRP3 folds into an auto-inhibited structure where the LRR domain interacts with the NBD and folds over the molecule, preventing nucleotide binding and activation (Ting *et al* 2008). This is corroborated by the evidence that missense Tyr859Cys mutations in the LRR domain found in atypical autoinflammatory disorder patients exhibit enhanced ASC speck formation and Caspase-1 processing, indicating an important role of the LRR in setting the activation threshold of NLRP3 (Jeru *et al* 2010). Therefore, it appears that, upon activation, NLRP3 undergoes conformational change allowing the LRR to release the protein into an active formation and replacing the NACHT-bound ADP with ATP to allow formation of the multimeric inflammasome complex.

It has been hypothesised that HSP90 and SGT1 cellular chaperones may be central to this process; indeed, the HSP90/SGT1 complex is indispensable for inflammasome activation (Mayor *et al* 2007). Furthermore, HSP90/SGT-1 associates with Ca^{2+} sensing proteins, including S100 and a diverse range of kinases and ubiquitin remodelling proteins, potentially linking some of the diverse activation stimuli of the NLRP3 inflammasome (Kadota *et al* 2010). One such kinase which has recently been highlighted as having a crucial role in NLRP3 activation is NEK7, a member of the NIMA family of kinases which regulate cell cycle progression and is a crucial regulator of NLRP3. NEK7 is fundamental for survival, with NEK7 -/- mice undergoing embryonic lethality. NEK7/NLRP3 interactions regulate inflammasome and speck assembly independent of NEK7 kinase activity (He *et al* 2016).

The binding of ATP to NACHT is the trigger required to allow the critical homotypic interactions between the pyrin domains of NLRP3 and ASC, essential for the formation of the mature inflammasome (Abderrazak *et al* 2015). The interaction between NLRP3 and ASC serves as a site of nucleation for further ASC/ASC interactions, allowing the formation of a filamentous ASC spindle which in turn allows the nucleation of Caspase-1 filaments, recruited to ASC via CARD domain homotypic interactions, shown in Figure 1.17 (Lu and Wu 2014).

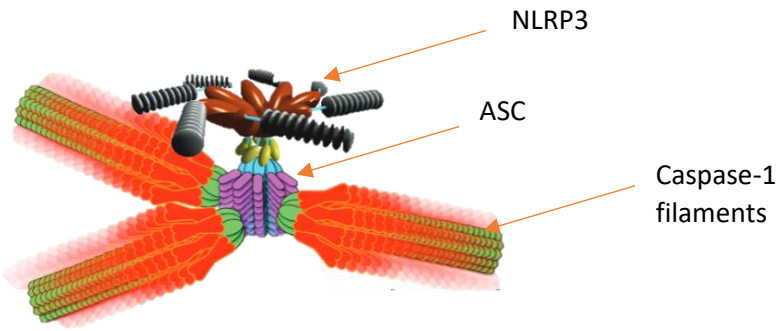

Figure 1.17. The formation of the multimeric NLRP3 inflammasome complex. Activated NLRP3 forms a point of nucleation for ASC oligomers via PYD/PYD homotypic interactions, which in turn provides nucleation for Caspase-1 fibrils through CARD/CARD interactions (Image edited from Lu et al 2014).

The formation of the Caspase-1 fibrils catalyses the conversion of pro-Caspase-1 zymogen to the active Caspase p10/p20 heterodimer through autolytic cleavage (Franchi *et al* 2009). This activated caspase then performs the final and critical step in inflammasome activation, the proteolytic cleavage of the precursors pro-IL-1β and pro-IL-18 to yield the pro-inflammatory cytokines IL-1β and IL-18, alongside a range of non-canonical substrates (Sollberger *et al* 2012). Caspase-1 activation has also been implicated in other processes such as cell membrane repair through SREBP1 activation and interactions with caveolae and regulation of cellular metabolic processes, including glycolytic enzyme cleavage and regulation of triglyceride metabolism, independently of IL-1β or IL-18 (Kotas *et al* 2013).

1.14 - Non-Canonical inflammasome activation

Whilst the mechanisms underlying canonical NLRP3 activation are still unclear, non-canonical activation mechanisms, where Caspase-11 in mice and Caspases 4 or 5 in humans are recruited to the complex in place of Caspase-1, are even more obscure. Non-canonical NLRP3 activation occurs during gram negative bacterial infection and its effects resemble canonical activation, with secretion of IL-1 family cytokines, Gasdermin cleavage and pyroptotic events (Pellegrini *et al* 2017). The realisation that non-canonical caspases may be important in NLRP3 activation was hindered by the proximity of Caspase-1 and Caspase-11 on chromosome 10 in mice; Caspase-1 knockout mice also lacked Caspase-11. The generation of Caspase-1 null mice with functional Caspase-11 suggested that Caspase-11 could not directly process the pro-cytokines but augmented the capacity of Caspase-1 to cleave pro-IL-1β in response to both canonical and non-canonical activators (Man *et al* 2017). To further complicate matters, other groups have reported that human Caspases 4 and 5 have some capacity to process IL-1β independently of Caspase-1 (Schmid-Burgk *et al* 2015).

1.15- IL-1β secretion and release of inflammasome components

The exact mechanism by which IL-1β produced by the NLRP3 inflammasome is released from the cell to act as a pro-inflammatory cytokine are still obscure; the process does not follow the canonical ER/Golgi secretion system and numerous mechanisms have been proposed. These include endosomal/lysosomal populations of IL-1β being released when autophagy is inhibited, microvesicular shedding, and release from pyroptotic cells as membrane integrity decreased (Luheshi *et al* 2012). Alongside IL-1β and IL-18 secretion, ASC and Caspase-1 may be released from the cell; in primed macrophages activated with ATP or Nigericin, ASC foci capable of activating Caspase-1 were detected outside of the cell within 20 minutes of stimulation (Baroja-Mazo *et al* 2014). Furthermore, extracellular ASC foci may propagate other roles independently of NLRP3 and Caspase-1 through the mediation of apoptosis or nucleating further ASC foci in neighbouring cells through phagocytic uptake and propagation of NLRP3 inflammasome activation (Franklin *et al* 2014; Franklin *et al* 2018). Interestingly, this behaviour of ASC as a highly oligomeric, fibril-forming molecule is reminiscent of prionoid

proteins such as β-amyloid. Indeed, it has been shown that ASC released from cells upon pyroptosis can be a target for autoantibodies in autoinflammatory disease.

1.16 - IL-1β signalling in health and disease

IL-1β induces potent pro-inflammatory effects through binding its cell surface receptor; IL-1R has high intracellular domain homology with the TLRs, generating the TIR superfamily, critical mediators of innate inflammatory responses (Dunne and O'Neill 2003). Both IL-1α and IL-1β can bind the IL-1R to induce differing signalling responses (O'Neill and Greene 1998). The IL-1R contains three extracellular IgG domains which when bound to ligand form a question mark shaped structure, enveloping and grasping the ligand in a similar manner to the interactions of the FGFR / FGF (Ve, Williams and Kobe 2015). However, unlike the binary FGFR – FGF complex, the IL-1R complex is heterotrimeric in nature, consisting of the primary receptor subunit, the ligand and a receptor accessory protein IL-1RAP which stabilises the IL-1R as well as being crucial for the recruitment of intracellular effectors such as MYD-88 for effective signal transduction (Smeets *et al* 2005).

IL-1R ligand binding triggers four identified signalling kinase cascades, NF-κB, ERK1, ERK2 and JNK (Dunne and O'Neill 2003),all of which have roles in priming of the NLRP3 inflammasome, demonstrating an element of self-propagation that might favour a chronic inflammatory state. Aside from their roles in the activation of the inflammasome, these pathways are also central regulators of a range of other pro-inflammatory pathways including inducing IL-6, TNFα, cyclo-oxygenase's and prostaglandins and matrix metalloproteases, some of the core signalling mechanisms for the inflammatory response (Tornatore *et al* 2012).

Unsurprisingly, due to this diverse range of pro-inflammatory effects, IL-1β has been demonstrated to be central to the pathogenesis of a wide range of inflammatory diseases including rheumatoid arthritis, T2 diabetes mellitus and Alzheimer's disease (Dinarello 2011; Parajuli *et al* 2013). Despite this, direct therapeutic mediation of IL-1β signalling has so far only had limited success, with the IL-1R antagonist Anakinra and the IL-1β specific mAb canakinumab both having limited effectiveness in multiple studies in a variety of conditions (Mertens and Singh 2009; Howard *et al* 2014). Direct modulation of the mechanisms

underlying IL-1β secretion may have potential as therapeutics in a range of conditions; indeed, MCC950, an orally active, specific inhibitor of both canonical and non-canonical NLRP3 inflammasome activation, attenuated disease in experimental models of multiple sclerosis and neonatal fatal cryopyrin associated periodic syndromes (Coll *et al* 2015). MCC950 inhibits NLRP3/Caspase-1 interactions; the generation of Caspase-1 P10/P20 was dose dependently inhibited while pro-Caspase-1 levels remained unchanged. No clinical trials of MCC950 are yet published, and there remains a major unmet therapeutic need for effective regulation of NLRP3 activation in a range of inflammatory conditions.

1.17- NLRP3 mediated pyroptosis

Programmed cell death is a necessity in tissue homeostasis and remodelling, however the induction of pyroptosis through NLRP3 activation, inflammasome formation and subsequent Caspase-1 cleavage differs from more controlled forms of cell death such as apoptosis (Miao *et al* 2011). Pyroptosis was discerned as a distinct form of cell death in studies investigating *Salmonella typhimurium* induced macrophage cell death; it differs from apoptosis in that inflammatory Caspases 1,4 and 5 are activated in humans as opposed to apoptotic Caspases 2,3,6,7,8, and 9. Further differences include a lack of PARP1 and ICAD cleavage and morphological and functional differences with cell swelling and pore formation observed in pyroptotic cells (Abe and Morrell 2016).

Pyroptosis is predominantly a response to infectious agents, including *Salmonella* and *Shigella* species in macrophages; however, a broadening role for pyroptosis in a variety of pathologies is emerging. Whilst the importance in disease and mechanisms of pyroptosis are still in the process of becoming understood, the biological role is to prevent the spread of bacterial infection in a two-fold manner, first by the direct disruption of the intracellular microbial niche through cell death and pyroptosis induced intracellular traps, and second by driving inflammation through the release of intracellular contents, which recruits circulating immune cells to the site of infection (Shao *et al* 2017).

The mechanism by which pyroptosis occurs has glaring similarities to the formation of MAC on the cell surface, with an intracellular pore formed by the activated Caspase-1 substrate

Gasdermin D (GSDM D). Upon Caspase-1/4/5/11 activation through the formation of the respective inflammasome, GSDM D is cleaved, removing the autoinhibitory C terminal domain (Rathkey *et al* 2017). The active 30 kDa N terminal domain then oligomerises into 16mer pores of a diameter of 12-14 nm which result in lytic cell death through chemiosmotic flux, cell swelling and eventual lysis. The parallels between Gasdermin oligomerisation and MAC formation are clear; however, the membrane localisation (intracellular v extracellular formation) and pore size (12 nm v 24 nm) differ (Kayagaki *et al* 2015). A schematic for Gasdermin D mediated pyroptosis is shown in Figure 1.18.

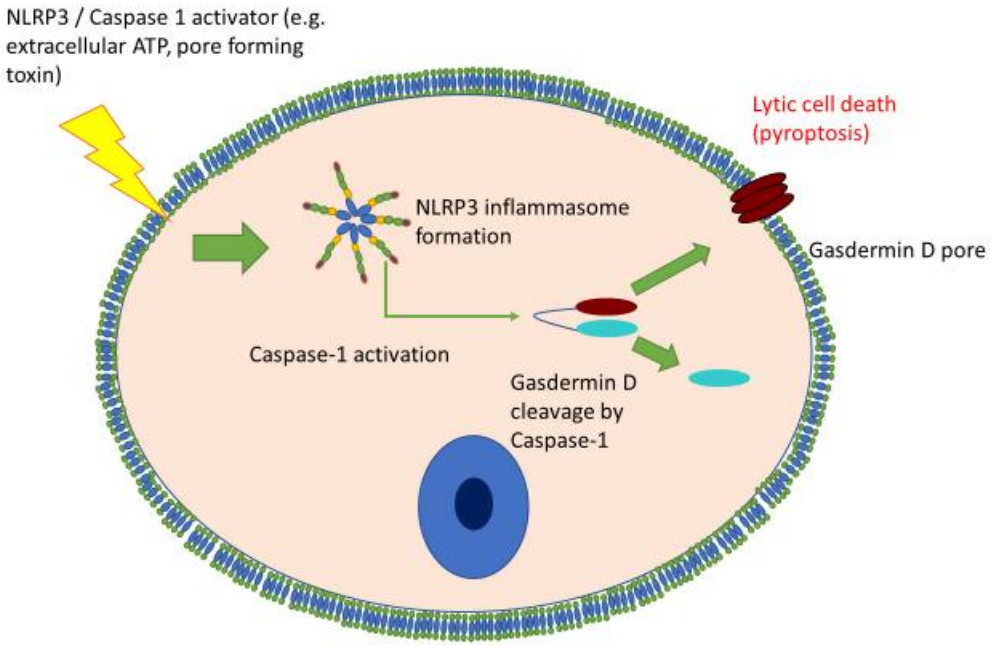

Figure 1.18. Schematic diagram of Caspase-1 mediated pyroptosis. The activation of NLRP3 through PAMP / DAMPs results in inflammasome activation and oligomerisation. This in turn allows the autocatalytic cleavage of Caspase-1 in to its active form. Activated Caspase-1 may in turn may cleave substrate proteins, including Gasdermin D. Upon cleavage, GSDM D N terminal domains may oligomerise to form large pores in the cell membrane to allow cytokine release alongside inducing the osmotic lysis which is commonplace in pyroptosis (Image based on content from Shao et al 2017).

Whilst pyroptosis is a distinctly different form of death to apoptosis, it shares many characteristics with other forms of inflammatory cell death, such as necroptosis. The induction of necroptosis is canonically through TNFαR signalling, the recruitment, dimerization and phosphorylation of RIPK1 and subsequent interaction with RIPK3. The formation of the RIPK1/RIPK3 complex allows phosphorylation and oligomerisation of MLKL, which integrates in to the cell membrane resulting in rupture and lytic cell death (Bergsbaken *et al* 2009).

The similarities between pyroptosis and necroptosis may stem from the direct and indirect interactions between the two pathways. Many of the mechanisms mediating RIPK1 activation and subsequently activated by RIPK1 are shared with established NLRP3 pathways. K63 ubiquitination is crucial for both NLRP3 and RIPK1 activation, a role for TAK1 has been established in the activation of both pathways, both pathways modulate NF-κB signalling and both undergo regulation through A20 activation (Yuan *et al* 2018).

Unsurprisingly, direct modulation of NLRP3 activation by RIPK1/3 has also been described. The formation of phospho-MLKL on the surface in response to necroptotic stimuli induced NLRP3 activation in a Caspase-1 and potassium efflux dependent manner. Furthermore, many of the inflammatory effects of necroptosis on bystander cells, notably NF-κB activation, are dependent on NLRP3 activation, suggesting a pro-inflammatory, death inducing synergism between the pathways (Conos *et al* 2017).

1.18- The role of complement in the activation of the NLRP3 inflammasome

As previously discussed, the complement pathway and NLR inflammasomes are linchpins of the innate immune system, underpinning the body's ability to induce and control inflammation in response to infection; however, either or both pathways may become dysregulated and be causative or contributing agents of disease. Unsurprisingly, a large degree of interaction and synergism has evolved between these two innate inflammatory pathways in order to mount an optimal response. Over recent years the extent of interaction between the two systems has become increasingly clear, with roles demonstrated for multiple complement components in the modulation of the inflammasome response.

1.18.1- Complement anaphylatoxins and NLRP3 activation

The anaphylatoxins C3a and C5a have long been shown to be important mediators of inflammation through signalling through their respective receptors. However, recent advances have linked the anaphylatoxins with the priming and activation of the NLRP3 inflammasome. C3a was shown to modulate the release of ATP from the cell when present alongside LPS, which in turn activated the inflammasome by the well described extracellular ATP / P2XR mechanism. This modulation was dependent on ERK1/2 signalling; however, the release mechanism of ATP from the cell remained elusive (Asgari *et al* 2013).

The role of C5a in NLRP3 priming and activation is slightly better documented, with roles being demonstrated in AMD and photo-oxidative retinal damage, cholesterol and uric acid crystal induced NLRP3 activation and sepsis (Samstad *et al* 2015). In the uric acid crystal model of gout, C5a primed the inflammasome to induce a far more robust IL-1β response independent of phagocytic crystal uptake and dependent on K^+ efflux, PLC signalling and Cathepsin B activity (An *et al* 2014). The potentiation of MSU crystal induced activation may well be attributable to the extensive interactions between C5a and TLR signalling, likely via activation of NF-κB signalling. C5a binding C5aR1 has been shown to induce NF-κB signalling in monocytes and robustly induce the expression of NF-κB mediated pro-inflammatory cytokines such as IL-8 and IL-6 (Hsu *et al* 1999). Therefore, the anaphylatoxins can deliver the central priming signal for NLRP3 activation, rendering cells sensitive to activating stimuli such as crystalline/prion structures inducing frustrated phagocytosis, extracellular ATP and pore forming toxins; the last of these can also be generated from complement activation in the form of the MAC. However, a separate study investigating the role of C5a in inflammasome priming and activation in a gout model suggested that C5a induced a strong oxidative burst through the generation of ROS, but had no direct effect on upregulation of NLRP3, ASC or Caspase-1, suggesting that C5a priming effects are mediated through ROS signalling.

1.18.2- The Membrane attack complex and NLRP3 activation

The role of the MAC in activating the inflammasome is relatively poorly understood, with only four papers directly linking sublytic MAC formation to the generation of IL-1β and NLRP3 activation (Triantafilou *et al* 2013; Laudisi *et al* 2013, Mosser *et al* 2016, Kumar *et al* 2018). The first paper from our group demonstrated that sublytic MAC deposition is capable of driving IL-1β secretion and NLRP3 activation in lung epithelial cells (Triantafilou *et al* 2013). The experiments demonstrated that the effect was C5, C6 and C9 dependent and also sensitive to heat inactivation, demonstrating that the effects were indeed MAC dependent. The mechanism by which sublytic MAC induced these effects was demonstrated through shRNA silencing to be NLRP3 and ASC dependent. The effects were also shown to be Ca^{2+} flux dependant and requiring Ca^{2+} release from intracellular stores through IP3/RYR channels; the induced ion flux resulted in mitochondrial dysfunction through Ca^{2+} uptake (Triantafilou *et al* 2013).

The conclusions of our group (Triantafilou *et al* 2013) were supported by the demonstration that non-lethal MAC induced inflammasome activation in murine bone marrow derived dendritic cells in a Ca^{2+} and K^{+} dependent manner, through pre-treatment with BAPTA-AM and elevated extracellular KCl both statistically significantly inhibiting IL-1β release (Laudisi *et al* 2013). The experimental model used by Laudisi *et al* circumvented the possible effects of using polyclonal antiserum to sensitise cells to complement and any possibility of antibody or CD59 mediated signalling events having roles in NLRP3 activation using heterologous serum (rabbit serum titrated on mouse bone marrow derived dendritic cells).

Further evidence supporting non-lethal MAC induces NLRP3 activation was demonstrated in LPS primed, murine bone marrow derived macrophages (Mosser *et al* 2016). The activation of complement by inulin, zymosan and *Leishmania major* in the presence of complete serum, but not heat inactivated or complement terminal pathway depleted serum produced robust IL-1β responses. Furthermore, the reactive lysis system of purified complement components was shown to induce IL-1β release upon the formation of complete MAC (C5b-9) but not any intermediate states. The molecular mechanisms proposed for the release of IL-1β were K^{+} efflux, including the inhibition of K^{+} gated channels, and ROS production, whereas a role for Ca^{2+} was not explored (Mosser *et al* 2016).

Finally, the significance of complement mediated NLRP3 activation was demonstrated *in vivo* in a mouse model of uveitis, where C9 -/- mice demonstrated reduced IL-1β, NLRP3 and Caspase-1 at the protein level relative to wild type, although histological retinal damage was not significantly changed (Kumar *et al* 2018). Interestingly, treatment with a lentivral expression vector generating soluble CD59 caused reduction in inflammasome activation (IL-1β and Caspase P20) but also reduced the histological damage of the disease, suggesting further anti-inflammatory roles for CD59 beyond only regulating complement terminal pathway and subsequently inflammasome activation (Kumar *et al* 2018).

Therefore, the published literature from our group and others linking sublethal MAC and NLRP3 activation is predominantly concordant, with ion fluxes, ROS production and mitochondrial dysfunction being the demonstrated mechanisms (Triantafilou *et al* 2013, Laudisi *et al* 2013, Suresh *et al* 2016). How the perturbations in Ca^{2+} / K^{+} influence NLRP3 remain unclear across the literature surrounding inflammasomes, multiple mechanisms likely exist. Furthermore, the mechanism by which complement can potentially both prime and activate the inflammasome in A549 cells is still unclear (Triantafilou *et al* 2013). A summary schematic of the proposed mechanisms of MAC induced NLRP3 activation from the current literature is shown in Figure 1.19.

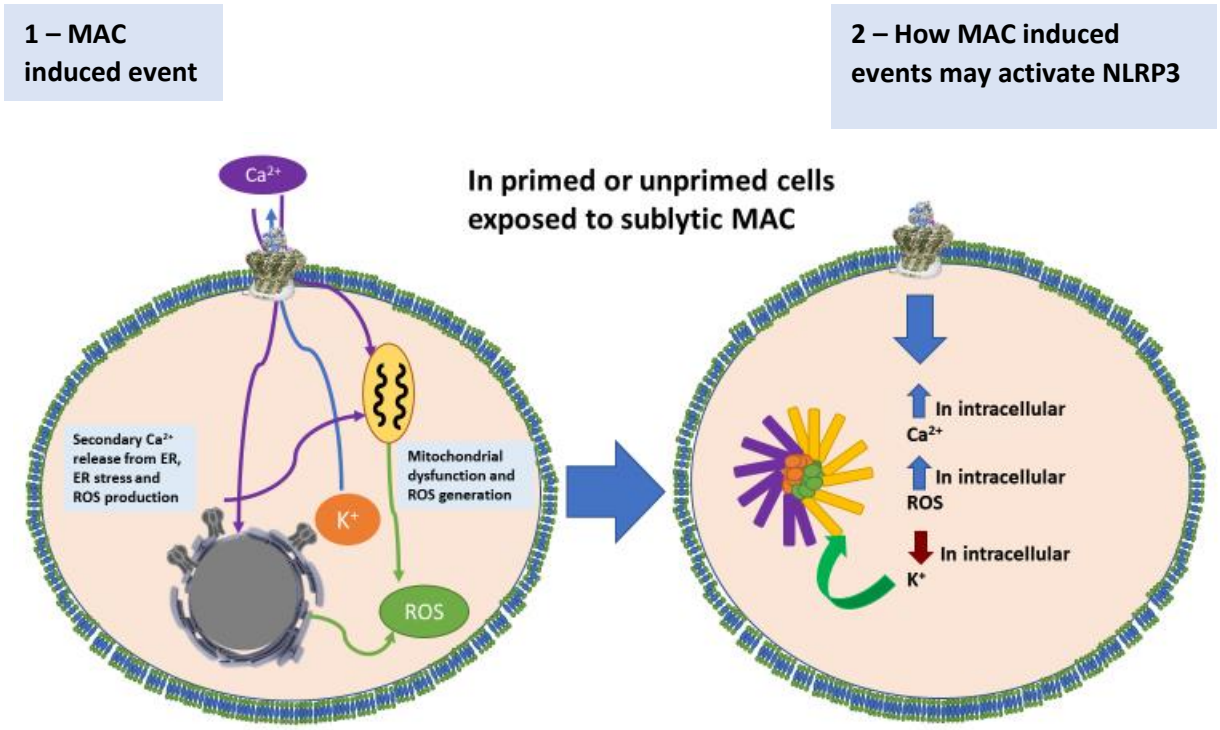

Figure 1.19. Schematic of mechanisms of sublytic MAC mediated NLRP3 activation demonstrated in the published literature. A combination of Ca2+ influx and secondary release from intracellular stores, K+ efflux and ROS mediated NLRP3 activation have all been demonstrated to have a role in activation (Triantafilou et al 2013; Laudisi et al 2013; Mosser et al 2016). MAC image sourced from Menny et al 2018.

1.19- Rheumatoid Arthritis

Rheumatoid arthritis (RA) is the most common inflammatory joint disorder, affecting around 1% of the UK adult population; however, with the aging western population these figures are expected to continue to rise (Sacks *et al* 2010; Humphreys *et al* 2012). RA is currently diagnosed and defined by the 2010 ACR scoring system which accounts for the number and sites of joints experiencing synovitis, serological abnormalities, elevation of acute phase response proteins and the duration of symptoms (Aletaha *et al* 2010). If left untreated, the disease manifests in inflammatory and debilitating changes to the joint culminating in bone and cartilage erosion, synovial hyperplasia and neovascularisation, chronic inflammation and stretching and deformity of tendons (Venables and Maini 2015).

Current treatment for RA focusses on the class of drugs known as DMARDs (Disease Modifying Anti-Rheumatic Drugs) – which have been the mainstay of RA treatment since the 1970's (Kahlenberg and Fox 2011). The most commonly administered DMARD is methotrexate (MTX) which can be taken orally or subcutaneously at a relatively low dose (10-25 mg / week) and is generally well tolerated with limited side effects, although GI, bone marrow and liver toxicity can occur in rare cases. The effectiveness of MTX is substantial in a subset of RA patients, with one third of patients demonstrating no radiographical progression after a year of MTX treatment, which can be further enhanced when combined with targeted biological therapies (Weinblatt 2013). Despite MTX being frequently prescribed, the exact anti-inflammatory mechanism it exerts is unclear. Originally, it was believed the antagonism of folate biosynthesis induced by MTX would inhibit the proliferation of the pro-inflammatory cells mediating RA; however, further theories including inhibition of toxic spermine synthesis, depletion of intracellular glutathione and increase of extracellular adenosine have all been proposed (Cronstein 2005).

The localised changes in the morphology and inflammatory state of the joint are preceded by serological changes such as anti-citrullinated protein antibody (ACPA) and rheumatoid factor (RF) immune complexes, indicating that the scope of the disease exceeds the affected joints (Shi *et al* 2014). The evidence for RA to be considered a systemic inflammatory condition rather than a localised joint pathology is strong, with extra-articular manifestations such as cardiovascular, haematological and renal co-morbidities more frequent in aggressive RA (predominantly RF/HLA-DR4 positive patients) (Cojocaru *et al* 2010).

The aetiology of RA is still unclear; although a range of genetic and environmental factors have all been associated with the induction of RA, no defining mechanism has yet been proposed. The most strongly associated genetic factor for RA is within the human leukocyte antigen (HLA) cluster, involved in antigen presentation to T cells. The highly polymorphic N terminal HLA region was found to be most associated with RA, with mutations in residues 70-74 being dubbed the susceptibility epitope (SE) and enabling the presentation of self-derived peptides as auto-antigens, including citrullinated cartilage and synovial components (Scally *et al* 2013). However, HLA mutations alone are not sufficient to induce the disease phenotype (not all individuals with the SE go on to develop RA) – highlighting further factors including smoking, obesity and chronic systemic inflammation (Crowson *et al* 2013).

The “normal”, healthy synovium functions to encapsulate and protect the joint, as well as providing lubrication in the form of synovial fluid and supplying nutrients to the cartilage. It is a loose array of cells embedded in extracellular matrix (ECM) with roughly equal proportions of fibroblast like synoviocytes (FLS) and macrophage like synoviocytes (Bartok and Firestein 2009). Under non-pathological conditions, FLS line the joint in a layer 1-2 cells deep, are relatively inactive in terms of secreted enzymes and cytokines and have a relatively low turnover rate due to a propensity to resist apoptosis (Firestein 2003).

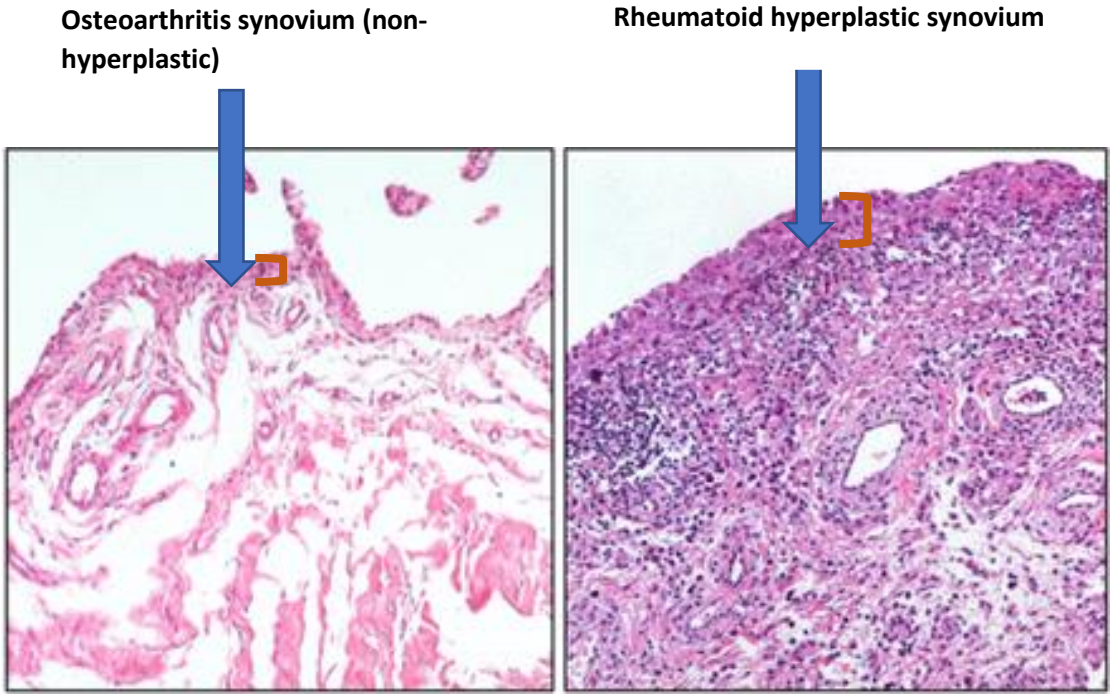

Figure 1.20. Electron micrograph demonstrating intimal synovial lining hyperplasia in RA – the FLS become activated and display an aggressive, invasive and hyperplastic phenotype relative to an OA joint (Image edited from Firestein 2003).

This ordered architecture becomes highly hyperplastic and disordered in the inflammatory RA phenotype, with massive increases of FLS in the intimal layer, up to 20 cells thick, as well as invasion into the local cartilage resulting in joint destruction. Alongside this, osteoclasts become activated and differentiated through the pro-inflammatory cytokine environment through the actions of RANKL, IL-17, TNFα and IL-1β resulting in localised bone erosion and resorption, further compromising joint integrity (Schett 2007). Furthermore, once the inflammatory state is established in the joint chemotactic signalling induces immune cell

infiltration, including B and T cells, mast cells and macrophages, which exacerbate the condition through recognition of autoantigens and inflammatory cytokine secretion (Kinne 2000; Mellado et al 2015).

The initial event mediating this transition from the healthy synovium to that seen in RA is unclear, however it appears to precede adaptive immune cell infiltration into the joint and therefore may well be mediated by the innate immune system interacting with the resident synovial cells (Burmester *et al* 2014).

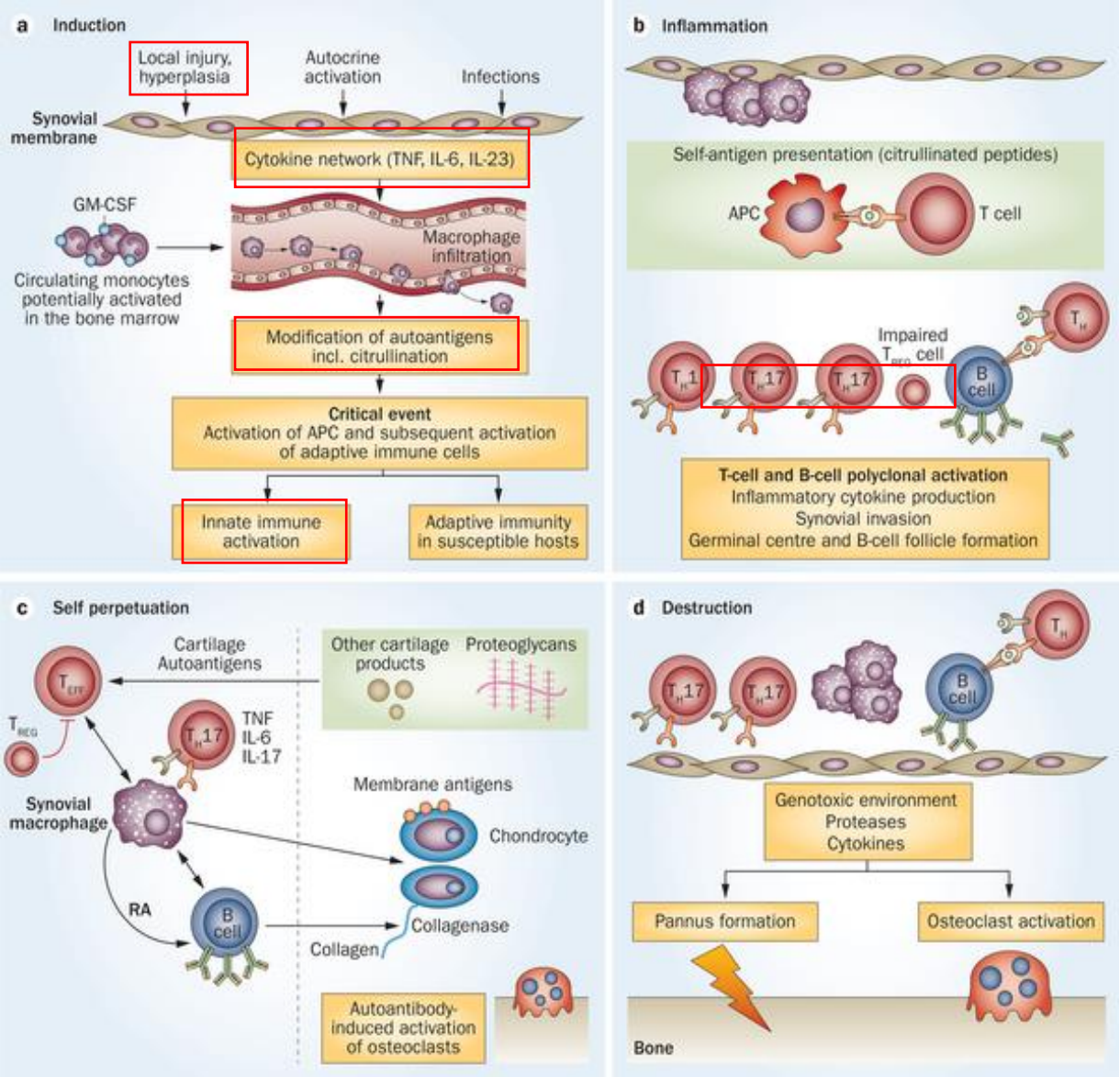

Figure 1.21. A potential chronology for the series of events underlying RA, with the innate immune system and the local synovial cells being central to the initiating events of the condition. Highlighted boxes denote stages in RA pathology in which NLRP3 or complement have been implicated (Image edited from Burmester et al 2014).

As previously mentioned, complement activation is one of the fundamental branches of the innate immune system, a potent mediator of inflammation; it is therefore, unsurprisingly, implicated in the pathogenesis of RA. Reports of a role of complement in RA date back to the 1980's, when it was found that most RA patients had elevated complement activation markers C3dg and sC5b9 in the synovial fluid, and around a third had elevated levels in the serum (Mollnes *et al* 1986). Since then, a plethora of studies have found links between complement activation and RA, including the realisation that complement components are locally synthesised within the joint, predominantly by macrophage like synoviocytes, and that complement gene expression is upregulated in RA compared to healthy and OA synovium (Firestein *et al* 1991; Neumann *et al* 2001). The concept that complement is not merely upregulated but has a central role in the pathogenesis of RA is supported by studies in mouse collagen induced arthritis (CAIA) models where histopathology scores were reduced by 52%, 94% and 65% respectively for C3aR, C5aR and C6 knockout mice (Banda *et al* 2012; Mehta *et al* 2015). These data collectively show that, in mouse models at least, both the chemotactic anaphylatoxins (C5a and C3a) and the membrane attack complex (inhibited in C6 deficiency) have substantial roles in arthritis.

As previously discussed, the complement system is capable of interacting with and activating other innate immune inflammatory pathways, including the NLRs. The NLRs and their predominant activation products IL-1β and IL-18 have also been shown to have a central role in RA, although attempts at therapeutic modulation of these pathways has so far only had modest efficacy. The observation that IL-1β levels were elevated and correlated with some disease parameters in RA dates back to the early 1990's; synovial fluid IL-1β concentration was found to be 10-fold higher in RA relative to OA and correlated to morphological patterns in the joint (Kahle *et al* 1992). Upregulation in IL-1β is not concomitantly matched with increases in its receptor antagonist IL-1Ra, leading to dysregulation of IL-1β signalling. However, when therapeutic intervention in IL-1β signalling was attempted using the IL-1β receptor antagonist Anakinra only modest clinical improvements in ACR20 were achieved (15% greater than placebo controls), considerably less effective than biologics targeting other systems such as TNFα (Mertens and Singh 2009). This lack of efficacy of Anakinra may be

because IL-1β can exert cellular effects through binding a relatively small number of IL-1R on a cell, making adequate dosing of a competitive IL-1β receptor blocker difficult (Kay and Calabrese 2004). Recent advances in the understanding of IL-1β secretion and maturation has led to the development of the previously mentioned MCC950, a specific inhibitor of the NLRP3 inflammasome, which could potentially be a far more efficacious method of therapeutic intervention, alone or potentially coupled with receptor antagonism.

The potential of IL-1β and NLRP3 to induce RA was recently demonstrated in a mouse model where TNFAIP3 (Also known as A20), which has multiple SNPs linked to RA, was demonstrated to be a negative regulator of NLRP3 and IL-1β in mice, with A20 -/- mice exhibiting polyarthritis resembling RA. These symptoms were not rescued by deletion of the TNFαR but were rescued by IL-1βR / NLRP3 / Caspase-1 knockout, indicating that the effects observed were induced by the NLRP3 / IL-1β signalling axis (Vande Walle *et al* 2014). This is also reinforced by human genetic studies associating NLRP3 polymorphisms such as rs35829419 C>A with an increased risk of RA (Wang *et al* 2015).

Therefore, understanding the interplay between the complement and NLR systems may be crucial to understand the mechanisms involved in the early pro-inflammatory and chemotactic events underlying the induction of RA.

1.20– Project aims and objectives

In the body of research described in this thesis I intend to dissect the molecular mechanisms underpinning the observations that sublytic MAC can activate NLRP3 and highlight the individual proteins and pathways which transduce these signals from the MAC to the intracellular inflammasome complex. This will be performed in both primary cells and cell line models. The overarching aim is to highlight signal transduction pathways linking sublytic MAC deposition and NLRP3 activation, the amelioration of which may offset MAC induced inflammation in disease. Furthermore, it has become apparent that NLRP3 and complement have further interactions, through both susceptibility to MAC mediated death and regulator expression in synovial cell lines. These new areas of interaction remain largely unexplored and will begin to be demonstrated and discussed in this body of work.

The hypothesis underpinning this work is that there are conserved signalling mechanisms linking MAC deposition and NLRP3 activation, and that further, currently undefined, links between the two systems exist.

Therefore, the key aims of this body of work are to:

1) Demonstrate sublytic MAC generation and determine the effects of sublytic MAC on NLRP3 activation and IL-1β secretion;
2) Address the broad molecular mechanisms by which sublytic MAC activates NLRP3;
3) Investigate how these triggers may induce NLRP3 activation through intracellular signalling cascades and modulate MAC mediated inflammasome activation;
4) Investigate the broader interactions of NLRP3 and MAC, particularly in complement regulator expression and MAC mediated cell death.

2 – Materials and Methods

2.1 -Lists of consumables, antibodies and cell signalling inhibitors and buffer recipes:

Table of buffer recipes:

Buffer name	Chemical composition
1x PBS	0.137 M NaCl, 2.7 mM KCl, 10 mM Na_2HPO_4, 1.8 mM KH_2PO_4, pH 7.4
Western blot running buffer (1x)	25 mM TRIS, 191 mM Glycine, 1% (w/v) SDS, pH 8.3
Western blot transfer buffer (1x)	25 mM TRIS, 191 mM Glycine, 20% v/v Methanol, pH 8.3
Reducing SDS PAGE buffer	125 mM TRIS, 20% v/v Glycerol, 4% w/v SDS, 0.05% w/ Bromophenol blue, 5% v/v β-Mercaptoethanol, pH 6.8
CFD buffer (Oxoid)	1 tablet per 100 ml of distilled water - 0.575 g/l Barbitone, 8.5 g/l NaCl, 0.168 g/l $MgCl_2$, 0.028 g/l $CaCl_2$, 0.185 g/l soluble Barbitone, pH 7.4
Alternative pathway buffer	CFD buffer + 10 mM EGTA, pH 7.4
TAE buffer (50x)	242 g TRIS, 18.61 g EDTA, 57.1 ml Glacial Acetic acid in 1 L ddH2O, pH 8.5
PBS-T	1x PBS , 0.05 – 0.1 % v/v TWEEN 20, pH 7.4
FACS buffer	1x PBS, 1& w/v BSA, pH 7.4, 0.22 µM filtered
ELISA reagent diluent	1x PBS, 1% BSA, pH 7.4, 0.22 µM filtered
HiTRAP Buffer B	0.1 M Sodium acetate ($C_2H_3NaO_2$), 0.5 M NaCl, pH 4
AKTA affinity elution buffer	0.1 M Glycine, 10 mM TRIS, pH 3, 0.22 µm filtered
AKTA affinity running buffer	10 mM TRIS, 150 mM NaCl, pH 7.4, 0.22 µm filtered
HiTRAP Buffer A	0.5 M ethanolamine, 0.5 M NaCl, pH 8.3
HiTRAP ligand binding buffer	0.2 M NaHCO3, 0.5 M NaCl, pH 8.3, 0.22 µm filtered
Western blot stripping buffer	200 mM Glycine, 1% w/v SDS, 1% v/v TWEEN, pH 2.2
3 A cell media supplement	1 mM Sodium pyruvate, 2 mM L-Glutamine, 50 µM Penicillin Streptomycin

Table 2: Commonly used buffer recipes for experiments performed within the thesis

Kit / Reagent	Source	Product number
Human IL-1β ELISA Duoset	R&D systems	DY401
LDH cell viability assay kit	Thermofisher	88954
ROS / RNS assay kit	Abcam	ab139476
Fluo-3-AM Calcium sensitive dye	Molecular Probes	F-21395
Propidium Iodide	Sigma Aldrich	P-4170
Western blot film	GE Healthcare	28906838
Western blot ECL reagent	Thermofisher	32106
RIPA lysis buffer	Thermofisher	8990
Protease Inhibitor tablets	Roche	4693159001
Pre-cast 4-20% gradient SDS PAGE gels	BioRad	4568094
Pageruler Plus pre-stained protein ladder	Thermofisher	26619
RPMI cell media	Gibco	11530586
Foetal Calf Serum (FCS)	Thermofisher	10500056
Complement Fixation Diluent (CFD)	Oxoid	BR0016
HiTRAP NHS activated affinity columns	GE Healthcare	17071601
Lipopolysaccharide (LPS)	Sigma Aldrich	L3024-5MG
Complement C5a	Comptech	A144
Complement Factor B	Comptech	A135
Complement Factor D	Comptech	A136
Cobra Venom Factor	Sigma Aldrich	233552-M
Triton X 100	Sigma Aldrich	T8787-50ML
Guinea Pig red blood cells in Alsever's solution	TCS Biosciences	PB029AP
Sheep red blood cells in Alsever's solution	TCS Biosciences	SB0629
Lipofectamine 2000	Thermofisher	11668027
NLRP3 gRNA	Thermofisher	A35509
Cas9 mRNA	Thermofisher	A29378
Dimethyl Sulphoxide (DMSO)	Sigma Aldrich	D2650-100ML
Mass ruler mixed range DNA ladder	Thermofisher	SM0403
One step RT PCR reagent set	Invitrogen	12574018
Mammalian Cell miniprep Kit	Sigma Aldrich	RTN70-1KT
pCW-CAS9 Expression Vector	Addgene	50661
Puromycin	Invivogen	ant-pr-1
Doxycycline Hyclate	Sigma Aldrich	D9891-1G
Bovine Serum Albumin (BSA)	Sigma Aldrich	A7906
Skimmed Milk Powder	Sigma Aldrich	70166-500G
Micro BCA assay Kit	Thermofisher	23235
TMRE mitochondrial stress kit	Abcam	ab113852
Caspase-glo 1 activity assay	Promega	G9951
Propidium Iodide	Sigma Aldrich	P4170-10MG

Table 3: List of consumable, kits and reagents used within the thesis.

Compound name	Target	Carrier Solvent	Stock concentration	Working concentration	Supplier	Catalogue number
MCC950	NLRP3	DMSO	20 mM	10 µM	Invivogen	inh-mcc
Ac-YVAD-CMK	Caspase 1	DMSO	10 mM	55 µM	Invivogen	inh-yvad
Z-VAD-FMK	Pan Caspase	DMSO	20 mM	20 µM	Invivogen	tlrl-vad
LY294002	PI3K	DMSO	2 mM	100 µM	Invivogen	tlrl-ly29
Perifosine	AKT	DMSO	10 mM	50 µM	Invivogen	tlrl-peri
Necrostatin 1	RIPK1	DMSO	5 mM	50 µM	Sigma Aldrich	N9307
C16	PKR	DMSO	10 mM	50 µM	Sigma Aldrich	I9785
H18	PKA	DMSO	5 mM	50 µM	Tocris	2910
BAPTA-AM	Intracellular Calcium	DMSO	2 mM	100 µM	Tocris	2787
Xestospongin C	IP3R Calcium channels	DMSO	2 mM	10 µM	Tocris	1280
AG490	JAK2	DMSO	10 mM	50 µM	Invivogen	tlrl-ag4
Geldanamycin	HSP90	DMSO	1 mM	10 µM	Invivogen	ant-gl-5
Everolimus	mTORC1	DMSO	18 µM	300 nM	Invivogen	tlrl-eve
PD98059	ERK 1/2	DMSO		50 µM	Invivogen	tlrl-pd98
NAC	Intracellular ROS	H_2O	200 mM	5 mM	Sigma Aldrich	A7250
SP600125	JNK	DMSO	10 mM	50 µM	Invivogen	tlrl-sp60
AKT 1/2	AKT	DMSO	20 mM	10 µM	Sigma Aldrich	A6730
LB100	PP2A	DMSO	5 mM	5µM	Selleck chem	S7537

Table 4: List of cell signalling inhibitors used in experiments. All DMSO reconstituted inhibitors were made under sterile conditions using tissue culture grade DMSO. All stock solutions of inhibitors were aliquoted and stored at -20°C prior to use. When stated in experiments, vehicle controls were used with the highest concentration of DMSO solvent to be used as a solvent for any compounds in that assay (between 1:100 and 1:1000 dilution v/v)

Antibody target	Supplier	Host species	Catalogue number
COS-1 antiserum (polyclonal antiserum against COS-1 kidney cell line derived from Cercopithecus aethiops)	In house	Rabbit	N/A
Anti-Human C3b FITC	Biolegend	Mouse	846108
BRIC 229 anti-CD59	Bristol Regional Immunohematology Centre	Mouse	N/A
BRIC 225 anti-CD55	Bristol Regional Immunohematology Centre	Mouse	N/A
Anti-FLAG epitope antibody	Thermofisher	Mouse	MA1-91878
Eculizumab - anti-C5 antibody	Alexion	Humanised mouse	N/A
SKY 59 anti-C5 antibody	Roche (see publication Fukazawa *et al* 2017)	Humanised Rabbit	N/A
Anti-C6 (27D1)	In house	Mouse	N/A
Anti-C7 (23D10)	In house	Mouse	N/A
Anti-C8 (J1)	In house	Mouse	N/A
Anti-C9 (B7)	In house	Mouse	N/A
Anti-Caspase-1 P10	Santa-Cruz biotech	Mouse	SC-56036
Anti NLRP3	CST	Rabbit	13158S
Anti IL-1β	CST	Mouse	12242S
Anti β actin HRP conjugate	Thermofisher	Mouse	MA5-15739-HRP
MEM43 anti-CD59	Grown in house (Originally from Vaclav Horejsi, Prague, Czech Republic)	Mouse	N/A
Cholera toxin B subunit Alexa 488 conjugate	Thermofisher	N/A	C34775
Anti Mouse Alexa 488	Thermofisher	Goat	A-11001
Anti Mouse Alexa 546	Thermofisher	Goat	A-11030
Anti-Mouse HRP	Jackson Labs	Goat	115-035-003
Anti-Rabbit HRP	Jackson Labs	Goat	111-035-144

Table 5: Table of primary and secondary antibodies used in the thesis.

2.2 - Cell culture techniques and conditions – THP-1 cell line

THP-1 cells were a kind gift from Prof Phil Taylor (Cardiff). THP-1 cells are a spontaneously immortalised monocyte cell line derived from a childhood M5 leukaemia patient and represent a well-established *In Vitro* model for monocytic cells (Bosshart and Heinzelmann 2016). Cells were cultured in upright, sterile T175 flasks in complete medium (RPMI medium + 10% v/v FCS and 3A supplement), with medium being replaced or cells passaged every 2-3 days. Cells were maintained at densities no greater than $1x10^6$ cells ml^{-1} in culture in a sterile incubator at 37˚C in 5% CO_2. To passage, cells were centrifuged at 300 x g for 5 minutes and the media aspirated, cells resuspended in complete medium and split into fresh T175 flasks in a 1:4 ratio. To freeze cells down for storage, the centrifuged cell pellet was resuspended in cryotubes in freezing medium (10% v/v DMSO, 90% FCS v/v), placed in a cell freezing container containing methanol, and transferred to -80˚C freezer overnight prior to long term storage in liquid nitrogen.

2.3 - Cell culture techniques and conditions – SW 982 cell line

SW 982 synovial cells were received as a kind gift from Prof Kathy Triantafilou (Cardiff). The SW 982 line is derived from synovial sarcoma cells and has been validated as a model for RA studies (Chang *et al* 2014). Cells were cultured in complete medium (RPMI medium + 10% FCS and 3A supplement). Cells were passaged every 2-3 days upon reaching 80-90% confluency. To passage these adherent cells, media was aspirated, cell monolayers were washed with 5 ml of sterile PBS and 3 ml of Trypsin-EDTA added for 5 minutes at 37˚C. The flasks were agitated and visually checked for cell de-adherence using a light microscope. Trypsin was then neutralised using 12 ml of media +10% FCS to prevent cell damage, cells centrifuged at 300 x g for 5 minutes and the supernatant aspirated. Cells were split in a 1:2 ratio to facilitate cell to cell contact, which helps maintain cell phenotype and growth. To freeze cells for long term storage, cells were harvested as above, and the same cryopreservation protocol was used as for THP-1 cells.

2.4 – Cell culture techniques and conditions – Thawing of frozen cell stocks

To bring up cells from frozen cell stocks, aliquots from liquid nitrogen were rapidly defrosted at 37˚C in a water bath. Defrosted cells were immediately centrifuged at 300 x g for 5 minutes to remove the freezing media and minimise DMSO cytotoxicity. The freezing media was aspirated, and cells resuspended in 5 ml of appropriate media. Resuspended cells were then seeded into flasks as with normal tissue culture protocols.

2.5 - Isolation of primary monocytes and differentiation to macrophages

Primary monocytes were enriched from 20 ml of concentrated donor blood cells from the GSK BDU based on CD14 expression. Ficoll (15 ml) was added to two Accuspin 50 ml tubes and centrifuged for 5 minutes at 300 x g at room temperature to allow the Ficoll to flow through the membrane. The cone tubing was then cut, and the blood collected into a 50 ml Falcon tube, with the cone subsequently being flushed using 10 ml of PBS to ensure maximal recovery. The volume of collected blood (circa 20 ml) was made up to 40 ml in sterile PBS and inverted to mix, then gently layered on top of the Ficoll in the Accuspin tubes and centrifuged at 400 x g for 20 minutes at room temperature without a deceleration brake.

The PBMC layer at the interface of the plasma and Ficoll was then removed using a sterile Pasteur pipette and transferred to a fresh Falcon tube before being made up to 50 ml using sterile PBS. Cells were then centrifuged at 300 x g for 10 minutes, the supernatant discarded, and pellets resuspended in a final volume of 50 ml of sterile PBS. After a second centrifugation step at 300 x g for 10 minutes, supernatant was discarded, and the cells resuspended in 1 ml of ice-cold MACS buffer (5 mM EDTA, 0.05% BSA in PBS without Ca^{2+} and Mg^{2+}). Anti CD14 magnetic beads (100 µl) were then added to the cell suspension and incubated for 15 minutes at 4˚C. Miltenyi columns were prewashed with MACS buffer and placed on the magnetic stand before the cell suspension was loaded; cells bound to CD14 beads were trapped in the columns by the magnetic field. The columns were removed from the magnetic stands, cells

eluted by washing with 3 x 5 ml of Miltenyi buffer and collected in fresh Falcon tubes. The cell suspensions were then centrifuged at 300 x g for 5 minutes with a deceleration brake, the supernatant aspirated and the cells resuspended in 10 ml of RPMI media + 5% v/v FCS. Cell number and viability was determined using the Vicell cell counter, with around $1x10^8$ cells recovered. Viability was recorded at 99% by Trypan blue exclusion. Cells were then diluted to $1x10^6$ cells ml^{-1} in cell media with 100 ng/ml M-CSF and 1x pen/strep to induce cell differentiation into macrophages and plated in to 24 well plates for 5 days to mature.

2.5 – Purification of complement terminal pathway components

Donor plasma was received from the Wales Blood Bank in expired platelet bags. Plasma was rendered acellular by centrifugation at 3000 x g for 15 minutes and the plasma aspirated from the pellet. The plasma was 0.22 µm filtered before loading on to the AKTA FPLC. All complement components were purified using affinity chromatography on columns generated through the coupling of in-house anti complement terminal pathway antibodies to HiTRAP NHS activated columns. Between 50 and 100 ml of donor plasma was loaded on to the column per purification run, with run through plasma being collected and run over the column again to maximise purification yields.

HiTrap affinity columns were activated using ice cold 1 mM HCl before washing with coupling buffer. Monoclonal antibodies against terminal pathway components in coupling buffer were then added to the column and incubated for 4 hours at 4˚C. After washing and blocking of the column using alternate perfusions of HiTRAP Buffer A and Buffer B, the column was stored in 10 mM TRIS, 0.02% NaN_3 until use. Coupling efficiency was determined through measurement of 280 nm absorbance of antibody solution prior to and post coupling and was generally around 90%. For protein purifications, the AKTA FPLC was equilibrated in 10 mM TRIS, 150 mM NaCl pH 7.4. The affinity column was then inserted into the system and five column volumes (CVs) of 10 mM TRIS, 150 mM NaCl pH 7.4 buffer were applied at a low flow rate of 0.5 ml $minute^{-1}$ to equilibrate the column matrix. Filtered (0.22 µm) pooled human plasma was loaded on to the column, followed by 5 CV's of running buffer to remove any non-specifically bound protein. Bound protein was then eluted using 0.1 M Glycine, 10 mM TRIS

pH 3 and collected in 1 ml fractions. These were immediately neutralised with the addition of 100 µl of 1M TRIS pH 10. The protein-containing eluted fractions were identified by absorbance or protein assay, then pooled and dialysed overnight at 4˚C in to CFD buffer. The dialysed protein was then tested for protein content using absorbance at 280 nm on a Nanodrop or Pierce protein assay, purity and identity by SDS PAGE, Western blotting and ELISA based methods, and function using haemolytic assays. Functional, pure protein was stored at -80°C in aliquots to prevent excessive freeze thaw cycles at a concentration of greater than 1 mg/ml in CFD buffer.

The affinity column was then re-equilibrated by washing in five CV's of running buffer before storage in 10 mM TRIS, 0.02% NaN_3 , pH 7.4 at 4˚C. The AKTA system was then washed into water and finally 20% v/v ethanol solution for storage. Due to the viscosity of plasma, the system required frequent cleaning using water and 0.5 M sodium hydroxide to prevent residue build up, as well as online filter replacement after every few runs.

2.6 - Purification of Cobra Venom Factor (CVF)

CVF is a 144 kDa protease with C3 and C5 convertase activity found in Cobra venom. Whole cobra venom was previously purchased from Sigma and stored at -80˚C until use. The lyophilised venom was reconstituted in 10 mM TRIS buffer pH 7.4 with 10 mM EDTA to prevent any degradation by Ca^{2+}-dependent venom proteases. The reconstituted venom was centrifuged at 10,000 x g in a 100 kDa cut off Vivaspin 500 spin column; removing all proteins below 100 kDa, whilst concentrating those heavier than 100 kDa. The concentrated protein was then reconstituted to 1 ml using 10 mM TRIS buffer without EDTA. The cobra venom was then loaded onto a MONOQ ion exchange column on the AKTA purification system via the sample injection loop and flushed through with TRIS running buffer. A linear elution gradient of 0-100% 0.5 M NaCl over 20 CV's was used to elute the proteins dependent on charge.

Eluted, protein-containing fractions were then collected and kept separate for assaying CVF functionality by haemolytic assays. A NHS – CVF control was used to ensure no spontaneous haemolysis of GPE's by NHS, but phospholipases were not removed, which may explain the haemolytic properties of the void volume elution peak in later experiments (Figures 3.6 and

3.7) (Vogel and Müller-Eberhard 1984). Functionally positive fractions were subsequently pooled and dialysed into CFD overnight at 4˚C before SDS PAGE and Coomassie staining to verify protein identity. CVF containing fractions were then pooled and protein concentration measured using the micro BCA system.

The AKTA system was subsequently returned in to water and ethanol and the MONOQ column stored in 20% ethanol until further use.

2.7 - Micro BCA assay for protein quantification

To accurately determine complement protein or CVF concentrations, the Pierce Micro BCA kit from Thermofisher was used. BSA standards were generated in PBS from 200 to 0.5 µg/ml. Then the amount of working reagent required for the assay was calculated (150 µl of working reagent / well in a 96 well plate format). The working reagent was then generated using a 25:24:1 ration of kit reagents A, B and C respectively. The samples of unknown concentration were diluted 1:10, 1:50 and 1:100 in PBS in triplicate to ensure distribution within the working range of the assay. Diluted samples and standards were added to the Nunclon 96 well, clear, flat bottomed plate at 150 µl / well. The working reagent was then added at 150 µl / well and mixed vigorously on a plate shaker for 30 seconds before sealing the plate and incubating at 37˚C for 2 hours. The plate was cooled to room temperature for 10 minutes before reading the absorbance at 562 nm in a plate reader. The blank absorbance values were subtracted from the other wells before fitting a polynomial standard curve to the standard samples and interpolating the unknown samples to the curve.

2.8 - Generation of C5b6 complexes

To have a functional reactive lysis system for stimulations purified C5b6 complex was required as an initiator for subsequent C7, C8 and C9 binding to generate fully formed MAC. The purification of C5b6 was performed through firstly purifying C5, C6 and CVF as previously described to provide the raw materials for the reaction, alongside commercial FB and FD (Comptech). The protocol used was derived from a published paper and scaled down to the protein quantities available (DiScipio *et al* 1983). CVF (100 µg), Factor B (10 µg/ml) and Factor D (1 µg/ml) were mixed in CFD buffer and incubated for 1 hour at 37˚C in a water bath to allow the formation of CVFBb complexes, an alternative pathway C5 convertase analogue. The newly generated CVFBb complexes were added to 1 mg of C5 and C6 in CFD buffer and incubated overnight at 37˚C to allow cleavage of C5 and subsequent C5b C6 binding. The overnight reaction mixture was then dialysed into 10 mM Tris buffer for 4 hours to allow purification of C5b6 by ion exchange chromatography. The CVFBb generated C5b6 reaction mixture was concentrated to 200 µl volume using a 100 kDa cut off Vivapsin concentrator. This was then loaded via the sample loop on to the Mono Q anion exchange column and eluted with a linear gradient of 10 mM to 1M NaCl. The eluted C5b6 fractions were assayed for haemolytic activity and checked for purity by SDS PAGE. Pure, functional C5b6 was then aliquoted and stored at -80 ˚C until use

2.9 - Coomassie staining of protein preparations

To verify protein purity and molecular weight SDS PAGE and Coomassie staining was used. Precast 4-20% BIS-acrylamide gradient gels, or hand-cast 10% acrylamide gels with a 4% stacking gel were used for electrophoresis. Samples were diluted to load 2 µg of protein per lane under reducing or non-reducing loading buffers. All diluted samples were heated to induce protein denaturation at 90˚C for 10 minutes in a heat block. To determine molecular weights of protein bands, the Pageruler plus pre-stained molecular weight marker (Thermofisher) was used, with 7.5 µl of pre-stained ladder loaded in lane one per gel. SDS PAGE was subsequently performed at 120 V for one hour or until the Coomassie dye front

reached the bottom of the gel. Gels were then stained using Coomassie dye solution (50% methanol, 50% H_2O v/v, 0.02% Coomassie powder w/v) for a minimum of 1 hour at room temperature with gentle agitation. The gels were then removed from the staining trays and added to the de-stain solution (50% H_2O, 40% Methanol, 10% glacial acetic acid v/v), changing the wash every 15 minutes until the background gel stain was removed. The gels were then imaged using the Thermofisher MyECL imaging system.

2.10 – Haemolytic assays

2.10.1 Reactive lysis Haemolytic assay

To determine the functional activity of purified complement terminal pathway components and Cobra venom factor, haemolytic assays were used. Guinea pig erythrocytes in Alsever's solution were inverted to ensure even distribution of cells before 1 ml was taken from the stock and added to 20 ml of APB. The cell suspension was subsequently centrifuged at 300 x g for 5 minutes to pellet erythrocytes. The APB supernatant was aspirated, and the erythrocyte pellet resuspended in 20 ml of APB, and the process repeated until the supernatant was clear and colourless indicating no background haemolysis. An aliquot (400 µl) of the set erythrocyte pellet was then aspirated and added to 20 ml of pre-warmed (37°C) APB to generate a 2% erythrocyte suspension. To perform the assay, 50 µl of 2% erythrocyte suspension was added per well in a 96 well, U bottomed plate. 50 µl of APB was then added to each well. Purified terminal pathway components diluted in CFD buffer were then sequentially added and the reaction volume made up to 150 µl with APB. In all assays, C5b6 or C56 was first added at the concentration stated (titrated up to 0.5 µg/ml for C5b6 and 10 µg/ml for C56) and incubated for 10 minutes at room temperature; C7 was subsequently added in at least two times molar excess compared to C5b6 (5 µg/ml) and incubated for a further 15 minutes at 37˚C. C8 and C9 were then added at roughly equimolar levels to C7 (5 µg/ml) for a further 45 minutes at 37˚C. The negative control comprised 50 µl of erythrocytes in 100 µl of APB; the positive (100% lysis) control comprised of 50 µl of erythrocytes in 100 µl water + 1% TWEEN. For validation of terminal pathway component function, C7 + C8 + C9 were added in the absence of C5b6.

After incubation to allow MAC mediated erythrocyte lysis, 96 well U bottomed plates were centrifuged at 300 x g for 5 minutes to pellet non-lysed erythrocytes and debris. 100 µl of the resultant supernatant was then carefully aspirated and transferred to a 96 well flat-bottomed plate. Absorbance was then measured at 405 nm, the closest available wavelength to the haemoglobin absorbance wavelength of 412 nm on the Magellan plate reader, and red cell cell lysis subsequently quantified relative to positive and negative controls.

To confirm the necessity of sequential addition of complement terminal pathway components to allow MAC formation on the cell surface, C5b6, C7, C8 and C9 were pre-incubated together for 30 minutes at 37˚C at the same concentration as in the reactive lysis assays above. The incubated components were then added to Guinea pig erythrocytes and incubated for 45 minutes at 37˚C as previously described for reactive lysis haemolytic assays and haemolysis measured in the same manner. Percentage haemolysis was calculated by:

Percentage haemolysis = ((Absorbance sample- negative control)/(Positive control- negative control)) x 100

Negative control = Erythrocytes in AP buffer

Positive control = Erythrocytes in H_2O + 1% v/v TWEEN 20

2.10.2 Cobra venom factor haemolytic assay and classical pathway assays

A variation of the reactive lysis assay was performed to determine the functionality of purified CVF. A titration of protein-containing fractions from the cobra venom MONOQ elution (7.5% - 0.1% v/v) was added to Guinea Pig erythrocytes in a 96-well U-bottomed plate with a constant dose of 10% final volume (15 µl) NHS. The remaining assay volume up to 150 µl was made up with APB. The plate was incubated at 37°C for 45 minutes, as described for the reactive lysis system. NHS only and MONOQ elution fraction only controls were included and haemolysis contingent on CVF activation of complement measured, alongside positive and negative controls of APB and 1% Triton X respectively. After CVF + NHS incubation with Guinea Pig erythrocytes, the U-bottomed plate was centrifuged, supernatant transferred, and haemolysis measured at 405 nm as previously described.

To determine the efficiency of complement component depletion from NHS, a classical pathway haemolytic assay was employed. Guinea pig erythrocytes were replaced with Sheep erythrocytes which are more resistant to complement mediated lysis and do not lyse directly with NHS. Sheep erythrocytes were therefore sensitised to human complement using anti-Sheep erythrocyte antibody (Amboceptor), diluted 1:2000 and added in equal volumes to a 2% suspension of Sheep erythrocytes in CFD for 30 minutes at 37^{o}C. After washing, the sensitised cells were incubated with a titration of NHS, or the comparable complement depleted serum with or without reconstitution with purified complement proteins for 30 minutes at 37°C; haemolysis was measured as above, and data analysed to confirm efficiency of depletion and capacity to restore lytic activity with complement component restoration. Percentage haemolysis was calculated by:

Percentage haemolysis = ((Sample - Negative control) / (Positive control - Negative control)) x 100

Negative control = Sensitised erythrocytes in CFD buffer

Positive control = Erythrocytes in H_2O + 1% v/v TWEEN 20

2.11 – Determining cell viability through Propidium Iodide staining

To ensure that experimental doses of MAC were sublytic, PI staining was performed by flow cytometry or plate-based fluorescence assays. For flow cytometry, cells were seeded at 1x10^{6} cells / ml in sterile 96 well U bottom plates in complete medium. Media was then replaced and cells sensitised to complement with a titration of the in-house heat inactivated COS-1 antiserum (rabbit polyclonal antiserum against the COS-1 kidney cell line from Cercopithecus aethiops, previously heat inactivated) for 20 minutes at room temperature prior to centrifugation at 300 x g and washing of the cells with 200 µl of sterile PBS. Cells were resuspended in complete medium and pooled NHS or C5 depleted serum was titrated on the cells to provide a source of complement. Complement titrations were incubated for 1 hour at 37˚C to allow complement mediated cell death. Cells were centrifuged at 300 x g and washed twice in 200 µl of sterile PBS. The cell pellet was then resuspended in 200 µl of FACS buffer

and cells stained using 10 µg/ml PI in the dark for 10 minutes at room temperature before running on the FACS Calibur flow cytometer. Relevant controls of unstained, unstimulated, antiserum only or NHS only, and positive control of cells incubated with 2% v/v Triton X were utilised to enable quantification of cell death and ensure complement dependence. PI fluorescence was measured in the FL2 channel on the flow cytometer on a log10 scale and analysed on Flowing software 2.0. Percentage cell death was calculated by subtracting unstained and unstimulated positive PI staining from the stimulated value. PI positivity was based on the gate around the Triton X-100 positive control.

Percentage complement mediated cell death was calculated as percentage cells falling in the PI positive gate and the following formula:

((Sample - Negative control) / (Positive control - Negative control)) x 100

Negative control = Unstimulated cells
Positive control = Cells + 1% v/v Triton X-100

A representative FSC/SSC scatterplot and gating is shown below in Figure 2.1.

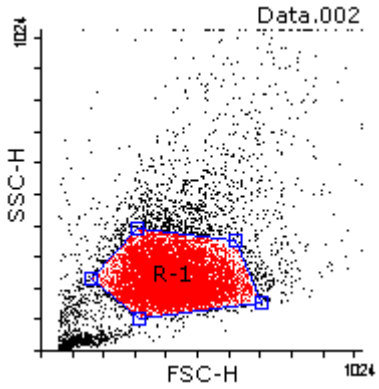

Figure 2.1. Representative FSC/SSC scatterplot with gating around intact cells

For measurement of reactive lysis mediated cell death on THP-1 cells, the reactive lysis haemolytic protocol described above was used for the formation of the MAC; cells were then resuspended in FACS buffer containing PI and viability assessed as above by flow cytometry analysis. A dose of C5b6 that, with the other terminal pathway components in molar excess, yielded cell death below a 5% threshold was defined as sublytic and subsequently utilised in stimulation experiments.

For kinetic, plate-based killing assays, the Clariostar fluorescent plate reader was used. SW 982 cells were seeded at $2x10^4$/ well in 200 µl of complete medium in opaque, sterile plates and left overnight to adhere to the plate under normal cell culture conditions. On the day of the experiment, complete medium was replaced, and cells were sensitised to complement using COS-1 antiserum as previously described. Cells were washed using 1x sterile PBS and before 200 µl of complete medium was added, alongside 10 µg/ml PI and the plate transported to the clariostar plate reader. The plate reader was configured with an excitation / emission profile of 480 / 630 nm respectively and a gain of 800. Baseline PI fluorescence was measured from the cells (prior to the addition of NHS, HI NHS, complement depleted NHS or Triton X at the given final concentrations (% v/v). The PI fluorescence at time 0 was subtracted as a baseline, with subsequent changes measured over the course of up to 1 hour. Fluorescence curves were then generated in MARS data analysis software and transposed into GraphPad PRISM.

Percent cell death was calculated using the equation: Percentage cell death = ((Sample– Negative control) / (Positive control – Negative control)) x 100

Negative control = reading for the well at time 0 (prior to NHS addition)

Positive control = Cells + 1% v/v Triton X-100

2.12 – Measuring cell viability through Lactate Dehydrogenase release (LDH)

To eliminate any possibility that non-viable adherent cells were lost during the PI workflow, such as during the washing step prior to de-attachment from the growing surface, an LDH viability assay was used (Thermofisher). The lyophilised LDH reagent was dissolved in 11.4 ml ddH_2O and added to 0.6 ml of LDH buffer immediately prior to the experiment. Any unused reagent was stored at -20˚C protected from direct light until use. Following manufacturer's instructions, cells were seeded in a sterile 96 well, flat bottomed plate overnight at a density of $2x10^4$ cells per well in 200 µl of complete medium. These cells were then washed with 1x sterile PBS and 200 µl of complete media replaced on the day of the experiment. The cells were subsequently sensitised to complement with COS-1 antiserum in complete medium as described previously. After sensitisation, cells were washed in 1x PBS and resuspended in 200

µl of complete medium. NHS, C5 depleted NHS or HI NHS were then titrated on the cells for 1 hour to induce complement mediated cell death. In instances where cell signalling inhibitors were utilised to modulate cell death in response to complement, these were applied for 30 minutes prior to the antiserum sensitisation step. Positive and negative controls of 1x (final concentration) lysis buffer and sterile water respectively were added to the complete medium, alongside appropriate serum only, antiserum only and unstimulated controls. Cell death was quantified relative to the negative and positive controls using the same equation as with PI staining, with the slight modification that the negative control used was a serum only sample as NHS gives a background signal in an LDH assay.

After the one-hour stimulation for complement mediated cell death, 50 µl of cell supernatant was aspirated per well from samples and controls and mixed with 50 µl of the assay working reagent in a fresh, flat bottomed, clear 96 well plate for 30 minutes at room temperature protected from light. The reaction was stopped through the addition of 50 µl of 1M acetic acid, absorbance read at 492 nm on the Magellan plate reader and cell death was quantified relative to the negative and positive controls using the equation given above, and killing curves generated in GraphPad PRISM.

The calculation used to determine percentage cell death by LDH release was therefore:

Percentage LDH release = ((Sample - Negative control) / (Positive control - Negative control)) x 100

Negative control = Cells + NHS without sensitising antibody

Positive control = Cells + 1x final concentration lysis buffer

2.13 - Cell stimulation using reactive lysis system generated sublytic MAC

In assays where complement mediated inflammasome activation was investigated, $2x10^5$ cells (THP-1 monocytes or monocyte derived macrophages) were seeded in 96 well or 24 well plates in 200 µl or 500 µl of complete media, at concentrations of $1x10^6$ and $4x10^5$ cells /ml respectively). Cells were subsequently primed with 25 ng/ml C5a (Native protein purified from pooled human serum, Comptech) for 4 hours prior to MAC assembly. C5b6 (titrated up to 3 µg/ml) was then deposited on the cells at the stated dose for 10 minutes at room temperature to allow cell membrane binding, C7 was then added for 15 minutes at 37˚C at over two times molar excess relative to C5b6 (5 µg/ml to all samples) to ensure that the initiation of MAC formation was the titrated C5b6. After C7 binding, cells were centrifuged at 300 x g and medium aspirated and replaced. The wash step performed was to eliminate C5b67 soluble complexes which may bind the subsequently added C8 and C9 proteins, allowing lower doses of complement components to be utilised and optimising the system. C8 and C9 were again added in two times molar excess relative to the C5b6 initiating complex (5 µg/ml for both) and subsequently incubated for the stated times for the experimental stimulation. All times stated are relative to the final addition of C8 and C9 rather than the initiation of complex formation with C5b6.

After incubation with sublytic MAC, THP-1 monocytes were centrifuged at 300 x g, cell supernatant aspirated, and the pellet washed with sterile PBS. Adherent monocyte required no centrifugation and supernatant was directly aspirated. Cells were then lysed using RIPA buffer + protease inhibitor cocktail and agitated on a plate shaker for 15 minutes prior to centrifugation at 10,000 x g to remove cell debris and allow lysate to be transferred to fresh Eppendorf tubes. Both lysates and supernatants were stored at -20˚C prior to analysis. A schematic overview of the stimulation procedure is shown Figure 2.2.

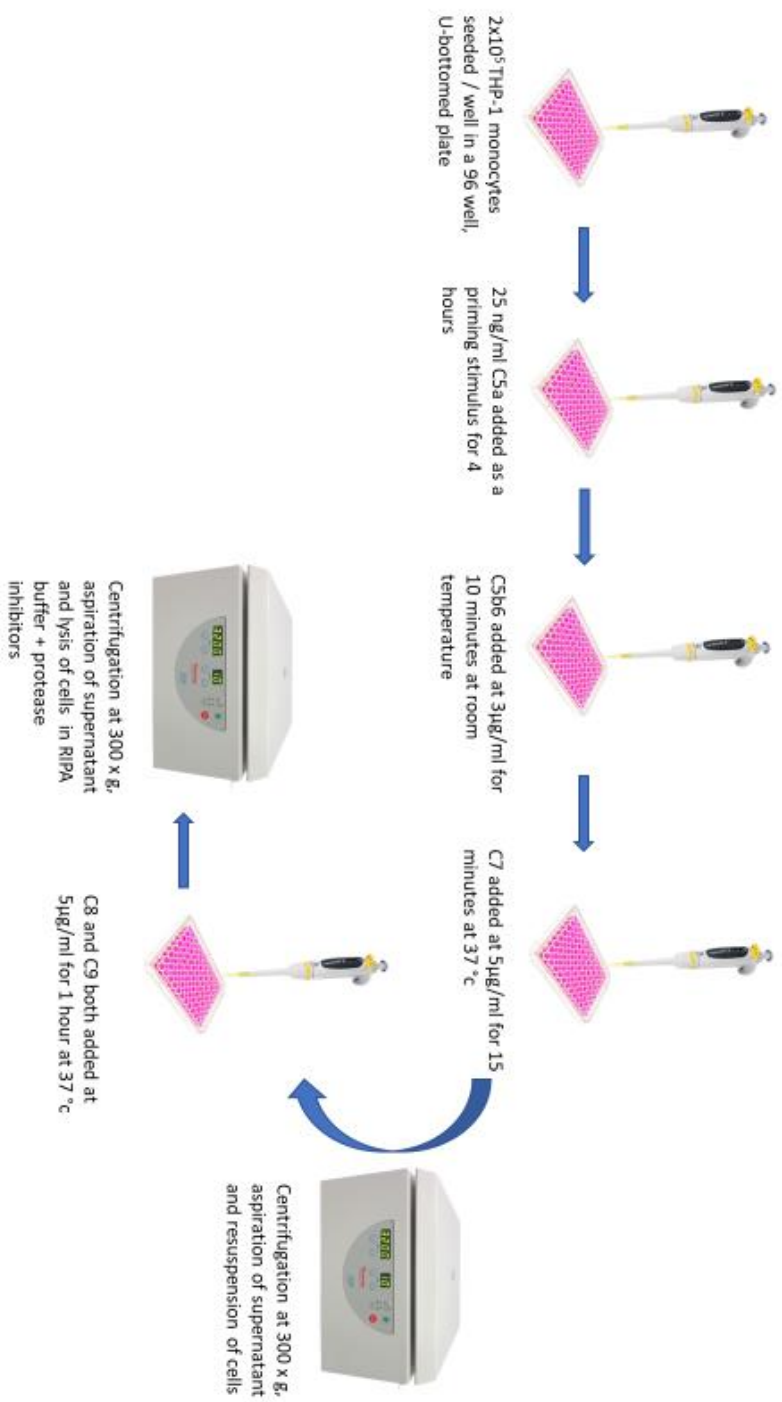

Figure 2.2 – Schematic of reactive lysis stimulation protocol for THP-1 monocytes and primary macrophages.

2.14 - Cell stimulations using Classical pathway generated sublytic MAC

THP-1 cells were harvested and seeded at $2x10^5$ cells per well at a concentration of $1x10^6$ cells / ml in a sterile 96 well U bottom plate in complete medium. To prime NLRP3 activation, LPS (Sigma) was added to the cells at 100 ng/ml for 4 hours at 37˚C to prime inflammasome activation. If cell signalling inhibitors were then used to investigate mechanisms of NLRP3 activation, THP-1 cells were washed with 1x sterile PBS and resuspended in 200 µl of complete medium and the inhibitors, at the stated doses (300 nM – 100 µM, dependent on the inhibitor working concentration as described in reagent manufacturer's instructions), were applied for 45 minutes at 37˚C after priming but prior to cell sensitisation to complement. Cells were washed in 1x sterile PBS and resuspended in 200 µl complete cell media before sensitisation to complement using COS-1 antiserum as previously described. Cells were subsequently washed in 1x sterile PBS and resuspended in 200 µl of complete medium and NHS, HI NHS or complement component depleted NHS added at a sublytic dose for 1 hour. Cells were then centrifuged at 300 x g, supernatant aspirated, and cells lysed as described in the previous section. A schematic for the Classical pathway system is shown in Figure 2.3.

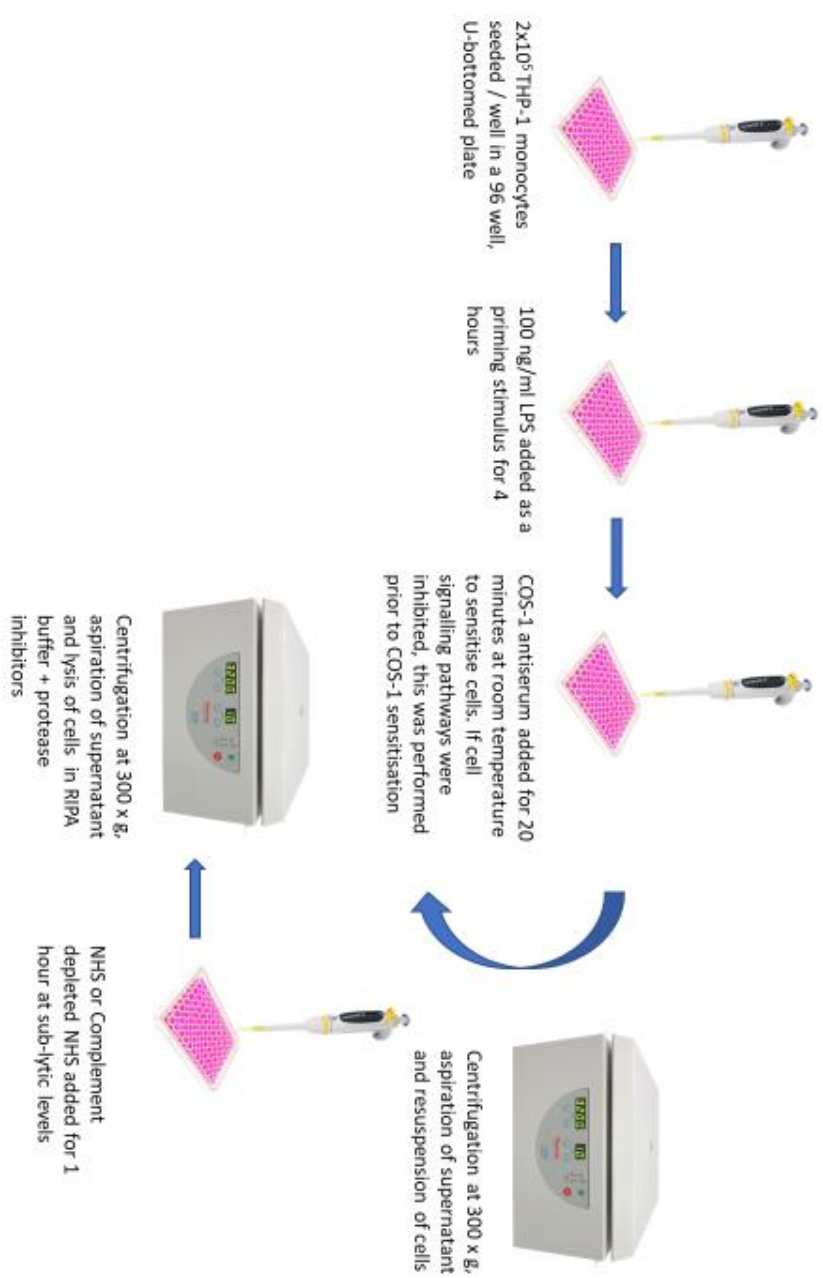

Figure 2.3. A schematic overview of the classical pathway stimulation procedure using COS-1 antiserum and NHS.

2.15 – Flow cytometry staining for complement activation

2.15.1 Flow cytometry staining for C3b deposition

To demonstrate that complement was the responsible factor for the observed effects, staining for complement components by flow cytometry was used. THP-1 cells were seeded at $2x10^5$ cells / well at a concentration of $1x10^6$ cells/ml in 96 well, sterile U-bottom 96 well plates in complete cell media. Cells were sensitised to complement as previously described using COS-1 antiserum at titrated doses for 20 minutes at room temperature. Cells were subsequently washed with 1x sterile PBS and resuspended at $1x10^6$ cells/ml in complete medium prior to addition of NHS / C5 depleted serum at the denoted concentration for 1 hour at 37˚C. Cells were washed in 1x sterile PBS and resuspended in 100 µl FACS buffer, prior to staining on ice, protected from light with anti-C3b monoclonal FITC conjugate (Biolegend) diluted 1:50 in FACS buffer for 30 minutes. Cells were washed twice with sterile PBS, resuspended in 200 µl of FACS buffer and assayed for fluorescence on the FACS Calibur using the FL1 channel and mean fluorescence quantified. Data were subsequently analysed on Flowing Software 2.0 and GraphPad PRISM 5.

For C3b staining on SW 982 cells, cells were first trypsinised (1x Trypsin, 10 mM EDTA solution, Gibco) to disassociate the cells from the flask. This step was essential as disassociation with 10 mM EDTA was slow and trypsinisation after complement deposition degraded C3b on the cell surface and ablated FACS signals. $2x10^5$ cells were then resuspended per sample in 200 µl of complete medium in 96 well U bottom plates prior to complement activation and deposition as previously described. SW 982 cells were stained, washed and analysed in an identical manner to THP-1 cells.

2.15.2 Flow cytometry staining for C9 deposition

To stain for C9 (as a surrogate for MAC) deposition, a similar protocol was used. $2x10^5$ THP-1 cells were seeded per sample at $1x10^6$ cells/ml, prior to sensitisation and stimulation with complement as previously described for 5 minutes. After 5 minutes, cells were centrifuged at 300 x g and fixed in 4% PFA solution at 4°C for 20 minutes. The shorter incubation and requirement for cell fixing is reflective of the more transient nature of C9/MAC deposition on the cell surface, in contrast to C3b which is retained for longer periods (Morgan 1988). Cells were stained for C9 deposition using in house B7 anti-C9 neo-epitope antibody (10 µg/ml) or appropriate isotype control for 20 minutes at room temperature. Cells were subsequently centrifuged at 300 x g and washed twice with 1x sterile PBS. Cell were then incubated with the appropriate secondary antibody, anti-mouse IgG Alexa 546, for a further 20 minutes. Cells were washed twice in FACS buffer and then analysed for fluorescence using FACS Calibur as described above.

2.16 - Determining cell surface complement regulator expression

SW 982 synoviocytes were seeded in 6 well plates overnight at $1x10^6$ cells per well and a concentration of $1x10^6$ cells / ml. Cell medium was replaced on the day of the experiment and any cell signalling inhibitors added for 1 hour at the designated dose. Cells were then washed with 1 ml of sterile PBS per well, before trypsinisation with 0.7 ml Trypsin per well at 37˚C for 10 minutes. The trypsin was subsequently neutralised with 0.7 ml of complete medium per well before cells were transferred to sterile Eppendorf tubes and centrifuged at 300 x g for five minutes and supernatant aspirated. Cells were then fixed in 4% PFA solution for 20 minutes at 4˚C to preserve expression profiles through the staining process, washed and resuspended in 200 µl FACS buffer prior to staining. For intracellular antigens, cells were stained in FACS buffer containing 0.1% v/v Triton X for both primary and secondary antibodies. CD59 was detected with the mouse monoclonal antibodies BRIC 229 or MEM 43, whilst CD55 was detected using BRIC 215. All antibodies were used at 10 µg/ml, for 30 minutes on ice in FACS buffer. Cells were then centrifuged at 300 x g and washed with sterile PBS before incubation with appropriate conjugated secondary antibodies at 1:100 dilution in FACS buffer for 30 minutes on ice and protected from light. Cells were again washed in 1x

sterile PBS and resuspended in 200 µl of FACS buffer prior to data acquisition on the FACS Calibur. Data were analysed using Flowing Software 2.0 and GraphPad PRISM 5.

2.17 – Investigating the role of CD59 in C3b deposition and cell death

To investigate the role of CD59 in regulating C3b deposition and cell death, THP-1 monocytes were seeded in complete cell media at $1x10^5$ cells per well at a concentration of 1x106 cells / ml in a sterile 96 well U bottom plate. Cells were sensitised to complement as previously described using COS-1 antiserum, with and without CD59 function blocking antibody BRIC 229 at 10 µg/ml. Cells were then centrifuged at 300 x g, washed in 1x sterile PBS and resuspended in complete cell medium and MAC generated using titrations of NHS or C5 depleted serum as a control for 1 hour at 37˚C. The attacked cells were then washed and stained for cell death with 10 µg/ml Propidium Iodide for 10 minutes at room temperature and for C3b deposition as described above using anti C3b-FITC antibody (Biolegend) on ice for 30 minutes. Cells were then washed with 200 µl of sterile PBS twice before transfer to FACS tubes and running on the FACS Calibur flow cytometer. Subsequently, the data were analysed using Flowing software 2.0 and GraphPad PRISM 5.

2.18 - Confocal microscopy imaging of complement regulator expression and complement cell surface deposition

To further demonstrate different levels of complement regulator and terminal pathway product deposition on the cell surface, confocal microscopy was used to visualise cells. WT and NLRP3 -/- SW 982 synovial cells were seeded at $4x10^4$ cells per well in an 8 well glass chamber slide and allowed to adhere to the glass overnight at 37°C. Cells were washed with 300 µl 1x sterile PBS prior to fixation with 4% PFA for 20 minutes at room temperature. Cells were washed prior to staining with primary antibody. In the case of CD59 surface staining, no permeabilizing agent was used, however, when intracellular expression was investigated 0.1% v/v Triton-X 100 was included in the primary and secondary antibody solutions. Primary antibody was diluted to appropriate concentration (20 µg/ml in the case of MEM43) in PBS,

0.2% w/v BSA, 0.2% w/v NaN_3. Cells were incubated with primary antibody for 2 hours at room temperature. Cells were thoroughly washed with sterile PBS prior to secondary antibody addition at 4 µg/ml in PBS, 0.2% w/v BSA for 2 hours at room temperature protected from direct light. Directly conjugated Cholera Toxin B subunit Alexa 488 (Thermofisher) was used to detect lipid raft membrane regions through binding to the GM1 sphingolipid at the same time as secondary antibody at 1 µg/ml final concentration. Cells were again washed thoroughly with 3x 300 µl of sterile PBS, then incubated with a 1:2000 dilution of TOPRO, a carbocyanine nuclear stain, in PBS for 10 minutes at room temperature protected.

The cell casket was removed, the glue lifted using a razor blade and peeled off evenly to allow mounting. A drop of vectashield was applied over each well and a coverslip applied over each half of the slide. This was pressed down using a pipette tip and excess vectashield removed using tissue. The coverslip was fixed using nail varnish and allowed to dry.

Cells were imaged using the ZEISS confocal microscope using a 1.4 NA 63x Zeiss objective lens. The system was equilibrated, the far-red, red and green laser gains were optimised for each experiment, and images visualised and saved using the Zen Black software. Colocalisation of markers was performed using the Zen Blue software, with a Pearson's co-efficient greater than 0.5 taken as significant colocalization.

2.19 - Western blotting

Cell lysates were collected as previously described in the cell stimulation protocols. Cell lysate was aliquoted then mixed in equal volume with 2x reducing Western blot loading buffer, boiled at 90˚C for 10 minutes to ensure protein denaturation and allowed to cool prior to loading. Precast gels (4-20% gradient BioRad gels) or hand cast gels (10-15% running, 3.5%-4.5% stacking) were then loaded in separate wells with 5 µl of chromogenic molecular weight ladder and 25 µl of cell lysate + loading buffer. Gels were run in SDS PAGE running buffer for a minimum of one hour at 120 V constant voltage at room temperature or until the gel dye front reached the bottom of the gel.

For gel transfer to nitrocellulose membrane a wet transfer system was used. Sponges, filter paper and nitrocellulose membrane were soaked in transfer buffer and then assembled

sequentially in the cassette, with a roller used to eliminate bubbles. The cassette was placed in the transfer buffer filled transfer tank and an ice block added to cool the buffer; voltage was set at 100 V for one hour. Complete transfer of the chromogenic ladder was checked to confirm effective protein transfer to the membrane.

Membranes were then blocked for a minimum of 1 hour at room temperature with 5% non-fat dry milk powder in 1x PBS + 0.1% v/v TWEEN to prevent nonspecific antibody binding to the membrane. Primary antibodies were incubated with the membrane overnight at a 1/1000 dilution at 4˚C in 5% w/v BSA in 1x PBS + 0.1% TWEEN with constant gentle agitation. Primary antibodies were reused up to three times with storage at -20˚C. Membranes were subsequently washed three times with 1x PBS + 0.1% TWEEN for 5 minutes at room temperature to remove any nonspecific primary antibody binding. The appropriate secondary antibody was then added in PBS, 5% w/v BSA, 0.1% TWEEN and incubated for 1 hour at room temperature with constant gentle agitation. Membranes were then washed three times (10 minutes each) in 1x PBS + 0.1% TWEEN and a final 10-minute wash in 1x PBS, then probed using ECL reagents as per the manufacturer's instructions. The membrane was soaked in ECL detection reagent and excess was removed by blotting; the membrane was then wrapped in clingfilm and images captured using the Thermofisher MyECL system or through exposure to autoradiography film. Molecular weights of protein bands were measured relative to the markers and band density assessed by densitometry (ImageStudio lite; Licor).

One set of Western blot experiments (IL-1β in cell lysates from primary macrophages stimulated with reactive lysis) was performed at the GSK site in Stevenage and therefore had a modified protocol. Differentiated primary macrophages were stimulated with C5a and reactive lysis MAC as described and $1x10^6$ cells were lysed in 200 µl of RIPA buffer with protease inhibitor cocktail. Cell lysate was loaded on 4-12% gradient BIS-TRIS gels and run under a constant Voltage of 120V for 1 hour. 5µl of Chameleon molecular weight marker was loaded in lane 1 of each gel. Protein was transferred to PVDF membrane using the semi-dry Invitrogen power blotting system for 8 minutes. Membranes were washed in PBS 0.1% v/v TWEEN as previously described and blocked in PBS + 5% w/v BSA for 1 hour. To probe for IL-1β, mouse anti human IL-1β (CST) was diluted 1:1000 in PBS 5% w/v BSA for 1 hour at room temperature and rabbit anti human β-actin (1:10,000 – CST). Membranes were subsequently washed with PBS 0.1% V/V TWEEN and probed with the respective LICOR secondary

antibodies (Goat anti-rabbit 800 CW and Donkey anti-mouse 680 CW) for 1 hour at room temperature. The two secondary antibodies allow detection of IL-1β and β-actin on the membrane simultaneously at the respective wavelengths. Membranes were washed 3 x 15 minutes in PBS + 0.1% V/V TWEEN before a 30-minute wash in deionized H_2O. All steps after the addition of the secondary antibodies were performed protected from direct light. Washed membranes were then visualised at 680 and 800nm on the ODYSSEY system and images at each wavelength saved.

2.20 - Quantification of IL-1β secretion by ELISA

To measure mature IL-1β secretion from cells, a duo set kit from R&D systems was used as per the manufacturer's instructions. A 96 well Nunclon plate was coated with a 1/120 (v/v) dilution of capture antibody in PBS for 2 hours at 37˚C or overnight at room temperature. The plate was then washed twice using PBS + 0.05% TWEEN, blocked with 300 µl per well of PBS + 1% w/v BSA for 1 hour at 37˚C and washed again. A dilution series of IL-1β standard from 500-7.2 pg/ml was generated in cell culture medium and 100 µl added to wells in duplicate to generate a standard curve. Diluted sample supernatants (100 µl) were added to sample wells and incubated for 1 hour at 37˚C. Wells were washed and detection antibody (100 µl/well at 1/60 (v/v) in PBS + 1% BSA) added for 1 hour at 37˚C. After washing, 100 µl of Streptavidin-HRP (1/40 (v/v) in PBS + 1% BSA) was added per well for 20 minutes at 37˚C. Wells were again washed and 100 µl of TMB substrate solution added per well for 20 minutes at room temperature. The chromogenic reaction was stopped by addition of 50 µl per well of 10% v/v H_2SO_4. The colour change was subsequently read at 490 nm on the Magellan plate reader. A standard curve was then generated, and sample unknown values interpolated using PRISM 5 analysis software.

2.21 – CaspaseGlo assay for Caspase 1 activation

Alongside IL-1β secretion, the cleavage of Caspase-1 is an important marker for NLRP3 activation. While this can be detected by western blotting for Caspase activation fragments, I selected a semi quantitative technique, the CaspaseGlo kit from Promega. This assay utilises a synthetic Caspase-1 substrate which, when cleaved by Caspase-1, generates a luminescent signal, which is used to quantify levels of Caspase activation relative to controls. A schematic of the reaction is shown in Figure 2.4.

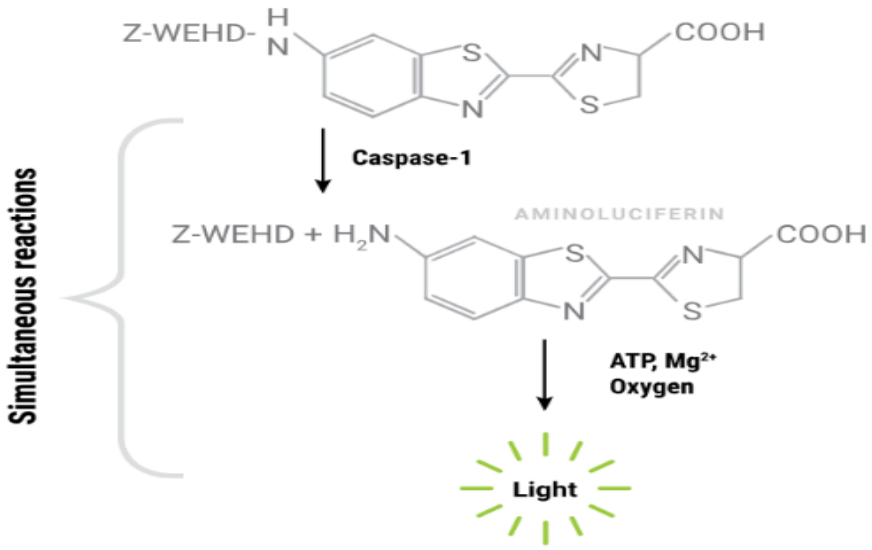

Figure 2.4. Schematic of the luminescent reaction used to generate Caspase-1 glo signal. The synthetic Caspase-1 substrate Z-WEHD is cleaved by the activated Caspase, generating Aminoluceferin, which in turn emits a quantifiable luminescent signal proportional to the amounts of activated Caspase-1. Image sourced from Promega website.

THP-1 cells were seeded at $2x10^5$ / well in a 96 well, U bottomed plate while SW 982 cells were seeded directly to opaque, sterile plates. THP-1 and SW 982 cells were sensitised to complement deposition and subjected to sublytic complement deposition using NHS or C5 depleted serum for one hour. The cells were then added to the Caspase-1 luminescent substrate and incubated in the dark at room temperature for 90 minutes prior to transfer to white, flat bottomed, sterile 96 well plates; luminescence values were recorded on the Clariostar plate reader. Data was then analysed in GraphPad Prism 5 software.

2.22 - Measuring calcium flux in response to sublytic MAC

THP-1 monocytes were cultured in complete medium; $2x10^5$ cells/well were seeded in U bottomed 96 well plates. The fluorescent Calcium binding dye Fluo-3-AM (Thermofisher) was reconstituted in DMSO to make a 221 µM stock, before adding to the cells at a 1:100 final dilution (2.2 µM) and incubating for one hour at 37˚C away from direct light. The lipophilic dye was taken up by the cells and trapped by cytosolic esterase cleavage of the AM (acetoxy-methyl) group (Figure 2.4). The cells were then sensitised to complement as previously described, washed and resuspended in 200 µl of CFD buffer +/- 10 mM EGTA. Cells were exposed to NHS or C5 depleted serum and incubated at room temperature to allow quick loading on the cytometer or plate reader for the designated length of time before running on the flow cytometer and measurement of FL1 fluorescence.

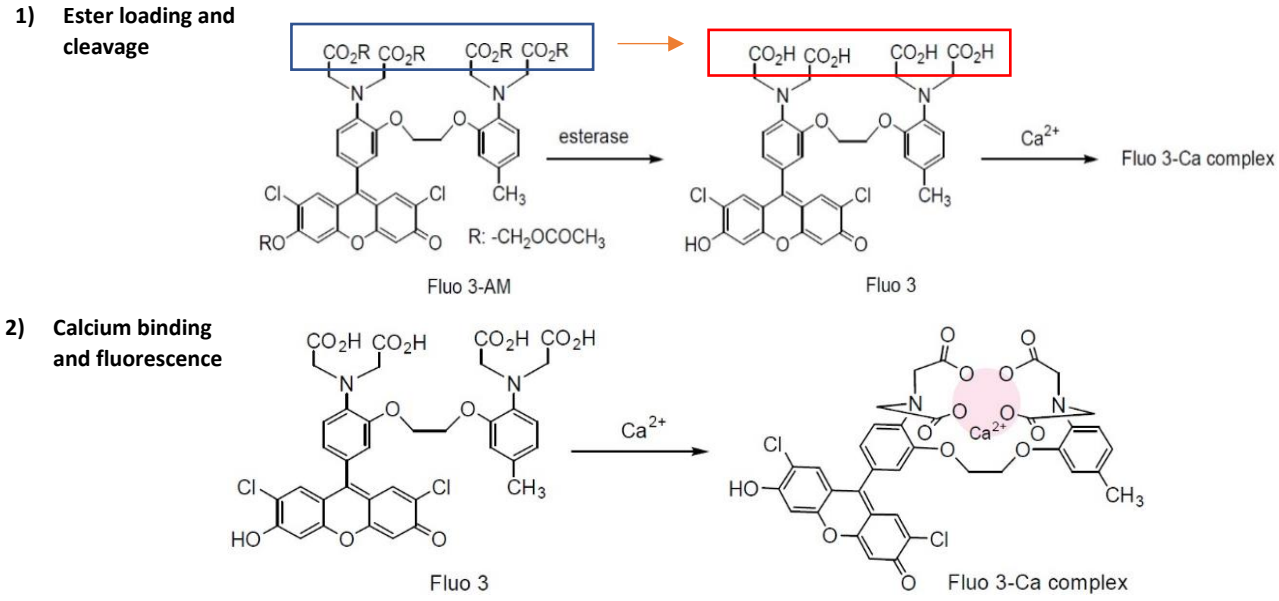

Figure 2.5. Schematic of methyl ester loading to the cell. Cell permeable, non-polarised methyl esters are added to the cells and incubated for 30 minutes – 1 hour at 37°C to allow the uptake across the cell membrane. Upon entering the cell, esterase cleavage generates a polarised molecule which is cell membrane impermeable and can then interact with intracellular charged groups such as Calcium or ROS, generating a fluorescent signal. Images edited from Dojindo website.

For measurement of calcium flux using the Clariostar plate reader, $2x10^5$ THP-1 cells or $2x10^4$ SW 982 synoviocytes were loaded with Fluo-3 by incubation with Fluo-3-AM as described, sensitised using COS-1 antiserum , transferred to white, flat bottomed plates in complete

medium and loaded in the plate reader set with a focal height of 7.7 mm, gain of 1000 and excitation/emission of 505/525 nm respectively. Cells were then stimulated with NHS, HI NHS or C5 depleted NHS, and calcium flux measured by increased fluorescence. Fluorescence readings were taken at least every 1 minute for at least 10 minutes from each well. If signalling inhibitors, such as BAPTA-AM or Xestospongin C were used, these were pre-incubated with the cells prior to COS-1 sensitisation at the stated doses for 45 minutes. Data was subsequently analysed using the MARS analysis software and curves generated using GraphPad Prism representing the changes in fluorescence over time in each replicate. Changes in Calcium concentrations were measured using the following formula:

$[Ca^{2+}]$ = Kd (325 nM for Fluo-3-AM) x ((Fluorescence of signal – Minimal Fluorescence (unstimulated cells)) / ((Maximal Fluorescence (Triton X control) – Minimal Fluorescence)).

2.23- Measuring mitochondrial potential

To determine whether sublytic MAC induced mitochondrial depolarisation, the mitochondrial selective dye tetramethyl rhodamine ethyl ester (TMRE) was used. TMRE is retained in polarised mitochondria where the mitochondrial membrane H^+ gradient is intact, yielding a fluorescent signal, and is lost upon membrane depolarisation. $2x10^5$ THP-1 cells were seeded in a 96 well, U bottomed plate at a density of $1x10^6$ cells/ml. In experiments where cell signalling inhibitors were used, cells were initially incubated with cell signalling inhibitors for 45 minutes at the relevant working concentrations. Cells were then incubated with TMRE at a concentration of 200 nM for 20 minutes at 37°C to load cells with TMRE. Cells were then washed with 1x PBS and sensitised to complement using the COS-1 antiserum as previously described. Cells were subsequently washed with 1x PBS prior to resuspension in complete medium and sublytic MAC deposition for 30 minutes. C5 depleted serum, antiserum only, unstimulated and unstained controls were also included. FCCP (carbonyl cyanide 4-(trifluoromethoxy) phenylhydrazone), an ionophore that causes mitochondrial depolarisation, was used as positive control. Fluorescence was measured by either flow cytometry or fluorescent plate reader; loss of fluorescence was indicative of a reduction in mitochondrial potential an indicator of mitochondrial dysfunction. Data were analysed using

Flowingsoftware 2.0 or MARS data analysis platform, dependent on the platform used, and outputs created in GraphPad PRISM 5.

2.24 - Generating NLRP3 KO SW 982 synoviocytes via CRISPR Cas9 system

CRISPR/Cas9 genome manipulation allows, specific, targeted gene editing using the Cas9 endonuclease. To target the Cas9 endonuclease to a DNA region, a short transcript containing a scaffold region (also known as Tracr RNA) and a complementary sequence (collectively called gRNA) to the target DNA must bind the Cas9 complex and orientate it adjacent to the Cas9 cleavage motif, known as a protospacer adjacent motif (PAM) site. The cleavage of target DNA is dependent on the homology of the gRNA with the complementary sequence to anchor the endonuclease in place. Upon effective Cas9 binding, the two endonuclease domains undergo conformational change, and each mediates a single DNA strand cleavage event, cumulatively creating a double strand break (DSB). The repair of the induced DSB can then be dictated in the experiment. The provision of a suitable DNA template to integrate into the blunt ended DSB allows precise genome editing with homology directed repair. If knocking out of gene expression is desired, no template DNA is provided; there is a propensity for inaccurate repair of blunt-ended DSB's, resulting in frame shifts in the target gene, introducing premature stop codons and/or missense mutations. A schematic for CRISPR Cas9 utilisation for both homology-directed repair and non-homologous end joining, mediating DSB's for missense mutations, is shown in Figure 2.6.

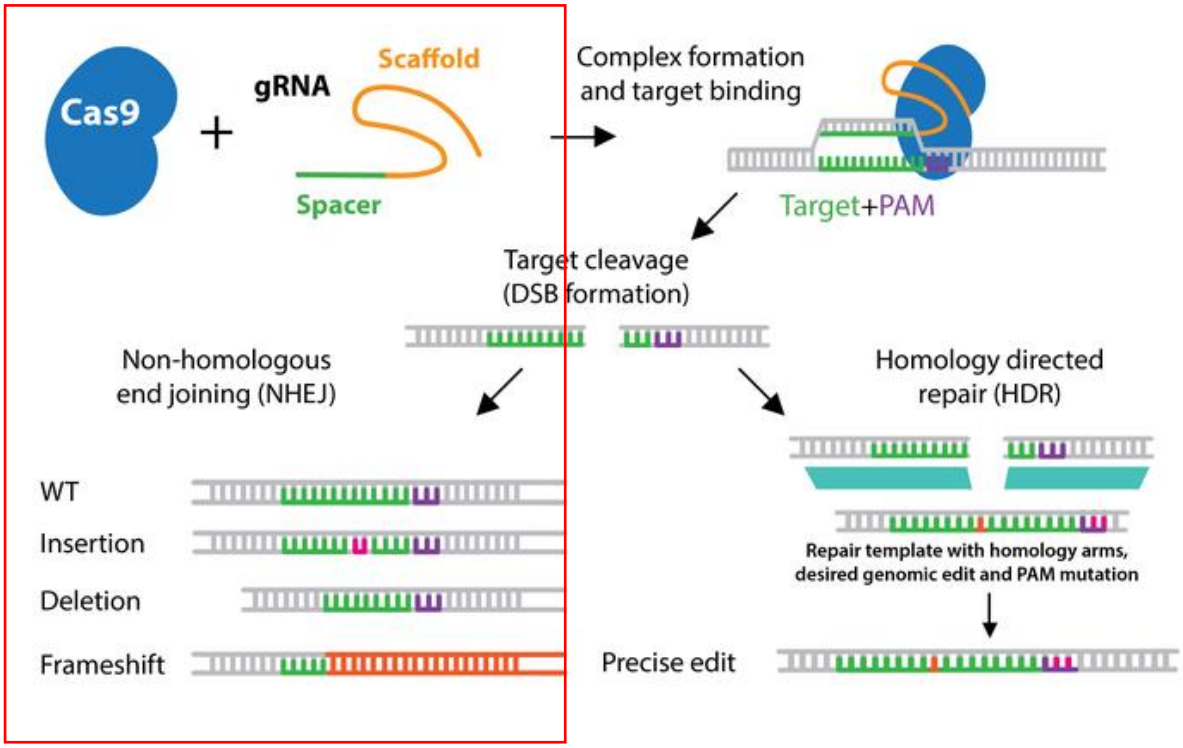

Figure 2.6. Schematic of CRISPR Cas9 mediated DNA manipulation, with the used workflow of NHEJ for gene knockout highlighted. Image adapted from https://www.addgene.org/crispr/guide/.

The CRISPR experiment was performed at GSK in the Catalyst/C3 DPU labs in Stevenage. The resources for the experiment were all sourced from Thermofisher, with 4 gRNAs against NLRP3 selected from predefined libraries. SW 982 cells were seeded at a density of $1x10^6$ cells $well^{-1}$ in a 6 well plate and allowed to adhere overnight at 37°C in a 5% CO_2 incubator. On the day of transfection, Cas9 mRNA (0.5 µg), NLRP3 gRNA (325 ng/ml) and Lipofectamine 3000 (5.2 µl) were aliquoted separately into 250 µl of OPTIMEM medium and liposomes allowed to form for 5 minutes at room temperature. The composition of each tube is shown below in Table 4. Two gRNAs were used per sample to maximise the probability of frame shift mutations. The tubes containing the RNA mix were then combined with the liposomes for 15 minutes at room temperature to allow RNA: Lipid complexes to form prior to addition to SW 982 cells in OPTIMEM for 6 hours at 37°C. After 6 hours, media was replaced, cell colonies selected, allowed to recover from transfection and assayed for NLRP3 expression by Western blot / RT PCR.

Tube	Condition			
	Untransfected	**gRNA pair 1**	**gRNA pair 2**	**Mock transfected control**
1	250µl OPTIMEM	250µl OPTIMEM	250µl OPTIMEM	250µl OPTIMEM
		gRNA 1 (325ng/ml) CRISPR1098152_CR	gRNA 3 (325ng/ml) CRISPR1098159_CR	
		gRNA 2 (325ng/ml) CRISPR1098154_CR	gRNA 4 (325ng/ml) CRISPR1098157_CR	
		0.5µg CAS9 mRNA	0.5µg CAS9 mRNA	0.5µg CAS9 mRNA
2	250µl OPTIMEM	250µl OPTIMEM	250µl OPTIMEM	250µl OPTIMEM
		5.2µl Lipofectamine	5.2µl Lipofectamine	5.2µl Lipofectamine

Table 6: Plan of CRISPR/CAS9 transfection for WT SW 982 cells. gRNA's against NLRP3 were acquired from Thermofisher TRUE guide range and used in pairs to ensure effective targeting of all NLRP3 isoforms. Untransfected and mock transfected (Cas9 mRNA + lipofectamine – gRNA control) were used to compare to the targeted transfections.

2.25– Pouring Agar plates and clone selection

To generate further CRISPR/Cas9 based knockouts a different system was utilised. Firstly, cells were transfected with an inducible Cas9 expression plasmid, pCW-Cas9 supplied by Addgene which allowed for positive selection through Puromycin resistance, with a subsequent second transfection of gRNA and screening for loss of gene expression of the protein of interest. A map of the plasmid is shown below in Figure 2.7. The total plasmid consists of 11,885 bp and contains the Cas9 gene under a TET-on inducible promoter and a Puromycin selection marker.

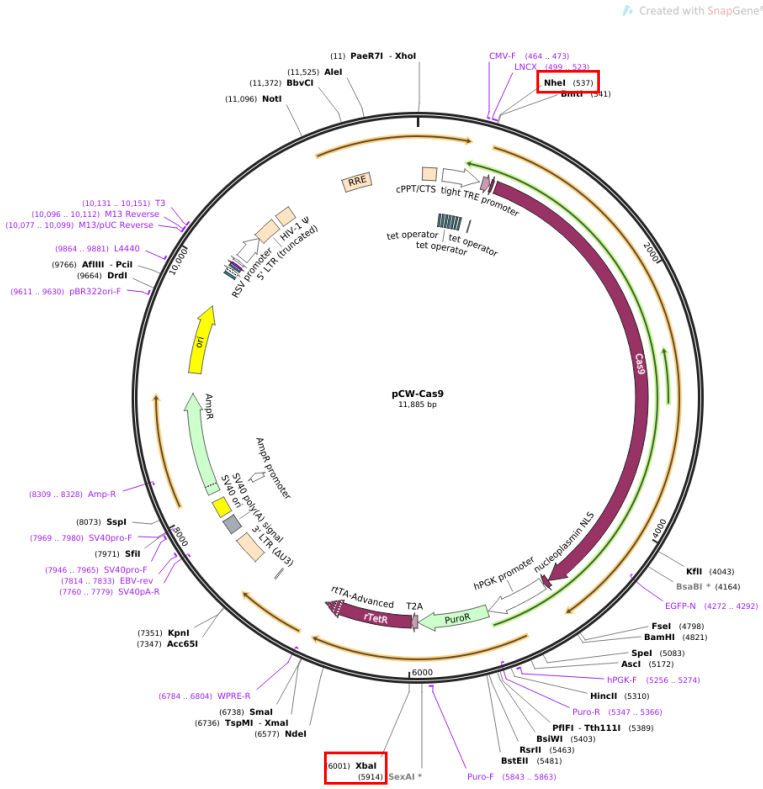

Figure 2.7. pCW-Cas9 gene map. The total plasmid construct consists of 11,885bp and contains the Cas9 gene under an inducible TET ON promoter allowing expression to be transient and potentially limit off target gene editing effects. The puromycin resistance gene allows positive survival selection of transfected cells. The plasmid contains restriction enzyme sites for XBA1 and NHEL1 at 6001 and 537 respectively, allowing a restriction digest of the plasmid with these enzymes to generate two fragments of roughly 5.5 kb and 6.5 kb. Image adapted from Addgene website (https://www.addgene.org/50661/).

The initial step of this workflow was the purification of the pCW-cas9 vector from Addgene, deposited by Eric Lander and David Sabbiatani and first described by Wang *et al* 2014. The vector was supplied in bacterial stabs set in agar, which were stored at 4˚C prior to use Agar stock was generated by adding 15 g of agar powder per litre of Luria Broth (LB) medium and microwaved until the agar was dissolved. The solution was then allowed to cool to room temperature prior to the addition of 10 µg/ml Puromycin to the solution. Agar solution (10 ml) was poured into each of 8 plates and allowed to set at room temperature. To generate bacterial colonies, cells from the bacterial stab were streaked on the selective agar plates using a sterile pipette tip.

The streaked plates were then inverted to prevent condensation dripping onto the cells and sealed with parafilm prior to overnight incubation at 37˚C to allow colony growth.

After the overnight incubation, plates were checked visually, and individual colonies carefully selected using a sterile pipette tip and transferred to 30 ml of prewarmed LB broth containing 10 µg/ml Puromycin. These cultures were then incubated at 37˚C with constant agitation overnight to allow liquid culture growth, apparent by the increased turbidity of the culture.

2.26 – Purification of pCW-Cas9 plasmid DNA

To purify plasmid DNA from the clonal liquid cultures the Invitrogen PureLink Maxiprep kit was used. The overnight liquid colonies were firstly centrifuged at 600 x g for 10 minutes to pellet bacteria. The Maxiprep column was equilibrated in 30 ml of buffer EQ1 (0.1 M sodium acetate, 0.6 M NaCl, 0.15 % v/v Triton X) using gravity flow. The resuspension buffer R3 (50 mM TRIS-HCl, 10 mM EDTA, pH 8.0) was prepared through the addition of RNase A to a final concentration of 100 µg/ml in 100 ml prior to use to eliminate RNA contamination. Pelleted bacteria were resuspended in buffer R3 in a sterile hood, with gentle inversion and shaking until the suspension was homogenous. 10 ml of Lysis buffer L7 (0.2 M NaOH, 1% w/v SDS) was then added to the suspension, mixed by inversion and incubated for five minutes at room temperature to allow bacterial lysis. The DNA from the lysed bacterial cells was then precipitated to remove debris through the addition of 10 ml precipitation buffer N3 (3.1 M Potassium acetate, pH 5.5) and inverted until the mixture was homogenous, with the precipitated DNA subsequently loaded on to the Maxiprep column and allowed to gravity flow through the column. The flow through from the precipitated lysate was discarded alongside the inner filtration cartridge, before washing the column with 50 ml of wash buffer W8 (0.1 M Sodium acetate, 825 mM NaCl, pH 5.0). The flow through from the wash step was discarded and a fresh sterile 50 ml tube was placed under the column for elution. Bound plasmid DNA was eluted from the column with 15 ml of elution buffer E4 (100 mM TRIS-HCl, 1.25 M NaCl, pH 8.5) through gravity flow. The eluted DNA was then precipitated by adding 10.5 ml of isopropanol, mixing and centrifugation at 12,000 x g for 30 minutes at 4˚C. The supernatant was discarded, the pellet was resuspended in 5 ml 70% ethanol and centrifuged

at 12,000 x g for 5 minutes. The supernatant was removed and the pellet air dried for 10 minutes then resuspended in 500 µl of TE buffer. DNA concentration was measured by nanodrop, aliquoted and stored frozen at -20˚C until use.

2.27- Restriction enzyme digestion and agarose gel electrophoresis of pCW-CAS9 plasmid

To verify that the purified plasmid DNA was intact, pure and encoding the correct sequence, the purified DNA was run on an agarose gel, with and without restriction enzyme digestion. To perform the restriction digest, 1 µg of plasmid DNA was added to 1 activity unit (the amount of enzyme required to digest 1 µg of substrate DNA in a 50 µl volume in 60 minutes) of both XBA1 and NHEL in a 30 µL reaction volume containing 0.1 mg/ml BSA in NEB broad spectrum restriction enzyme buffer for 1 hour at 37°C. A 1% agarose gel made from 1% agarose solution in 1x TAE buffer containing 50 µg of Ethidium Bromide to allow visualisation of DNA was used to resolve the digestion products. The gel was placed in the gel docking system with a 10-well comb inserted for sample loading immersed in 1x TAE buffer in the gel tank, a DNA samples and broad range molecular weight marker (10 kb-100 bp,) were loaded and electrophoresis performed at a constant voltage of 100 V for 1 hour. Resolution was checked using UV imaging and the gel run for up to a further hour to increase the high kb resolution needed to differentiate the restriction digest products. Images were captured using the Thermofisher MyECL system and shown in Figure 2.8.

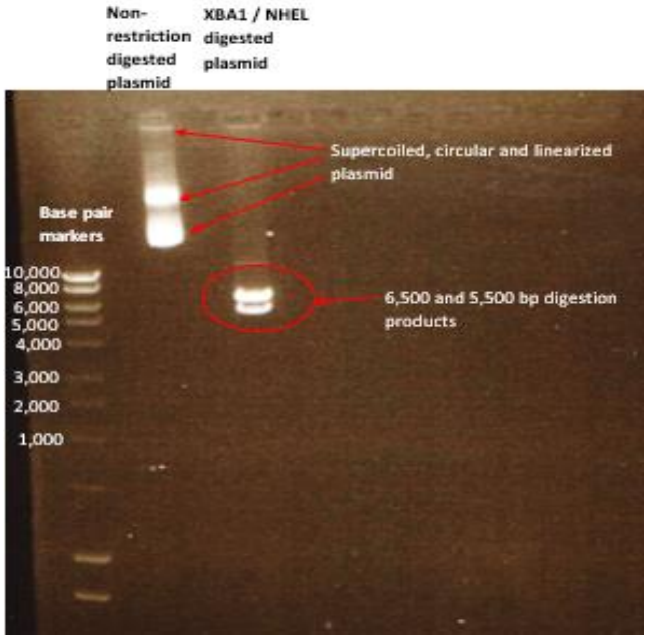

Figure 2.8. Agarose gel electrophoresis of purified pCW-CAS9 vector. Intact pCW-CAS9 vector s 11,800 bp and above the heaviest base pair marker, but observable in its linearized, circular and supercoiled structures in Lane 2. The double restriction digest of the plasmid using XBA1 and NHEL1 generated the expected 6,500 and 5,500 bp fragments observed in Lane 4. The lack of multiple bands indicates little DNA degradation and allows confidence in identity, purity and quality of the plasmid DNA for subsequent transfections.

2.28- Transfection of pCW-Cas9 vector in to SW 982 cells

To generate an inducible Cas9 expressing synovial cell line, SW 982 cells were lipofectamine transfected with the purified pCW-Cas9 vector and transfected cells selected through puromycin resistance. The day before the experiment, $2x10^5$ WT SW 982 cells were seeded per well in a 24 well plate in 500 µl of complete medium and left overnight to adhere. On the day of the experiment, cells were washed and 1 ml of OPTIMEM added per well. Concurrently, DNA: lipid complexes were prepared. A titration of plasmid DNA (2-8 µg) was diluted in 500 µl of OPTIMEM and lipofectamine dilutions were prepared in separate sterile Eppendorf tubes (2-10 µl of lipofectamine in 50 µl of OPTIMEM). The DNA and lipofectamine were then combined to allow DNA: Lipid complexes to form and incubated for 20 minutes at room temperature, then added to the cells for 6 hours at 37˚C. The medium was changed back to complete medium for 24 hours post transfection. Positive selection was then performed by

adding 5 μM Puromycin to the medium for 48 hours after transfection. Cell islands were then allowed to grow in the absence of Puromycin and expanded to T175 flasks.

To verify that the T175 cultures retained the plasmid after growth in the absence of Puromycin containing selection media, $2x10^5$ WT and pCW-Cas9 treated cells were seeded at a density of $4x10^5$ cells /ml in a sterile 24 well TC plate and allowed to adhere overnight. Cells were then subjected to a titration of Puromycin (2.5-0.1 μM) in complete cell medium for 48 hours and cell viability measured through trypan blue exclusion, relative to unstimulated (complete medium – Puromycin) and positive control (complete medium + 1% Triton X) shown in Figure 2.9.

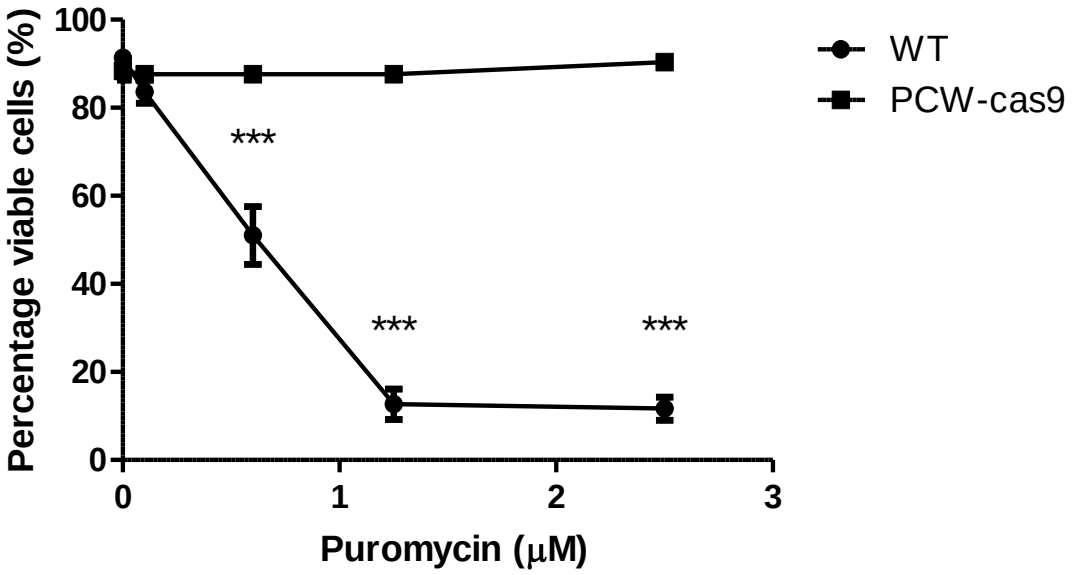

*Figure 2.9. Trypan blue exclusion of WT and PCW-CAS9 transfected SW 982 cells treated with a titration of Puromycin for 48 hours. PCW-Cas9 transfected SW 982 cells demonstrated statistically significant protection to Puromycin mediated cell death relative to WT controls, validating transfection and construct expression. Data presented as mean +/- SEM from a single experiment, representative of two experiments. Data analysed by two-way ANOVA (*** = P<0.001.)*

2.29 - Purification of total RNA from SW 982 synoviocytes

To verify the loss of expression of NLRP3 from the CRISPR/Cas9 treated cells, RNA was collected for analysis with reverse transcriptase PCR (RT-PCR). The mRNA extraction was performed using the Sigma GeneElute mammalian total RNA miniprep kit. The buffers provided with this kit came supplied, and details of formulation are not available on the company website. $2x10^5$ SW 982 WT and CRISPR/Cas9 treated cells were seeded per well at a density of $4x10^5$ cells/ml in a 24 well, sterile, flat bottomed sterile plate and allowed to adhere overnight at 37°C. On the day of the experiment, complete media was replaced (500 µl) and cells were primed with 100 ng/ml LPS for 4 hours to elevate NLRP3 expression or left unstimulated as controls. The cells were washed using 1x sterile PBS and lysed in 250 µl RNA extraction buffer + 1:1000 v/v β mercaptoethanol. Cell lysate was then mixed with 250 µl of 70% ethanol solution, then added to the RNA binding column, centrifuged at 13,000 x g for 15 seconds, and the flow through discarded. The column was washed with 500 µl of wash buffer W3136 and centrifuged at 13,000 x g for 15 seconds, washed again with 500 µl of buffer W3261, then eluted using 50 µl of buffer E8024 and centrifugation at 13,000 x g for 1 minute through the column. Eluent was collected, concentration and A260/280 nm ratio measured on the Nanodrop, and mRNA was stored at -80°C until use.

2.30 - Reverse Transcriptase PCR

To perform the RT-PCR, the Superscript III One-step RT-PCR kit (Thermofisher) was used. The procedure was performed as recommended in the generic guide provided with the kit. The primer pair used for NLRP3 amplification was purchased from Thermofisher (Primer ID: Hs00315580_CE, forward primer sequence: TCTCACTTCAATCCACTGGTTGATA, reverse primer sequence: TTAGCCAAATGCTTACCAGAAAGTT, expected amplicon length: 499 bp).

The PCR reaction mixture was prepared with 21 µl of diluted template RNA added per tube giving final concentrations of 200 ng of RNA per tube to ensure template mRNA was within optimal range for amplification. The concentration of RNA from samples taken from stimulated SW 982 cells was measured by Nanodrop A230 nm to ensure equal loading in to

the PCR tubes. The remaining PCR mixture consisted of 25 µl of 2x reaction mixture (Superscript One step PCR Kit), 21 µl of sample RNA (diluted in RNA free water with 200 ng of total RNA per sample), 1 µl of forward and reverse primers and 2 µl of Superscript III RT / Platinum Taq mix added per PCR tube.

To perform RT-PCR, the thermocycler was preheated to 54°C for 15 minutes prior to experiment starting. The thermocycling protocol was as follows: CDNA synthesis and denaturation at 54°C for 20 minutes, followed by pre-denaturation at 94°C for 2 minutes. Amplification was performed by cDNA denaturation at 94°C for 15 seconds, annealing at 63°C (average of calculated optimum annealing temperatures of forward and reverse primers, 61.2°C and 64.4°C respectively). Extension was performed for 1 minute each cycle for the 499 bp expected amplification product. Denaturation, annealing and extension was performed for 40 cycles and a final extension step added at the end of the final cycle at 68°C for 5 minutes.

Following the RT-PCR process, half (25 µl) of RT-PCR product was then mixed 1:1 with 2x agarose gel loading dye and loaded on to a 1% agarose gel containing 50 µg of Ethidium Bromide for DNA visualisation. The agarose gel electrophoresis was performed as previously described, until the loading dye front had migrated at least half the length of the gel. A broad range molecular weight marker (10kb-80bp) was used to measure PCR product bp size. The gel was subsequently visualised using the Thermofisher MyECL system.

Chapter 3: Establishment of protocols for complement attack on nucleated cells

3.1- Introduction

To mimic the effects of complement activation *In vivo*, systems had to be generated which would allow complement activation on target cells, from a serum or purified protein source, at a sublytic level (<10% cell death above baseline). The establishment of a reproducible sub-lethal system is crucial to allow the dissection of lytic and non-lytic effects of MAC on inflammatory signalling.

Previous work on MAC mediated activation of NLRP3 has utilised a variety of methods for this process. One method utilised heterologous serum to circumvent the need for sensitisation with antibody, subsequently demonstrating a complement mediated induction of IL-1β secretion and Caspase-1 release at sublytic levels in LPS primed Dendritic cells (Laudisi *et al* 2013). In other studies, the capacity of complement activators which are avidly opsonised was investigated in the context of NLRP3 activation. Whilst the focus of the work was on C3 products and NLRP3 activation, an experiment using reactive lysis generated MAC was performed and robust IL-1β production demonstrated; however, percentage cell viability in response to attack was not reported (Suresh *et al* 2016).

Another paper, published by our group, measured non-lytic MAC in the context of NLRP3 activation using homologous serum in a CP system (rabbit polyclonal anti-CD59 as a complement activator) and demonstrated clear titrations of cell death and C9 deposition on the cell surface as well as terminal pathway dependency using complement depleted sera (Triantafilou *et al* 2013).

Despite the differences in experimental procedure, each of these studies came to the same conclusion; the MAC is needed for complement mediated NLRP3 activation. It is therefore critical to demonstrate that the systems used in this body of work firstly replicate this dependence on MAC, whilst also maintaining the clear separation of lytic and sublytic MAC activities. This was investigated using both reactive lysis and CP systems, optimised for the subsequent experiments investigating NLRP3 activation.

3.2 - Methods of purification and validation of function of complement terminal pathway components from normal human serum

Complement terminal pathway components are abundant in NHS, with C5 the most abundant at ~80 μg/ml; however, the acute phase nature of the terminal pathway components, with the exception of C7, can result in higher concentrations in disease (Noris and Remuzzi 2013). To purify these proteins via classical chromatography methods requires large volumes of serum and a multistep process requiring salt cuts, ion exchange and size exclusion chromatography to yield a pure final product (Van den Berg 2000). However, affinity chromatography utilising monoclonal antibodies against terminal pathway proteins allows efficient purifications in a single step. Affinity columns comprising monoclonal antibodies against C5, C6, C7, C8 and C9 immobilised on Sepharose were generated as described in materials and methods Purification was performed on donor plasma from expired platelet bags, with 50 – 100 ml of donor plasma applied to the column twice to maximise purification yields. An example chromatogram for purification of C9 from 50 ml pooled human plasma is shown in Figure 3.1. Purified affinity eluents were collected, and fractions pooled and dialysed in to CFD overnight at 4°C. Purified components were then subjected to SDS PAGE with Coomassie staining or western blotting to verify protein identity (Figures 3.2 and 3.3

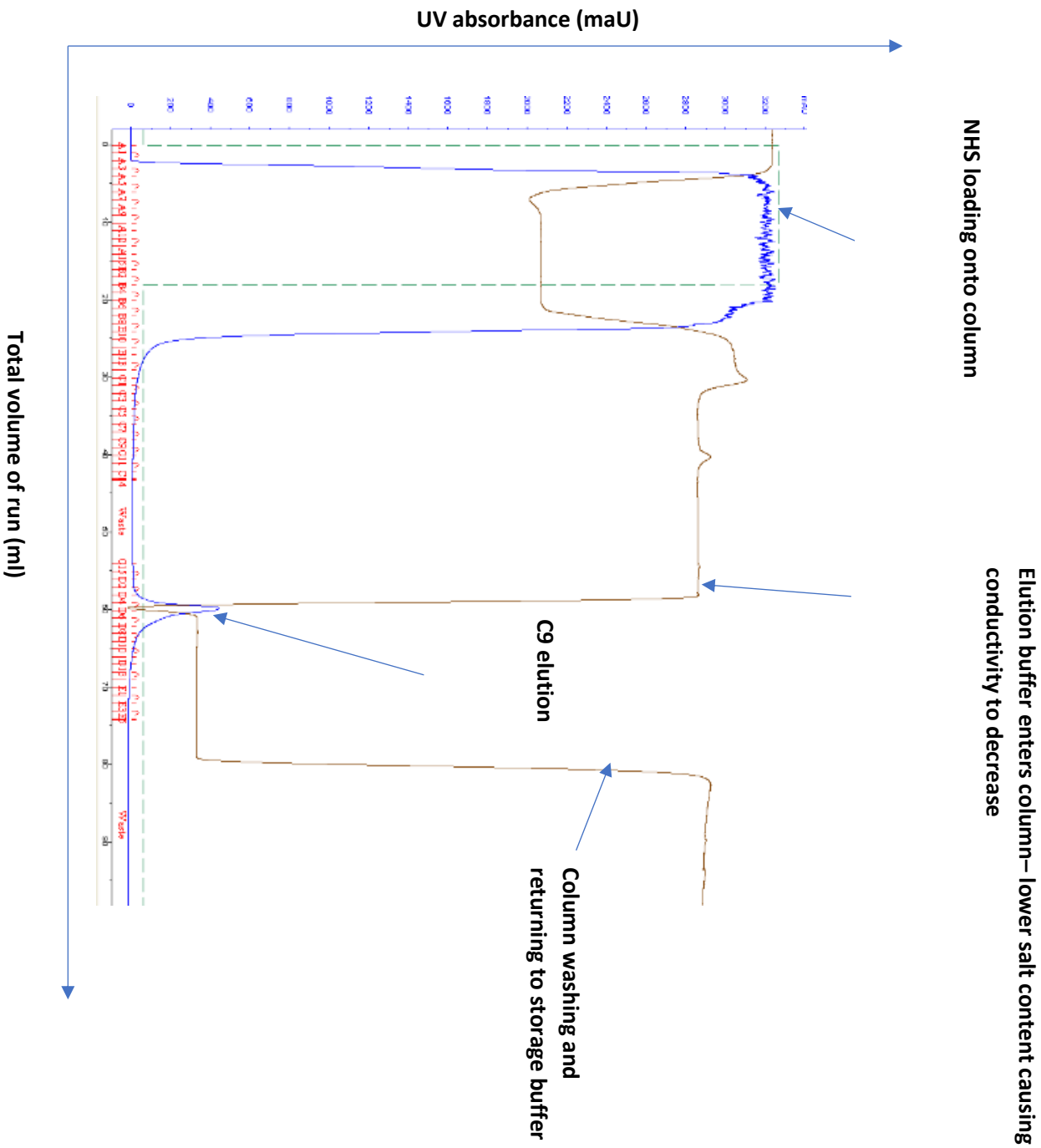

Figure 3.1. Representative chromatogram of complement component C9 purification by affinity chromatography using a Hi-TRAP NHS activated column with 23mg of B7 (in house anti C9 antibody) coupled. 50 ml of pooled NHS was loaded onto the column under low salt, natural pH conditions (10 mM TRIS, 150 mM NaCl, pH 7.4) to facilitate protein binding to the column coupled antibody. NHS loading on the column generates, a large, saturating UV signal (initial blue peak) due to the high protein content. As the pooled NHS is washed off the column, the UV signal drops and the buffer flows to the waste valve. The bound protein is then eluted using 5x column volumes of elution buffer(1 M Glycine, 10 mM TRIS pH 4). Protein positive fractions were immediately neutralised with 100 µl of 1 M TRIS pH 10, pooled and dialysed overnight into CFD buffer at 4˚C prior to testing for function and purity.

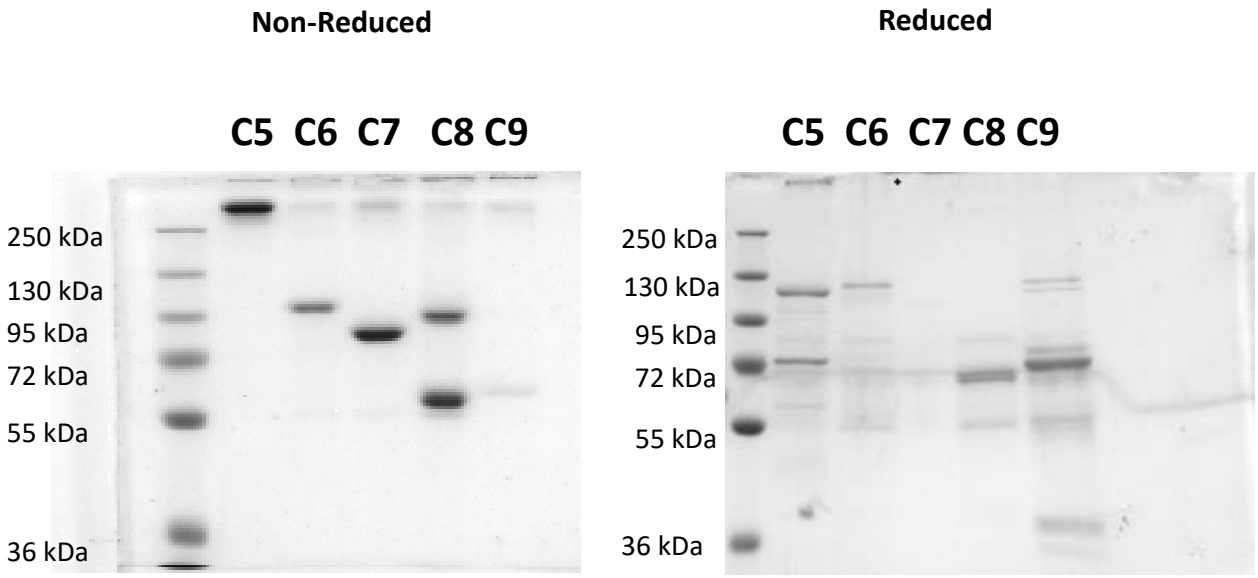

Figure 3.2. Coomassie stained SDS PAGE of purified complement terminal pathway components. 1 µg of purified protein from affinity purifications was denatured (90 °C for 10 minutes) and loaded on to 4-20% gradient polyacrylamide gels (BioRad) under reducing or non-reducing conditions. Pageruler Plus pre-stained protein ladder (Thermofisher) was loaded in to Lane 1 of both gels. SDS-PAGE was performed under a constant Voltage of 120V for 1 hour. Gels were then stained using Coomassie staining solution for at least 1 hour at room temperature. Gels were subsequently destained using destain solution with 5x 10-minute washes. Gels were then visualised using the Thermofisher MyECL system. C5 molecular weight – 183 kDa, α chain 110 kDa, β chain 75 kDa. C6 molecular weight – 95 kDa, C7 molecular weight – 110 kDa but runs around 86 kDa under SDS PAGE (Stahl et al 2000) C8 – 163 kDa intact, upon reduction α/β chains run at 64 kDa and γ at 24 kDa, C9 molecular weight 79 kDa.

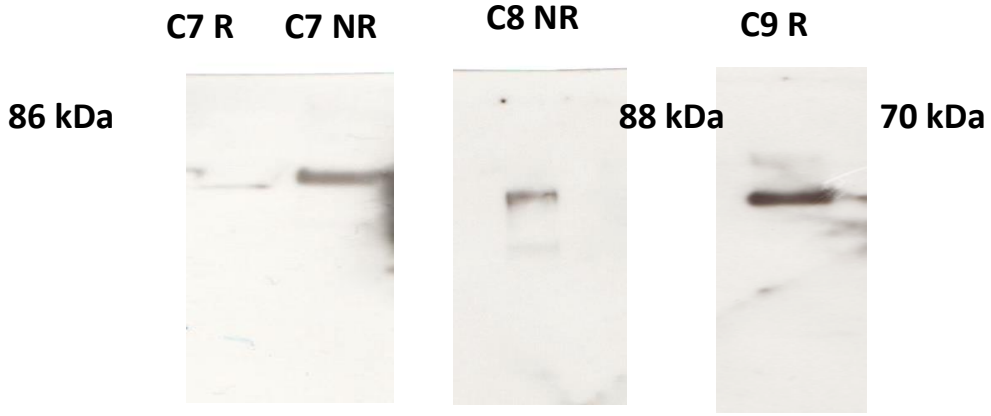

Figure 3.3. Western blots of purified C7, C8 and C9 proteins. 1 µg of purified protein from pooled stocks was denatured at 90 °C for 10 minutes and loaded under reducing or non-reducing conditions on a BioRad precast 4-20% gradient polyacrylamide gel. Samples were then subjected to SDS PAGE for 1 hour at a constant voltage of 120 V. Gels were removed and transferred onto nitrocellulose membranes for 1 hour at 100 V using the wet transfer system. Effective protein transfer was denoted by the transfer of the pre-stained Pageruler Plus ladder to the membrane. Membranes were blocked with PBS 5% w/v skimmed milk powder for 1 hour at room temperature, washed using PBS 0.1% v/v TWEEN and probed for the respective proteins (C7 – In house 27D10 anti human C7 polyclonal, C8 – In house J1 mouse anti human C8 monoclonal, C9 – In house rabbit anti human C9 polyclonal). Primary antibodies were used at 1/1000 dilution. Membranes were washed using PS 0.1% v/v TWEEN 3x15 minutes and before respective secondary antibodies were applied at 1/5000 dilution in PBS 5% w/v BSA. Membranes were again washed for 3x 15 minutes in PBS 01% w/v TWEEN and before 1 x 30-minute wash in ddH_2O. Chemiluminescent visualisation was performed using ECL reagents from GE as per manufacturer's instructions and exposed to Amersham Hyper film for 3 minutes for final blots.

To generate an active C5b6 complex, two methods were employed. Initially, a freeze thaw method was used due to the difficulty in generating C5b6 (Dessauer *et al* 1985). To form an active complex, purified C5 and C6 were mixed in an equimolar ratio and incubated at 4˚C for one hour. The mixture was subsequently frozen at -80˚C for 24 hours before rapid defrosting in a water bath at 37˚C. The reaction of C5 and C6 in this manner yields no detectable C5a biological activity; however, it enables generation of a MAC precursor with lytic function similar to the native C5b6 complex. A drawback to this method is that the C56 complex generated through freeze thaw is unstable and rapidly decays, requiring the thawed product to be used within 3 hours and kept on ice to preserve activity (Cole thesis 2005).

To determine this activity for future experiments on nucleated cells, the C56 complex was incubated on guinea pig erythrocytes (GPE) in a reactive lysis haemolytic assay. GPE's were used for reactive lysis assays due to the lack of expression of CD59 on the cell surface, rendering the cells highly sensitive to complement mediated lysis (Boshra *et al* 2017). A titration of initiating C56 complex was applied to a fixed dilution of GPE for 10 minutes at room temperature in CFD + 10 mM EGTA before C7 addition in molar excess and a further 15-minute incubation at 37˚C for 15 minutes. C8 and C9 were then added at a molar excess to the C5-7 complex and incubated for a further hour at 37˚C. Intact GPE were pelleted by centrifugation at 4˚C at 300 x g for 10 minutes and 100 µl of the haemoglobin containing supernatant aspirated and transferred to a 96 well, flat bottomed clear plate. Absorbance at 405nm was measured, corresponding to released haemoglobin and shown in Figure 3.4 A/B. Positive and negative controls (GPE + water, 1% TWEEN 20 positive and GPE + CFD only negative) were employed as well as a GPE's + C56 exposed + 10% NHS with 10 mM EDTA as a source of terminal pathway components. This was to ensure any negative results were due to a lack of C56 function as opposed to a problem with the preparation of any other terminal pathway components. A major caveat of this method is the inability to effectively quantify the conversion of C5 and C6 to the functional C56 complex; hence, the stated doses of C56 complex in Figure 3.4 assume complete conversion of C5 and C6 to C56; however, efficiency is likely low and the actual working concentration of complex far lower.

Percentage haemolysis was quantified by the equation: Percentage haemolysis = ((Positive control – Negative control) – (Sample – Negative control)) x 100.

In this experiment, the negative controls was GPE's in 100 µl of CFD only without the addition of any complement components. The relatively high rates of background haemolysis (around 8-10%) of negative control samples (such as C56 only) may be attributable to the multiple rounds of pipetting in this method incomplete dialysis of the elution buffers used in component purification which may slightly alter absorbance values.

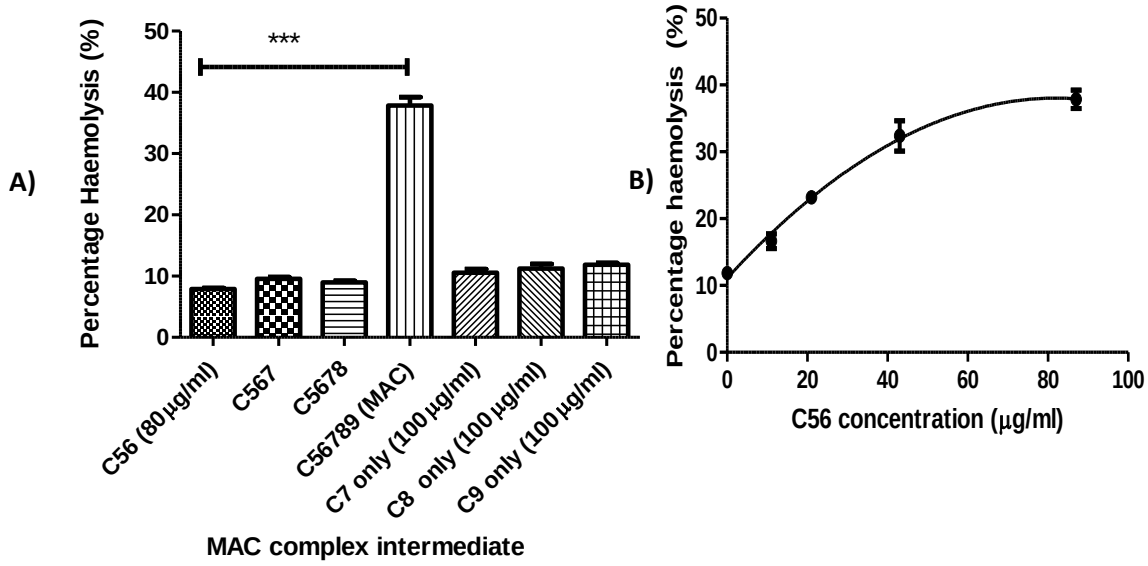

Figure 3.4.A. Titration of haemolytic activity of C56 generated by freeze thaw of purified C5 and C6 proteins. The MAC complex was assembled as described above with the C56 initiating complex as the limiting component by concentration. C56 was added to guinea pig erythrocytes in 96 well, U bottom plates at the denoted concentrations for 10 minutes at room temperature in CFD buffer. C7 was subsequently added in molar excess (80 µg/ml) for 15 minutes at 37 °C. C8 and C9 were subsequently added (both at 80 µg/ml) for 45 minutes at 37 °C. Plates were centrifuged, cells pelleted and haemoglobin containing supernatant transferred to flat bottom plates and absorbance at 405nm measured. Percentage haemolysis was quantified relative to CFD only negative and water + 0.1% v/v positive controls. Haemolytic activity of the complex was fully dependent on the addition of C9 as C56, C567 and C5678 complexes exhibited no significant increases in haemolysis at any concentrations of C56 used . The haemolytic capacity was also demonstrated to be independent of C9 addition alone, as the C9 only control failed to induce haemolysis. Data was analysed using a one-way ANOVA with a Dunnett post-hoc test to compare all groups of the assembling MAC complex to the complete MAC sample. The MAC induced haemolysis was statistically significantly higher than initiating complex or components alone (One-way ANOVA with Dunnett post-hoc test, all groups compared to C56789 $P < 0.001$). Data presented as the mean +/- SEM from a single experiment, representative of three independent experiments. B. A titration of haemolysis induced by MAC (C56-9) relative to the amount of C56 initially deposited on the cells with constant concentrations of C7-C9 used. This demonstrates a C56 dose dependent response. Representative data from one of three independent experiments. Data displayed as mean +/- SEM.

To circumvent the issues surrounding the C56 system, predominantly the inaccurate quantification of the initiating complex, methods of generating a C5b6 complex were explored. Initially, C7 depletion of serum utilising affinity chromatography prior to activation using zymosan (1 mg/ml) was attempted to arrest complement activation at the C5b6 stage and then subsequent purification via SEC / Mono Q cation exchange. However, C7 depletion of NHS to an extent sufficient to limit complement activation at the C5b6 stage was not achieved with the affinity columns available or generated at that time. Residual haemolytic activity was present in NHS despite low volumes of donor normal human serum (10 ml) being run over the available anti-C7 affinity columns at the time three times ; therefore, an alternative method was required. It should be noted, superior affinity columns were generated later and used to effectively deplete C7 from NHS to generate C7 depleted NHS. A second way of generating C5b6 is via the activation of purified proteins through the C3/C5 convertase analogue cobra venom factor (CVF) from *Naja Naja Kouathia* which activates both C5 and C3, making it ideal for this application.

3.3 - Purification of CVF from whole cobra venom and validation of function

CVF is a 146 kDa protease which is the complement activating agent in Cobra venom. Whole cobra venom was obtained and lyophilised, reconstituted in 1 ml of 10 mM TRIS buffer pH 7.2 containing 10 mM EDTA. This solution was loaded onto a Mono Q anion exchange column and eluted using a linear gradient of 0-0.5 M NaCl, with a final 1 M NaCl wash to clean the column. Protein containing fractions were collected and stored on ice prior to assaying complement activating function, with the MONO Q AKTA trace show in Figure 3.5.

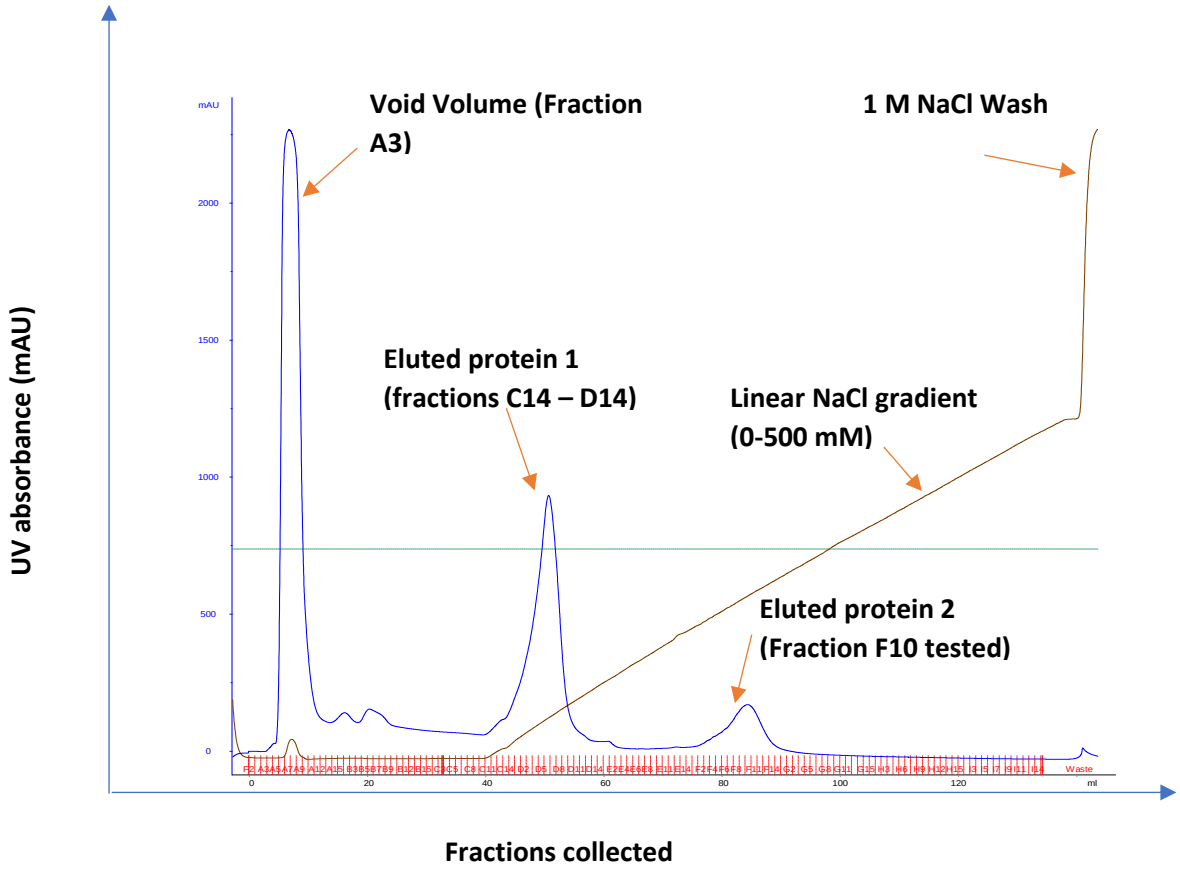

Figure 3.5. AKTA trace of Mono Q anion exchange column elution of Cobra venom. 10 ml of reconstituted cobra venom was concentrated using 100 kDa cut off spin columns through centrifugation at 10,000 x g and was reconstituted in 10 mM TRIS buffer. Reconstituted venom was loaded on to the AKTA via a 1 ml loading loop. The AKTA programme was then run and the sample loop loaded on to the Mono Q anion exchange column. Large amounts of protein came through the column in the void volume, as determined by the large UV peak (Blue) in the early fractions. This is most likely caused by proteins with a positive net charge at pH 7.4 and therefore did not interact with the positively charged MONOQ column matrix. The protein which bound the matrix was then eluted with a linear gradient of NaCl (0-0.5 M) and protein containing fraction peaks pooled and assayed for haemolytic function. The column was flushed through with 1 M NaCl to ensure no protein remained bound. Eluted, protein containing fractions were collected and kept separate to test for functionality by haemolytic assays.

To test the haemolytic capacity of the eluted fractions, fractions from each of the protein peaks eluted were added to Guinea Pig erythrocytes in CFD + 10 mM EGTA to prevent classical pathway activation of NHS. The addition of 10% NHS provided a source of complement; however, without a functional CVF protein there would be no complement activation due to the EGTA preventing classical pathway activation on GPE cells, with the haemolytic titrations of each purification fraction shown in Figure 3.6.

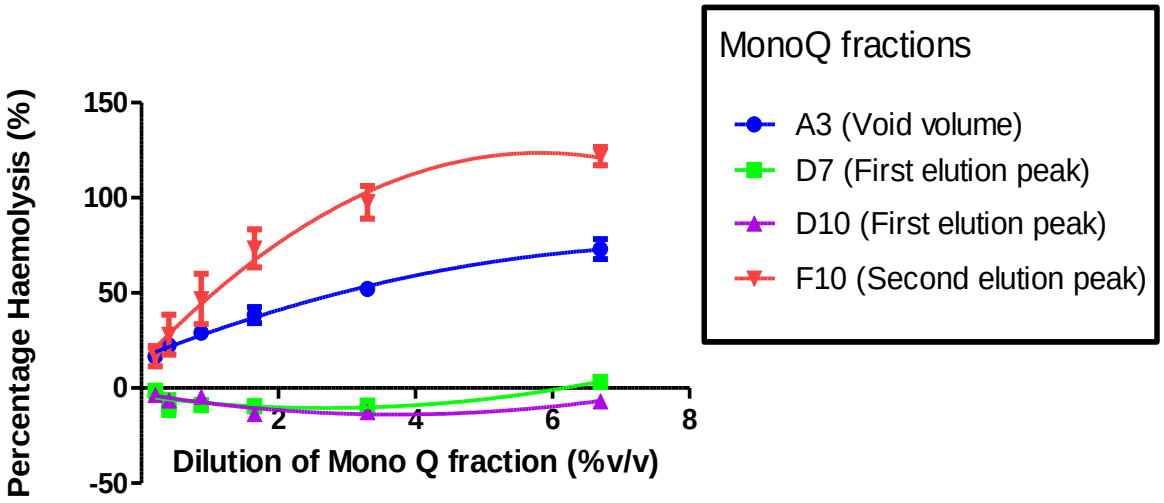

Figure 3.6. CVF Mono Q fractions corresponding to elution protein peaks were assayed for haemolytic capacity. GPEs in CFD + 10 mM EGTA were incubated with serial dilutions of the Mono Q fractions as denoted, in the presence of 10% v/v NHS as a source of complement for 1 hour at 37 ˚C in 96 well, U-bottomed plates. Plates were subsequently centrifuged, GPEs pelleted and haemoglobin containing supernatant transferred to flat bottom plates for absorbance reading at 405 nm. Percentage haemolysis was quantified relative to water + 0.1% TWEEN positive and 10% NHS with no CVF negative controls. Run through fractions (A3) and second eluted peak (F10) demonstrated titratable haemolytic activity whilst D10 (first eluted peak on the NaCl gradient) did not. The haemolytic capacity of A3 may be derived from Cobra venom phospholipases which did not bind the Mono Q column at the given pH. Haemolytic capacity of F10 fraction was statistically significantly higher than D10 and D7 fractions, with no significant difference observed between F10 and A3 fractions (P<0.01, One-way ANOVA with Dunnett post-hoc test, comparing all groups to F10 fraction).

The fractions in the peak including F10 demonstrated haemolytic capacity, but not the peak corresponding to the D10 fraction. Therefore, to confirm the identity of the haemolytic agent as CVF and to determine the protein purity of the second eluent peak, fractions F6-F12 were pooled and SDS PAGE was performed under both reducing and non-reducing conditions with 2.5 µg of protein loaded per lane on a 4-20% gradient gel (Figure 3.7). The multichain structure of CVF consists of a 68.5 kDa α chain, a 48.5 kDa ß chain and a 32 kDa Y chain, disulphide linked to generate the functional protein at 144 kDa. Aliquots of CVF were then frozen at -20˚C until use. From an initial 100 mg of lyophilised total cobra venom, 1.2 mg of purified CVF was obtained.

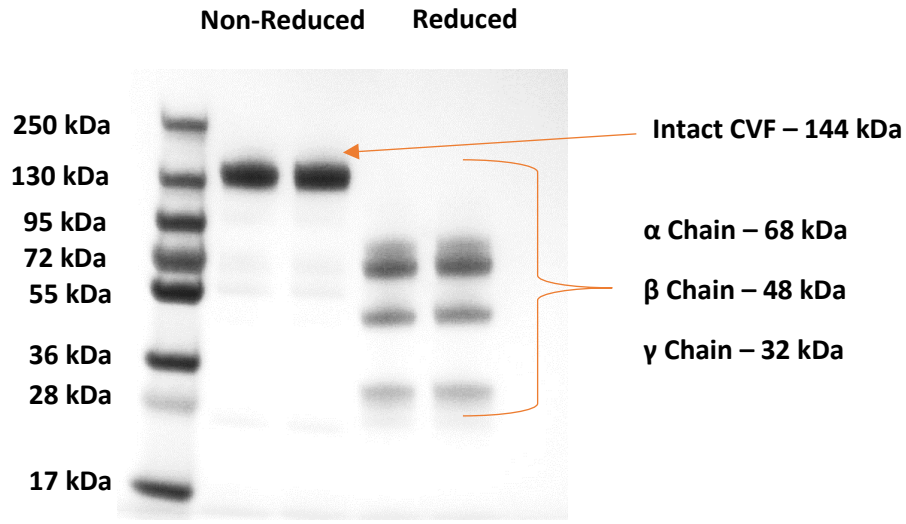

Figure 3.7. SDS PAGE of fractions F6 – F12 from Mono Q purification of CVF from whole Cobra venom (Naja Naja Kaouthia). 2.5 µg of pooled protein from Mono Q elution fractions F6-F12 was denatured at 90 °C for 10 minutes and loaded on a 4-20% gradient polyacrylamide gel under reducing or non-reducing conditions. Gels were subjected to SDS PAGE at a constant voltage of 120 V for 1 hour, before gels were stained in Coomassie solution for 1 hour at room temperature. Gels were subsequently washed and destained as previously described, and visualised using the Thermofisher MyECL system.Intact CVF, which is retained in the non-reduced samples, was observed at around 140 kDa as expected, whereas the α, ß and γ chains were generated upon reduction at 68, 48 and 32 kDa respectively.

3.4 – Generation and purification of functional C5b6 complexes

Purified CVF was then utilised to generate C5b6 complexes using a modification of a published method (DiScipio *et al* 1983). CVF (10 µg) was incubated with 10 µg of FB and 1 µg of FD in CFD buffer at 37˚C for 15 minutes to form a functional CVFBb convertase. C5 and C6 (1 mg of each component) were added and incubated in the presence of the convertase overnight at 37˚C. The product was then dialysed at 4˚C into size exclusion chromatography buffer (10 mM sodium phosphate, 150 mM NaCl pH 7), concentrated to a 1 ml final volume using Vivaspin 500 centrifugation column with a 100 kDa MW cut off, and injected into an equilibrated SD200 size exclusion chromatography column on the AKTA FPLC, with the resulting chromatogram shown in Figure 3.8. Protein-containing peaks from the SEC experiment were collected and assayed for haemolytic capacity.

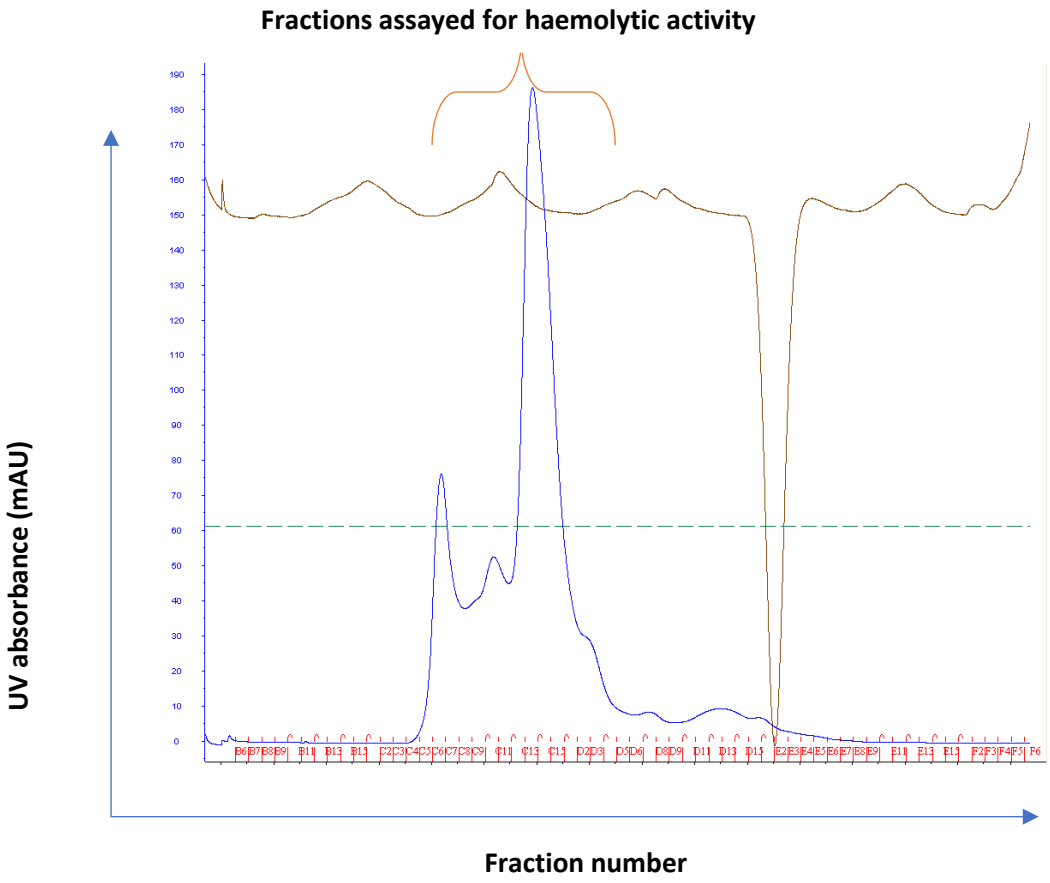

Figure 3.8. Size exclusion chromatography (SEC) trace of C5b6 preparation using CVFBb to cleave C5; generated C5b then binds C6 to form active C5b6 complexes. The reaction mixture of the C5, C6, FB, FD and CVF reaction described above was concentrated using 100 kDa cut off spin columns and loaded on to a Superdex 200 size exclusion column on the AKTA FPLC system in 10 mM TRIS, 150 mM NaCl via sample loop. The loop was subsequently flushed through with 10 mM TRIS, 150 mM NaCl and loaded on to the Superdex column. Protein containing peaks were retained for individual testing for haemolytic activity and SDS PAGE analysis.

To determine if any of the protein-containing fractions contained C5b6 as opposed to individual complement components or CVF, haemolysis and SDS PAGE were performed. From each of the SEC fractions 15 µl was removed, mixed with an equal volume of 2x non-reducing SDS loading buffer, separated on a BioRad 4-20% gel and Coomassie stained. Commercially available C5b6 was run alongside the fractions to demonstrate the expected banding patterns. SEC fractions C10 to C15 displayed a similar banding pattern to commercial C5b6 with bands tentatively identified as C5α', C5β and C6 co-eluting in the same fractions, shown in Figure 3.9.A, with the subsequent haemolytic testing shown in Figure 3.9.B.

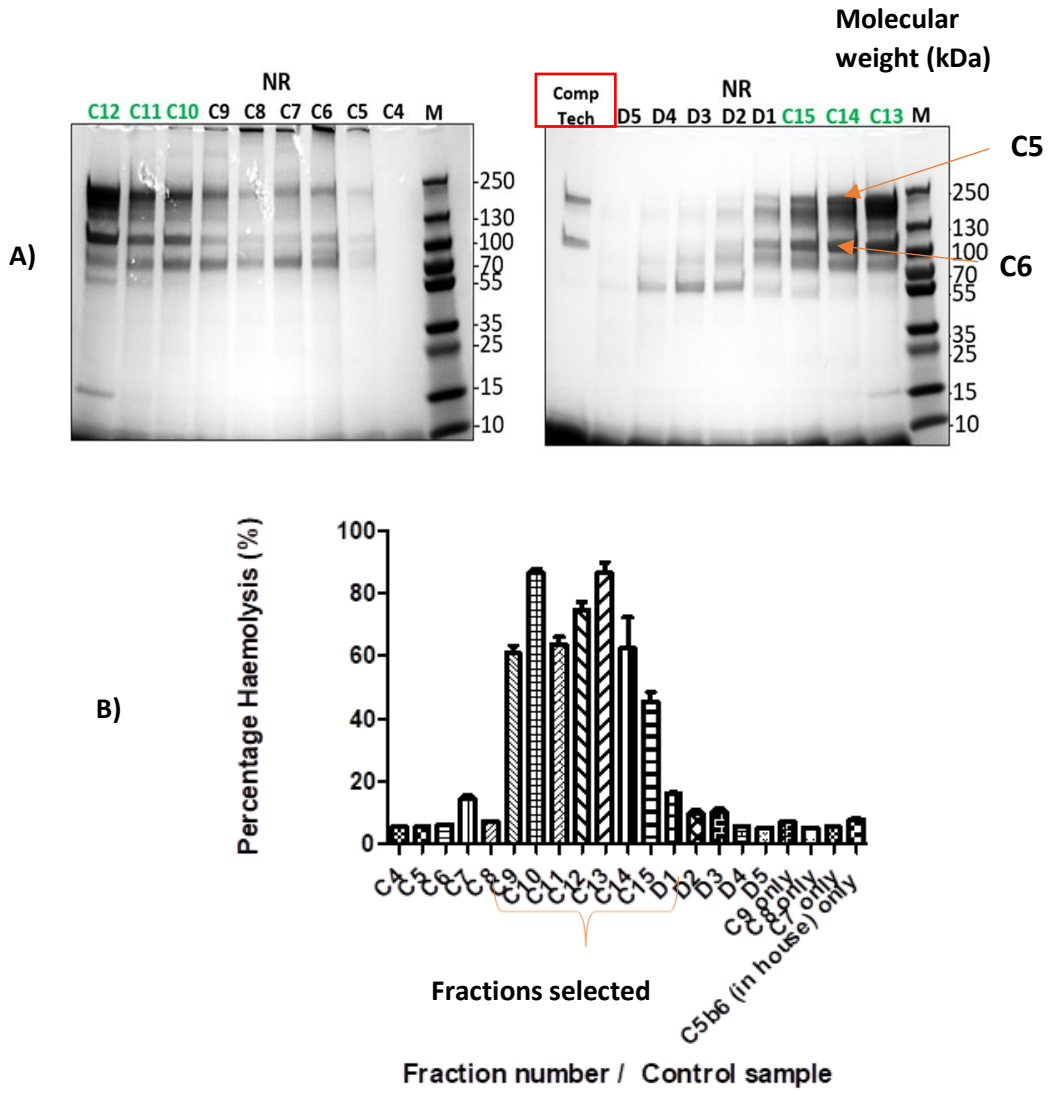

Figure 3.9.A. SDS PAGE of SEC fractions for C5b6 generation. 2.5 µl of each size exclusion chromatography fraction was loaded under non-reducing conditions on a BioRad 4-20% gel at a constant voltage of 120V for 1 hour. Gels were subsequently coomassie-stained and destained as previously described and images captured using the Thermofisher system. Commercially sourced C5b6 (Comptech) was also run on the gel to compare with the generated protein. M – molecular weight marker, C4 – D5 represent SEC fractions collected and compared to Comptech C5b6 protein (LH lane, RH gel). B. Haemolytic Screening of SEC fractions. GPE cells were incubated in CFD buffer in a 96 well U bottomed plate with 10 µl of SEC fractions for 10 minutes at room temperature, then with C7 (80 µg /ml) for 15 minutes at 37˚C, and finally with C8 and C9 (both 80 µg/ml) for 1 hour at 37˚C. Cells were centrifuged at 300 x g for 5 minutes to pellet intact GPE, supernatant was transferred to a flat bottomed 96 well plate and absorbance read at 405 nm. Percentage haemolysis was quantified relative to water + 1% TWEEN positive and CFD only negative controls. Data presented as mean +/- SEM from a single experiment, representative of two experiments.

Fractions C9 to C15 from the SEC elution demonstrated both similar Coomassie staining pattern to commercial C5b6 and haemolytic capacity and were therefore pooled, dialysed overnight at 4˚C into CFD and aliquoted and stored at -80˚C as a stock solution of C5b6 at 200 µg/ml until use. A final QC check was performed on the pooled C5b6 stock after dialysis to ensure function in the RL system; the stock was haemolytically active in this system (Figure 3.10). Further validation of the methodology of forming the MAC sequentially in a membrane associated manner as opposed to fluid phase assembly and insertion was performed by separately adding the MAC components in the fluid phase before exposing GPE cells to the soluble MAC complexes (Figure 3.10).

To perform this experiment, variations of the reactive lysis haemolytic assay protocol were used. Guine pig erythrocytes (2% v/v final concentration) were incubated in U-bottomed 96 well plates in 100 µl of CFD buffer. In a separate plate, C5b6 titrations (0.001 µg/ml – 0.5 µg/ml) were incubated with C7 + C8 + C9 (all at 1 µg/ml final concentration) in 50 µl of CFD for 30 minutes at 37° C. After the 30-minute incubation, C5b6 only (at the stated concentrations) was added to one set of triplicate titrations and incubated for 10 minutes at room temperature. Subsequently, C7 was added to this titration at 1 µg/ml and incubated at 37°C for 15 minutes. Finally, C8 and C9 were also added to the cells, both at 1 µg/ml, for 45 minutes at 37°C. At this point, the pre-incubated C5b6-9 from the second plate was transferred to GPEs in CFD to give a corresponding titration of pre-incubated components and also incubated on the GPEs for 45 minutes at 37°C. After incubation, U bottomed plates were centrifuged, supernatant transferred to a flat-bottomed plate and absorbance at 405nm measured as previously described. Concurrent with literature, C5b6-9 incubated in the absence of cells demonstrated minimal haemolytic activity, highlighting fluid phase C8 binding to C5b67 is a potent inhibitor of MAC mediated haemolysis (Nemerow, Yamamoto and Lint 1979).

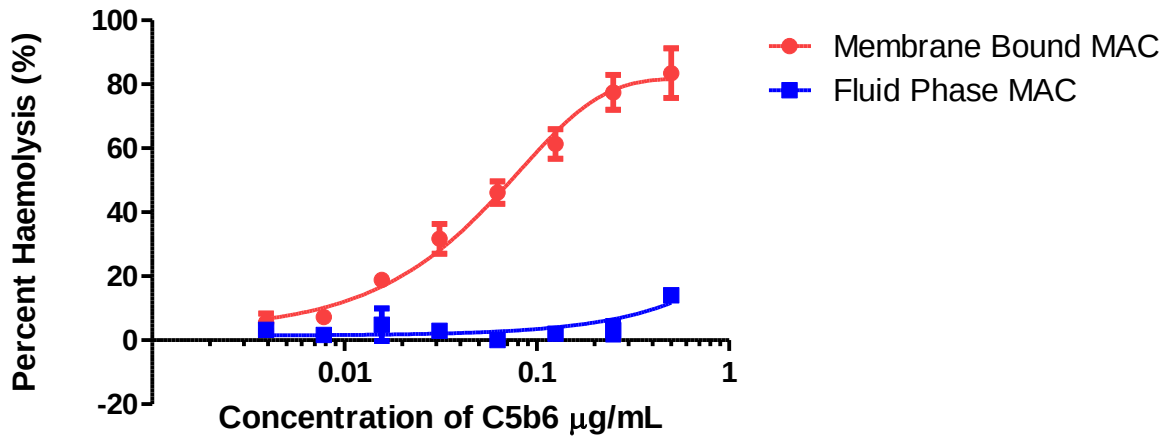

Figure 3.10. Pooled C5b6 fractions from SEC purification retain haemolytic capacity in RL system, whereas preincubated C5b6-9 in the absence of GPEs has minimal haemolytic capacity. GPEs (2% v/v final concentration) were incubated in a U-bottomed 96 well plate in 100 µl of CFD buffer. In a separate plate, fluid phase C5b6-9 was generated with a titration of C5b6 from 0.001 µg/ml – 0.5 µg/ml and all other components (C7+C8+C9) at 1 µg/ml together in CFD for 30 minutes at 37°C. A second titration was performed with identical concentrations of components sequentially added to GPEs. C5b6 was incubated on GPEs for 10 minutes at room temperature, C7 for 15 minutes at 37°C and C8 + C9 for 45 minutes at 37°C. The pre-incubated C5b6-9 complexes were added to the GPEs at the same time as the C8+C9 as the sequential component addition protocol. C5b6 complexes pre-incubated with C7, C8 and C9 in the absence of GPE at 37˚C for 45 minutes were haemolytically inactive; membrane bound MAC statistically significantly increased haemolysis relative to fluid phase MAC (Two-way ANOVA P=0.007). Data presented as mean +/- SEM from a single triplicate experiment representative of three independent experiments.

3.5 - Generation and validation of classical pathway system of MAC deposition

Nucleated cells exhibit a much higher resistance to MAC mediated lysis compared to erythrocytes due to their ability to mitigate MAC-induced chemiosmotic flux through expression of regulators, endocytosis and exocytosis of MAC pores, and active ion pumps to offset ion leak through the MAC pore. Due to this, effects of RL-generated MAC on nucleated cell death in my hands was limited and difficult to titrate in the manner performed on GPE's; it was therefore not possible to titrate a maximum sublytic dose using the RL system, reducing its value for investigating sublytic effects. To overcome this problem, a second system utilising classical pathway activation was optimised and titrated to identify maximum sublytic condition, with Propidium iodide staining and LDH release from THP-1 cells both used as measures of cell death, shown in Figure 3.11.

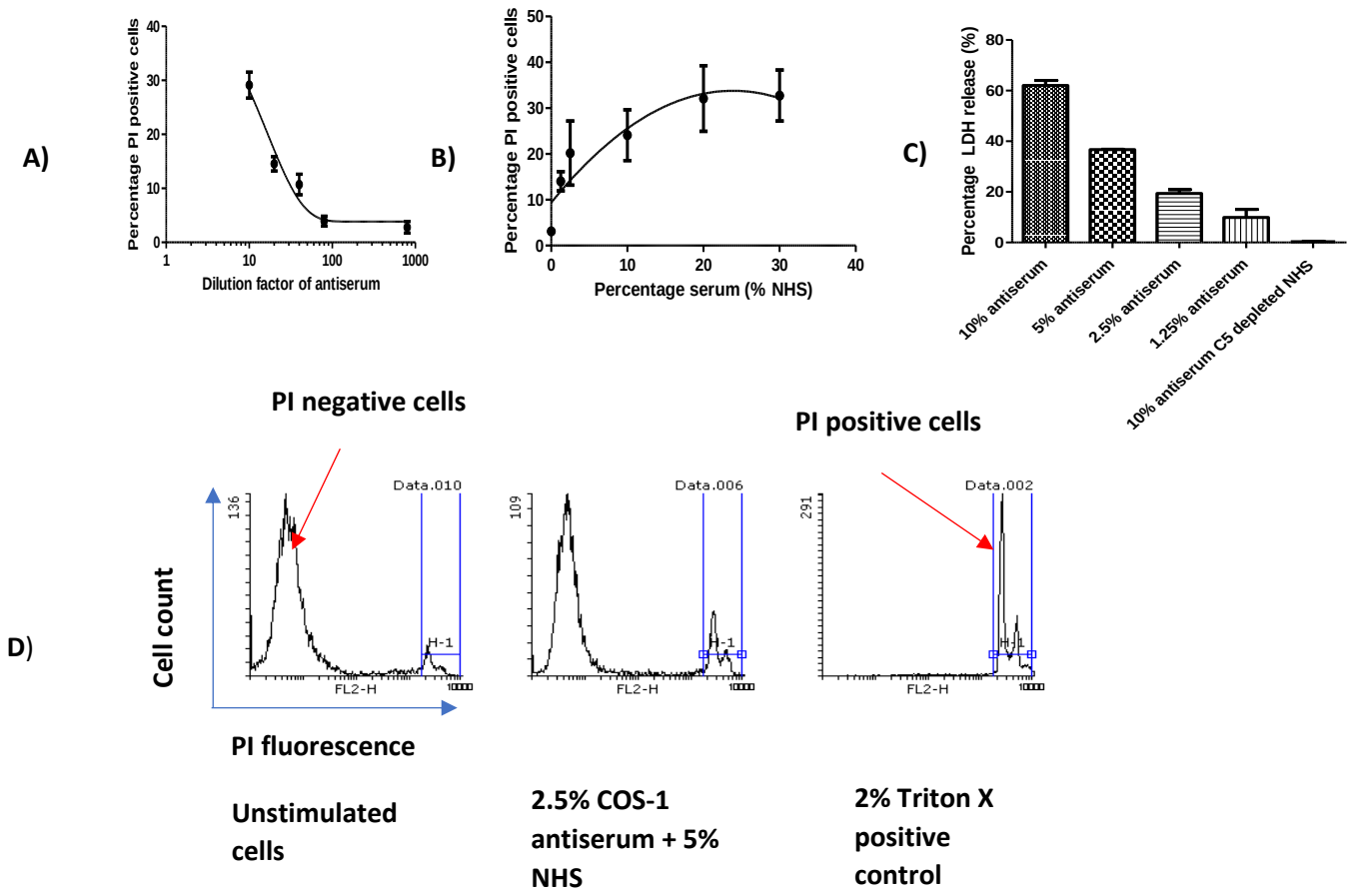

Figure 3.11. A. Classical pathway activation on THP-1 cells sensitised with COS-1 antiserum. 2x10^5 THP-1 cells seeded at a density of 1x10^6 cells /ml were incubated with titrations of COS-1 antiserum (10% - 0.1% v/v) for 20 minutes at room temperature in complete RPMI media. Cells were centrifuged at 300 x g for 5 minutes to pellet cells and remove unbound antibody before resuspension in complete RPMI and incubating with NHS / C5 depleted serum (5% v/v) for 1 hour at 37^{o}C. Cells were subsequently washed and resuspended into 200 µl FACS buffer and 10 µg/ml PI added. Cells were protected from direct light and analysed on the FACS Calibur flow cytometer. As positive control, cells were lysed with 2% Triton and PI positive cells gated relative to this. Negative controls included antiserum only, NHS only, and sensitised cells incubated with C5 depleted serum; all demonstrated <10% cell death (Data for negative controls not shown in figure). B. 2x10^5 THP-1 cells seeded at a density of 1x10^6 cells/ml were incubated with a constant dose of COS-1 sensitising antiserum (5%) in complete RPMI media in 96 well U bottom plates for 20 minutes at room temperature. Cells were centrifuged, resuspended and exposed to a titration of NHS (0-30% v/v). Cells were washed, resuspended in FACS buffer, PI added and assayed on the FACS Calibur as previously described. Data presented from a single triplicate experiment, representative of more than three independent experiments. C. LDH release assay. 2x10^5 THP-1 monocytes were seeded at a density of 1x10^6 cells/ml in a sterile 96 well U bottomed plate in complete RPMI media and COS-1 antiserum titrated from 10% to 1.25% v/v as previously described to sensitise the cells to complement. NHS or C5 depleted NHS were added at 5% v/v final concentration for 1 hour at 37 °C in complete RPMI media. Plates were then centrifuged and 50 µl cell supernatant transferred to new plate where LDH reagent was added 1:1 with supernatant and incubated protected from direct light for 45 minutes at room temperature. The assay was stopped using 50 µl of 10% acetic acid and absorbance read at 490 nm on the Magellan plate reader. Percentage LDH release was quantified relative to 1x lysis buffer and 5% NHS – antiserum activator positive and negative controls. demonstrating a dose dependent increase in LDH release with increased sensitising dose of COS-1 antiserum. Data displayed as mean +/- SEM from a single triplicate experiment, representative of three independent experiments. D. Example PI histograms for unstimulated, sublytic MAC attacked and triton-lysed positive control cells with the PI positive gate used for quantification displayed from samples stimulated with the methodology described for 3.11.A.

The dose of NHS / sensitising antiserum required to generated sublytic attack varied between experiments, presumably dependent on the original growth phase and confluence of the cells at the time of harvesting for the experiment; therefore, the sublytic dose was titrated prior to each experiment. Of note, C5 depleted serum demonstrated no significant cell death, allowing confidence the cytotoxicity induced was MAC dependent. The timescale in which the cell death was observed (1 hour), suggests an inflammatory and rapid form of death is involved in MAC-mediated nucleated cell death, as proposed by others (Elmore 2007).

3.6 - Measuring complement deposition on THP-1 cell surface

To further demonstrate complement activation on the THP-1 cell surface in the classical pathway sublytic attack system, flow cytometry staining for C3b and C9 was performed. For C9 staining, due to the transient nature of MAC deposition with cells rapidly shedding MAC through endocytosis and exocytosis, cells were fixed prior to staining, whereas the more stable C3 fragments did not require fixation. Cell stimulation and staining was performed as described in the materials and methods.

Antibody-sensitised THP-1 cells incubated with 5% NHS showed strong staining for C9, indicative of MAC formation, whereas all controls were negative (Figure 3.12). C9-staining was serum dose dependent and absent when sensitised cells were incubated with C5-depleted serum, demonstrating that there is complement terminal pathway deposition alongside the previously described decreases in cell viability.

A)

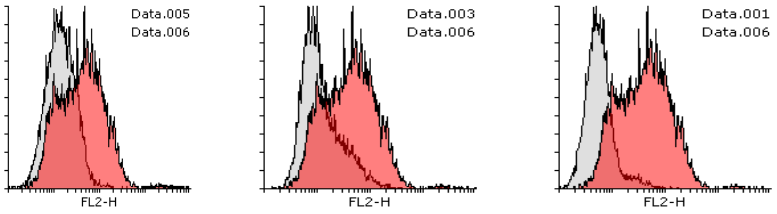

Unstained (Grey) v 5% NHS + COS 1 (Red)

Isotype control (Grey) v 5% NHS + COS-1 (Red)

NHS -COS1 (Grey) v 5% NHS + COS1 (Red)

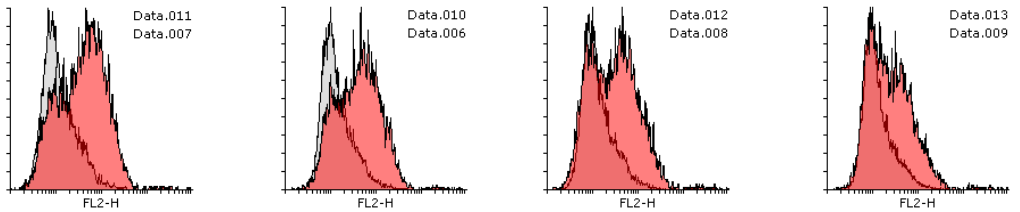

5% C5 depleted serum + COS-1 (Grey) v 5% NHS + COS-1 (Red)

2.5% C5 depleted serum + COS-1 (Grey) v 2.5% NHS + COS-1 (Red)

1.25% C5 depleted serum + COS-1 (Grey) v 1.25% NHS + COS-1 (Red)

0.5% C5 depleted serum + COS-1 (Grey) v 0.5% NHS + COS-1 (Red)

B)

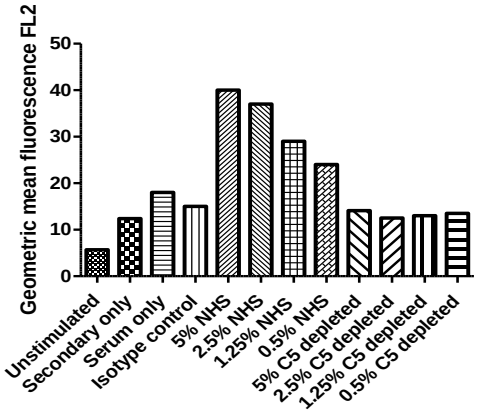

Figure 3.12.A. C9/MAC staining on THP-1 monocyte cell line. 2x10 [5] THP-1 cells were seeded at a concentration of 1x10[6] cells/ml in complete RPMI media and were sensitised to complement with 2.5% v/v COS-1 antiserum for 20 minutes at room temperature. Cells were washed with sterile PBS and resuspended in 200 µl of RPMI containing NHS or C5 depleted serum at the stated concentrations (all described as final % v/v) for 10 minutes at 37˚C. Plates were then centrifuged at 300 x g for 5 minutes, RPMI supernatant aspirated and cells fixed in 4% v/v PFA at 4˚C for 30 minutes. Cells were washed twice with sterile PBS and stained using the mouse monoclonal anti-C9 neoepitope antibody B7 (10 µg/ml in FACS buffer, on ice for 30 minutes) and subsequently rabbit anti-mouse IgG Alexa 546 (1/50 v/v dilution in FACS buffer protected from light for 20 minutes). Cells were again washed twice with sterile PBS and resuspended in 200 µl of FACS buffer and transferred to FACS tubes before fluorescence was measured on the FACS Calibur. Controls of unstained, Mouse IgG and 5% NHS without sensitising antibody were also used. B. Quantification of Geometric mean fluorescence of controls, NHS and C5 depleted serum titrations. Data presented from single replicates of a single experiment, representative of three independent experiments.

To verify complement activation was occurring on the cell surface, staining for C3b deposition was also performed. This was also undertaken to address recent observations in the literature that CD59/CD46/CD55 triple knockout cells demonstrated C3b deposition without a complement activator present, whereas CD55/ CD46 KO cells did not (Thielen *et al* 2017). This led to a proposed hypothesis that CD59 has roles beyond the regulation of the terminal pathway and may also regulate at the C3 convertase level. To address this, cells were sensitised as described in the materials and methods but also with and without the CD59 blocking antibody BRIC 229. It was hypothesised that if CD59 activity influenced C3b deposition in this system, cells with CD59 inhibition would have increased C3b staining. To verify that CD59 function was effectively inhibited, cell viability was also measured. A reduction in cell viability relative to cells with retained CD59 function was taken as an indicator that cell surface function was effectively inhibited.

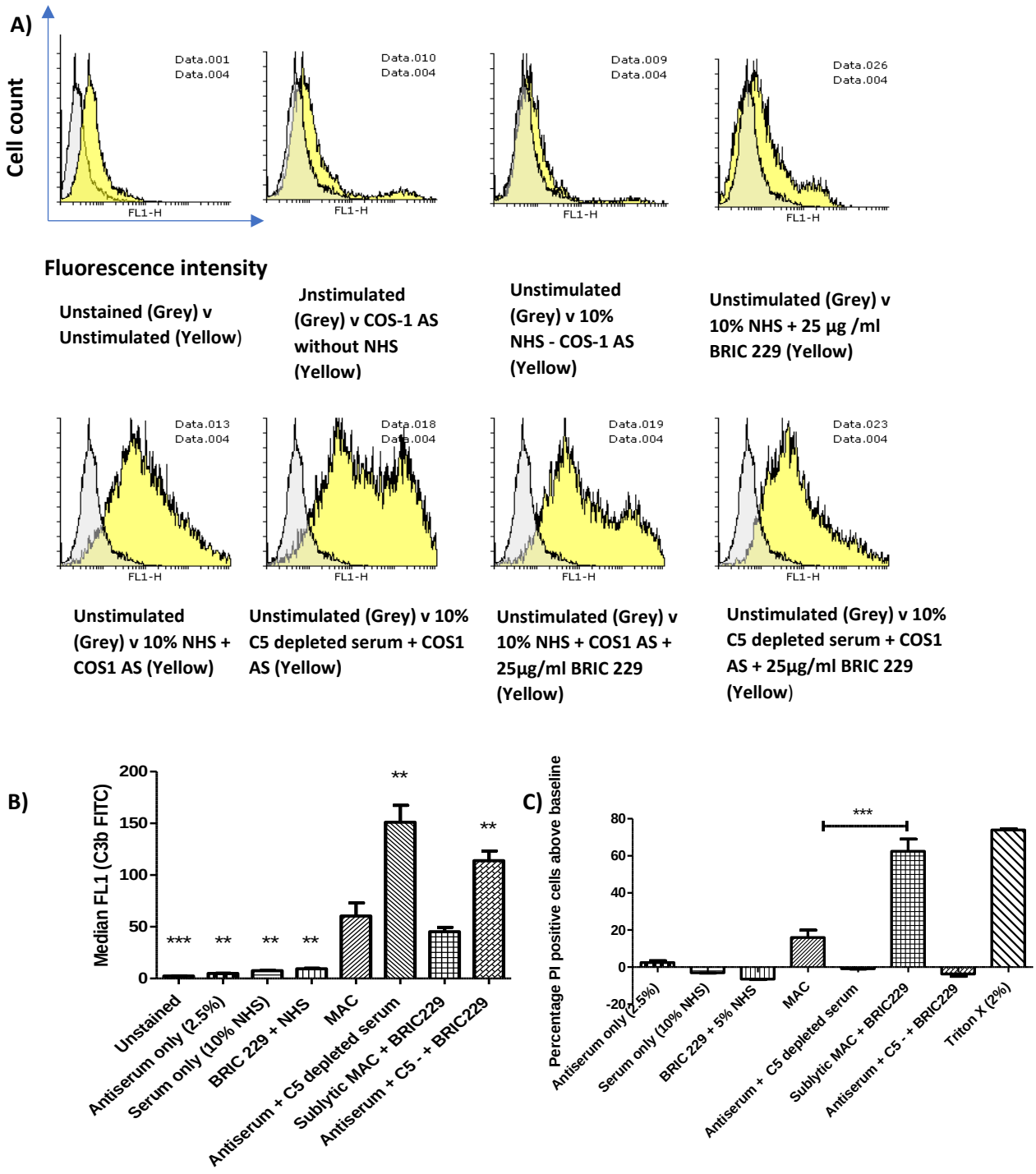

Figure 3.13.A. Histogram overlays of C3b staining relative to unstimulated samples, C5 depleted serum generated a double-peak pattern of C3b staining not observed with NHS. Histograms presented representative of triplicate samples. C3b deposition and cell death in THP-1 monocytes. 2x10^5 THP-2 monocytes were seeded at a density of 1x10^6 cells/ml in complete RPMI media. Cells were sensitised to complement using 2.5% v/v COS-1 antiserum as previously described +/- 25 µg/ml BRIC 229 for 20 minutes at room temperature. Cells were subsequently washed and resuspended in complete RPMI prior to complement deposition (5% v/v NHS or C5 depleted NHS) for 1 hour at 37 °C. Cells were centrifuged and resuspended in FACS buffer, prior to staining with Biolegend anti-C3b FITC antibody at a 1:100 dilution for 20 minutes protected from direct light. Cells were washed and resuspended in FACS buffer and transferred to FACS tubes before fluorescence measured on the FL-1 channel of the FACS Calibur. B. Quantification of mean fluorescence intensity of FITC-C3b staining of THP-1 monocytes from A. Significance determined by one-way ANOVA with Dunnett post-hoc test. Statistical significance tested relative to MAC without BRIC 229 sample. C. Comparison of PI positive THP-1 cells across control and stimulated samples with unstimulated

*control baseline subtracted. Experimental conditions were as described in 3.13.A for the stimulation of THP-1 cells. Upon stimulation with complement (COS-1 antiserum +/- BRIC 229 and NHS / C5 depleted NHS) cells were resuspended in FACS buffer and PI staining performed as previously described. Above baseline cell death was only observed with NHS + sensitising antiserum, which was statistically significantly increased with the addition of BRIC 229 anti-CD59 antibody. Data presented as the mean +/- SEM from a single experiment, representative of three independent experiments. Significance determined by One-Way ANOVA with Dunnett post-hoc test relative to MAC sample (** = P<0.01. *** = P<0.001).*

Whilst the previous experiments demonstrated no role for CD59 inhibition in C3b regulation, there was an interesting observation in that C5-depleted NHS, which caused neither haemolysis nor nucleated cell death, deposited more C3b on the cell surface than the same dose of NHS. To explore whether this was an artefact of the C5 depletion process yielding an increased level of C3 activation, or if the lack of terminal pathway has a real effect on activation and amplification, follow up experiments were performed. NHS was pre-incubated (30 minutes at room temperature) with Eculizumab at a dose sufficient to inhibit all C5 activity. The inhibitory concentration of Eculizumab was calculated as around 1.5x molar ratio of antibody to final C5 concentration. As NHS was used at 5% v/v final concentration, with an estimated C5 concentration of 80 µg/ml in NHS, final C5 concentrations in this system were estimated as 4 µg/ml. As C5 has a molecular mass of 180 kDa and IgG has a molecular mass of 160 kDa, 6 µg/ ml of Eculizumab was used to completely inhibit C5 activity. NHS, C5 depleted NHS or NHS + eculizumab were then incubated with complement sensitised THP-1 cells as above and C3b deposition measured. NHS with Eculizumab generated a similar C3b staining pattern to that seen in C5-depleted serum with a highly C3b positive population not present in NHS-treated samples (Figure 3.14). Negative controls of NHS without an activating antiserum and heat inactivated NHS + antiserum were used to validate the experiment.

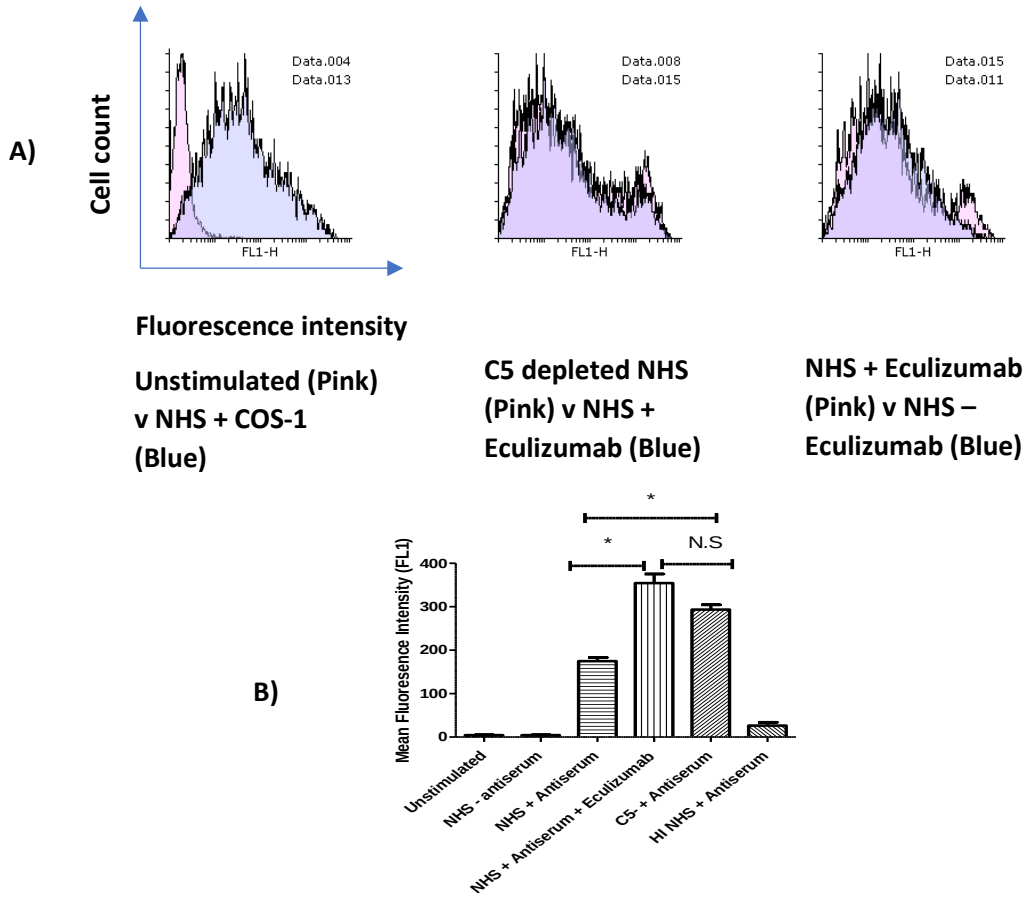

*Figure 3.14. A. Representative overlay histograms of stimulation conditions, demonstrating the similar staining patterns of C5 depleted serum and Eculizumab treated NHS, both generating a population of highly C3b positive cells. $2x10^5$ THP-1 cells at a concentration of $1x10^6$ cells /ml in a sterile 96 well U bottomed plate were sensitised to complement using 2.5% COS-1 antiserum (v/v) in complete RPMI media as previously described. Cells were subsequently washed with sterile PBS and resuspended in complete media, prior to NHS, C5 depleted NHS or NHS pre-incubated with eculizumab addition to the cells for 30 minutes at 37°C. Cells were subsequently washed with sterile PBS and resuspended in FACS buffer prior to staining for C3b deposition using the Biolegend anti-C3b FITC antibody at a 1:100 dilution. Cells were washed with sterile PBS and resuspended in FACS buffer before fluorescence was analysed on the FACS Calibur. B. Quantification of C3b staining on THP-1 cells incubated with NHS, NHS + Eculizumab or C5 depleted NHS as described in 3.14.A. Both eculizumab pre-treated NHS and C5 depleted NHS deposited significantly more C3b than NHS on COS-1 sensitised THP-1 cells in this system (One-way ANOVA with Dunnett post-hoc test comparing to NHS + antiserum sample. Data presented as Mean +/- SEM from a single experiment, representative of three independent experiments. * = P<0.05).*

The finding that either C5 depletion or C5 inhibition markedly increased C3b deposition on THP-1 cells was unexpected; this could have real impact if excessive C3b deposition is occurring on nucleated cells exposed to plasma in patients on Eculizumab.

To further investigate whether this observed elevated C3b deposition was specific to C5 depletion and inhibition or a general phenomenon of terminal pathway inhibition, an in house anti-C7 inhibitory antibody (23D10) was used alongside Eculizumab. In contrast to the results obtained with C5 blockade or depletion, blocking terminal MAC formation at the C7

stage did not statistically significantly affect the levels of C3b deposition on the cells (Figure 3.15 A and B).

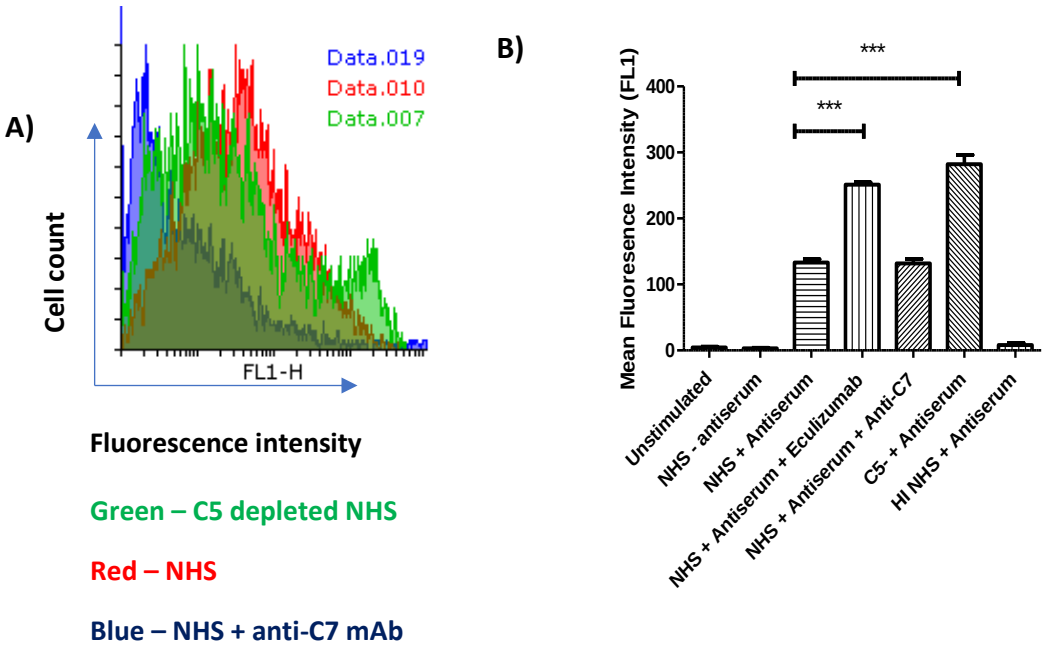

*Figure 3.15 A. FACS profiles of C3b staining on THP-1 cells sensitised to complement and stimulated with NHS, C5 depleted NHS or NHS + in house anti-C7 antibody incubated with NHS prior to addition to sensitised cells. . 2x10^5 THP-1 monocytes were seeded at a density of 1x10^6 cells/ml in complete RPMI media. Cells were sensitised to complement using 2.5% v/v COS-1 antiserum as previously described. Cells were subsequently washed with sterile PBS and resuspended in complete media, prior to NHS, C5 depleted NHS or NHS pre-incubated with eculizumab or in house anti-C7 antibody. Sources of complement were added to the cells for 30 minutes at 37°C. Cells were subsequently washed with sterile PBS and resuspended in FACS buffer prior to staining for C3b deposition using the Biolegend anti-C3b FITC antibody at a 1:100 dilution. Cells were washed with sterile PBS and resuspended in FACS buffer before fluorescence was analysed on the FACS Calibur B. Mean fluorescence of THP-1 cells treated with NHS, C5 depleted NHS, NHS + Eculizumab and NHS + anti-C7 blocking antibody, stained for C3b deposition. Intact cells were gated on forward and side scatter. B. Quantification of mean C3b staining fluorescence intensity from 3.15.A. Statistically significant differences were determined using One-Way ANOVA with Dunnett Post hoc test comparing samples to antiserum + NHS (***= P<0.001)*

The finding that MAC block at the C7 stage, in contrast to block at the C5 stage, did not increase C3b staining on NHS-exposed THP-1 cells is intriguing. As both blocking mAbs prevent lytic cell death, this is unlikely to be a consequence of differences in cell loss. One possibility is that C5 block, by preventing C5 interaction with the convertase, allows more C3 to be cleaved by the convertase, whereas C7 block does not alter C5 interactions or impact convertase function.

3.7 - The induction of Ca^{2+} flux in response to MAC deposition

One of the crucial mechanisms of MAC induced cell signalling is via the induction of elevated cytosolic Ca^{2+} concentrations. The elevation of cytosolic Ca^{2+} from the nanomolar range in unstimulated cells to several micromolar upon MAC deposition has been implicated as an important trigger, not only in MAC induced inflammatory cell signalling, but also in the repair processes and resistance of cells to MAC mediated death (Morgan and Campbell 1985). Therefore, it was crucial to ensure that the expected Ca^{2+} flux was observed with the systems used in these experiments. Methods were modified from previously published work from our group showing that sublytic MAC induced Ca^{2+} flux using the fluorescent dye Fluo-3-AM by flow cytometry (Triantafilou *et al* 2013). Fluo-3-AM is a cell permeable esterified compound which becomes de-esterified by cytosolic esterases, trapping the dye in the cytoplasm. Intracellular Fluo-3 fluorescence at 525 nm upon Ca^{2+} binding can be measured through the FL-1 channel on a flow cytometer. Fluo-3-loaded cells were sensitised as before and incubated with NHS or C5 depleted serum or NHS + 10 mM EDTA to prevent complement terminal pathway activation and alternative pathway amplification respectively. Incubation with a sublytic dose of NHS caused an increase in fluorescence signal, indicative of increased intracellular Ca^{2+} , after 10 and 15 minutes at 37^{o}C and persisting for at least 20 minutes (Figure 3.16 A/B). EDTA-treated NHS did not cause a change in fluorescence at these times and C5-depleted serum caused a small increase in fluorescence, possibly due to C3 cleavage product (C3a or C3b) signalling through cognate receptors. To generate time resolved data, a plate-based assay was used. Cells were loaded with dye and sensitised as with the flow protocol, however sensitised cells were then resuspended in CFD buffer, transferred to 96 well, opaque plates and stimulated with NHS / C5 depleted NHS and fluorescence at 515 nm recorded (Figure 3.16 C).

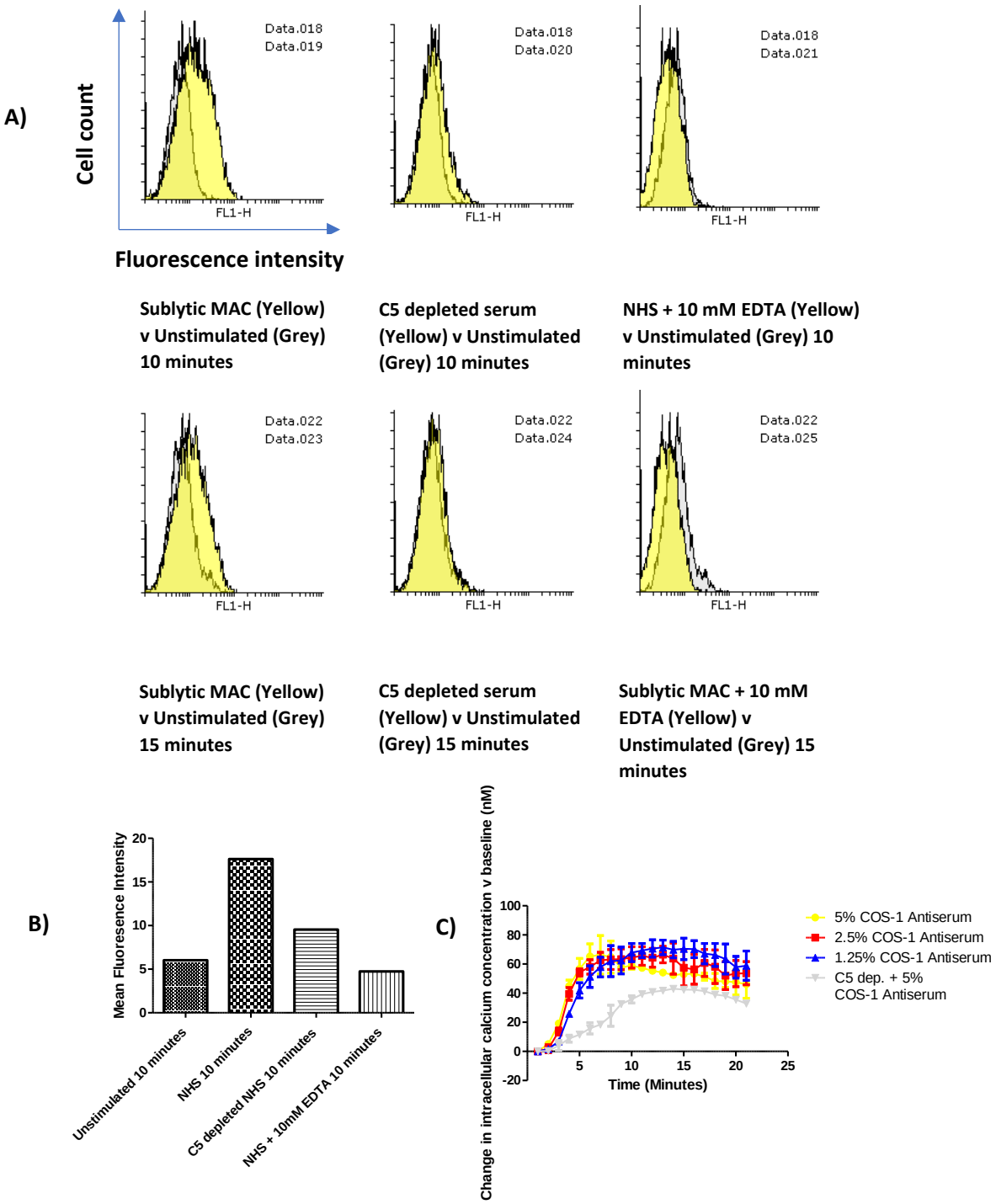

Figure 3.16. Calcium flux in response to sublytic MAC deposition on THP-1 monocytes. 2x10^5 THP-1 cells were loaded with the Calcium sensitive dye Fluo-3-AM at 2.5 µM for 45 minutes at 37˚C in complete RPMI in 96 well, U-bottomed plates. Cells were washed and sensitised to complement using COS-1 antiserum as previously described. Cells were then exposed to NHS, NHS containing EDTA or C5 depleted serum and fluorescence measured on different platforms. A. Fluorescence was measured over time in each condition via FACS analysis and data analysed using Flowing software 2.0. Data are from a single experiment, representative of three independent experiments. B. Bar graph showing mean fluorescence intensities in the different conditions at 10 minutes. C. Quantification of changes in MAC mediated increases in intracellular Ca^{2+} over time in a fluorescence plate reader. 2x10^5 COS-1 sensitised THP-1 cells were transferred to opaque, black plates for plate reader fluorescence reading (505 nm / 525 nm excitation / emission). Baseline fluorescence was obtained from unstimulated cells, and maximal fluorescence was obtained at the end of the experiment through adding 2% Triton X to control wells. Change in fluorescence at 515 nm was converted to Ca^{2+} concentration through the equation $[Ca^{2+}]$ = Kd (325 nM for Fluo-3-AM) x ((Fluorescence of signal – Minimal Fluorescence (unstimulated cells)) / (Maximal Fluorescence (Triton X control) – Minimal Fluorescence). Data presented as mean +/- SEM from one experimental set of triplicate values, representative of three independent experiments.

3.8 - Sublytic complement deposition affects the intracellular oxidative state

A second important consequence of sublytic MAC deposition on nucleated cells is the production and release of ROS/ RNS. Whilst sublytic MAC deposition has been demonstrated to induce ROS secretion from monocytes, the intracellular generation of ROS and the nature of the ROS generated has largely been unexplored. Sublytic MAC deposition on rat mesangial cells was demonstrated to induce the release of O^{2-} and H_2O_2: driving tissue damage, but the intracellular signalling responsible was not explored (Couser *et al* 1986). The importance of these observations, and further delineating MAC mediated ROS/RNS production is the pleiotropic roles ROS performs as a secondary messenger within the cell, activating a host of inflammatory and cell death associated mechanisms; including the NLRP3 inflammasome.

Cellular ROS / Superoxide production was tested using a detection kit (Abcam) that allows analysis of two subsets of intracellular ROS through flow cytometry. The two dyes are dihydrofluorescin esters which are cell permeable; however, upon cell entry the compounds are deacetylated by intracellular esterases to trap the non-fluorescent precursor compounds in the cell where they can be oxidised by ROS / Superoxide and generate fluorescent products. The exact probe molecular identities are not disclosed by the manufacturer. The green probe (FL-1 channel) allows measurement of hydrogen peroxide, peroxynitrite, hydroxyl radicals, nitric oxide and peroxy radicals; the orange probe (FL2 channel) allows the measurement of Superoxide and hypochlorous acid radicals, cumulatively allowing a thorough investigation into ROS/RNS production within the cell in response to MAC stimulation. THP-1 monocytes ($2x10^5$) were loaded with a 1:2000 dilution of the respective ROS/RNS probes reconstituted in dimethylformamide (DMF) for 30 minutes; DMF was used as solvent as DMSO can modulate ROS signalling and may generate spurious results. Cells loaded with the respective dyes were subsequently antibody using COS-1 antiserum sensitised as previously described (2.5% v/v final concentration), washed and resuspended in NHS / C5 depleted serum for 20 minutes prior to further centrifugation and resuspension in FACS buffer. Cells were then analysed on the Becton Dickenson FACS Calibur and plots generated using Flowing software 2. Due to the overlapping fluorescence spectra of the dyes and difficulties encountered in compensation, cells were stained separately with the individual dyes, shown in Figure 3.17.

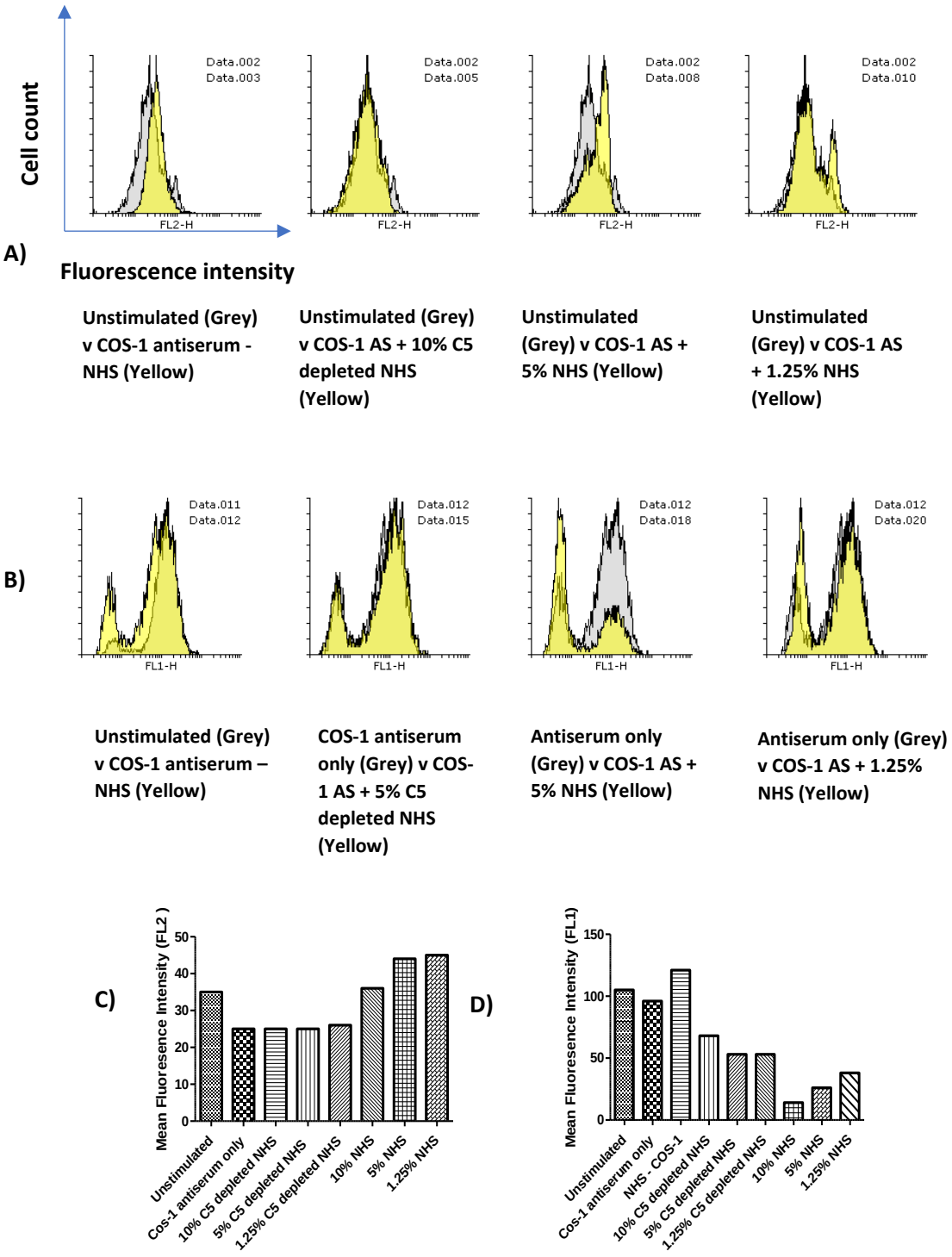

Figure 3.17. Deposition of sublytic MAC on THP-1 cells alters the cell redox potential through generation of superoxide. A. 2x10^5 THP-1 cells were loaded with the ROS sensitive dyes (Abcam) at the recommended 1:2000 dilution in DMF for 45 minutes at 37˚C in complete RPMI in 96 well, U-bottomed plates. Cells were washed and sensitised to complement using COS-1 antiserum as previously described. Cells were then exposed to NHS, NHS containing EDTA or C5 depleted serum and fluorescence measured on different platforms. A. Fluorescence was measured at 30 minutes each condition via FACS analysis and data analysed using Flowing software 2.0. Data are from a single experiment, representative of three independent experiments Sublytic MAC causes an elevation of superoxide derived ROS/RNS in a dose dependent manner relative to unstimulated controls, which is not observed when C5 depleted serum is used. B. C5 depleted serum does not alter the oxidative stress / hydroxyl radical staining of the cells; however, sublytic MAC causes a shift with a decrease of FL-1 fluorescence. C. Quantification of FL2 mean fluorescence from A. D. Quantification of mean FL1 fluorescence from B. Data presented from an individual, single replicate experiment, representative of three independent experiments.

The observation that sublytic MAC generates an elevation of intracellular superoxide (A and C) and a decrease in hydroxyl radical states (B and D) was unexpected, however the literature of MAC driven ROS production is relatively scarce, with a single paper highlighting an elevation of superoxide production on rat mesangial cells, but not addressing other oxygen or nitrile species (Adler *et al* 1986). A possible explanation for the reduction in fluorescence signal in regard to the hydroxyl radical stain might be that the dye leaked from the cells upon MAC deposition and membrane disruption; however, decrease in signal was only seen for the green (FL1) channel, not the orange (FL2), making non-specific dye release from damaged cells an unlikely explanation. Therefore, the observed dichotomy of elevated superoxide and reduction of hydroxyl staining suggests a real phenomenon with marked changes in Oxygen and Nitrile species.

3.9 - Conclusions of Chapter three

In this section of work, I have demonstrated that sublytic MAC may be generated from the reactive lysis and serum / antibody systems. The purification and validation of individual terminal pathway components, C5b6, CVF and the CVFBb complex, which together were subsequently utilised to generate functional reactive lysis systems, was shown. Both early complement (C3b) and terminal pathway (C9) deposition could be demonstrated on THP-1 cells subjected to sublytic MAC using a classical pathway system.

In contrast to recent reports from other groups, blockade of CD59 caused no significant differences in C3b deposition in complement attacked cells with the functional blocking of CD59 using BRIC229; large changes in C9/MAC staining and cell death were observed, validating that CD59 function was impaired (Thielen *et al* 2017). The literature suggesting CD59 was implicated in C3 regulation was derived from the observation that only cells deficient in CD46/CD55/CD59 were susceptible to spontaneous C3 deposition when exposed to NHS, whereas CD46/CD55 deficient cells did not undergo spontaneous C3 deposition as determined by FACS. Due to the contrasting methods used, the differences are hard to verify.

Most likely, this difference is attributable to MAC mediated damage driving further C3b deposition on these cells, which is then not regulated by CD55 / CD46 (Thielen *et al* 2017).

From this set of experiments, a further interesting observation was made that C5 depleted NHS, used as a control to demonstrate that cell death or sublytic effects were terminal pathway dependent, caused increased C3b deposition on the cell surface relative to the same dilution of NHS alone. To verify this, NHS was incubated with a C5 blocking concentration of Eculizumab prior to addition to sensitised cells and compared to NHS – Eculizumab and C5 depleted NHS samples. The C3b staining pattern and intensity was comparable between C5 depleted NHS and NHS + Eculizumab, and significantly increased relative to NHS alone. Interestingly, the strongly C3 fragment positive populations observed with C5 depleted and Eculizumab treated NHS samples has also been observed in PNH patients, where CD59 negative RBC's had two distinct C3 fragment positive and negative populations (Sica *et al* 2018). Comparative FACS dot plots are shown in Figure 3.18.

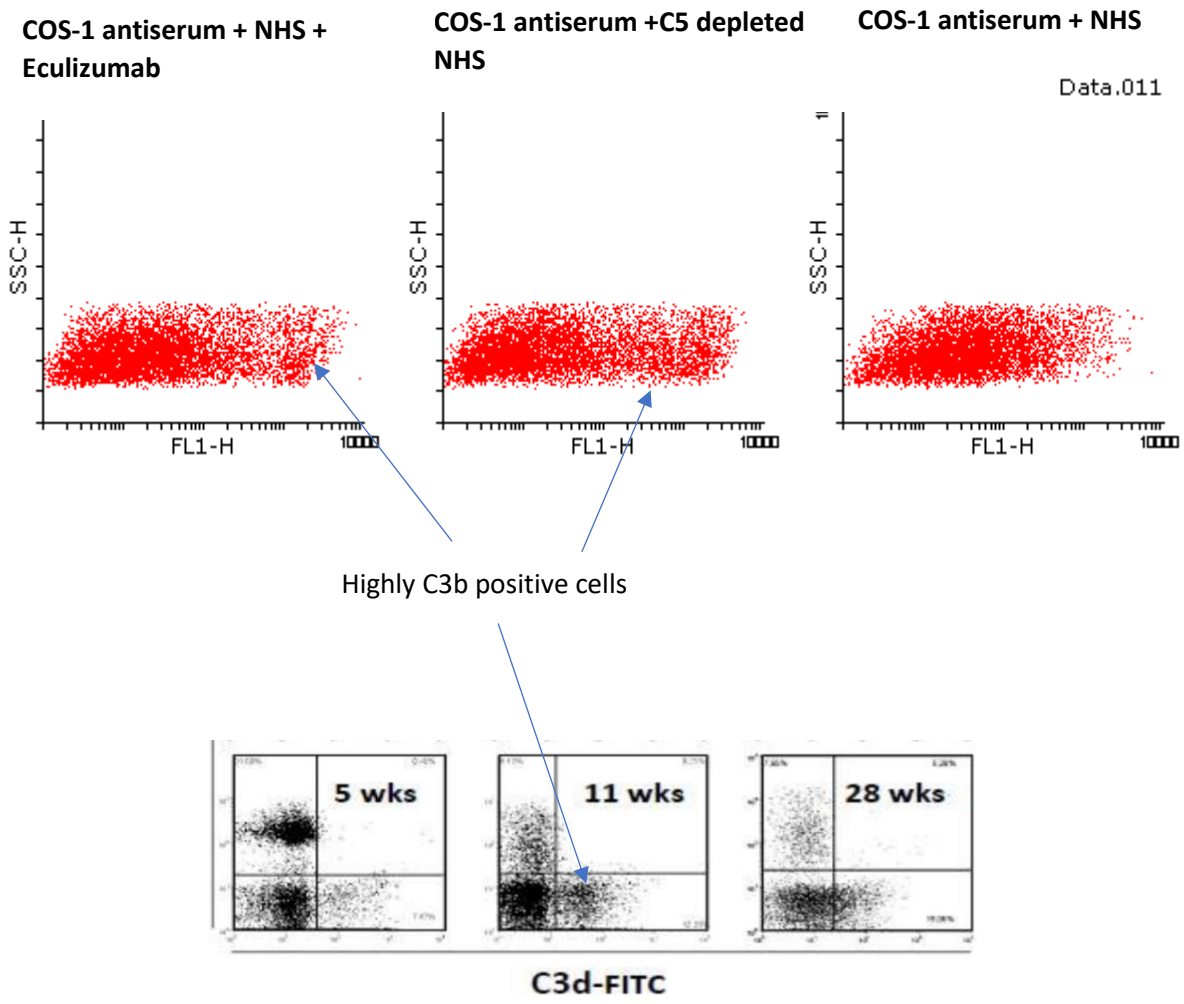

Figure 3.18 – Comparative C3b staining dot plots between classical pathway stimulated THP-1 cells (histogram data described in Figure 3.14) and C3d staining on PNH patient erythrocytes (Y axis CD59, dot plots sourced from Sica et al 2018). PNH patients on stable eculizumab treatment (e.g. 11 weeks of treatment) demonstrate CD59 negative, C3b positive cells distinct from the C3 negative main population, similar to the subpopulations observed in these experiments, suggesting that the observed effects of C5 inhibition in this system may be replicated in vivo.

To further investigate whether this was a C5 specific effect or a general observation with terminal pathway inhibition, an anti-C7 antibody was also tested in the same experimental system. Surprisingly, the effects of C7 inhibition differed from that of C5 inhibition or depletion. C7 inhibited NHS had comparable levels of C3b deposition on the THP-1 cell surface to NHS without terminal pathway inhibition, as opposed to C5 depleted NHS which demonstrated significantly increased C3b deposition. This suggests that there may be a mechanism by which C5 inhibition or depletion impacts the activity of the C3 convertase. One possible explanation for this could be that the C5 convertase still retains a low affinity for C3, therefore, in the absence of C5 interaction, more C3 is cleaved and deposited on the cell

surface whereas in C7 inhibited serum the C5 convertase can still preferentially bind the C5 ligand. This has direct impact, if further explored, on patients treated with Eculizumab. If C5 inhibition elevates C3b deposition in response to complement activation, but C7 inhibition results in comparable C3b surface levels to NHS, some effects of Eculizumab on processes such as extravascular haemolysis may be attenuated, which would be beneficial for the patient (Hill *et al* 2010; Gottleib *et al* 2012; Sica *et al* 2018).

The fundamental hallmarks of MAC deposition which pertain to NLRP3 activation, including Calcium flux and ROS generation have been observed in systems with MAC being formed, but not in C5 depleted controls, demonstrating specificity to MAC mediated effects in the systems used. The sharp, rapid increase in intracellular Calcium in response to sublytic MAC, but not C5 depleted serum or serum inhibited with 10 mM EDTA validates that Calcium flux is MAC dependent and is not induced by antibody deposition on the cell surface.

The observation of a differential ROS/RNS profile, with MAC mediating an increase in a superoxide detecting agent whilst cocommitantly decreasing staining for oxidative stress was surprising. The distinction of ROS species generated in response to sublytic MAC in THP-1 cells is poorly defined and understanding these differences may have important connotations in cell signalling, survival and recovery.

The generation of the sublytic MAC system utilising COS-1 antiserum and NHS allowed the investigation of both sublytic and lytic MAC on nucleated cells in subsequent chapters. Other sensitising antibodies including monoclonal anti-HLA and anti-CD15 (TG1) and polyclonal anti-CD59 failed to effectively activate complement and allow titratable cell death (data not shown). The sublytic threshold demonstrated in the COS-1 system on THP-1 monocytes was 2.5% (v/v) COS-1 antiserum to sensitise the cells to complement attack, with 5% (v/v) NHS to yield cell death <10% above baseline levels. This is comparable to the system used by our group previously to investigate the role of sublytic MAC in the activation of NLRP3 in A549 lung epithelial cells, in which 5% NHS was used, however the dose and duration of complement sensitisation using anti-CD59 polyclonal antiserum was not defined (Triantafilou *et al* 2013).

This work therefore lays the foundation to apply the protocols established here to observe the effects of sublytic MAC in the context of NLRP3 activation and manipulate some of the described responses, such as Calcium and ROS/RNS and observe the effects on NLRP3 activity.

Chapter 4: Investigating sublytic MAC induced inflammasome activation and IL-1β secretion in monocytic cells

4.1 - Introduction

In the previous chapter, the classical pathway and reactive lysis methods were established and demonstrated to deposit MAC on the cell surface. In this chapter, both systems were used to investigate the mechanisms by which sublytic MAC induced inflammasome activation and IL-1β secretion in monocytic cells. The activation of complement and MAC formation on nucleated cells has previously been demonstrated to induce NLRP3 activation and IL-1β secretion by our group in A549 lung epithelial cells, with others demonstrating similar effects in LPS primed human dendritic cells and mouse BMDM's; however, the current understanding of conserved and cell type specific inflammasome activation pathways in response to MAC remains unclear (Laudisi *et al* 2013; Triantafilou *et al* 2013; Suresh *et al* 2016). The absence of a general mechanism explaining how MAC induces NLRP3 activation is apparent from the lack of consensus of previous studies, with cellular perturbations such as Ca^{2+} influx, K^{+} efflux, ROS production and mitochondrial dysfunction all implicated by different studies. The range of different potential mechanisms explored in the current literature is summarised in Table 7.

Paper	Proposed mechanism(s) of sublytic MAC induced NLRP3 activation	Mechanism(s) of MAC mediated NLRP3 shown to have no effect in this system
Triantafilou *et al* 2013	Ca^{2+} influx, secondary calcium release from intracellular stores, mitochondrial dysfunction,	N/A
Laudisi *et al* 2013 (supplemental information)	Ca^{2+} influx, K^+ efflux	N/A
Suresh *et al* 2016	ROS production, K^+ efflux	P2XR7 -/- (ATP receptor) cells did not have significantly reduced MAC mediated IL-1β release compared to WT
Kumar *et al* 2018	N/A	N/A

Table 7: Summary of mechanisms of MAC mediated NLRP3 activation explored in existing literature.

Due to the range of mechanisms of MAC induced NLRP3 activation proposed in these papers, and the lack of any contraindicating evidence between papers, all these established NLRP3 activation pathways (Ca^{2+} influx and release from stores, K^+ efflux and ROS production) were investigated in this system. The objective of this was to demonstrate which cellular processes had effects on sublytic MAC mediated NLRP3 activation in this system, as well as attempt to establish any interaction between mechanisms, such as Ca^{2+} mediated mitochondrial dysfunction or ROS production. Alongside these broad cellular mechanisms, the effects of inhibiting sublytic MAC activated signalling pathways, such as AKT, PI3K, JNK1 and ERK in the context of NLRP3 activation and IL-1β secretion were explored to attempt to elucidate conserved signalling pathways linking MAC and NLRP3

4.2 - Investigating the mechanisms of sublytic MAC activation of NLRP3

THP-1 cells were stimulated using LPS priming with subsequent COS-1 antiserum sensitisation and NHS treatment to induce sublytic complement activation on the cell surface. $2x10^5$ THP-1 cells were seeded at a density of $1x10^6$ cells / ml in complete RPMI media in 96-well, U-bottomed sterile plates and primed with 100 ng/ml LPS for 4 hours. Cells were subsequently sensitised to complement using 2.5% (v/v) COS-1 antiserum and subject to sublytic attack using 5% (v/v) NHS or C5 depleted NHS as described in the materials and methods (Chapter 2, Section 2.14) for 1 hour prior to harvesting of supernatant for assay of IL-1β secretion (Figure 4.1.A). Sublytic MAC treatment statistically significantly increased IL-1β secretion relative to unstimulated controls and cells treated with C5 depleted NHS, the latter demonstrating MAC dependence. Stimulation of cells with sublytic MAC without a priming stimulus did not elicit an IL-1β response (data not shown).

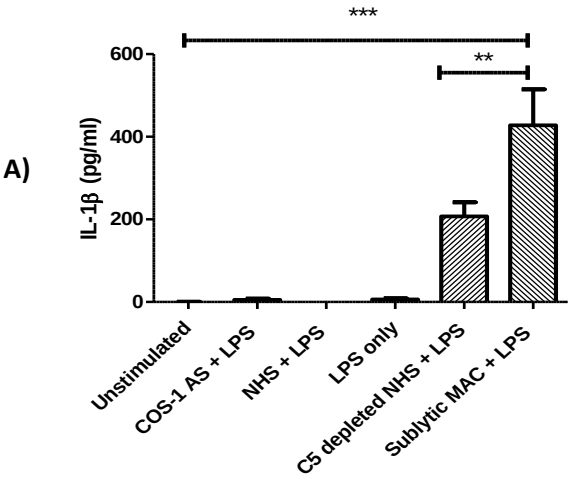

*Figure 4.1.A. $2x10^5$THP-1 monocytes were seeded at a density of $1x10^6$ cells /ml in complete RPMI media. Cells were then primed with 100 ng/ml LPS for 4 hours. Primed cells were subsequently exposed to a sublytic dose of COS-1 antiserum (2.5% v/v) + NHS or C5 depleted serum (5% v/v) as previously described. After one hour of sublytic MAC stimulation, cell supernatant was collected and IL-1β measured by ELISA. LPS primed THP-1 cells exposed to sublytic MAC generated statistically significantly more IL-1β than LPS primed alone, LPS + 2.5% v/v COS-1 antiserum without NHS, LPS + 5% v/v NHS without sensitising antiserum or LPS primed, COS-1 sensitised (2.5% v/v) and exposed to C5 depleted serum (5% v/v). Data presented as the mean +/- SEM from a single experiment, representative of three independent experiments. Statistical significance determined by one-way ANOVA with Dunnett post-hoc test, comparing all columns with Sublytic MAC + LPS. (*** = P<0.001, **= P<0.01).*

4.3 - Sublytic MAC induced IL-1β secretion is NLRP3 dependent

The mechanism by which sublytic MAC induces the observed IL-1β secretion is not defined in THP-1 cells, although the literature from other cell types would suggest it would be through canonical NLRP3 and Caspase-1 activation as Caspase-1 P10 / P20 generation has been demonstrated to accompany MAC mediated IL-1β secretion (Triantafilou *et al* 2013, Laudisi *et al* 2013, Suresh *et al* 2016). Therefore, $2x10^5$ THP-1 cells at a density of $1x10^6$ cells / ml in complete RPMI media were primed with 100 ng/ml LPS and stimulated with sublytic MAC (2.5% v/v sensitising COS-1 antiserum and 5% v/v NHS) as described in the previous section, but with the addition of pre-treatment with pharmacological modulators of NLRP3. Three inhibitors were selected: MCC950, a small molecule inhibitor of NLRP3; AC-YVAD-FMK, an inhibitor of Caspase-1; ZVAD-FMK, a pan-caspase inhibitor. These were selected to target different processes related to canonical or non-canonical inflammasome activation. If the induction of IL-1β synthesis and secretion was through canonical NLRP3 and Caspase-1 activation then MCC950, AC-YVAD-FMK and Z-VAD-FMK would all be expected to decrease the levels of cytokine released, whereas if secretion was via a non-canonical inflammasome forming with Caspases 4/5/11 Z-VAD-FMK would inhibit cytokine secretion, but AC-YVAD-FMK would be ineffective (Ding and Shao 2017). Each inhibitor was titrated across literature derived doses on LPS primed THP-1 cells and incubated for 45 minutes prior to sublytic MAC deposition; IL-1β secretion into the supernatant after MAC exposure was assayed by ELISA (Figure 4.2. A-C). The measured IL-1β levels were then compared to the LPS + MAC controls to determine significant changes in secretion. It was demonstrated that the NLRP3 and Caspase-1 specific inhibitors MCC950 and AC-YVAD-FMK caused dose dependent reductions in IL-1β secretion in response to sublytic MAC. NLRP3 inhibition through MCC950 also elicited a reduction of Caspase-1 activation in THP-1 cells in response to sublytic MAC, suggesting canonical NLRP3 activation was occurring (Figure 4.2.D).

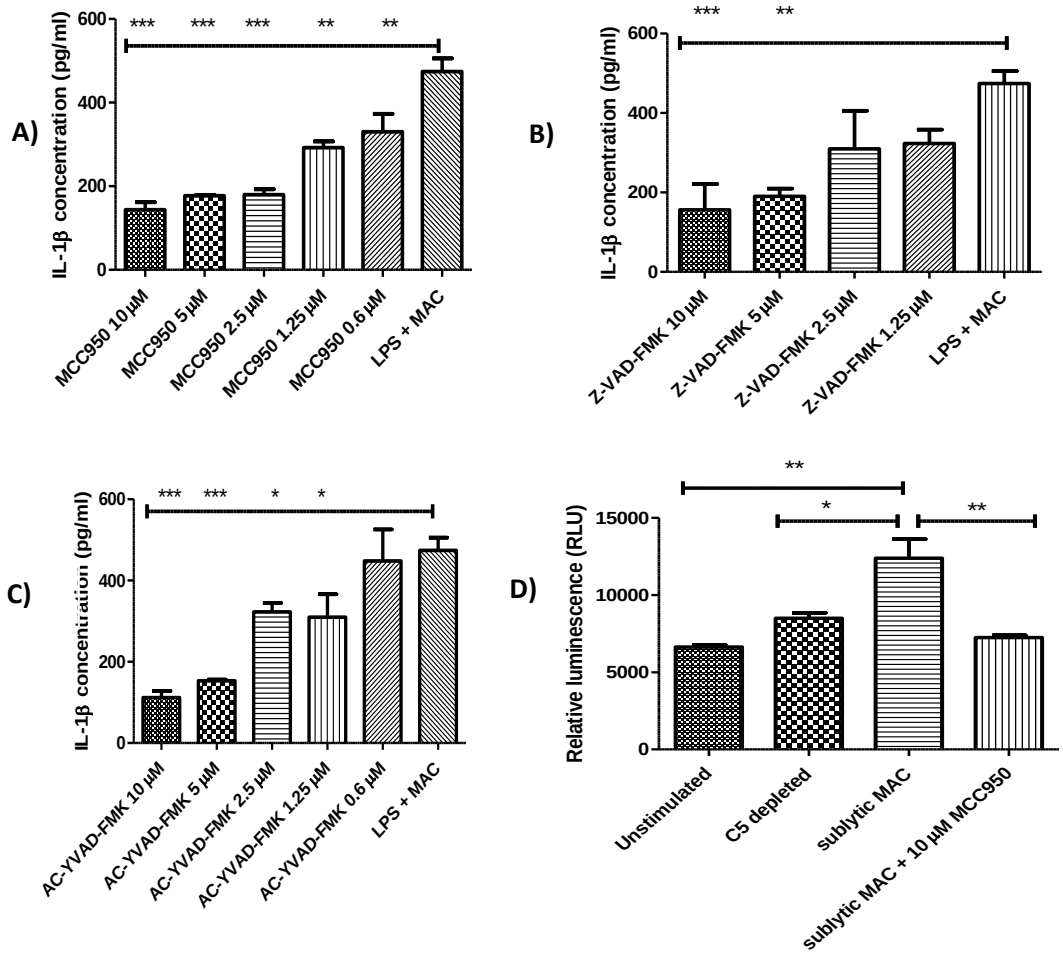

Figure 4.2. 2x10^{5}THP-1 monocytes were seeded at a density of 1x10^6 cells /ml in complete RPMI media. Cells were then primed with 100 ng/ml LPS for 4 hours. After LPS priming, cells were incubated with the denoted inflammasome inhibitors for 45 minutes at 37 °C. Primed cells were subsequently exposed to a sublytic dose of COS-1 antiserum (2.5% v/v) + NHS (5% v/v) as previously described. After one hour of sublytic MAC stimulation, cell supernatant was collected and IL-1ϐ measured by ELISA. A. IL-1ϐ secretion from LPS primed THP-1 cells pre-treated with MCC950 – the specific NLRP3 pharmacological inhibitor. B. IL-1ϐ secretion from LPS primed THP-1 cells pre-treated with Z -VAD- FMK, a pan-caspase inhibitor. C. IL-1ϐ secretion from LPS primed THP-1 cells pre-treated with AC-YVAD-FMK, a specific caspase 1 inhibitor. Data A-C presented as Mean +/- SEM from a single experiment, representative of three independent experiments. Statistical significance determined by one-way ANOVA with Dunnett post-hoc test (= P<0.05, ** = P<0.01, ***= P<0.001). D. Caspase-1 Glo luminescence readings. 2x10^{5}THP-1 monocytes were seeded at a density of 1x10^6 cells /ml in complete RPMI media. MCC950 treated samples were treated for 45 minutes prior to sublytic MAC deposition. Cells were sensitised to complement using COS-1 antiserum (2.5% v/v) and NHS / C5 depleted NHS (5% v/v) incubated with Caspase-1 glo reagent for 90 minutes prior to luminescence reading on the Clariostar plate reader. Data presented as mean +/- SEM from a single experiment, representative of three independent experiments. Statistical significance determined by one-way ANOVA with Dunnett post-hoc test, comparing all groups relative to sublytic MAC. (*=P<0.05, **=P<0.01).*

There was a clear, dose dependent inhibition of complement-driven IL-1β secretion upon incubation with MCC950 and AC-YVAD-FMK (Figure 4.2.A and C) and significant inhibition of Caspase-1 activation upon incubation with MCC950 (Figure 4.2.D). These data suggest that NLRP3 activity is crucial for Caspase-1 activation in response to sublytic MAC, that both NLRP3 and Caspase-1 function are crucial for MAC-induced IL-1β secretion. To ensure that NLRP3 and Caspase-1 specific inhibitors had no unexpected effects in modulating complement activation, thus decreasing MAC deposition and subsequent IL-1β release, a haemolytic assay was performed with sensitised Sheep erythrocytes incubated with NLRP3 and Caspase-1 inhibitors prior to NHS addition as a source of complement. Pre-treatment of Sheep erythrocytes with either inhibitors did not statistically significantly inhibit haemolysis; therefore, the repression of IL-1β secretion was assumed to be through modulation of intracellular signalling (Figure 4.3). From this I conclude that NLRP3 is the central mediator of sublytic MAC mediated IL-1β production and the resultant inflammatory effects in LPS-primed THP-1 cells.

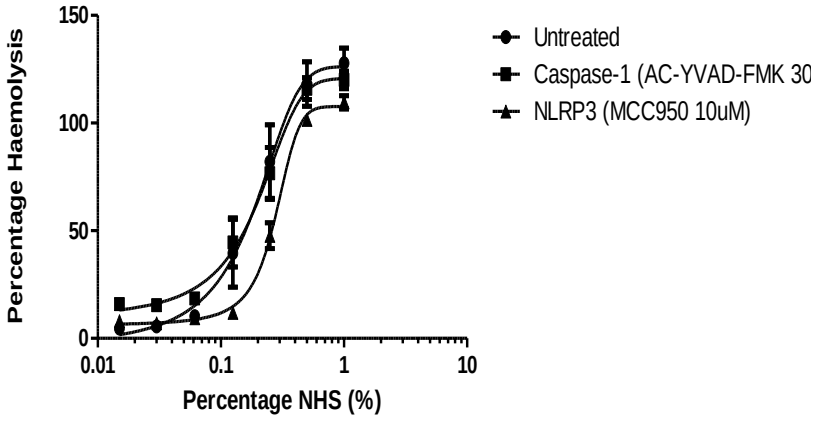

Figure 4.3.Haemolytic assay; sensitised sheep erythrocytes were pre-incubated with MCC950 or AC-YVAD-FMK for 30 minutes prior to complement deposition with NHS. 2% v/v sheep erythrocytes were sensitised to complement using ambocepter (1:2000 dilution in CFD) as previously described in 96 well, U bottomed plates. Sensitised erythrocytes were then plated in 96 well, U bottomed plates and MCC950 / AC-YVAD-FMK added at the denoted concentrations for 45 minutes at 37 °C. Sensitised, inhibitor treated cells were then exposed to a titration of NHS in CFD (1-0.01% v/v) for 45 minutes. Sheep erythrocytes were then centrifuged at 300 x g and cell supernatant transferred to a flat bottomed plate for absorbance readings at 405nm. Percentage haemolysis was quantified relative to CFD only and water + 0.1% v/v TWEEN positive and negative controls. The addition of either pharmacological agent had no statistically significant effects on erythrocyte lysis, therefore excluding the possibility the inhibitory effects demonstrated are through mitigation of complement activation in the context of sheep erythrocyte haemolysis. Data analysed by One-way ANOVA with Dunnett post-hoc test comparing AC-YVAD-FMK and MCC950 to control with no pharmacological inhibitors used. Data presented as mean +/- SEM from a single experiment, representative of three independent experiments.

4.4 - Molecular mechanisms of sublytic MAC activation of NLRP3 – Potassium Efflux

Potassium (K^+) efflux from the cell is one of the strongest current hypotheses for underlying activation mechanism of NLRP3, despite K^+ itself not being an established secondary messenger, in contrast to ROS and Ca^{2+}. A recent publication however points to a loss of membrane potential, for which K^+ and Ca^{2+} are both critical regulators, as the key factor in NLRP3 activation (Zhang *et al* 2018). To address the role of K^+ efflux in NLRP3 activation in THP-1 cells, increasing concentrations of K^+ were titrated into the stimulation medium. THP-1 cells were primed with 100 ng/ml LPS for 4 hours and sensitised as previously described using COS-1 antiserum. However, before cells were exposed to sublytic MAC, the stimulation medium was supplemented with titrated doses of sterile KCl (50-5 mM) and compared to control stimulus (RPMI without added KCl).

In concordance with published literature, elevated extracellular K^+ concentrations resulted in a repression of IL-1β secretion and Caspase-1 activity (Figures 4.4.1 A and C). However, whether this was due to a change in tonicity of the media with a resultant reduced osmotic potential, or due to the changes in free K^+ were unclear. Therefore, a second experiment was performed where the titrated KCl concentrations were reciprocated with an inverse titration of NaCl, giving a constant total added salt content to the media of 50 mM. The addition of NaCl, even in the absence of KCl, also abrogated IL-1β secretion, suggesting that the inhibitory effects of elevated KCl, in this instance at least, may be mediated by the altered osmotic potential or membrane potential rather than directly through K^+ gradients (Figures 4.4 B and C). The changes in salt concentration had no significant effects on the ELISA assay used to measure secreted IL-1β, as a 500 pg/ml standard used across the salt concentrations demonstrated non-significant differences in Abs 450 nm, allowing confidence in the data (Figure 4.4.D). Finally, to exclude the possibility that the Cl^- counterion was having effects on NLRP3 activation, $KHCO_3$ was used as an alternative salt, which also demonstrated capacity to inhibit sublytic MAC mediated IL-1β secretion (Figure 4.4.E). To ensure there were no large repressive effects on complement activation through adding hyperosmotic concentrations of salt to the stimulation media, a haemolysis assays was used. The addition of 50 mM of all salts had repressive effects in a classical haemolytic

assay, with KHCO3 and KCl significantly reducing haemolysis. This was probably through reducing the chemiosmotic gradient across the cell membrane, subsequently reducing haemolysis; however, it was demonstrated that complement activation was still occurring under the high salt conditions (Figure 4.4.F).

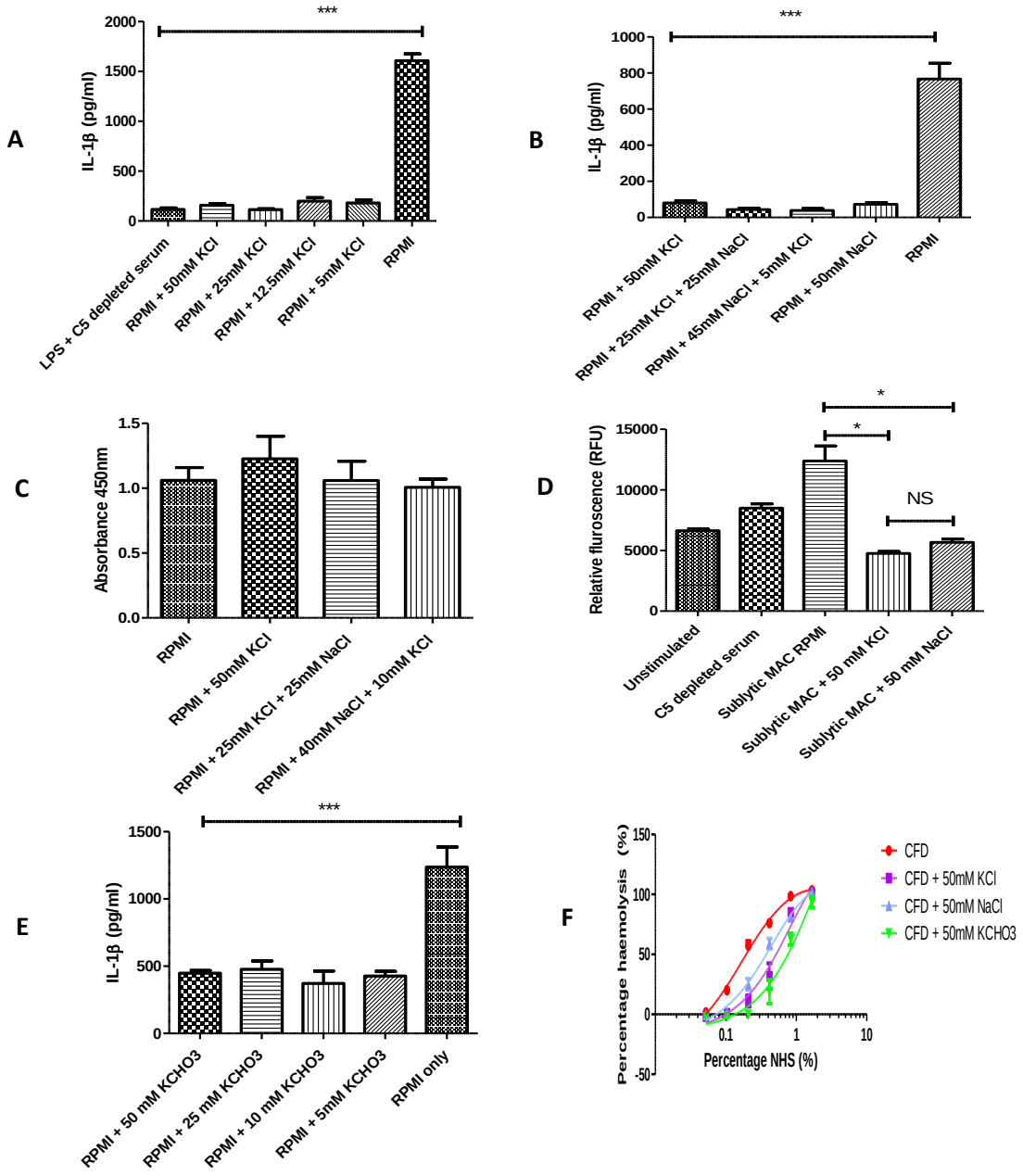

Figure 4.4.A. Complement-induced IL-1β secretion from LPS primed THP-1 monocytes with a titration of KCl added to stimulation media. 2x10^{5}THP-1 monocytes were seeded at a density of 1x10^6 cells /ml in complete RPMI media. Cells were then primed with 100 ng/ml LPS for 4 hours. Primed cells were subsequently exposed to a sublytic dose of COS-1 antiserum (2.5% v/v) + NHS or C5 depleted serum (5% v/v) as previously described + the denoted concentration of sterile KCl added to the stimulation media. Supernatants were then analysed by Il-1β ELISA for inflammasome activation. Data presented as mean +/- SEM from a single experiment, representative of three independent experiments. B. Samples were stimulated as in 4.4.A, however with changes in K$^+$ across the titration were matched with reciprocal changes in NaCl, to keep osmolarity and charge constant across the titration. All samples demonstrated statistically significant inhibition relative to RPMI with no added salt.

Data presented as mean +/- SEM from a single experiment, representative of three independent experiments. C. Changes in salt concentration had no effect on signal of IL-1β standard run at 500 pg/ml on the duo set ELISA, eliminating the possibility that changes in signal were due to salt interfering with the assay. D. CaspaseGlo assay determining the effects of the addition of monovalent cations to RPMI. Caspase-1 Glo luminescence readings. 2x10^{5}THP-1 monocytes were seeded at a density of 1x10^6 cells /ml in complete RPMI media. Cells were sensitised to complement using COS-1 antiserum (2.5% v/v) and NHS / C5 depleted NHS (5% v/v) with or without the addition of 50 mM sterile KCl/ NaCl and incubated with Caspase-1 glo reagent for 90 minutes prior to luminescence reading on the Clariostar plate reader. The addition of 50 mM NaCl or KCl to RPMI media significantly inhibited the activity of Caspase 1, however there was no significant difference between NaCl and KCl treated samples. Data presented as mean +/- SEM from a single experiment, representative of three independent experiments. E. Potassium hydrogen Carbonate ($KHCO_3$) was titrated as described for KCl in 4.4.A. The inhibitory effects of the addition of Potassium with a different counterion were measured by IL-1β ELISA as previously described. $KHCO_3$ demonstrated significant inhibition of IL-1β secretion, suggesting no role for Cl^- in the observed inhibition of MAC mediated NLRP3 activation. F. Haemolysis assay on complement sensitised sheep erythrocytes comparing the effects of additional KCl, NaCl and $KHCO_3$ on classical complement activation. Ambocepter sensitised erythrocytes were plated in 96 well, U bottomed plates and each salt was added at the denoted concentrations alongside NHS for 45 minutes at 37 °C. Sheep erythrocytes were then centrifuged at 300 x g and cell supernatant transferred to a flat bottomed plate for absorbance readings at 405nm. Percentage haemolysis was quantified relative to CFD only and water + 0.1% v/v TWEEN positive and negative controls. $KHCO_3$ and KCl *caused significant (P<0.05) inhibition of MAC mediated lysis of Sheep erythrocytes, however the difference for NaCl was non-significant. For all titration experiments, statistical analysis was performed by one-way ANOVA with Dunnett post-hoc test to compare test groups to buffer control (***=P<0.001; * = P<0.05).*

4.5 - Molecular mechanisms of sublytic MAC activation of NLRP3 – Calcium influx

The central role for Ca^{2+} flux in MAC mediated NLRP3 activation has been previously demonstrated by our group in A549 lung epithelial cells. In this cell type, chelation of intracellular Ca^{2+} by pre-incubation of the cells with cell permeable BAPTA-AM significantly inhibited IL-1β secretion, but this effect was also demonstrated with Xestospongin C, Dantrolene and 2-ABP, which inhibit secondary release of Ca^{2+} from ER stores through RYR and IP3R regulated channels (Triantafilou *et al* 2013). To determine if similar effects were seen in THP-1 cells, cells were primed with 100 ng/ml LPS for 4 hours as previously described. Subsequently, titrations of BAPTA-AM and Xestospongin C were added to the cells for 45 minutes. Cells were then washed, sensitised to complement and attacked with sublytic MAC and supernatants collected after 1 hour. Pre-incubation with either 100 µM BAPTA-AM or 10 µM Xestospongin C statistically significantly inhibited both IL-1β secretion and Caspase-1 activity (Figures 4.5. A-C).

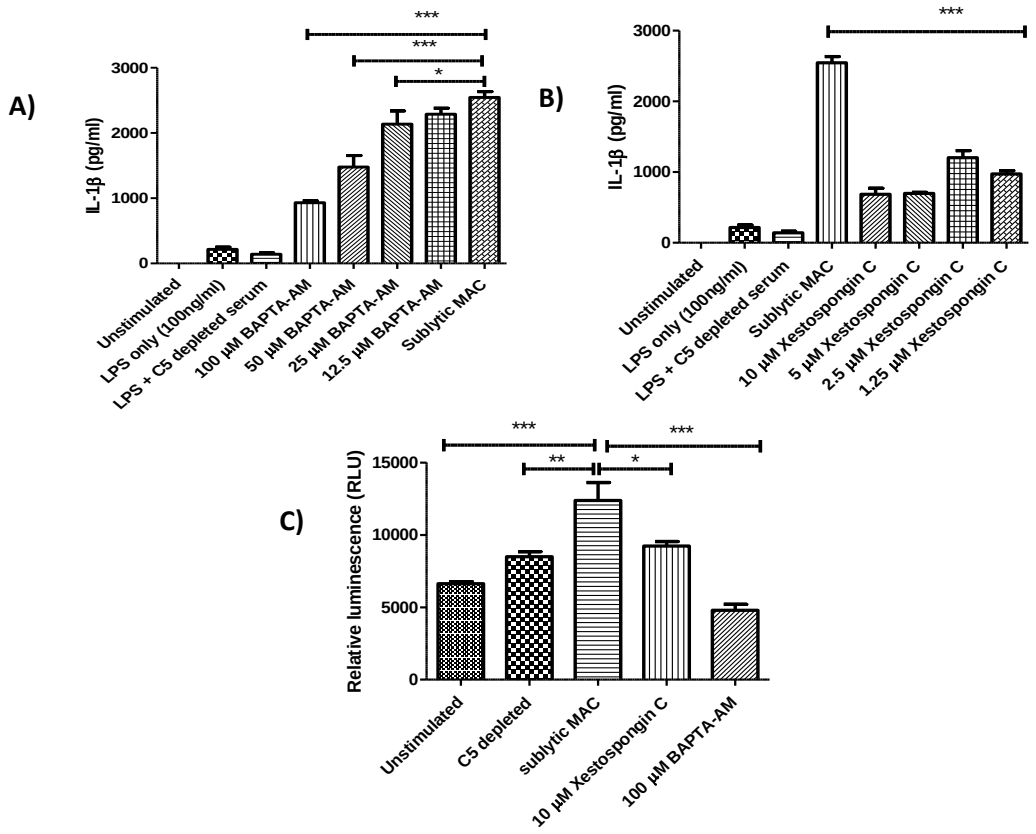

Figure 4.5.A. IL-1β secretion from LPS primed THP-1 cells in response to sublytic MAC with BAPTA-AM. 2x10^{5}THP-1 monocytes were seeded at a density of 1x10^6 cells /ml in complete RPMI media. Cells were then primed with 100 ng/ml LPS for 4 hours. After LPS priming, cells were incubated with the denoted concentration of BAPTA-AM for 45 minutes at 37 °C. Primed cells were subsequently exposed to a sublytic dose of COS-1 antiserum (2.5% v/v) + NHS (5% v/v) as previously described. After one hour of sublytic MAC stimulation, cell supernatant was collected and IL-1β measured by ELISA. Statistically significant inhibition of IL-1β secretion was observed with > 25 μM BAPTA-AM treatment relative to MAC treated control by One-Way ANOVA with Dunnet post-hoc test (=P<0.05, *** = P<0.001). Data displayed as the mean +/- SEM from a single experiment, representative of three independent experiments. B. IL-1β secretion from LPS primed THP-1 cells in response to sublytic MAC with pre-treatment using IP3R antagonist Xestospongin C. Cell stimulation protocol was performed as in 4.5.A, however Xestospongin C was titrated at the denoted concentrations in place of BAPTA-AM. Data presented mean +/- SEM from a single experiment, representative of three independent experiments. Statistical analysis was performed relative to MAC stimulated control by one-way ANOVA with Dunnett post-hoc test (*=P<0.05, *** = P<0.001). C. Caspase-1 glo assay comparing levels of Caspase-1 activity in sublytic MAC attacked cells, controls and cells pre-treated with the highest doses of Calcium signalling inhibitors prior to sublytic MAC deposition. 2x10^{5}THP-1 monocytes were seeded at a density of 1x10^6 cells /ml in complete RPMI media. BAPTA-AM / Xestospongin C treated samples were treated for 45 minutes prior to sublytic MAC deposition. Cells were sensitised to complement using COS-1 antiserum (2.5% v/v) and NHS / C5 depleted NHS (5% v/v) and incubated with Caspase-1 glo reagent for 90 minutes prior to luminescence reading on the Clariostar plate reader. A statistically significant decrease in Caspase-1 activity was observed with BAPTA-AM and Xestospongin C treatment relative to sublytic MAC control. Data presented as mean +/- SEM from a single experiment, representative of three independent experiments. Statistical analysis was performed by one-way ANOVA with Dunnett post-hoc test (*=P<0.05, *** = P<0.001).*

To observe the effects of BAPTA-AM or Xestospongin C treatment on MAC induced Ca^{2+} flux, Fluo-3-AM loaded THP-1 cells were pre-treated with 100 µM of BAPTA-AM or 10 µM of Xestospongin C prior to sensitisation with COS-1 antiserum. Cells were then attacked with sublytic doses of MAC and Ca^{2+} influx measured through fluorescence at 525 nm on the Clariostar plate reader. As previously shown, sublytic MAC induced a large Ca^{2+}influx compared to C5 depleted and HI NHS controls. The dose of BAPTA-AM previously demonstrating inhibition of IL-1β secretion also caused complete ablation of MAC mediated elevations of Ca^{2+} concentrations through chelation of Ca^{2+} and preventing binding to Fluo-3, whilst Xestospongin C treatment caused a slightly slower kinetic profile of Ca^{2+} influx to sublytic MAC treated cells that was not statistically significant, and similar levels of total Ca^{2+}influx. This, alongside the demonstrated inhibition of IL-1β release and Caspase-1 activation suggests not only that Ca^{2+}influx is an important mediator of sublytic MAC mediated NLRP3 activation, but that secondary release from ER stores is also an important signalling event mediating NLRP3 activation and IL-1β secretion, but IP3 receptor inhibition has no effect on the early Ca^{2+} flux events mediated by MAC (Figure 4.6).

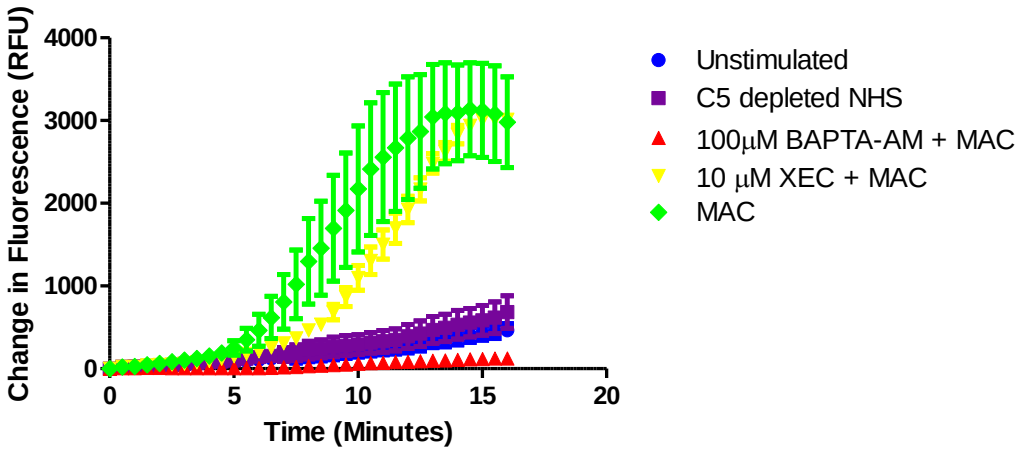

Figure 4.6. Kinetic profile of Ca^{2+} influx into Fluo-3 loaded THP-1 monocytes through sublytic MAC deposition. $2x10^5$ THP -1 monocytes were seeded at a density of $1x10^6$ cells / ml in complete RPMI media in sterile U-bottomed plates. Cells were incubated with the denoted concentrations of BAPTA-AM and Xestospongin C for 45 minutes in complete RPMI media. Cells were subsequently loaded with 2.5 μM Fluo-3 as previously described. Cells were then washed and sensitised to complement using 2.5% v/v COS-1 antiserum as previously described. Sensitised THP-1 cells were transferred to opaque, black plates for plate reader fluorescence reading (505 nm / 525 nm excitation / emission) in complete RPMI media. Baseline fluorescence was obtained from unstimulated cells, and maximal fluorescence was obtained at the end of the experiment through adding 2% Triton X to control wells. Immediately prior to plate loading, sensitised cells were exposed to sublytic NHS (5% v/v) or C5 depleted NHS and changes in Fluo-3 fluorescence measured over time. Data presented as the mean +/- SEM from a single experiment, representative of three independent experiments.

4.6 - Molecular mechanisms of sublytic MAC NLRP3 activation – ROS production and mitochondrial dysfunction

In the previous chapter, it was demonstrated that sublytic MAC deposition on THP-1 cells alters the ROS / RNS profile of the cells relative to C5 depleted controls. Elevations in cellular ROS have also been implicated in NLRP3 activation in response to sublytic MAC and can also be a downstream product of mitochondrial depolarisation which in turn, can be induced through elevated intracellular Ca^{2+}concentrations (Suresh *et al* 2016; Bertero and Maack 2018) . To determine if ROS production was an important mediator of NLRP3 activation in this system and test the interplay between ROS production and Ca^{2+} influx or mitochondrial depolarisation, sublytic MAC stimulations in the presence of the ROS scavenger N-Acetyl-Cysteine (NAC) were performed. Previous studies have demonstrated that NAC is an effective modulator of NLRP3 in various cell types undergoing challenge with an array of stimuli,

including inhibition of MAC induced IL-1β secretion, but not Caspase-1 activation (Suresh *et al* 2016; Cui *et al* 2017; Chimin *et al* 2017)

A titration was performed of literature derived doses of NAC on LPS primed THP-1 monocytes prior to sublytic MAC deposition; ≥ 2mM NAC statistically significantly inhibited sublytic MAC IL-1β secretion (Figure 4.7.A), however Caspase-1 activity was not statistically significantly changed relative to MAC only controls (Figure 4.7.B).

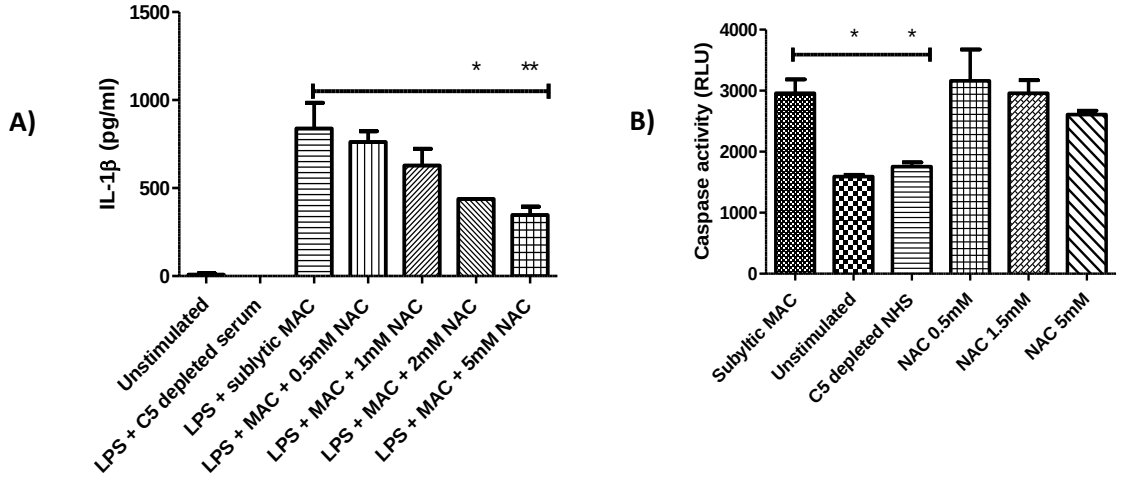

Figure 4.7.A. IL-1β secretion in from LPS primed THP-1 cells pre-treated with the ROS scavenger NAC. . 2x10^{5}THP-1 monocytes were seeded at a density of 1x10^6 cells /ml in complete RPMI media. Cells were then primed with 100 ng/ml LPS for 4 hours. After LPS priming, cells were incubated with the denoted concentration of NAC for 45 minutes at 37 °C. Primed cells were subsequently exposed to a sublytic dose of COS-1 antiserum (2.5% v/v) + NHS (5% v/v) as previously described. After one hour of sublytic MAC stimulation, cell supernatant was collected and IL-1β measured by ELISA. Treatment with ≥ 2 mM NAC significantly decreased IL-1β secretion relative to the LPS + MAC positive control. Data presented as the mean +/- SEM from a single experiment, representative of three independent experiments. Statistical significance was determined by one-way ANOVA with Dunnett post-hoc test comparing all groups to LPS + MAC control (= P,0.05, **= P<0.01). B. CaspaseGlo assay titrating NAC on THP-1 monocytes prior to sublytic MAC deposition. 2x10^{5}THP-1 monocytes were seeded at a density of 1x10^6 cells /ml in complete RPMI media. BAPTA-AM / Xestospongin C treated samples were treated for 45 minutes prior to sublytic MAC deposition. Cells were sensitised to complement using COS-1 antiserum (2.5% v/v) and NHS / C5 depleted NHS (5% v/v) and incubated with Caspase-1 glo reagent for 90 minutes prior to luminescence reading on the Clariostar plate reader. No statistically significant differences were observable between the sublytic MAC and sublytic MAC + NAC groups, however there was a trend towards inhibition with increasing NAC doses. Data presented as mean +/- SEM from a single experiment, representative of three independent experiments. Statistical significance was determined by one-way ANOVA with Dunnett post-hoc test comparing all groups to LPS + MAC control (* = P,0.05, **= P<0.01).*

Whilst NAC treatment significantly decreased IL-1β secretion, it failed to inhibit Caspase-1 activity , suggesting differences in cellular processes involved in the different events. To investigate this, BAPTA-AM and NAC were titrated on THP-1 monocytes prior to sublytic MAC deposition and superoxide production measured. It was hypothesised that if BAPTA-AM treatment affected superoxide production in response to sublytic MAC, it could provide

a link between Ca^{2+} and ROS mediated NLRP3 activation. However, the generation of superoxide in response to MAC was unaffected by BAPTA-AM across the titration of doses, whilst titration of NAC generated significant decreases in sublytic MAC induced superoxide (Figure 4.8).

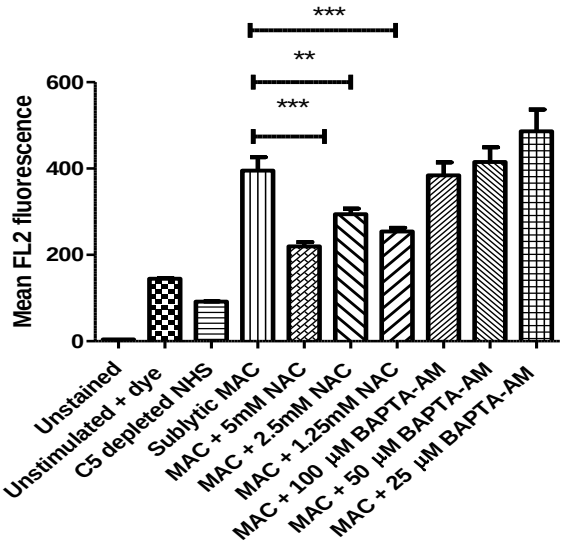

*Figure 4.8. Chelation of intracellular Calcium with BAPTA-AM has no effect on sublytic MAC mediated superoxide production, suggesting that the production of ROS is not Calcium dependent. In contrast, N-acetyl-cysteine reduced superoxide production in response to sublytic MAC. 2x10^5 THP-1 cells were loaded with the superoxide sensitive dye (Abcam) at the recommended 1:2000 dilution in DMF for 45 minutes at 37˚C in complete RPMI in 96 well, U-bottomed plates. Cells were washed and treated with NAC / BAPTA-AM at the denoted doses for 45 minutes at 37 °C. Cells were subsequently sensitised to complement using COS-1 antiserum (2.5% v/v) as previously described. Cells were then exposed to sublytic NHS or C5 depleted NHS (5% v/v) for 30 minutes, washed, resuspended in FACS buffer and run on the FACS Calibur as previously described. Data presented as the mean fluorescence +/- SEM from a single experiment, representative of three independent experiments. Data analysed by one-way ANOVA with Dunnett post-hoc test (*** = P < 0.001; **= P<0.01).*

These data suggest that there is no clear role for Ca^{2+}influx in superoxide production in response to sublytic MAC, again suggesting that the observed effects of the inhibitors of ROS and Ca^{2+}in terms of IL-1β secretion and Caspase-1 activity are independent. To further explore the potential of Ca^{2+} to induce other NLRP3 activating stimuli, the role of Calcium in the induction of mitochondrial depolarisation in response to sublytic MAC was investigated (Zhou *et al* 2018). One mechanism by which Calcium could induce secondary NLRP3 activators was through causing mitochondrial dysfunction. Mitochondria act as a nexus for NLRP3 activation through being a source of ROS, Cardiolipin and mitochondrial DNA, all of which have been demonstrated to function as NLRP3 activators (Cassell *et al* 2018). Firstly,

to verify that sublytic MAC causes mitochondrial dysfunction, a specific fluorescent dye for mitochondrial membrane polarisation, tetramethyl rhodamine ethyl ester (TMRE) was used. TMRE is a net positively charged molecule and becomes sequestered to the mitochondria; however, if the mitochondrial membrane potential becomes abrogated, a common feature of dysfunction, the dye is no longer retained, resulting in a decrease of fluorescent signal. The mitochondrial uncoupling ionophore Carbonyl Cyanide 4-Trifluoromethoxy phenylhydrazone (FCCP) was used as a chemical agent mediating uncoupling as a positive control.

Sublytic MAC deposition on THP-1 monocytes triggered a dose dependent and significant decrease in TMRE fluorescence at 549/575 nm on the Clariostar plate reader, indicating that MAC deposition caused mitochondrial depolarisation, an indicator of dysfunction (Figure 4.9.A).

To investigate the role of Calcium in sublytic MAC mediated mitochondrial damage, the chelator BAPTA-AM and the IP3R antagonist Xestospongin C were used and mitochondrial potential measured. Treatment with BAPTA-AM induced a lower TMRE stain in response to sublytic MAC but did not alter TMRE staining in the absence of MAC. Together with the data shown previously that BAPTA-AM treatment inhibits IL-1β secretion, Caspase-1 activation and elevation of intracellular Calcium concentrations, this suggests that ROS and mitochondrial dysfunction are distinctly different NLRP3 activating events from Calcium influx in this system (Figure 4.9.B).

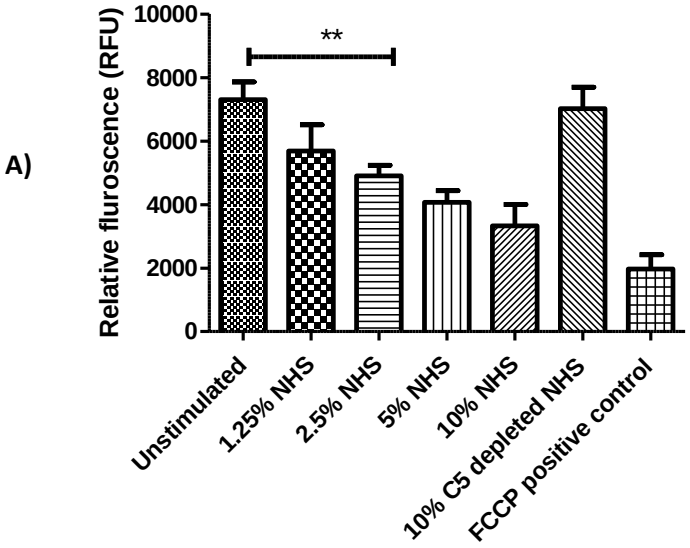

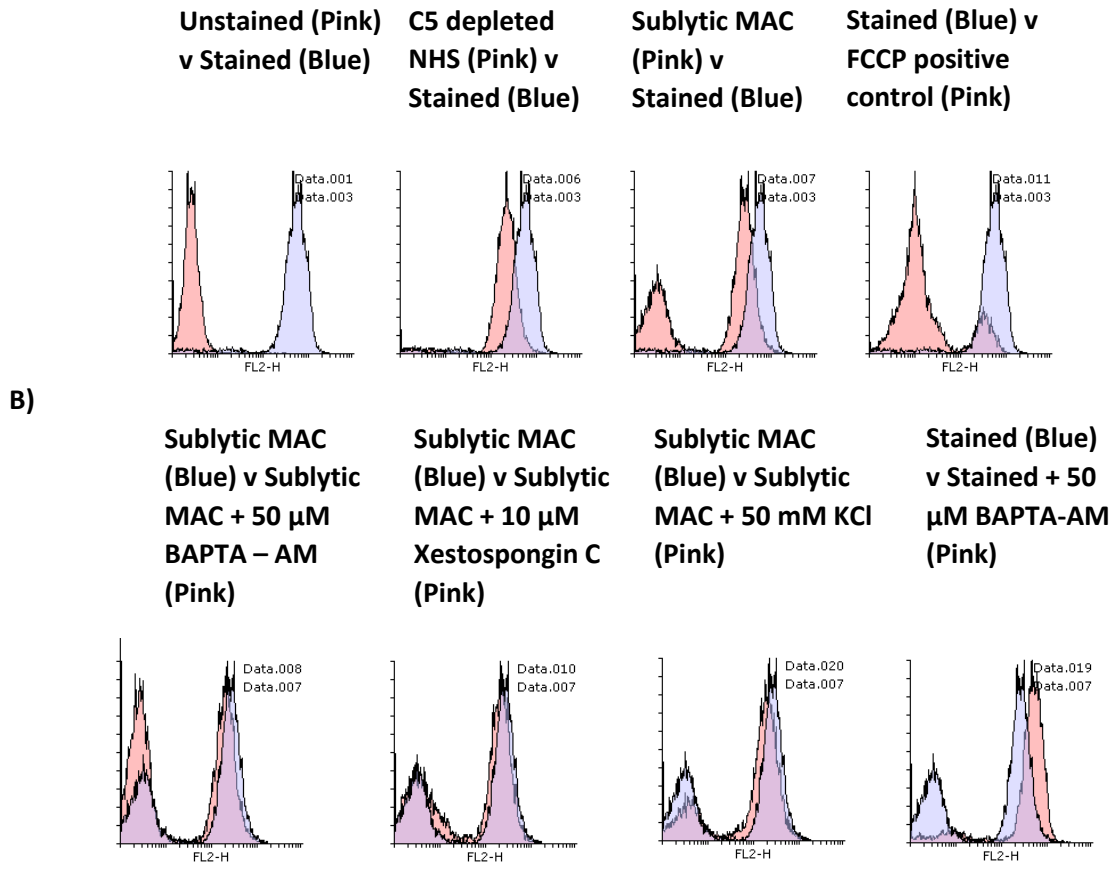

Figure 4.9.A. TMRE staining of mitochondria in THP-1 cells measured using the Clariostar plate reader. 2x10^5 THP-1 cells seeded at density of 1x10^6 cells / ml in complete RPMI media were preloaded with 500 nM TMRE for 30 minutes at 37°C. Cells were subsequently sensitised to complement using COS-1 antiserum (2.5% v/v) and exposed to a titration of sublytic – lytic complement with (1.25% - 10% v/v) NHS or C5 depleted NHS as a negative control for 1 hour. A 20 µM FCCP positive control was used as to generate a high level of mitochondrial dysfunction, resulting in a low TMRE stain. Data presented as the mean +/- SEM from a single experiment, representative of three independent experiments. Statistical significance was determined by one-way ANOVA with Dunnett post-hoc test comparing all groups to unstimulated control (= P,0.05, **= P<0.01) B. The same experiment was performed by flow cytometry to ensure the signal was from intact cells through FSC/SSC gating. 2x10^5 THP-1 cells were loaded with TMRE as described in A. Samples exposed to cell signalling modulators*

were incubated with BAPTA-AM / Xestospongin C were incubated with the denoted concentrations at 37 °C for 45 minutes. Cells were then sensitised to complement using 2.5% v/v COS-1 antiserum and stimulated with sublytic MAC (5% v/v) NHS or C5 depleted NHS for 1 hour. Intact cells stimulated with sublytic MAC generated a negative TMRE peak, which was not present in C5 depleted controls or antiserum only controls. BAPTA-AM treatment of cells caused decreased TMRE staining, suggesting that chelation of intracellular calcium was increasing mitochondrial dysfunction. Data presented from a single experiment, representative of three independent experiments.

4.7 - Inhibition of sublytic MAC activated kinases and their roles in NLRP3 activation

The induction of sublytic MAC signalling can occur through a variety of intracellular signalling pathways, the roles of which in inducing inflammation are unclear. As both Calcium and ROS induced by sublytic MAC were demonstrated to activate NLRP3 in the previous set of experiments, both triggering stimuli derived signalling pathways may be the secondary mediators of the signalling effects. Many downstream kinases and signalling pathways have been linked to sublytic MAC deposition on the cell, with some of these potentially influencing cell viability and cytokine production. As described in the introduction, sublytic MAC deposition elicits a range of cytoplasmic kinase responses (Section 1.6). From the established literature, the targeting of relevant kinases to sublytic MAC signalling may yield suggestions as to how the previously described diverse stimuli for NLRP3 activation coalesce, as well as provide potential targets for therapeutic inhibition. Therefore, pharmacological agents against known sublytic MAC mediated signalling pathways were used in a similar manner to the inhibitors of NLRP3 activation used previously. The signalling pathways inhibited were selected based on previous association with sublytic MAC mediated signalling (Towner *et al* 2016). A schematic of the signalling pathways targeted in this experiment and the inhibitors used to do so is shown in Figure 4.10. A wide range of Calcium induced kinases were targeted including PI3K (LY294002)/ AKT signalling (Perifosine), mTOR (Everolimus), ERK (PD98059) and JAK (AG490), and the effect of inhibition of these pathways on IL-1β secretion examined (Figure 4.11).

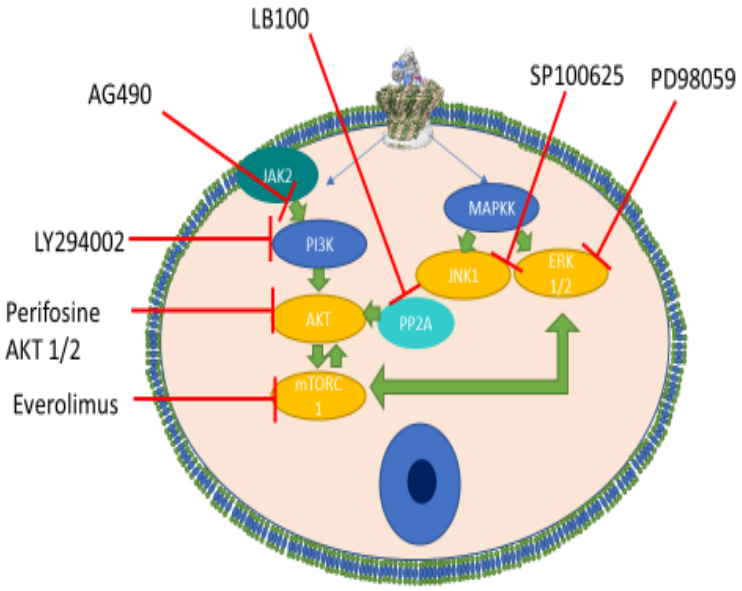

Other inhibitors	Molecular target	Rationale
Geldanamycin	HSP90	HSP90 has been shown to chaperone NLRP3 and facilitate activation
H18	PKA (cAMP singalling)	PKA signalling was significantly changed with sublytic MAC attack at transcriptional level, PKA / cAMP are implicated as negative regulators of NLRP3 activation
Necrostatin-1	RIPK1	RIPK1/RIPK3 mediated necroptosis has been demonstrated to partially mediated MAC mediated cell death and activate NLRP3 in separate studies

Figure 4.10 – Schematic of sublytic MAC activated cell signalling pathways and the inhibitors used to modulate their activation. Cryo-EM image of the MAC edited from Menny et al 2018.

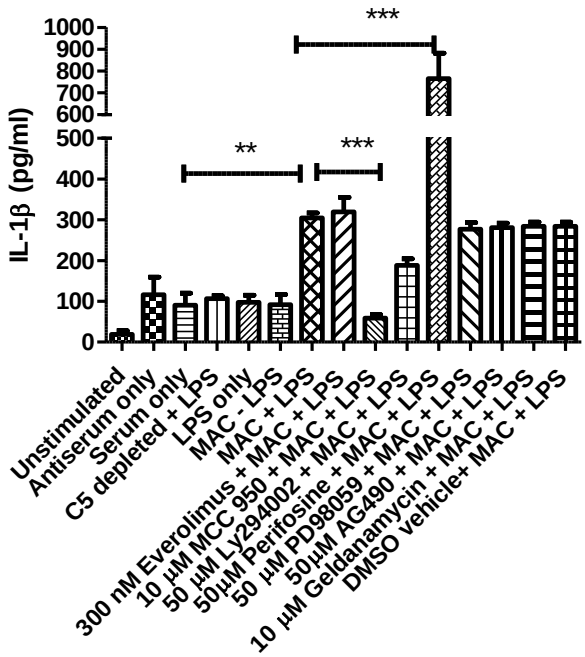

*Figure 4.11. 2x10^{5}THP-1 monocytes were seeded at a density of 1x10^6 cells /ml in complete RPMI media. Cells were then primed with 100 ng/ml LPS for 4 hours. Primed cells were subsequently incubated with the denoted concentrations of each cell signalling inhibitor for 45 minutes. Cells were then washed and exposed to a sublytic dose of COS-1 antiserum (2.5% v/v) + NHS or C5 depleted serum (5% v/v) as previously described. Supernatants were then analysed by Il-1β ELISA for inflammasome activation. Data presented as mean +/- SEM from a single experiment, representative of three independent experiments Data represents mean +/- SEM from a single triplicate experiment, representative of three independent experiments. Statistical significance determined by one-way ANOVA with Dunnett post-hoc test comparing all groups to MAC + LPS control. Only Perifosine and MCC950 treatment caused statistically significant changes in IL-1β secretion (***=P<0.001).*

Across the range of pharmacological inhibitors sublytic MAC mediated activated kinases used, only Perifosine caused statistically significant changes in IL-1β secretion, alongside the MCC950 negative control (Figure 4.11). Due to the large effect of AKT inhibition through Perifosine on IL-1β secretion and the relatively small changes caused by inhibitors of other pathways, the mechanism by which Perifosine mediates changes in NLRP3 activity were investigated. Perifosine is an Alkyl phospholipid which acts as a novel AKT inhibitor by restricting AKT translocation to the cell membrane and interactions of the Pleckstrin homology domain with binding partners (Richardson *et al* 2012). To determine whether Perifosine acts independently of MAC, a second experiment was performed titrating Perifosine to see if the effects were dose dependent, whilst investigating if the effects were MAC mediated or simply caused by administration of Perifosine to primed cells or unstimulated cells and exploring the effects of Perifosine in Caspase-1 activation in response to sublytic MAC (Figure 4.12 A /B).

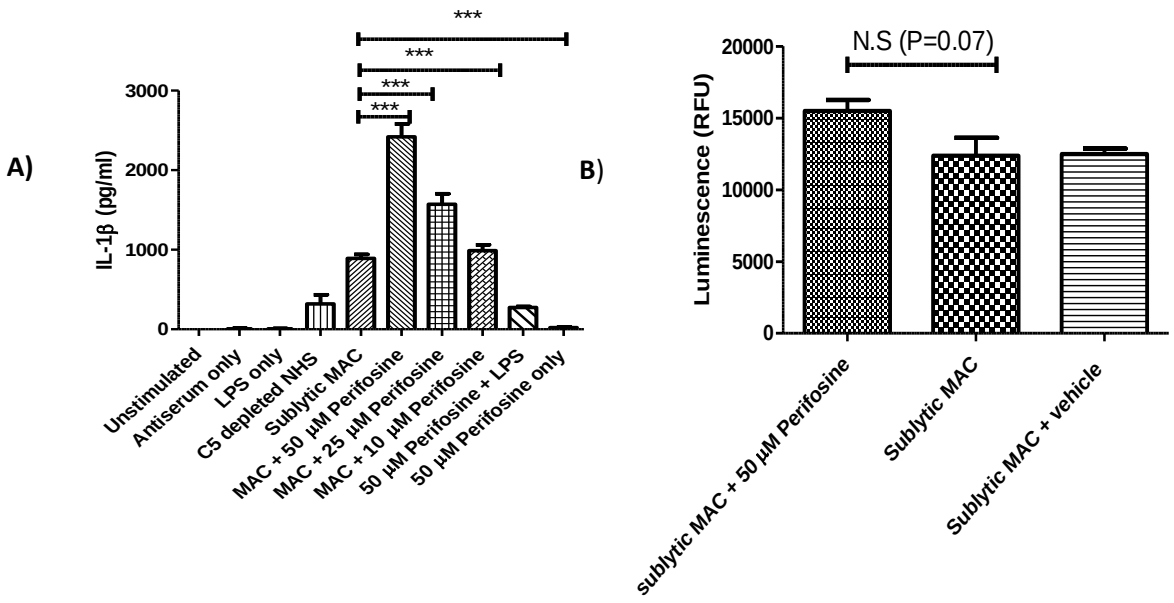

*Figure 4.12.A. The effects of Perifosine titration on IL-1β release in THP-1 monocytes. 2x10^{5}THP-1 monocytes were seeded at a density of 1x10^6 cells /ml in complete RPMI media. Cells were then primed with 100 ng/ml LPS for 4 hours. Primed cells were subsequently incubated with the denoted concentrations of each Perifosine for 45 minutes. Cells were then washed and resuspended in complete RPMI and exposed to a sublytic dose of COS-1 antiserum (2.5% v/v) + NHS or C5 depleted serum (5% v/v) as previously described. Supernatants were then analysed by Il-1β ELISA for inflammasome activation. The effects of perifosine on LPS primed cells or previously unstimulated cells was significantly less than sublytic MAC stimulated cells, suggesting that Perifosine's effect is through synergism with MAC rather than an independent mechanism. Data presented as the mean +/- SEM from a single experiment, representative of three independent experiments. Data analysed by one-way ANOVA with Dunnett post-hoc test relative to sublytic MAC treated samples(*** = P < 0.001; **= P<0.01). B. Pre-treatment of cells with 50 µM Perifosine caused a non-statistically significant trend towards an increase in sublytic MAC mediated activation of Caspase-1 (P=0.07, students T-test), measured using the Caspase-1 Glo system. 2x10^{5}THP-1 monocytes were seeded at a density of 1x10^6 cells /ml in complete RPMI media. Perifosine treated samples were treated for 45 minutes prior to sublytic MAC deposition. Cells were sensitised to complement using COS-1 antiserum (2.5% v/v) and NHS / C5 depleted NHS (5% v/v) and incubated with Caspase-1 glo reagent for 90 minutes prior to luminescence reading on the Clariostar plate reader. Data presented as Mean +/- SEM from a single experiment, representative of three independent experiments.*

The data demonstrate that Perifosine increased sublytic MAC-induced IL1β secretion in a dose dependent manner but did not alter secretion from LPS primed or non-primed THP-1 cells. The effects of modulating other portions of the AKT signalling pathway with sublytic MAC were investigated. Perifosine, LY294002 (PI3K inhibitor, upstream of AKT in canonical signalling (Figure 4.12), LB100 (specific PP2A inhibitor, prevents dephosphorylation of AKT and increases activity), AKT 1/2 (alternative AKT inhibitor) and everolimus (mTOR inhibitor) were all utilised to determine if the effects of Perifosine were AKT signalling specific or due to off target effects of the drug, shown in Figure 4.13.

Of all the compounds used, only Perifosine induced significant changes in sublytic MAC mediated inflammasome activation, suggesting that the effects were non-specifically linked to the compound (Figure 4.13). This may be through the induction of TNFα-R signalling and activation of the RIPK1/3 necroptosome complex which has been described previously (Conos *et al* 2017). This was supported by the dose dependent increases in cell death with Perifosine after 4 hours, suggesting the induction of cell death pathways and with a chronology supporting a necroptotic pathway and in line with literature suggesting 20 µM and higher doses of Perifosine are capable of inducing necroptotic death in THP-1 cells (Papa *et al* 2007).

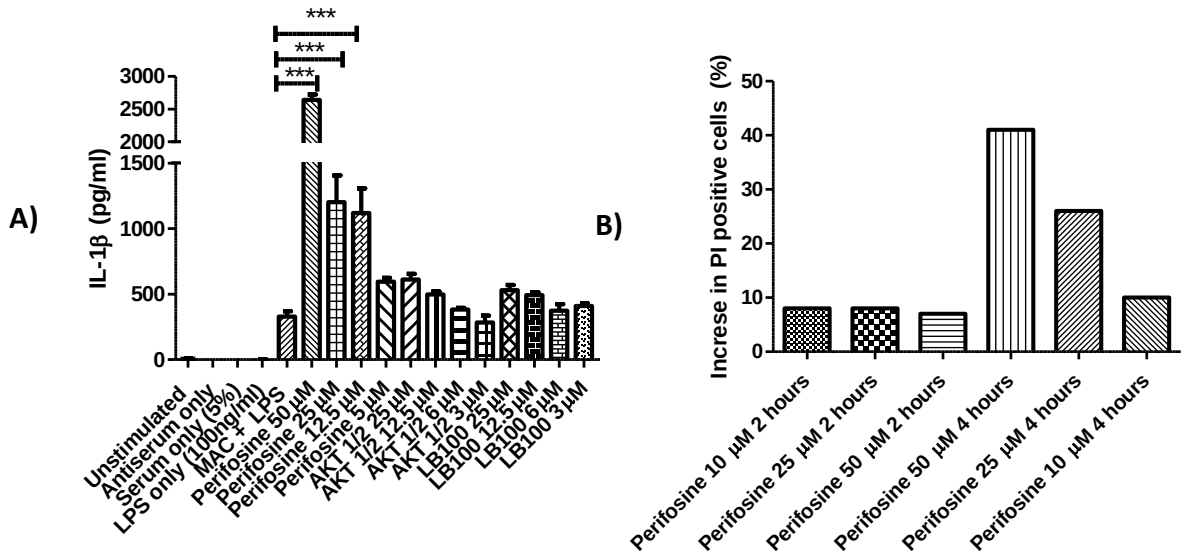

*Figure 4.13.A. Perifosine potentiates sublytic MAC activation of NLRP3 in an AKT independent manner. 2x10^{5}THP-1 monocytes were seeded at a density of 1x10^6 cells /ml in complete RPMI media in 96 well, U-bottomed plates. Cells were then primed with 100 ng/ml LPS for 4 hours. Primed cells were subsequently incubated with the denoted concentrations of Perifosine, AKT 1/2 and LB-100 in complete media for 45 minutes. Cells were then washed and resuspended in complete media and exposed to a sublytic dose of COS-1 antiserum (2.5% v/v) + NHS or C5 depleted serum (5% v/v) as previously described for 1 hour. Supernatants were then analysed by Il-1β ELISA for inflammasome activation. Only Perifosine statistically significantly increased IL-1β release relative to sublytic MAC treated cells, suggesting the other AKT pathway targeting compounds do not exert the same effects. Data presented as the mean +/- SEM from a single experiment, representative of three independent experiments. Data analysed by one-way ANOVA with Dunnett post-hoc test relative to sublytic MAC sample (*** = P < 0.001; **= P<0.01). B. Doses of Perifosine which were utilised in experiments induced large amounts of cell death within 4 hours of administration as determined by PI staining of cells on FACS. 2x10^5 THP-1 monocytes were seeded per well at a density of 1x10^6 cells / ml in 96 well plates and stimulated with the denoted concentrations of Perifosine for 2 or 4 hours at 37 ℃. Cells were subsequently centrifuged, washed and resuspended in FACS buffer and 10 µg/ml PI added as previously described and cell death measured by PI fluorescence on the FACS Calibur.*

Although the effects of Perifosine were not specific to AKT and caused elevated IL-1β release as opposed to the targeted decrease, it provided useful insights into the mechanisms underlying the activation process. MAC has been previously demonstrated to induce cell necroptosis, therefore if a pro-necrotic stimulus such as Perifosine caused an elevation in NLRP3 activation, it suggests an anti-necroptotic stimulus may provide the desired inhibitory effects (Lusthaus *et al* 2018). Furthermore, the incorporation of Perifosine into the cell membrane disrupts lipid raft structure due to the preferential incorporation of the phospholipid into cholesterol rich regions, suggesting that there may be links to lipid raft mediated signalling pathways and NLRP3 activation, with both mechanisms warranting further investigation.

To investigate whether necroptotic signalling was involved in MAC mediated NLRP3 activation and MAC mediated cell death, one of the inhibitors utilised in the published work (Lusthaus *et al* 2018), Necrostatin-1 (NEC) was utilised. NEC is widely utilised as an allosteric inhibitor of RIPK1; however, it may also influence cell fate through inhibition of the IDO pathway, which modulates immune tolerance as well as inflammatory responses. NEC was titrated on THP-1 cells at literature derived doses (50-10 μM) prior to attacking cells with a lytic dose of MAC (5% COS-1 antiserum, 10% NHS) and PI uptake measured. In contrast to the literature in other monocytic cell lines, in THP-1 cells there was no effect of NEC on rapid, lytic MAC mediated death (Lusthaus *et al* 2018) (Figure 4.14. A and B). However, whilst NEC pre-treatment did not cause protection from MAC mediated cell death, it may influence the activation of NLRP3 and IL-1β secretion, which had previously been demonstrated in BMDM's with other NLRP3 activators (Lawlor *et al* 2015). NEC was again titrated on primed cells prior to sublytic MAC deposition, and IL-1β secretion measured by ELISA. NEC pre-treatment did not cause statistically significant changes in IL-1β secretion at any of the experimental concentrations (Figure 4.14.C)

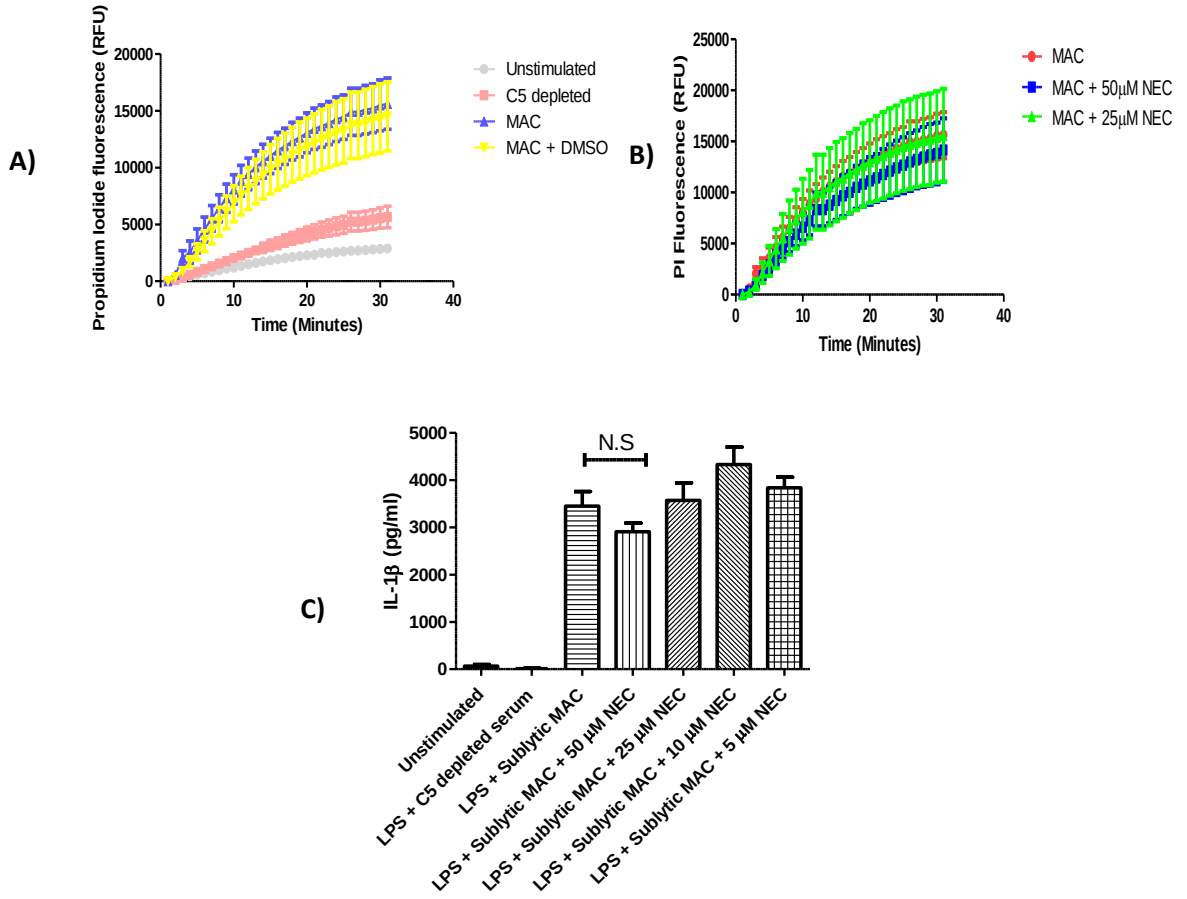

Figure 4.14.A/B. Kinetic assays for rates of PI uptake in THP-1 cells pre-treated with NEC for 45 minutes. 2x10^5 THP-1 cells were seeded / well in complete RPMI media. Cells were pre-treated with literature derived doses of Necrostatin-1 or DMSO vehicle control for 45 minutes. Cells were subsequently washed and resuspended in complete media prior to sensitisation to complement with 2.5% v/v COS-1 antiserum as previously described. Cells were subsequently transferred to black, opaque plates with 10 µg/ml Propidium Iodide. Cells were stimulated with 10% NHS as a lytic source of complement prior to loading on the Clariostar plate reader and fluorescence measured at 480 / 630 nm over half an hour. Treatment of THP-1 cells with Necrostatin-1 or the DMSO vehicle control generated no significant protection from MAC mediated cell death. Data presented as Mean +/- SEM from a single experiment, representative of three independent experiments. C. IL-1ß ELISA of supernatant from LPS primed, NEC-1 pre-treated cells (0-50 µM) exposed to sublytic MAC / C5 depleted serum. 2x10^{5}THP-1 monocytes were seeded at a density of 1x10^6 cells /ml in complete RPMI media in 96 well, U-bottomed plates. Cells were then primed with 100 ng/ml LPS for 4 hours. Primed cells were subsequently incubated with the denoted concentrations of Necrostatin-1 in complete media for 45 minutes. Cells were then washed and resuspended in complete media and exposed to a sublytic dose of COS-1 antiserum (2.5% v/v) + NHS or C5 depleted serum (5% v/v) as previously described for 1 hour. Supernatants were then analysed by Il-1ß ELISA for inflammasome activation. Whilst Necrostatin-1 treatment did generate a titratable effect on IL-1ß secretion, the changes in IL-1ß secretion were non-significant (one-way ANOVA with Dunnett post-hoc test comparing all samples to LPS + MAC control). Data presented as Mean +/- SEM from a single experiment, representative of three independent experiments.

NEC pre-treatment of THP-1 cells did not statistically effect IL-1β secretion (Figure 4.14.C.) or cell death (Figure 4.14.B.). Due to the lack of affect for NEC inhibition on IL-1β secretion, other targets were chosen from the previously mentioned work in the field of MAC mediated death signalling pathways which would align with the observation of Perifosine induced elevation of IL-1β secretion in this system. One of the pathways which may link Perifosine treatment and other MAC mediated affects is JNK signalling (Lusthaus *et al* 2018). Therefore, the effects of inhibiting JNK were explored in LPS primed THP-1 cells. Inhibition of JNK signalling alone generated a trend towards inhibition of IL-1β secretion inhibition in a dose dependent manner; however, this did not reach statistical significance (Figure 4.15.A) . In models of *Histoplasma capsilatum* activation of NLRP3 in dendritic cells, JNK signalling was augmented by ERK1/2, suggesting a more general role for MAPK in NLRP3 activation (Chang *et al* 2017). From this, a broader blockade of MAPK with both JNK and ERK1/2 inhibition was performed; this combination generated a statistically significant decrease in IL-1β and Caspase-1 activation relative to sublytic MAC alone controls (Figure 4.15. B/C).

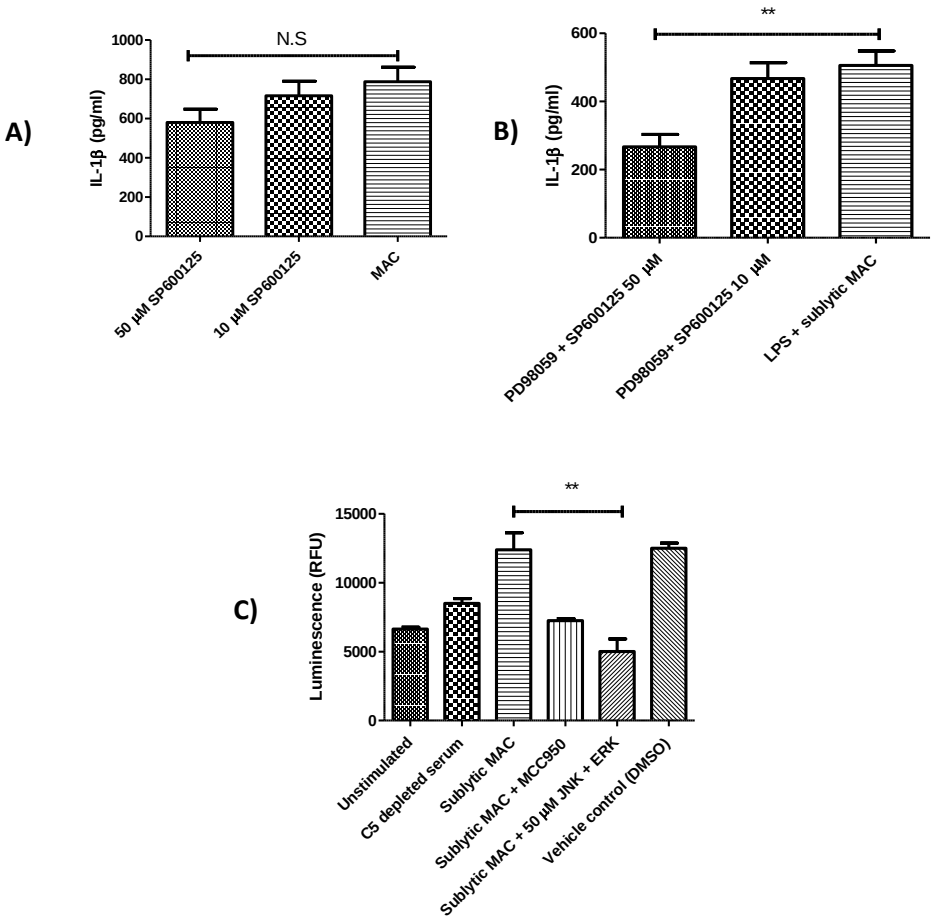

Figure 4.15. A. 2x10^5 THP-1 monocytes were seeded at a density of 1x10^6 cells/ ml in complete RPMI media in 96 well, U bottomed plates. Cells were subsequently primed with 100 ng/ml of LPS for 4 hours. Cells were washed and pre-treated with the denoted concentrations of the JNK inhibitor SP600125 for 45 minutes at 37 °C. Cells were washed and resuspended in complete media and exposed to 2.5% v/v COS-1 antiserum and 5% v/v NHS as previously described. Cell supernatant was collected and IL-1ϐ measured by ELISA. Pre-treatment with the JNK inhibitor SP600125 did not statistically significantly affect IL-1ϐ secretion, however demonstrated a dose dependent response (one-way ANOVA with Dunnet post-hoc test comparing samples to LPS + sublytic MAC). Data presented as mean +/- SEM. Data from a single experiment, representative of three independent experiments. B. 2x10^5 THP-1 monocytes were stimulated with the same method as A, however, cells were incubated with both SP600125 and the ERK inhibitor PD98059 at the denoted concentrations for 45 minutes at 37 °C prior to sublytic MAC deposition. IL-1ϐ secretion was statistically significantly lower with pre-treatment with both JNK and ERK inhibitors (One-way ANOVA with Dunnett post-hoc test comparing pre-treatments with LPS + sublytic MAC control. Data presented as mean +/- SEM from one experiment, representative of three independent experiments. C. 2x10^5 THP-1 monocytes were seeded at a density of 1x106 cells / ml in complete RPMI media in 96 well, U bottom plates. Cells were pre-treated with ERK and JNK inhibitors (PD98059 - 50 µM) and (SP600125 – 50 µM) for 45 minutes. Cells were washed and resuspended in complete media prior to stimulation with sublytic MAC (sensitisation with 2.5% v/v COS-1 antiserum for 20 minutes at room temperature and NHS 5% v/v). Caspase-1 activity was measured after 90 minutes using the Caspase-1 glo system on the Clariostar plate reader. Treatment of the cells with the combination of JNK and ERK inhibitors, both at 50 µM, yielded a statistically significant decrease in Caspase-1 luminescence (one-way ANOVA with Dunnett post-hoc test comparing all samples with sublytic MAC control). Data presented as mean +/- SEM from a single experiment, representative of three independent experiments.

4.8 - Sublytic MAC in the reactive lysis system induces IL-1β secretion from THP-1 cells and primary macrophages

To demonstrate the effects of sublytic MAC deposition on THP-1 and SW982 cells a reactive lysis (RL) system was also utilised. THP-1 monocytes were C5a primed (25 ng/ml) and C56 generated from the freeze thaw method as a source of complement terminal pathway activation. Cells were primed with 25 ng/ml C5a for 4 hours at 37˚C prior to deposition of C56. Cells were incubated with varying concentrations of C56 at room temperature for 10 minutes to allow interaction with the cell membranes prior to C7 addition in molar excess to the C56 with a further incubation for 15 minutes at 37˚C. Cells were then washed via centrifugation at 300 x g for 5 minutes and resuspension prior to C8 and C9 addition. Cells were then stimulated overnight with the C56-9 and the supernatant collected. The aspirated supernatant was then assayed for IL-1β content by ELISA (Figure 4.16 A/B).

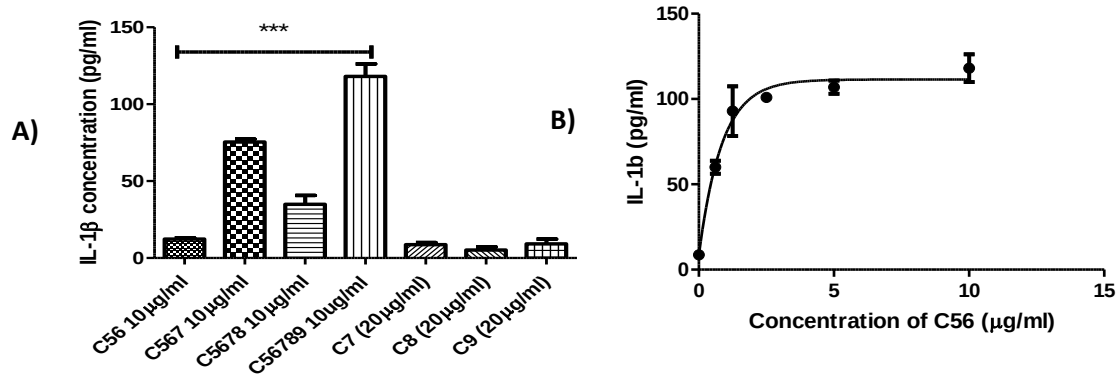

Figure 4.16.A. C56 mediated reactive lysis MAC formation on THP-1 monocytes induces IL-1β secretion. 2x10^5 THP-1 monocytes were seeded at a density of 1x10^6 cells/ ml in complete RPMI media in 96 well, U bottomed plates. Cells were subsequently primed with 100 ng/ml of LPS for 4 hours. C56 was added to the cells for 10 minutes at room temperature in complete RPMI media at the denoted concentrations (0-10 µg /ml). C7 was then added to the cells at 10 µg/ml for 15 minutes at 37 °C. Cells were subsequently washed and resuspended in complete media, before C8 and C9 were applied (10 µg/ml each) for 1 hour. IL-1β release was then measured by ELISA. The generation of maximal IL-1β was dependent on mature MAC (C56-9) and was titratable with the amount of C56 initially deposited on the cells. C7 / C8 / C9 alone had negligible effects in terms of IL-1β secretion. B. Titration of the C56 initiating complex with constant dose of C7 – C9 demonstrating a dose dependent IL-1β response. Data presented as mean +/ SEM from a single experiment, representative of three independent experiments.

To confirm the efficacy of the RL system, as well as investigate the capacity of complement to both prime and activate NLRP3 in myeloid lineage cells, primary macrophages were also stimulated with sublytic doses of MAC. CD14+ cells were purified from donor blood utilising the MACS purification system (Miltenyi Biotech), seeded $2x10^5$ cells / well at a density of $1x10^6$ cells/ml in RPMI media in 24 well plates and differentiated in to macrophages using 100 ng/ml GM-CSF in complete RPMI for 4 days at 37˚C as described in the materials and methods (Section 2.5).

On the day of the experiment, differentiated primary macrophages media was replaced and cells were primed with 25 ng/ml or 10 ng/ml C5a for 4 hours. Primed cells were then stimulated with reactive lysis MAC, generated sequentially as previously described, with 3 μg/ml or 0.75 μg/ml C5b6 + 3 μg/ml C7 C8 and C9 for 1 hour. Cells were then lysed in RIPA buffer containing complete protease inhibitor cocktail (Roche) and lysate probed for IL-1β on the ODYSSEY western blot platform (Section 2.19). Briefly, samples and chameleon pre-stained ladder were loaded on to 4-12% gradient BIS-TRIS gels and run at a constant voltage of 120 V for 1 hour. Protein content was then transferred to PVDF membrane using the Invitrogen power blotter system. Membranes were blocked for 1 hour in PBS 5% w/v BSA and membranes probed for IL-1β (mouse anti-human, CST) and β-actin (rabbit anti-human, CST) at 1:1000 dilutions respectively for 1 hour in PBS + 5% w/v BSA. Membranes were washed in PBS 0.1% TWEEN and probed with the respective secondary antibodies anti mouse 680nm and anti rabbit 800nm for 1 hour in PBS 5% w/v BSA protected from light. Membranes were then washed with PBS 0.1% v/v TWEEN and deionized H_2O. Membranes were then visualised using the ODDYSEY system, allow detection at 800nm (gel A – IL-1β) and 680nm (gel B – β-actin). Mature IL-1β was only detectable via western blot in cells stimulated with complete MAC (C5b-9) at the higher concentration (3 μg/ml C5b6 initiator) with a 25 ng/ml C5a priming stimulus, which was ablated by the treatment of cells with 10 μM MCC950 for 30 minutes before MAC deposition, demonstrating IL-1β maturation being dependent on NLRP3 activation (Figure 4.17 A.)

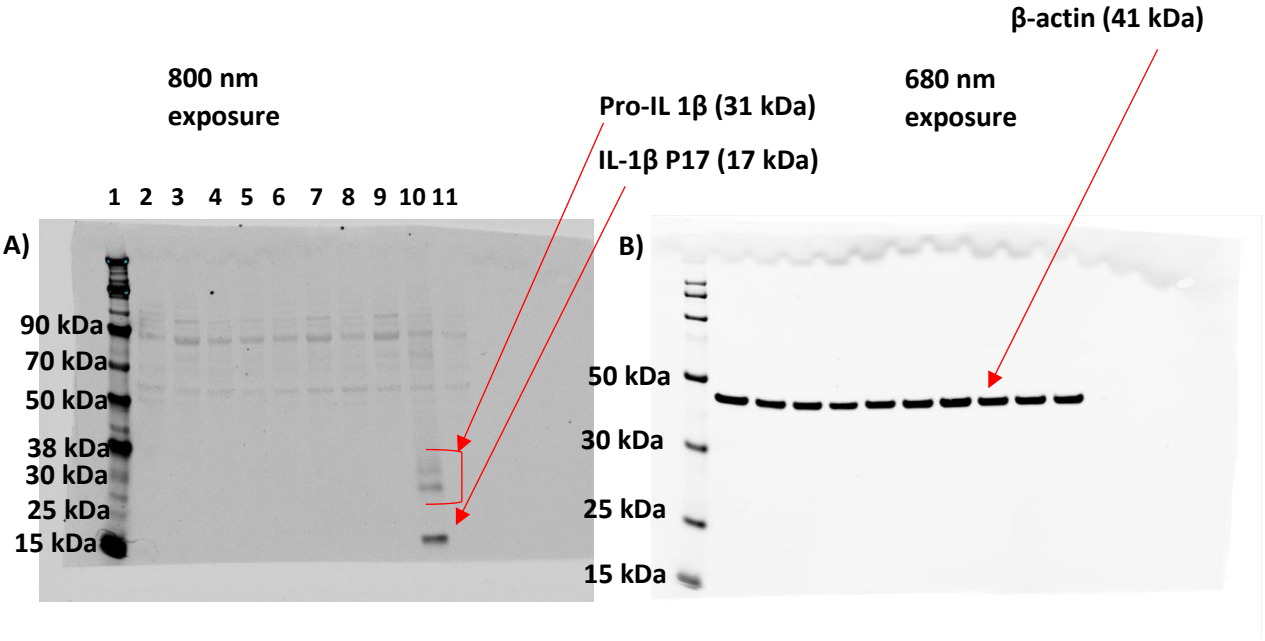

Figure 4.17.A. Sublytic MAC deposition on C5a primed primary macrophages induces IL-1β cleavage.2x10^5 myeloid derived macrophages were primed with 25 ng/ml or 10 ng/ml of C5a for 4 hours in complete RPMI media. Cells were washed and stimulated with reactive lysis MAC, with 0.75 µg/ml or 3 µg/ml initiating C5b6 complex. Cells incubated with MCC950 were incubated for 45 minutes at 37 °C prior to reactive lysis MAC assembly. Cells were stimulated with the denoted concentrations of C5b6 for 10 minutes at room temperature, before the addition of C7 at 5 µg/ml for 15 minutes at 37°C. Cells were washed and complete RPMI media replaced, prior to C8 and C9 addition at 5 µg/ml for 1 hour at 37 °C. Cells were subsequently lysed in 200 µl of RIPA buffer with protease inhibitors and cell lysates subjected to SDS PAGE on 4-12% gradient BIS-TRIS gels for 1 hour at a constant voltage of 120 V. Protein was transferred to PVDF membranes with the Invitrogen fastblot system and membranes blocked in PBS 5% w/v BSA. Membranes were probed with CST mouse anti-human IL-1β and rabbit anti human β-actin antibodies at 1:1000 dilutions. Membranes were washed and probed with the respective secondary antibodies coupled to 680 nm and 800 nm emitting fluorophores, and fluorescence captured on the ODYSSEY Western blot system. Production of IL-1β is dependent on full MAC C5b-9 deposition (Lane 10) and is inhibited by pre-treatment of the cells with 10 µM MCC950 for 30 minutes (Lane 11). Lane 1 – Molecular weight marker, 2 – Unstimulated cells, 3 – C5b6 only, Lane 4 – C7 only, Lane 5 – C8 only, Lane 6 – C9 only, Lane 7 – C5a only, Lane 8 – C5b67 + C5a, Lane 9 C5b678 + C5a, Lane 10 – C5a + MAC, Lane 11 – C5a + MAC + 10 µM MCC950. B. β-actin western blot of 4.16.A.

To obtain a more global view of effects induced by sublytic MAC on cells, RNA-Seq was performed on cells stimulated with sublytic, reactive lysis MAC and compared to C7 + C8 + C9 only controls. 2x10^5 THP-1 cells were seeded at a density of 1x10^6 cells/ml in 96 well U bottom plates in complete RPMI media. Cells were stimulated with reactive lysis MAC as previously described with 3 µg/ml C5b6 initiating complex + C7 to C9 in molar excess at 10 µg/ml and RNA extracted at 1 and 8 hours respectively. Stimulated samples were compared to a C7 + C8 + C9 control with no C5b6 initiating complex. After stimulation, mRNA was extracted and data analysis were performed by Dr You Zhou and David Lee, whilst the RNA SEQ was undertaken by Cardiff gene park.

In total, 307 genes from 61 pathways demonstrated significant differences between the control and stimulated samples. Interestingly, at 8 hours some of the highest Z scored pathways (those with the most significant changes in gene expression of pathway constituents) have connotations for NLRP3 activation and IL-1β signalling. Firstly, IL-1 signalling itself was highlighted as significantly altered at 8 hours relative to controls, reinforcing the data acquired the protein level. Further associated pathways with MAC deposition include Calcium induced signalling alongside pathways with implications in NLRP3 activity, for example, PKA signalling, which was highlighted as the most upregulated pathway after 8 hours is an established negative regulator of NLRP3 activation and may provide a negative feedback loop between sublytic MAC and NLRP3 (Gros and Gros 2016).

å	-log(B-H p-value)	Ratio	z-score	Molecules
Protein Kinase A Signaling	4.4	0.0553	-1.342	GNAS,PTPN23,YWHAE,YWHAB,PDE4A,GSK3A,PTP4A1,PTPN12,RAP1A,PTPRF,EP300,GNB1,PPP3CB,TGFB1,PPP3R1,PRKCD,PRKACA,GNB2,DUSP7,GNG5,SIRPA
RhoGDI Signaling	3.75	0.0756	1	GNB1,ACTR2,GNAS,WASF2,ACTB,GNA12,RHOT2,PAK2,GNB2,ARHGDIA,GNG5,ARHGAP1,EP300
Role of NFAT in Cardiac Hypertrophy	3.44	0.0684	#NUM!	GNAS,EP300,GNB1,PPP3CB,TGFB1,PRKCD,PPP3R1,MEF2D,PRKACA,GNB2,PIK3CB,MAP2K3,GNG5
Cardiac Hypertrophy Signaling	3.29	0.0601	-2.887	GNAS,GNA12,RHOT2,EP300,GNB1,PPP3CB,TGFB1,MEF2D,PPP3R1,PRKACA,GNB2,PIK3CB,MAP2K3,GNG5
fMLP Signaling in Neutrophils	3.21	0.082	-3	GNB1,ACTR2,GNAS,PPP3CB,WAS,PPP3R1,PRKCD,GNB2,PIK3CB,GNG5
Calcium-induced T Lymphocyte Apoptosis	2.93	0.117	2.449	PPP3CB,MEF2D,CD4-,PPP3R1,PRKCD,ATP2A2,EP300
Androgen Signaling	2.93	0.0818	-2	GNB1,POLR2A,GNAS,GNA12,PRKCD,GNB2,PRKACA,GNG5,EP300
Tec Kinase Signaling	2.93	0.0655	-1.89	GNB1,GNAS,WAS,GNA12,ACTB,PRKCD,RHOT2,PAK2,GNB2,PIK3CB,GNG5
IL-1 Signaling	2.75	0.087	-2.236	GNB1,GNAS,GNA12,TAB2,GNB2,PRKACA,MAP2K3,GNG5

Table 8. Table of highest Z-score, significantly changed ENSEMBL pathways from RNA-Seq analysis of reactive lysis stimulated THP-1 monocytes after 8 hours relative to unstimulated (C7+C8+C9) controls. 2x10^5 monocytes were seeded at a density of 1x10^6 cells/ml in complete RPMI media in sterile 96 well, U bottomed plates. Cells were stimulated with RL MAC as previously described. Briefly, cells were stimulated with 3 µg/ml C5b6 for 10 minutes at room temperature, followed by C7 at 5µg/ml for 15 minutes at 37 °C. Cells were subsequently stimulated with 5µg C8 and C9 for 1 or 8 hours. Stimulated cells were washed in sterile PBS and lysed in RNA extraction buffer before mRNA extraction and RNA SEQ were performed by Dr You Zhou, David Lee and Cardiff gene park. Changes in mRNA expression were categorised by ENSEMBL pathways, with the largest changes in mRNA expression at 8 hours having multiple pathways to the activation of NLRP3 include PKA signalling, Calcium induced signalling and IL-1 signalling, reinforcing the data generated through other methods.

Guided by the highly significant changes in PKA pathway component expression in the RNA-Seq analysis, and the known role of PKA in prostaglandin synthesis and NLRP3 regulation, inhibition of PKA in the context of MAC activation of NLRP3 was explored. PKA is a cAMP activated kinase which exerts a range of cellular effects, including in the context of NLRP3 activation the induction of prostaglandin biosynthesis through activation of PKC and induction of COX-2 expression, which results in PGE2 production from membrane lipids (Klein *et al* 2007). The induction of PGE2 production is important due to the established roles of prostaglandins as potent negative regulators of NLRP3 activation (Sokolowska *et al* 2015). Therefore, the MAC, by inducing the activation of PKA signalling, may be a negative feedback mechanism to limit the levels of NLRP3 activation either directly or through the cAMP-PKA-COX2-PGE2 pathway and prevent excessive cytokine production. To investigate this, the classical activation method was used with the specific PKA antagonist H-89 at literature derived doses to investigate whether PKA inhibition in cells exposed to sublytic MAC altered NLRP3 activity and the subsequent Caspase-1 activation and IL-1β release. H89 administration did not significantly affect IL-1β secretion and Caspase -1 activation; despite a slight trend towards an increase at higher doses (Figure 4.18).

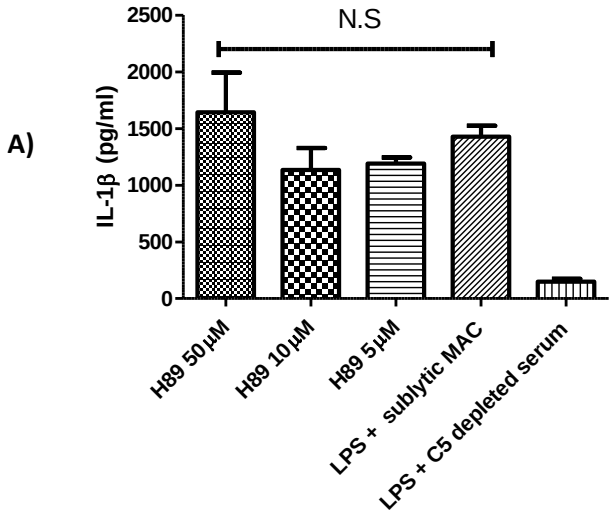

Figure 4.18. The PKA antagonist H89 did not statistically significant affect IL-1β secretion from LPS primed THP-1 cells exposed to sublytic MAC. 2x10^5 THP-1 cells were seeded at a density of 1x10^6 cells /m in complete RPMI media in 96 well, U bottomed plates. Cells were subsequently pre-treated with a titration of H89 hydrochloride (50 – 5 μM) , a potent PKA inhibitor, for 45 minutes prior to sublytic MAC deposition through sensitisation with 2.% v/v COS-1 antiserum and 5% v/v NHS. Cells were stimulated with sublytic MAC for 1 hour and supernatants assayed for IL-1β secretion by ELISA. H89 administration had no statistically significant effects on IL-1β release from LPS primed THP-1 cells (One-way ANOVA with Dunnett post-hoc test).

Whilst H89 pre-treatment had no statistically significant effects in these experiments, the timescale and conditions for inflammasome activation and the previous RNA-Seq experiments are markedly different, 1-hour MAC exposure versus 8 hours and reactive lysis versus classical activation. Therefore, the data do not rule out a role for PKA in cellular responses to sublytic MAC.

4.9 – Conclusions of Chapter 4

In this chapter I have demonstrated that sublytic MAC deposition on primed monocytic cells through both reactive lysis and classical activation methods results in IL-1β secretion and Caspase-1 activation in a NLRP3 dependent manner.

Upon investigating the mechanisms underlying NLRP3 activation in response to sublytic MAC, it was first shown that elevation of extracellular monovalent cations (K^+ and Na^+) through supplementation of the stimulation medium resulted in abrogation of NLRP3 activation, irrespective of the nature of the cation. Although K^+ ions have previously been implicated , my data show that either Na^+ or K^+ ions mediate the effect, provoking questions as to whether the retention of membrane and osmotic potential play roles in the activation process (Brough and Rivers-Aughty 2015).

The role of Ca^{2+} flux in sublytic MAC induced NLRP3 activation has previously been demonstrated by our group in A549 lung epithelial cells and was further investigated in these experiments (Triantafilou *et al* 2013) . In concordance with the literature, pre-treatment of LPS primed THP-1 cells with either BAPTA-AM or the IP3R antagonist Xestospongin C inhibited MAC-induced IL-1β secretion and Caspase-1 activation in a dose dependent manner (Figure 4.5. A-C). The involvement of IP3R-regulated calcium channels in NLRP3 activation links the ER network and ER stress with NLRP3 activation in response to sublytic MAC, with ER stress mediated NLRP3 activation previously reported in response to other stimuli (Li *et al* 2010). Understanding whether ER stress was a critical factor in sublytic MAC mediated NLRP3 was not directly investigated due to the time limitations of the project but may offer an interesting avenue for future research. However, the role of Ca^{2+} in

mediating ROS production, mitochondrial dysfunction and the role of ROS / RNS in NLRP3 activation were all explored to try and unify the hypotheses. Whilst ROS ablation through the ROS scavenger NAC dose dependently inhibited IL-1β secretion in response to MAC (Figure 4.7.A), it failed to inhibit Caspase-1 activity (Figure 4.7.B). This observed dichotomy is unexpected and not easily explained. It is possible that the inhibition of ROS signalling alters the inflammasome response to sublytic MAC by driving the cell signalling down a non-canonical inflammasome route through Caspase 4/5/11 activation, separating IL-1β secretion and Caspase-1, however, this has not been previously documented. The further observation that Superoxide production, the predominant ROS response to sublytic MAC in THP-1 cells demonstrated in Chapter 3 section 8, was unaffected by BAPTA-AM treatment (Figure 4.8), indicates that Calcium flux and ROS production are not tightly linked events. Loss of mitochondrial membrane potential, a marker for mitochondrial dysfunction, was dose dependently induced through complement MAC deposition. However, treatment with the Calcium chelator BAPTA-AM did not reduce mitochondrial depolarisation; indeed, Ca^{2+} chelation caused increased loss of membrane potential in MAC-attacked cells (Figure 4.9). Taken together the data show that Ca^{2+} flux, essential for MAC-mediated NLRP3 activation, is not acting through either ROS production or mitochondrial dysfunction in this system.

To observe any effects of the inhibition of kinases activated by sublytic MAC, a panel of pharmacological inhibitors were used (Figure 4.11). Only MCC950, which directly inhibits NLRP3, and the AKT inhibitor Perifosine had statistically significant effects on MAC-induced IL-1β secretion from the panel of molecules selected. The stark effects of Perifosine in upregulating IL-1β secretion were further explored. Firstly, it was demonstrated that Perifosine exerted a dose dependent effect on IL-1β secretion that was dependent on sublytic MAC deposition, as Perifosine alone or with an LPS prime did not induce IL-1β release (Figure 4.12.A). Other AKT inhibiting compounds such as the AKT 1/2 inhibitor, PP2A inhibitor, PI3K inhibitor and mTORC1 inhibitor all failed to induce the same increase in IL-1β release observed with Perifosine (Figures 4.11, 4.12 and 4.13). This then suggests that Perifosine mediated elevation of IL-1β release in response to sublytic MAC is not through AKT signalling. Whilst Perifosine is marketed as an AKT inhibitor, it has a range of effects on the cell, including the induction of cell death pathways and the activation of cell stress responses shown in Figure 4.19.

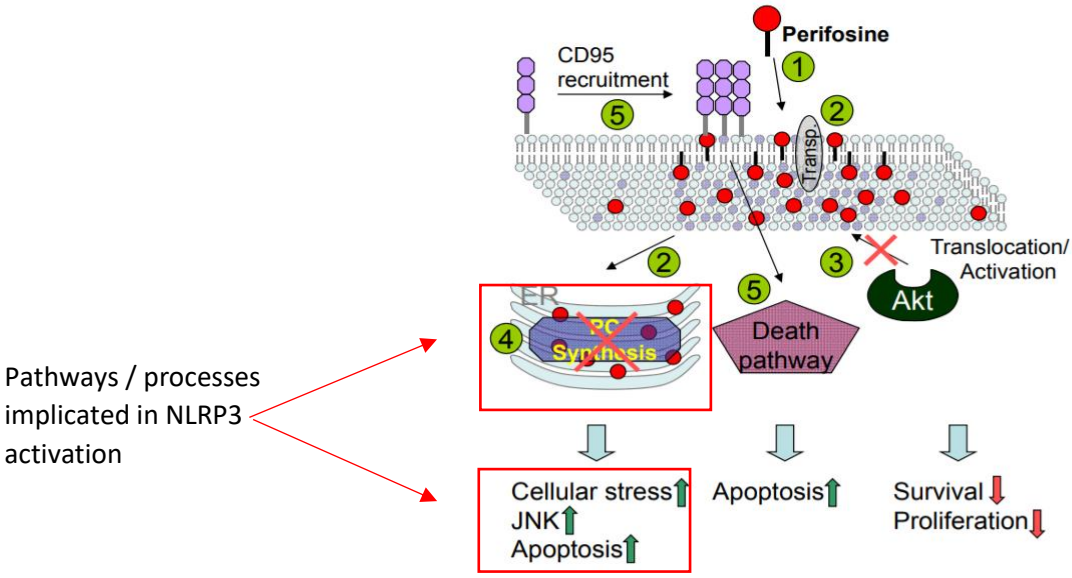

Figure 4.19. Schematic of the pleiotropic effects of Perifosine. Although Perifosine is marketed as an inhibitor of AKT translocation to the cell membrane and subsequent activation through PHD interactions, Perifosine also elicits an array of other effects. These include increasing cell stress through ER dysfunction and the induction of CD95 signalling which can invoke necrotic cell death pathways through RIPK1/3 activation. This in turn can induce cell death, cellular stress and activation of inflammatory MAPK's such as JNK. Image sourced from Fenestrele et al 2014.

Because the role of Perifosine in the induction of IL-1β could not be attributed to its function as an AKT inhibitor, I explored whether off-target effects of the molecule were responsible for the observed elevations of IL-1β secretion. One of these off-target effects is the activation of JNK signalling. JNK has previously been implicated in NLRP3 activation and linked to MAC mediated cell death as demonstrated in Figure 4.20 (Okada *et al* 2014; Lusthaus *et al* 2018). The specific JNK inhibitor, SP6100, caused a non-significant reduction in IL-1β secretion (Figure 4.15.A); however, the ERK pathway has also been implicated in NLRP3 activation but inhibition had no significant effects on IL-1β release alone (Figure 4.11) (Chang *et al* 2017).

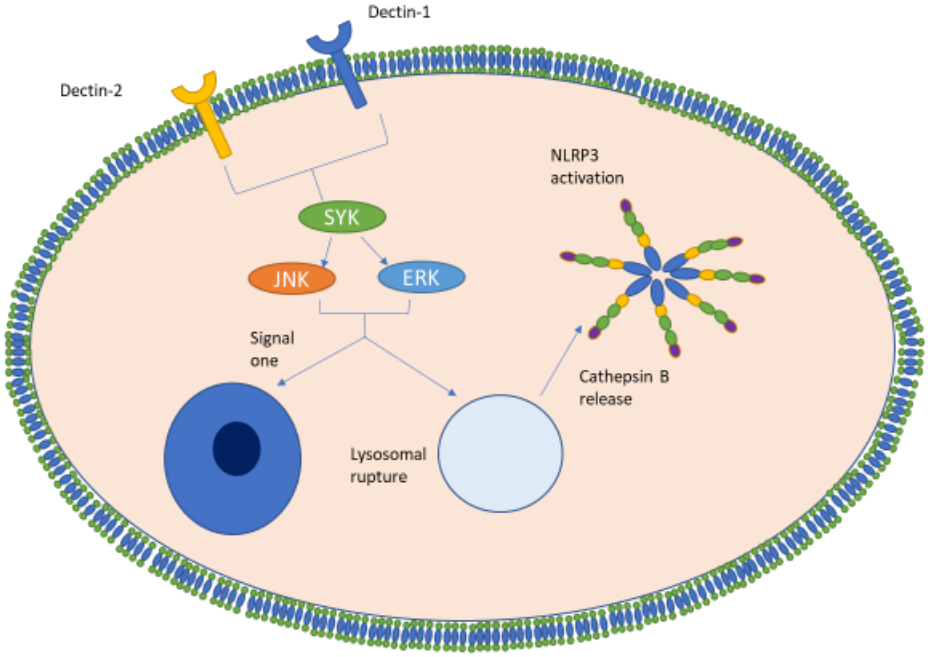

Figure 4.20– The role of MAPK's in the activation of NLRP3 in response to Dectin 1/2 activation. Both JNK and ERK were implicated in the induction of lysosomal destabilisation in the proposed model. Image based on Chang et al 2017.

The dual inhibition of both ERK and JNK in MAC-attacked cells demonstrated dose dependent inhibition of both IL-1β secretion and Caspase-1 activity (Figure 4.14. B /C). This provides evidence that some of the established intracellular signalling pathways in response to sublytic MAC have active roles in NLRP3 activation (Towner *et al* 2016). A possible mechanistic hypothesis, encompassing the multi-source data suggesting that IP3R mediated Ca^{2+} flux plays an important role in NLRP3 activation, is that ER stress is a central mediator of NLRP3 activation in response to MAC, as both ERK and JNK activation are inducible through ER stress responses (Figure 4.20), and IP3R localise on the ER, which also mediates ROS production; ER stress can thus potentially link the array of pathways proposed.

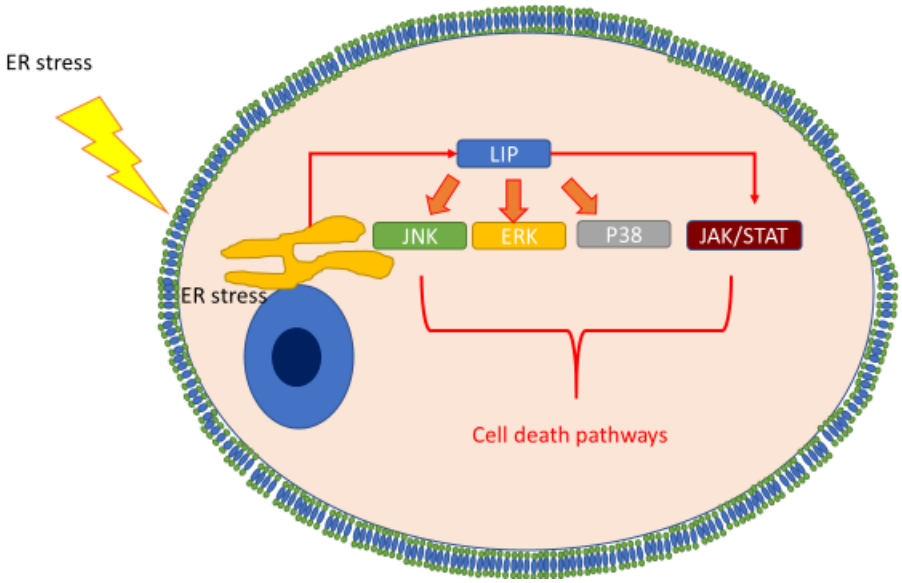

Figure 4.21. ER stress can mediate both JNK and ERK activation, as well as being the central organelle containing IP3R and being an important mediator of ROS/RNS production. Image based on diagram from Wasserman-Dozorets and Rubinstein 2017.

Direct testing of the effects of sublytic MAC on the ER was not performed due to time constraints, so whilst offering a potential hub for the observed mechanisms, further work is needed to verify the ER as the central organelle responsible for NLRP3 activation in this system, however, ER stress in response to sublytic MAC has been demonstrated in other studies (Cybulsky *et al* 2002) .

A second method of forming MAC on the cell surface was performed to verify the classical pathway results. MAC formation through reactive lysis on C5a primed THP-1 monocytes induced dose dependent IL-1β secretion (Figure 4.16.B.) that was dependent on the formation of complete MAC pores, with C56-8 intermediates or individual components not inducing cytokine secretion (Figure 4.16.A). This was also subsequently demonstrated on PBMC derived primary macrophages, with none of the individual components or intermediate complexes generating mature IL-1β detectable by Western blot (Figure 4.17 A/B). The IL-1β signal was also abrogated through the pre-treatment of the cells with MCC950, demonstrating the NLRP3 dependence of MAC-induced IL1β secretion.

Beyond the activation of NLRP3, reactive lysis derived MAC was also used to stimulate THP-1 monocytes and RNA-Seq performed by collaborators Dr You Zhou and David Lee, with the largest Z-Scoring ENSEMBL pathways shown in Table 8. The highlighted pathways have some biologically expected results such as Calcium and apoptotic pathways being highly upregulated, whilst others such as PKA signalling were of interest in terms of relaying inflammatory cell signalling. In preliminary experiments, PKA inhibition was explored in the context of NLRP3 activation; however, there was no statistically significant effect of PKA signalling inhibition on sublytic MAC mediated IL-1β secretion (Figure 4.18).

Chapter 5 - Investigating the roles of NLRP3 in MAC mediated nucleated cell death

5.1- Generation of SW 982 NLRP3-/- cells

As previously demonstrated by our group and others, MAC deposition on cells can instigate NLRP3 activation and subsequently Caspase-1 activity and IL-1β release (Triantafilou *et al* 2013; Laudisi *et al* 2013; Suresh *et al* 2016). Whilst MAC deposition on nucleated cells is generally non-lytic, large numbers of MAC complexes can result in a lytic form of cell death. As NLRP3 activation can also result in a lytic, necrotic form of cell death through Gasdermin D pore formation this raises the question of whether MAC mediated nucleated cell death functions, at least in part, through NLRP3 (Fink and Cookson 2006). There has been previous work demonstrating that MAC mediated cell death is partially transduced through intracellular signalling pathways; Caspase inhibition or blocking of necroptotic pathways partially ameliorated MAC mediated cell death, but no work has been published specifically focussing on the role of NLRP3 (Lusthaus *et al* 2018).

To investigate the role of NLRP3 in MAC signalling in a different cell type, SW 982 synoviocytes were used. These cells were edited using the CRISPR/Cas9 system with commercially sourced gRNA against Exon 1 of NLRP3 to induce frameshift mutations in the gene, resulting in a loss of expression as described in materials and methods (methods described in section 2.24). To verify the loss of NLRP3 expression, WT and CRISPR/CAS9 treated cells were tested for successful knockout by Reverse Transcriptase Polymerase chain reaction (RT-PCR) and Western blot for mRNA and protein expression respectively, with methods described in sections 2.19 and 2.30 respectively. Briefly, $2x10^5$ SW 982 synoviocytes were seeded / well in 24 well sterile plates in complete RPMI media and allowed to adhere overnight. Cells were then stimulated with LPS (100 ng/ml) for 4 hours to induce elevated NLRP3 expression. Cells were washed with sterile PBS before lysis in RIPA buffer (Western blot) or RNA extraction buffer + β-mercaptoethanol (RT PCR) and stored at -20°C until use. For RT-PCR, RNA purification and extraction was performed as described in section 2.29, prior to RNA quantification using absorbance at 260/230 nm on the Nanodrop system. 200 ng of sample mRNA was then added per PCR tube, and RT PCR performed as described in section 2.30. The resultant PCR product was then loaded on to agarose gel and

electrophoresis performed as previously described. As the mRNA loading in to the original RT-PCR reaction was equal, that was taken as a loading control for this experiment.

NLRP3 mRNA expression was detected in LPS primed SW 982 synoviocytes using RT-PCR followed by electrophoresis (Fig 5.1.1A); specific bands were present at the expected PCR product size in WT cells (expected amplification product size – 498 bp) and was absent in knockout cells. A rabbit monoclonal anti-NLRP3 antibody (CST) was used in Western blots to detect NLRP3 protein; although a non-specific band marginally heavier than NLRP3 was present in all cell lysates, the specific band representing the protein (circa 120 kDa) was present in WT LPS-primed cells but absent in KO cells (Fig 5.1.1B).

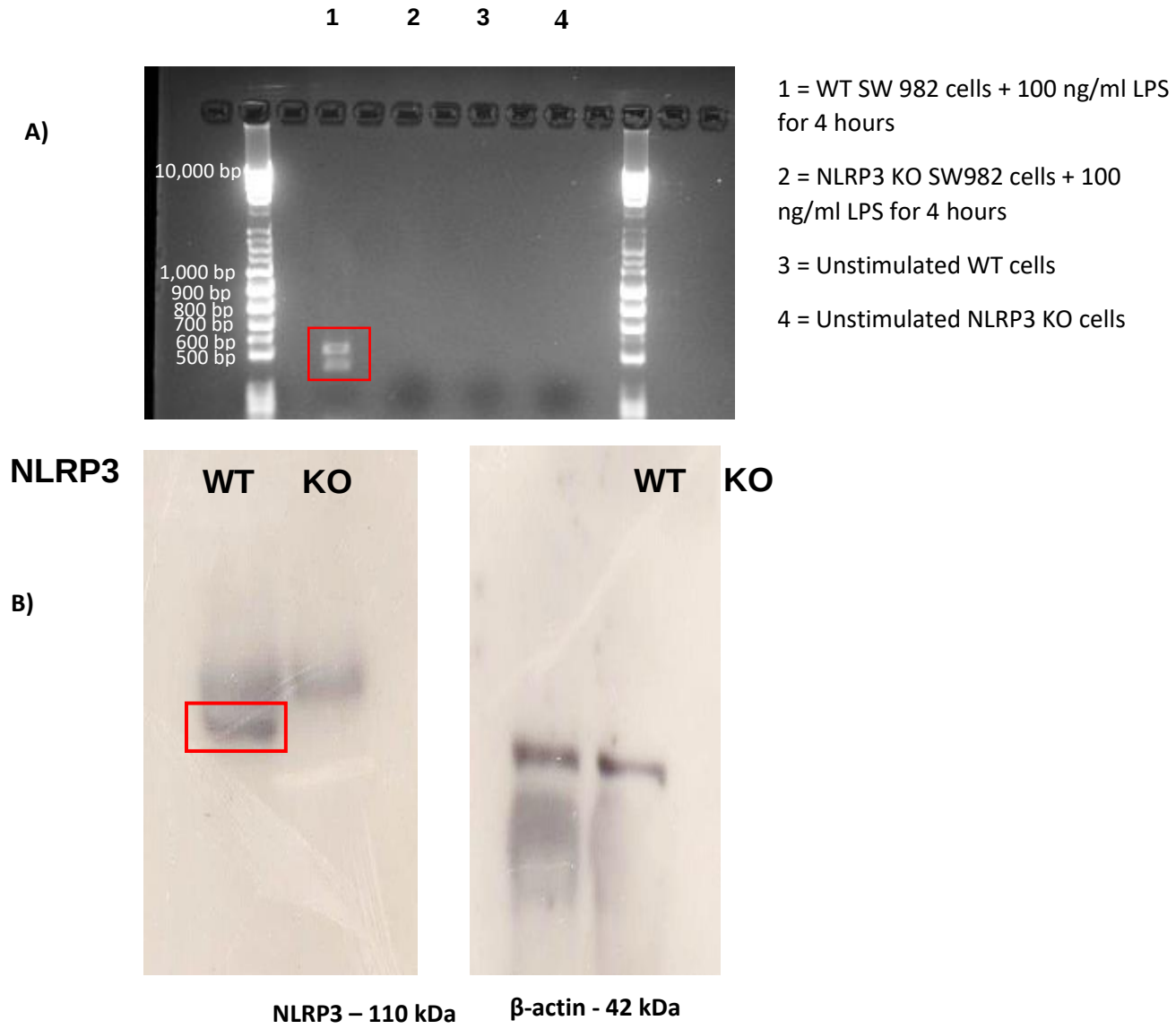

Figure 5.1.1. A. RT-PCR of NLRP3 expression from WT or NLRP3 KO cells. 2x10^{5}WT or KO SW 982 synoviocytes were seeded in 12 well plates in complete RPMI media and allowed to adhere overnight. On the day of the experiment, cell media was replaced, and relevant samples primed with LPS (100 ng/ml) for 4 hours. Cells were washed with sterile PBS and lysed in 100 µl of RNA extraction buffer + ß-mercaptoethanol. Extracted RNA was quantified on the Nanodrop and equal amounts of template RNA (200 ng/ sample) added to the RT PCR mixture as described in section 2.30. The resultant RT-PCR product was run on a 1% agarose gel and visualised using ethidium bromide on the Thermofisher MyECL system. The expected PCR amplicon length was 497 bp and was visualised in the WT cells primed with LPS, but not the NLRP3 KO cells or unprimed WT cells. 5.1.1.B. Western blot of NLRP3 expression in WT and NLRP3 KO SW 982 cells. Cells were seeded and stimulated with LPS as in A. After stimulation, cells were lysed using 100 µl of RIPA buffer + protease inhibitors. 15 µl of sample lysate was denatured at 90 °C for 10 minutes under reducing conditions and subjected to reducing SDS PAGE and Western blot analysis (CST mouse anti-human NLRP3 antibody and . NLRP3 WT cells demonstrated NLRP3 expression, which was absent in CRISPR/Cas9 treated cells. The membrane was then stripped and re-probed for ß-actin.

5.2 - Investigating the roles of NLRP3 in the cell response to MAC in SW 982 synoviocytes

After validating the absence of NLRP3 expression in the CRISPR/Cas9 treated cells, sublytic titrations of NHS were set up to observe differences in response to complement deposition in the presence and absence of NLRP3 expression. WT or NLRP3 KO SW 982 were seeded at $2x10^4$ cells per well in a 96 well plate and assay performed as described in the materials and methods. Briefly, seeded cells were allowed to adhere overnight in complete RPMI media. Cell media was then replaced on the day of the experiment and cells sensitised to complement using 2.5% v/v COS-1 antiserum as previously described, for 20 minutes at room temperature. Cell media was then replaced, and the cells exposed to titrations of NHS as a source of complement (5-0.25% v/v). Under the conditions used, WT cells were sensitive to killing in the LDH assay, with up to 50% cell death being observed at 2.5% NHS prior to a slight plateau at 5% NHS; in contrast, NLRP3 KO cells were highly resistant to lytic killing, with statistical significance across all titrated doses of NHS. Representative data shown below in Figure 5.2.

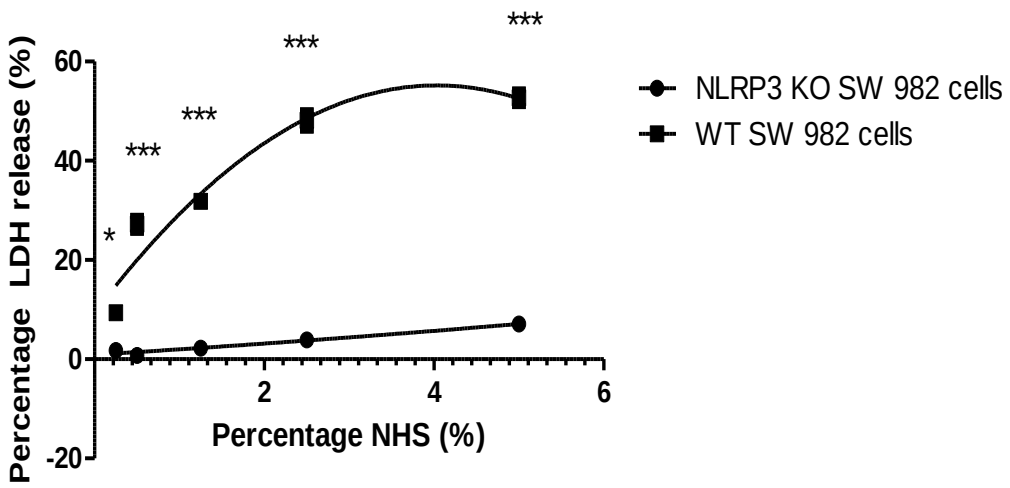

Dose of NHS	Difference	t	P value	Summary
5.000	45.63	22.35	P<0.001	***
2.500	44.23	21.66	P<0.001	***
1.250	29.54	14.47	P<0.001	***
0.5000	26.43	12.94	P<0.001	***
0.2500	7.651	3.747	P < 0.05	*

Figure 5.2. LDH release assay between WT and NLRP3 -/- SW 982 synoviocyte cells. 2x10^4 SW 982 WT and NLRP3 KO cells were seeded in 96 well sterile plates in complete RPMI media and allowed to adhere to the plate overnight. On the day of the experiment, and cell media replaced. Cells were sensitised with 2.5% v/v COS-1 antiserum at room temperature as previously described, prior to media being replaced and a titration of NHS (0.25 – 5% v/v) for 1 hour, alongside NHS without sensitising antibody negative and 1x final concentration lysis buffer positive control. 50 µl of cell supernatant was aspirated and mixed 1:1 with LDH buffer protected from direct light for 45 minutes. The LDH reaction was subsequently stopped with the addition of 50 µl of 10% v/v acetic acid and absorbance measured at 492 nm. The loss of NLRP3 resulted in a significant reduction in cell death and subsequent LDH release from the cells. This experiment was repeated >5 times. Data from a single representative experiment presented as the mean +/- SEM and analysed using a two-way ANOVA with a Bonferroni Post-hoc test in GraphPad Prism.

Due to the stark contrast in cell death readouts by LDH release, a second death assay was performed to confirm the results. This was performed by PI staining in both flow cytometry and 96 well plate-based formats.

To perform flow cytometry, adherent SW 982 cells were removed from the TC plastic surface using Trypsin EDTA solution and resuspended in sterile Eppendorf's in complete RPMI media prior to complement attack. Cells were then stimulated using COS-1 antiserum / NHS as previously described for the LDH assay. In flow cytometric assays, WT cells were lysed on exposure to complement (with the generation of a PI positive population, whereas while NLRP3 KO cells were resistant to killing, replicating the LDH assay findings (Figure 5.3).

WT Unstimulated (Pink) v 2% Triton X positive control (Blue)

WT Unstimulated (Pink) v NHS 10% + COS-1 (Blue)

WT Unstimulated (Pink) v NHS 5% + COS-1 (Blue)

WT Unstimulated (Pink) v NHS 2.5% + COS-1 (Blue)

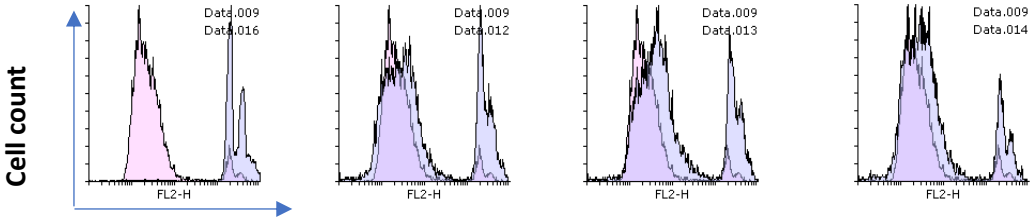

KO Unstimulated (Pink) v 2% Triton X positive control (Blue)

KO Unstimulated (Pink) v NHS 10% + COS-1 (Blue)

KO Unstimulated (Pink) v NHS 5% + COS-1 (Blue)

KO Unstimulated (Pink) v NHS 2.5% + COS-1 (Blue)

B)

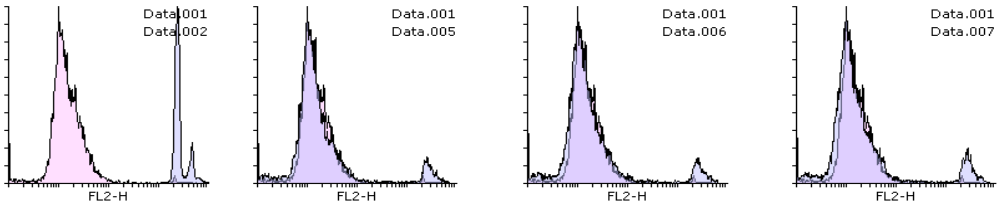

10% NHS WT (Blue) v NLRP3 -/- (Pink)

5% NHS WT (Blue) v NLRP3 -/- (Pink)

2.5% NHS WT (Blue) v NLRP3 -/- (Pink)

C)

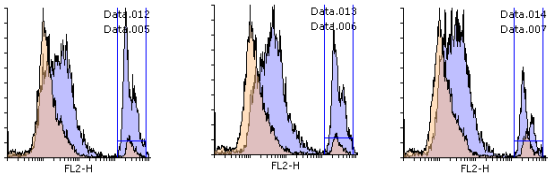

D)

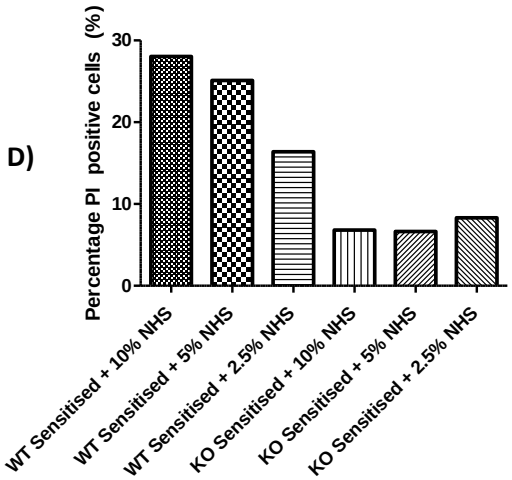

Figure 5.3.A. Flow cytometry analysis of SW 982 WT cells stained with Propidium iodide and attacked with complement or exposed to antiserum or serum only controls. 2x10^5 WT cells were trypsinised and sensitised to complement with 2.5% v/v COS-1 antiserum for 20 minutes at room temperature as previously described. Cells were then stimulated with a titration of NHS (2.5-10% v/v NHS) for 1 hour. Positive (1% v/v Triton X) and negative (unstimulated) cells were also included. Cells were subsequently stained using 10 µg/ml propidium iodide and fluorescence measured by flow cytometry on the FACS Calibur. WT SW 982 cells demonstrated an NHS dose dependent increase in PI positive staining B. NLRP3 -/- cells were sensitised to complement and stimulated with NHS as described for the WT cells. NLPR3 -/- cells demonstrated positive PI staining with the Triton X positive control, validating the assay, but were not lysed when exposed to complement attack. C. Direct comparison of PI staining histograms of WT cells (Blue) and NLRP3 -/- SW 982 cells (Pink) from A. and B. (Pink) across a titration of NHS doses for PI positive staining. D. Quantification of the PI positive gated populations from Figure C.

To ensure the that no PI positive NLRP3 -/- SW 982 cells were lost on the flow gating strategy, the change in PI mediated fluorescence over 1 hour of complement attack was also measured using the Clariostar fluorescent plate reader (Fig 5.4). Again, sensitised WT SW 982 cells exposed to NHS demonstrated an increase in PI fluorescence, beginning at around 8 minutes after initiation of complement attack, whereas the NLRP3 -/- SW 982 cells demonstrated comparable fluorescence to WT C5 depleted NHS controls confirming that the cells were not lysed in the absence of MAC.

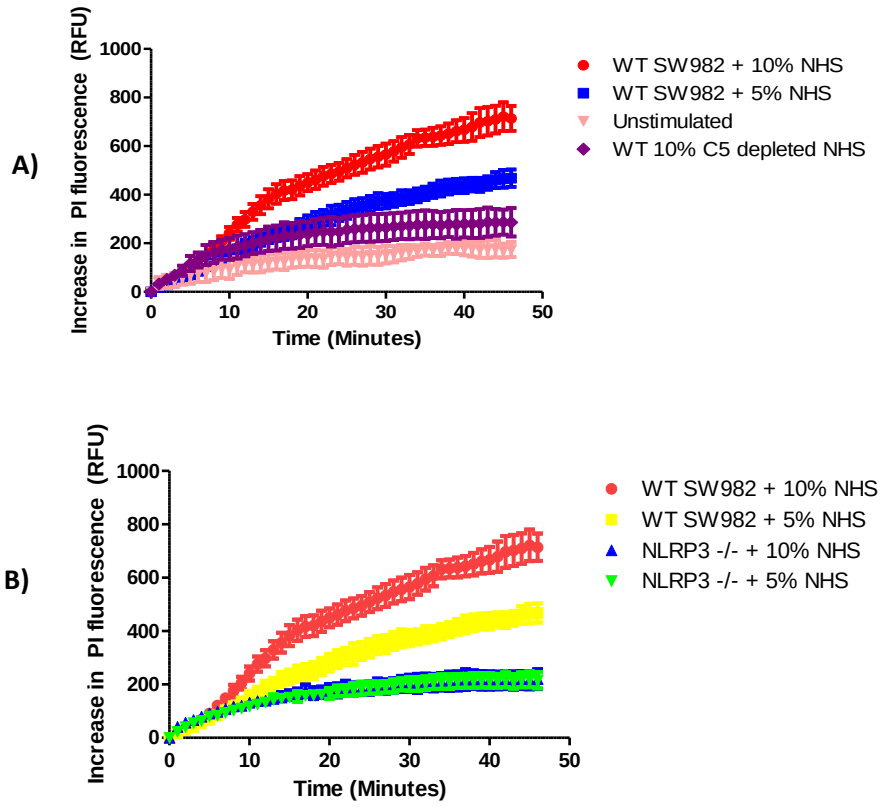

Figure 5.4.A. WT SW 982 cells demonstrated a dose dependent increase in PI fluorescence upon classical pathway activation. 2x10^4 WT SW 982 were seeded per well in 96 well opaque white plates. Cells were sensitised to complement using 2.5% v/v COS-1 antiserum for 20 minutes. Cell media was replaced, and 10 µg/ml of PI added to the cell media. Cells were subsequently stimulated with NHS or C5 depleted as described and changes in PI fluorescence measured over 45 minutes. A Statistically significant difference in fluorescence (P < 0.001) was observed between 10% NHS + COS-1 antibody and unstimulated and C5 depleted NHS controls, analysed by one-way ANOVA with Dunnett post-hoc test. Data presented as mean +/- SEM from a single experiment, representative of three independent experiments. B. Comparison of sensitised WT and NLRP3 -/- SW982 cells PI uptake in response to exposure to two doses of NHS as a source of complement. NLRP3 -/- in SW982 cells statistically significantly (P<0.001) reduced PI uptake compared to WT (one-way ANOVA with Bonferroni post-hoc test comparing serum doses between cell types). No statistically significant difference was observed dependent on NHS dose in NLRP3 -/- SW 982 cells. Data presented as mean +/- SEM from a single experiment, representative of three independent experiments.

Across both PI and LDH assays WT cells were consistently susceptible to MAC mediated cell death, whilst NLRP3 -/- cells were protected. To explore whether pharmacological inflammasome inhibition replicated this finding, MCC950, the specific NLRP3 inhibitor, was added to the cells at 10 µM as previously described in other studies (Coll *et al* 2015). Cells were then sensitised, exposed to NHS and lytic susceptibility assessed by PI uptake compared to cells without MCC950 treatment (Figure 5.5). Cells pre-treated with MCC950 demonstrated statistically significant protection from MAC mediated lytic death, albeit not to the same extent as the genetic knockout, further supporting a role for NLRP3 in

mediating cell death. The reasons for the less marked effect of pharmacological inhibition are unclear but may relate to longer term ablation of NLRP3 function, drug dose or efficacy in the system.

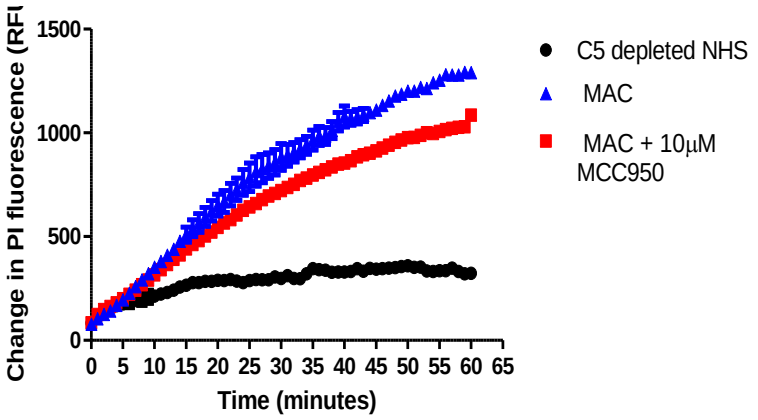

Bonferroni's Multiple Comparison Test	Mean Diff.	t	Significant? P < 0.05?	Summary	95% CI of diff
MAC + 10µM MCC950 vs MAC	-137.0	4.673	Yes	***	-195.1 to -78.96

Figure 5.5. PI uptake in of WT SW 982 synoviocytes in response to MAC in cells treated with 10 µM MCC950 v untreated over time. 2x10^4 WT SW 982 cells were seeded per well in opaque white plates in 200 µl of complete RPMI media and allowed to adhere to the plate overnight. On the day of the experiment, cell media was replaced with fresh complete RPMI. Samples pre-treated with 10 µM MCC950 were incubated at 37 °C for 45 minutes. After incubation, cell media was replaced, and cells sensitised to complement with 2.5% v/v COS-1 antiserum for 20 minutes at room temperature. Cell media was again replaced with complete RPMI and PI added at a final concentration of 10 µg/ml. Plates were then transported to the clariostar plate reader and PI fluorescence measured at an excitation / emission profile of 480 / 630 nm respectively and a gain of 800. MCC950 pre-treated samples exposed to MAC were compared with untreated cells and with C5 depleted NHS as a MAC-negative control. MCC950-treated cells showed statistically significantly reduced PI uptake relative to untreated cells on exposure to 10% NHS. Data presented as mean +/- SEM and analysed by One-way ANOVA with Bonferroni Post-Hoc test comparing all pairs of columns (P<0.001).

The role of necroptosis in MAC mediated cell death was also investigated. SW 982 cells were pre-incubated with a titration of Necrostatin-1, a RIP kinase inhibitor that blocks necroptotic killing, prior to complement sensitisation and attack with NHS / C5 depleted NHS. Cell viability was subsequently measured using the LDH release assay. SW 982 cells demonstrated dose-dependent protection from MAC mediated cell death with the addition of Necrostatin-1 (Figure 5.6).

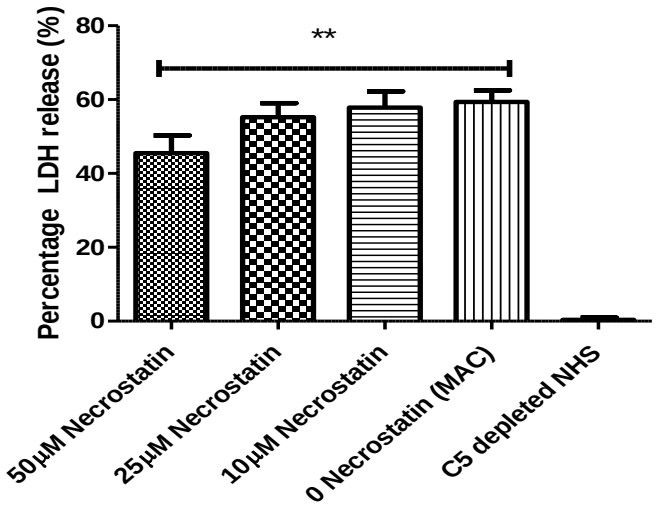

*Figure 5.6. LDH release assay with a pre-treatment titration of Necrostatin-1 on SW 982 synoviocytes prior to MAC deposition. 2x104 WT SW 982 cells were seeded per well in sterile 96 well plates in complete RPMI media and allowed to adhere to the plate overnight. On the day of the experiment, media was replaced, and cells treated with a titration of Necrostatin-1 (50-10 µM) for 45 minutes at 37 ˚C. Cells media was subsequently replaced cells sensitised to complement with 2.5% v/v COS-1 antiserum for 20 minutes at room temperature. Sensitised cells media was replaced and 5% v/v NHS / C5 depleted serum added to the cells for 1 hour at 37 ˚C, alongside NHS without sensitising antibody negative and 1x final concentration lysis buffer positive control. 50 µl of cell supernatant was aspirated and mixed 1:1 with LDH buffer, protected from direct light, for 45 minutes. The LDH reaction was subsequently stopped with the addition of 50 µl of 10% v/v acetic acid and absorbance measured at 492 nm. Pre-treatment with 50 µM Necrostatin-1 statistically significantly inhibited LDH release from the cells relative to untreated controls. Data presented as mean +/- SEM from a single experiment, representative of three independent experiments. Statistics performed with One-way ANOVA with Dunnett post-hoc test, comparing all samples with MAC treated controls (** = P ≤ 0.01) .*

To determine whether NLRP3 expression influenced Caspase-1 activity in response to MAC in SW 982 cells the Caspase-1 Glo assay was used as previously described in materials and methods and Chapter 4. WT and NLRP3 -/- SW 982 cells were LPS primed, sensitised and stimulated with complement and Caspase-1 glo reagent added for 1 hour. Luminescence was subsequently read on the Clariostar plate reader. Caspase-1 activity in NLRP3-/- cells was significantly lower that WT at both serum doses used for MAC challenge and was significantly inhibited through pre-treatment of the cells with the NLRP3 inhibitor MCC950 (Fig 5.7). LPS priming of WT SW 982 cells also caused non-significant increases in Caspase-1 activity relative to unstimulated WT controls, suggesting that levels of Caspase-1 activation may be occurring in response to the priming stimulus. No significant difference in Caspase-1 activity was observed between lytic (10% NHS) and sublytic (2.5% NHS) MAC on WT SW982 cells. These data suggest that MAC is activating Caspase-1 via NLRP3 in these cells as the response is lost in NLRP3 -/- cells; however, IL-1β secretion was not detectable in ELISA of

cell supernatants. This concurs with other reports which demonstrated undetectable levels of IL-1β release from SW 982 cells stimulated with canonical NLRP3 activators (Sugiyama *et al* 2014).

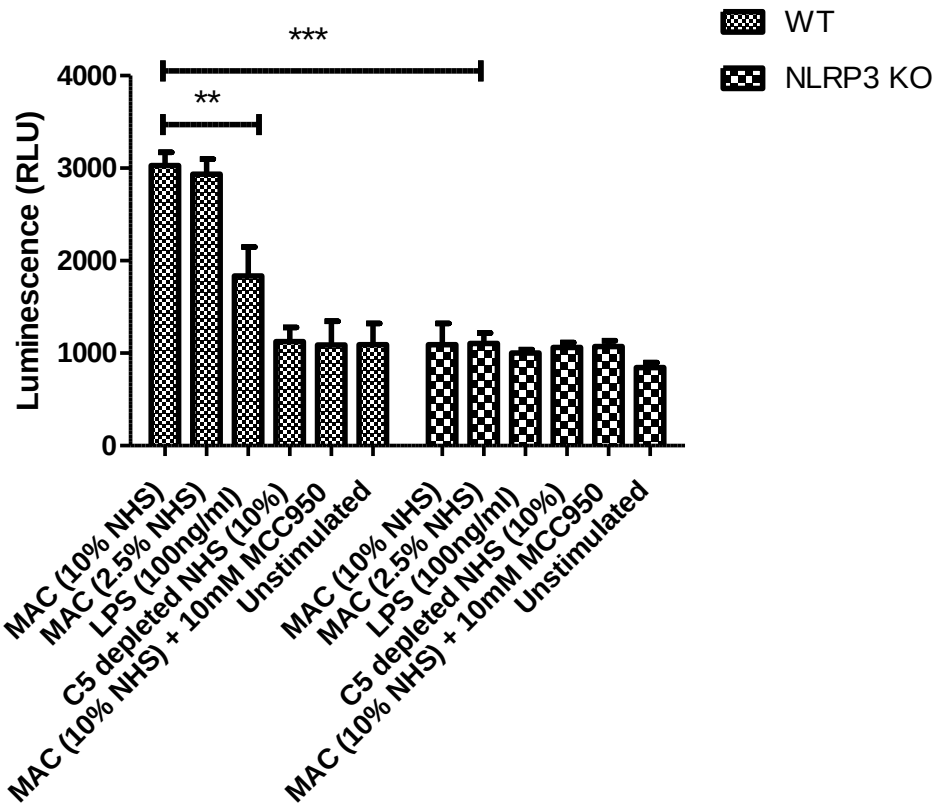

*Figure 5.7. Caspase-1 activity assay of NLRP3 -/- and WT SW 982 cells. WT and NLRP3 KO cells were seeded at 2x10^4 cells / well in opaque white plates in complete RPMI media and allowed to adhere overnight. On the day of the experiment, cells were primed with 100 ng/ml LPS for 4 hours at 37 °C. Cell media was subsequently replaced and 10 μM MCC950 control samples treated at 37 °C for 45 minutes. Cells were subsequently sensitised to complement with 2.5% v/v COS-1 antiserum for 20 minutes at room temperature. Cell media was replaced and cells stimulated with MAC at lytic (10% v/v) and non-lytic (2.5 % v/v) doses and incubated with Caspase-1 glo reagent for 90 minutes prior to luminescence reading on the Clariostar plate reader. Only WT cells demonstrated a statistically significant elevation of Caspase 1 activity in response to MAC. Data presented as mean +/- SEM from a single experiment, representative of three independent experiments. Data analysed using a one-way ANOVA with Dunnett post-hoc test to compare all columns to MAC 10% NHS WT sample(** = P ≤ 0.01, *** = P≤ 0.001).*

The data show, across multiple different platforms and assay techniques, that NLRP3 -/- and NLRP3 inhibitor treated SW 982 cells are significantly protected from complement mediated cell death compared to WT and untreated counterparts. Levels of Caspase-1 activation in response to MAC were significantly increased in the WT cells but not in NLRP3-/- cells relative to controls. The mechanism by which NLRP3 knockout or inhibition induces protection from lysis requires further investigation as is likely of importance in

understanding the effects of MAC on nucleated cell death pathways, including necroptosis as shown here.

As a first step in understanding mechanism, I tested whether complement was being activated to similar degrees on the surfaces of both cell types. While loss of NLRP3 has not been previously reported to alter cell surface protein expression, the observed lack of cell death could be due to an altered cell surface epitope profile, resulting in inefficient antibody binding from COS-1 antiserum and consequent lack of complement activation and MAC mediated death. WT and NLRP3 -/- SW 982 cells were stimulated with COS-1 antiserum and NHS as previously described, then stained for complement activation marker C3b as a marker of complement activation (Figure 5.8).

A)

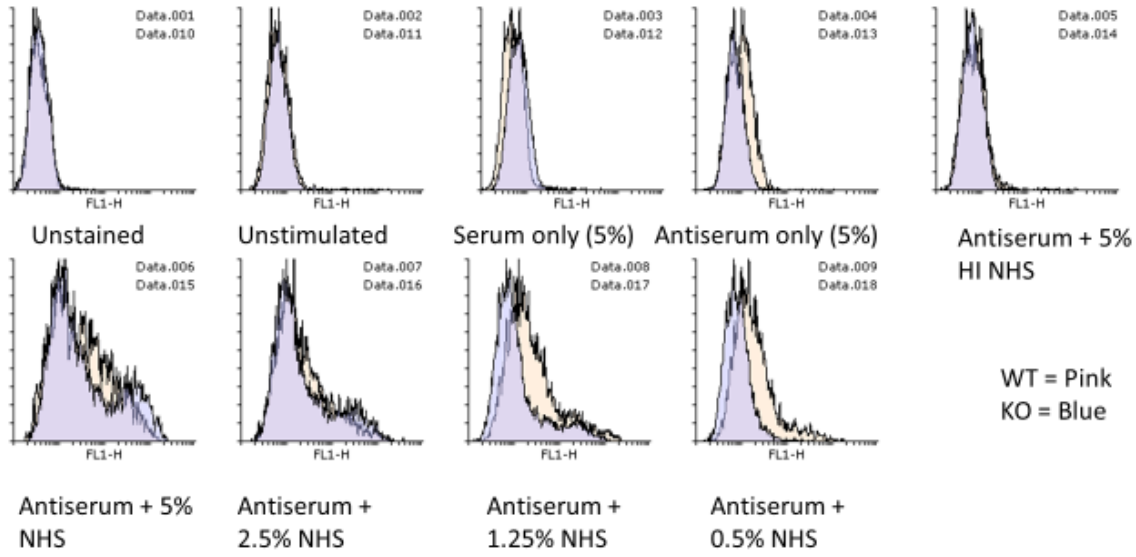

B)

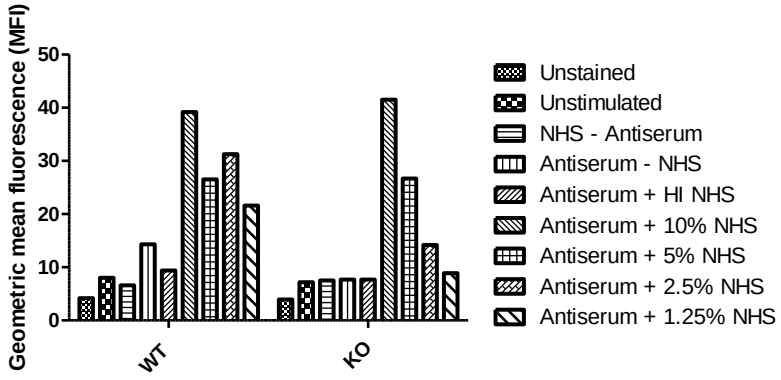

Figure 5.8.A. C3b staining of WT and NLRP3 -/- SW 982 synoviocytes. 2x10^5 WT and NLRP3 KO cells were trypsinised per sample and sensitised to complement with 2.5% v/v COS-1 antiserum in complete RPMI media for 20 minutes at room temperature in sterile Eppendorf's. After sensitisation, cells were centrifuged, media replaced, and 2.5% v/v NHS or HI NHS added for 1 hour at 37 °C as previously described. Cells were subsequently washed, fixed with 4% PFA for 20 minutes at 4 °C and then stained with a monoclonal anti-C3b FITC antibody (Biolegend) at a 1:50 dilution for 30 minutes protected from direct light. Cells were washed with sterile PBS and resuspended in 200 µl of FACS buffer and transferred to FACS to tubes prior to analysis by flow cytometry on the FACS Calibur and histograms generated using FlowingSoftware 2. The FL-1 fluorescence corresponding to C3b deposition was comparable between WT and NLRP3 -/- SW 982 cells at the NHS doses used in sublytic attack experiments (5%, 2.5%), indicating a similar capacity to fix complement on the surface using COS-1 antiserum at lower serum doses WT cells stained more strongly for C3b.B. Quantification of mean fluorescence from 5.8.A.

5.3 - Investigating whether NLRP3 modulates complement regulator expression on the SW 982 cell surface

The data above show that NLRPs-/- cells are protected from complement lysis when exposed to NHS, however, demonstrate C3 fragment deposition similar to WT. To further understand how NLRP3 expression and complement mediated cell death were linked, a key question was whether inhibition or deletion of NLRP3 altered the cell surface expression of complement regulators such as CD55 and CD59, which in turn might explain how NLRP3-/- cells are protected from complement lysis. Firstly, CD55 and CD59 expression was compared between the two cell types under unstimulated conditions by flow cytometry as described in the materials and methods. WT SW 982 cells showed specific staining for CD55 compared to various antibody controls and there was no significant difference in CD55 expression between WT and NLRP3-/- cells (Fig 5.9A); in contrast, WT SW 982 cells showed no specific staining for CD59 (except for a small positive sub-population apparent in the histograms) while NLRP3-/- cells expressed CD59 abundantly on the cell surface (Figure 5.9.B)

A)

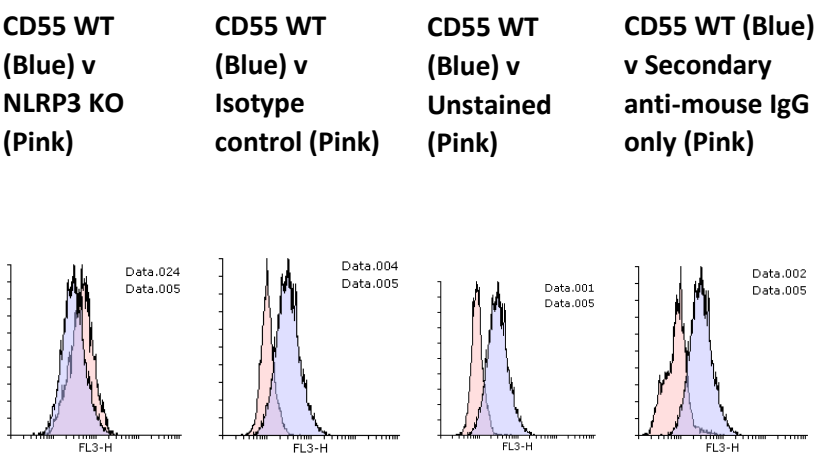

B)

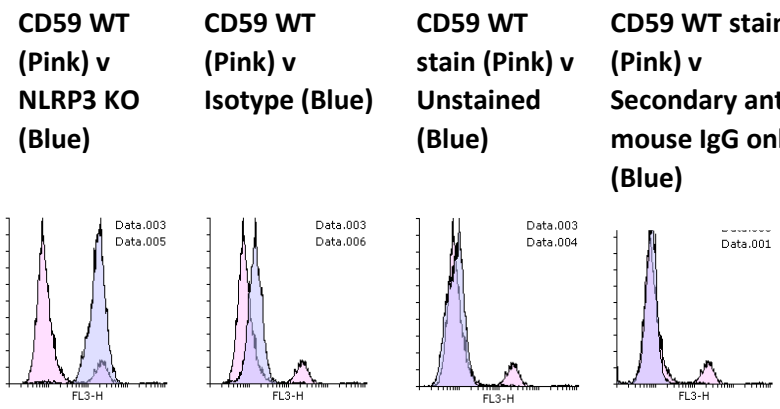

Figure 5.9. Analysis of CD55 and CD59 expression on WT and NLRP3 -/- SW 982 synoviocytes. A. Comparison of expression of CD55 between WT and NLRP3 KO cells. 2x10^5 WT and NLRP3 KO cells were trypsinised from the flask and transferred to sterile Eppendorf's. Cells were stained for CD55 with 10 µg/ml BRIC 215 in FACS buffer for 30 minutes at room temperature protected from direct light. Cells were washed twice with sterile PBS and were subsequently stained with 1:50 dilution of anti-mouse IgG Alexa 546 for 30 minutes in FACS buffer, protected from direct light. Cells were washed, resuspended in FACS buffer and transferred to FACS tubes before fluorescence was measured on the FACS Calibur. Both WT and NLRP3 -/- SW 982 cells stained positively for CD55, but with no significant differences between the two cell types. B. WT and NLRP3 KO cells were prepared as in A. Cells were subsequently stained for CD59 expression using 10 µg / ml MEM43 mAb in FACS buffer for 30 minutes at room temperature. Cells were washed twice with sterile PBS and resuspended in FACS buffer, before staining using a 1:50 dilution of anti-mouse IgG Alexa 546 for 30 minutes protected from direct light. Cells were washed, resuspended in FACS buffer and transferred in to FACS tubes. Fluorescence was subsequently recorded on the FACS Calibur. WT cells were negative for CD59 expression, except for a small positive subpopulation. NLRP3 -/- cells stained strongly and universally positive for CD59 expression, to the same level as the small CD59 positive subpopulation of the WT cells.

To further investigate the elevation of cell surface CD59 expression in NLRP3 -/- cells, both WT and NLRP3 -/- cells were treated with MCC950, the specific NLRP3 inhibitor, to determine if pharmacological inhibition could partially replicate the effects seen at the genetic level. Cells were pre-treated with a titration of MCC950 doses (10-1 µM) for 1 hour prior to staining for CD59 as previously described. Exposure of WT SW 982 cells to MCC950 caused a dose-dependent increase in CD59 expression; as anticipated, the NLRP3 inhibitor had no effect on CD59 expression in NLRP3-/- cells (Figure 5.10). Exposure to the higher doses of MCC950 increased CD59 expression in WT to levels similar to those in NLRP3-/- cells.

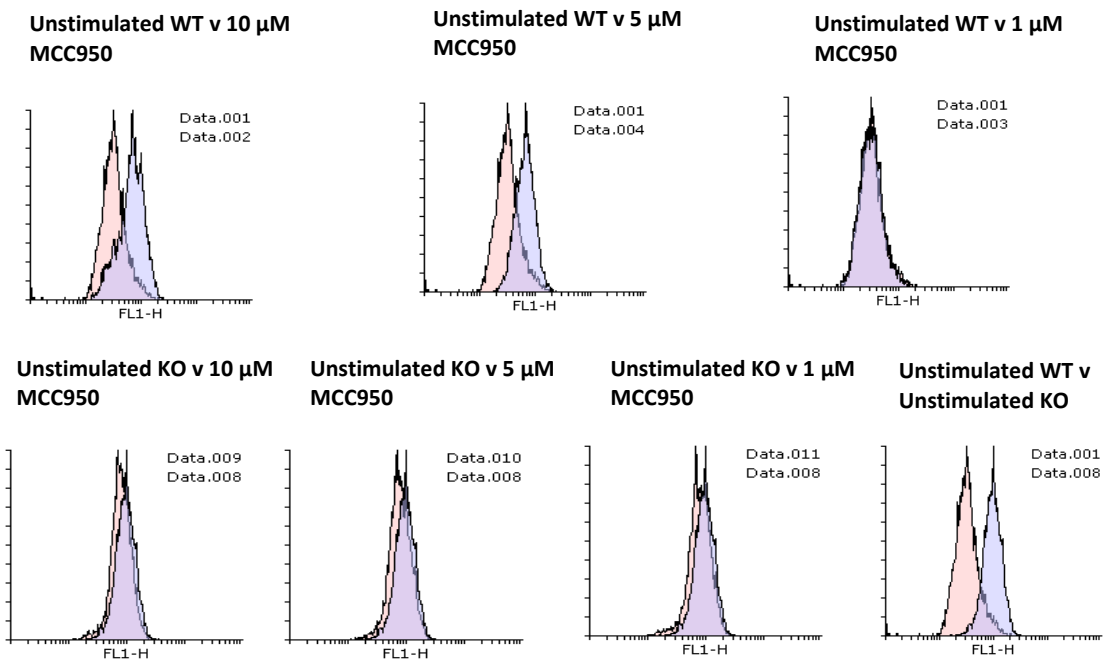

Figure 5.10. Changes in CD59 cell surface expression in response to treatment with MCC950. 2x10^5 WT and NLRP3 -/- SW 982 synoviocytes were trypsinised from flasks and resuspended in complete RPMI in sterile Eppendorf tubes. Cells were subsequently treated with a titration of MCC950 (10-1 µM) for 1 hour at 37°C prior in complete RPMI. Cells were then fixed in 4% v/v PFA at 4°C for 20 minutes. Cells were washed and stained for CD59 using 10 µg/ml MEM 43 in FACS buffer for 30 minutes. Cells were washed, resuspended in FACS buffer and stained using anti-mouse IgG FITC (1:50 dilution) as previously described. Cells were subsequently washed with sterile PBS, resuspended in FACS buffer and transferred to FACS tubes prior to fluorescence measurement using the FACS Calibur. Treatment of WT cells with MCC950 induced a dose dependent increase in CD59 staining on the cell surface, whereas the NLRP3 -/- cells exhibit no changes with drug administration.

The rapid changes in CD59 expression observed in the above experiments (within an hour of exposure to inhibitor) suggested a non-transcriptional / translational mechanism was responsible for the changes observed. This is supported by established literature demonstrating CD59 translocation from intracellular to cell surface localisations upon cell activation in neutrophils and as part of insulin secretion in β-cells of the Pancreas (Okada *et al* 1994;Renstrom *et al* 2016). Therefore, it was hypothesised that the differences in CD59 staining between WT and NLRP3-/- cells could be reduced or eliminated by permeabilising the cells with 0.1% Triton X after fixing to allow antibody staining of any intracellular CD59 stores. After permeabilization, apparent CD59 expression in WT cells was markedly increased and the differences in expression between WT and NLRP3-/- cells effectively lost (Figure 5.11)

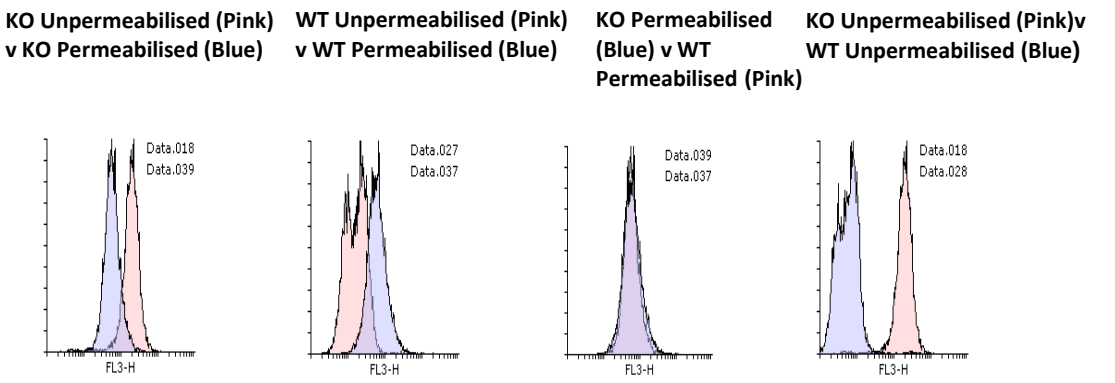

Figure 5.11. CD59 staining in permeabilised and non-permeabilised WT and NLRP3-/- SW 982 synoviocytes. 2x10^5 WT and NLRP3 KO cells were trypsinised and transferred to sterile Eppendorf tubes in complete RPMI media. Cells were subsequently fixed using 4% v/v PFA for 20 minutes at 4 °C. Cells were washed with sterile PBS, resuspended in FACS buffer and stained using 10 µg/ml BRIC 229 +/- 0.1% v/v Triton X (dependent on permeabilisation state) for 30 minutes. Cells were subsequently washed and resuspended in FACS buffer before the addition of anti-mouse Alexa 546 (1:50 dilution) in FACS buffer +/- 0.1% v/v Triton X 100 protected from direct light for 30 minutes. Cells were subsequently washed , resuspended in FACS buffer and fluorescence analysed on the FACS Calibur. WT SW 982 cells fluorescence increased upon permeabilization, whereas staining of KO cells was reduced. The overlay demonstrated that staining of the two permeabilised cell types was comparable, suggesting WT cells but not NLRP3-/- cells had stores of CD59 within the cell exposed on permeabilisation. Data analysed using Flowing software 2.

To verify the complement regulator data collected by flow cytometry, confocal microscopy was used. WT and NLRP3 -/- cells were seeded and stained for CD59 using MEM43 and Alexa 546-labelled secondary anti-mouse IgG, and a lipid raft marker, Cholera toxin subunit B labelled with Alexa 488, to determine cell surface localisation and visualised on the Zeiss

confocal microscope, as described in the materials and methods. Co-localisation of CD59 and Cholera toxin subunit B was determined using Zen black software, with a Pearson's coefficient > 0.5 taken as significant co-localisation. Whereas unpermeabilised WT cells were negative for CD59 staining, permeabilization revealed intracellular CD59 in a granular distribution; unpermeabilised NLRP3-/- cells stained strongly for CD59, partly co-localised with the lipid raft marker, and permeabilization reduced CD59 signal (Figure 5.12 and Table 7). The lack of CD59 positive staining for permeabilised NLP3 -/- cells may be explained by the lack of intracellular CD59 due to the high cell surface expression, and that permeabilising conditions may not be optimal for cell surface antigen staining.

	Alexa 546 (CD59)	Alexa 488 (Lipid rafts)	ToPRO (Nucleus)	Merge
Anti -mouse IgG Alexa 546 + ToPRO only				
Cholera toxin B Alexa 488 + ToPRO only				
NLRP3 -/- SW 982 cells non- permeabilised				

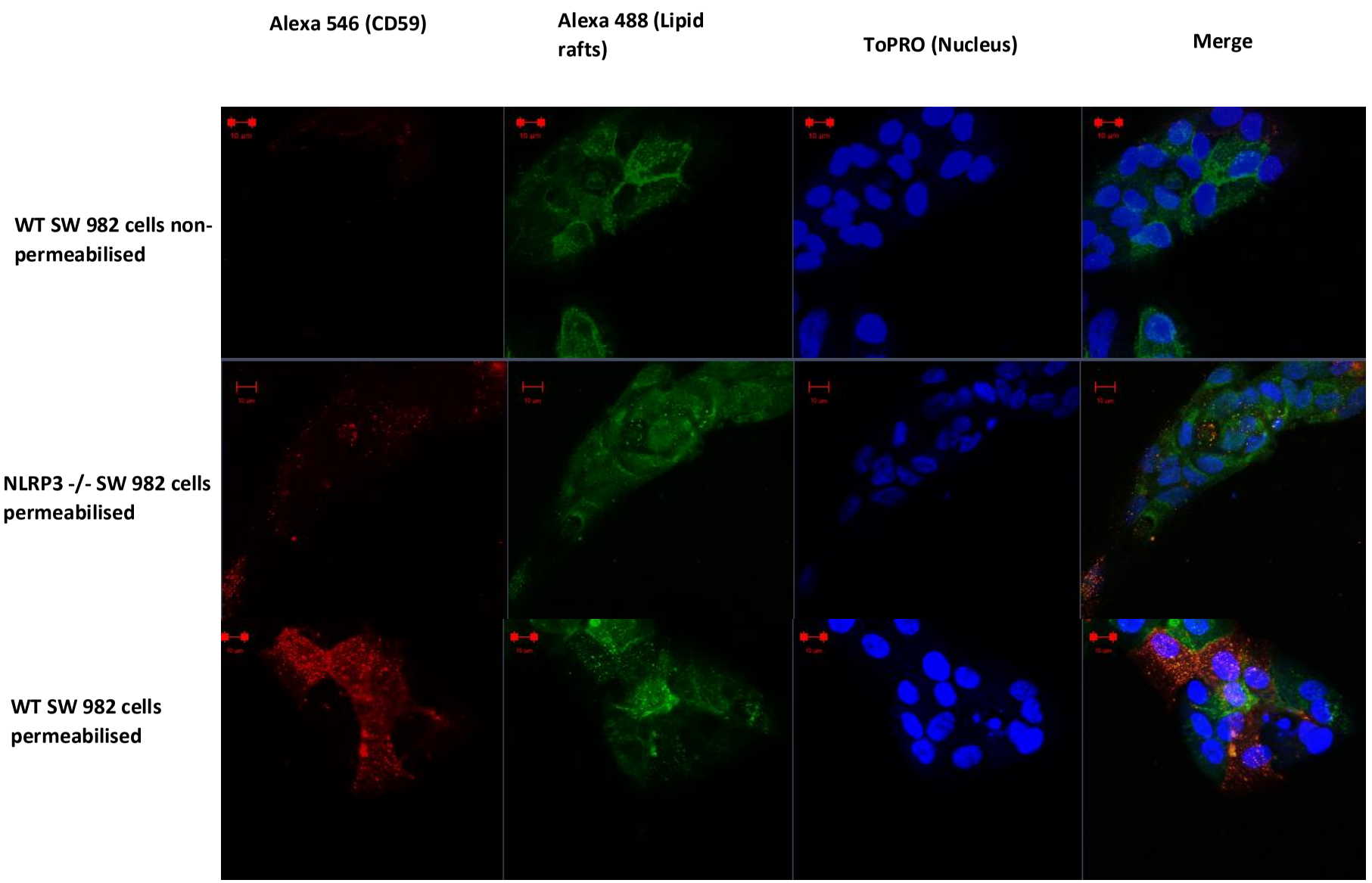
Alexa 546 (CD59)
Alexa 488 (Lipid rafts)
ToPRO (Nucleus)
Merge
WT SW 982 cells non-permeabilised
NLRP3 -/- SW 982 cells permeabilised
WT SW 982 cells permeabilised

Table 8

Sample	Pearson's co-efficient	Significant colocalisation
Anti-mouse Alexa-546 control	-0.003	No
Cholera Toxin B subunit Alexa 488 control	0.12	No
NLRP3 -/- SW982, non-permeabilised	0.73	Yes
NLRP3 -/- SW982, permeabilised	0.24	No
WT SW982 Non-permeabilised	0.35	No
WT SW982 permeabilised	0.31	No

Figure 5.12. Confocal microscopy of WT and NLRP3 -/- SW 982 cells probing for CD59 expression and lipid rafts. 4x10^4 WT and NLRP3 KO cells were seeded per well on sterile glass chamber slides and allowed to adhere to the surface overnight in complete RPMI media. On the day of the experiment, cells were fixed using 4% v/v PFA for 20 minutes at 4°C. Cells were subsequently washed with sterile PBS and stained with 10 µg/ml BRIC 229 +/- 0.1% v/v Triton X (dependent on permeabilisation state) for 30 minutes in sterile PBS + 0.2% w/v BSA. Cells were washed twice with sterile PBS before staining with anti-mouse Alexa 546 (1:50 dilution) in sterile PBS, 0.2% w/v BSA +/- 0.1% v/v Triton X 100 protected from direct light for 30 minutes. Samples stained for lipid rafts also had Cholera Toxin B- Alexa 488 conjugate added at 1 µg/ml at this stage. Cells were washed twice with sterile PBS, and nuclear visualisation was performed with a 1:2,000 dilution of ToPRO in sterile PBS protected from direct light for 10 minutes. The casket removed, and cover slips applied as per the materials and method (section 2.18). Cells were imaged using the ZEISS confocal microscope using a 1.4 NA 63x Zeiss objective lens SW 982 cells were demonstrated to have far lower cell surface CD59 staining when unpermeabilised, and poor colocalization between Alexa 488 and Alexa 546. NLRP3 -/- cells demonstrated strong cell surface expression of CD59 and co-localisation with lipid raft marker. Upon permeabilization, a large amount of signal is lost from the NLRP3 -/- cells, whereas the WT cells had strong staining of CD59 on- intracellular granules. Table 8. Quantification of Pearson's colocalisation co-efficient between Cholera toxin B Alexa 488 and MEM43 + anti mouse IgG 546. Only NLRP3 -/- SW 982 cells, non-permeabilised demonstrated significant colocalisation. Scale bars shown om images in the top left corner of images at 10 µm.

5.4 – Investigating the effect of inhibition of complement regulator function on susceptibility to MAC mediated cell death

NLRP3 -/- SW 982 cells were resistant to MAC mediated cell death, and, as shown above, had increased cell surface expression of CD59; this may regulate the levels of MAC deposited on the cell surface and effect the observed resistance. To test this, CD59 function was inhibited using the blocking mAb MEM43 on both WT and NLRP3 -/- cells.

Adherent WT and NLRP3 -/- SW 982 cells were sensitised using 2.5% COS-1 antiserum alone or with MEM43 and incubated with 10% NHS in the presence of 1 µM PI. Readings were taken on the Clariostar plate reader with excitation of 480 nm, a dichroic setting of 568nm and an emission of 615nm respectively. A positive control of 100% lysis was obtained through the addition of 1% Triton X to triplicate wells of WT and KO cells for 10 minutes at the end of the experiment

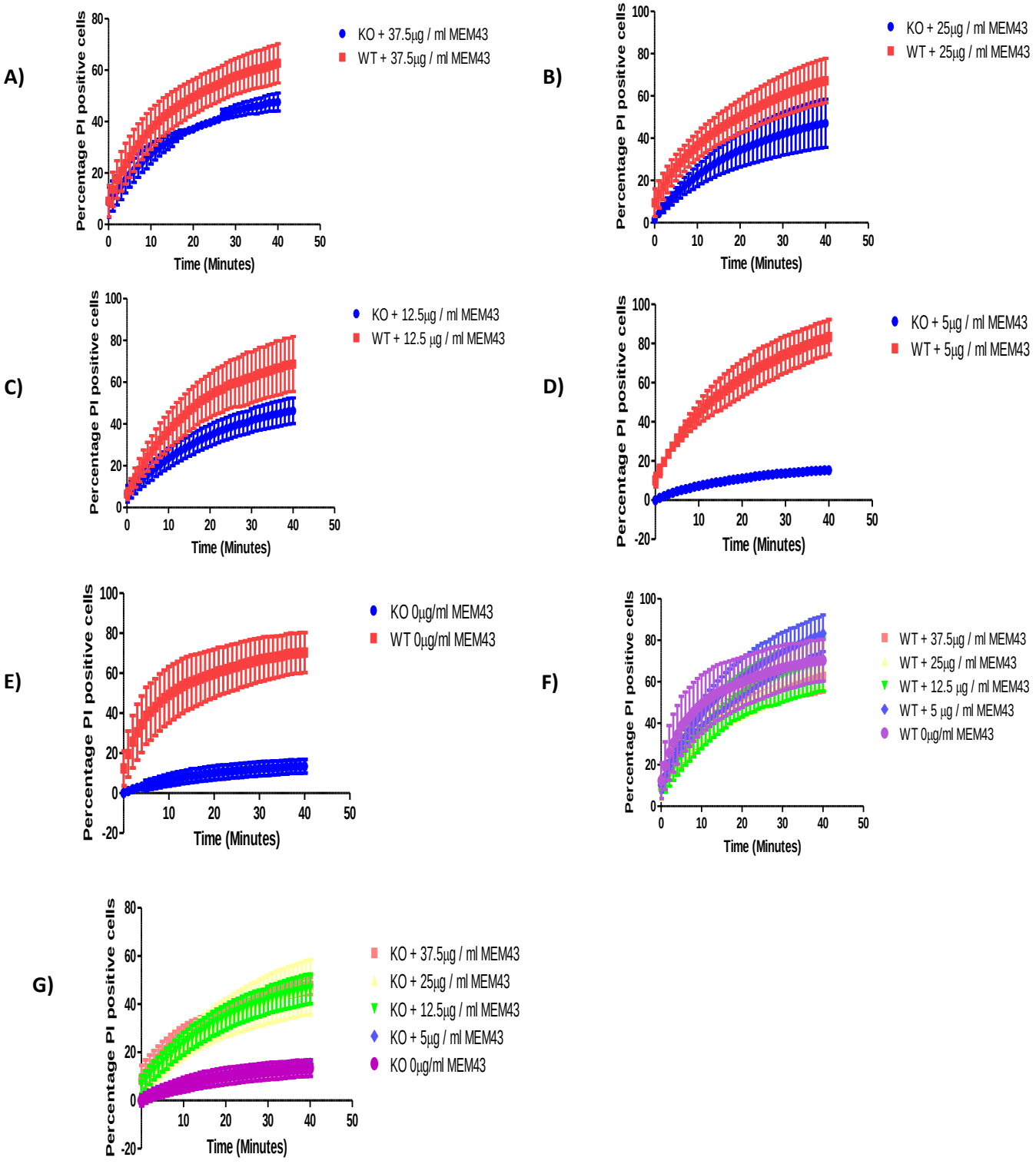

Figure 5.13.A-E.Percentage cell death of WT v NLRP3 KO SW 982 synoviocytes stimulated with lytic MAC over time. 2x10⁴ WT and NLRP3 KO cells were seeded / well in white, opaque plates in complete RPMI media and allowed to adhere to the plate overnight. On the day of the experiment, media was replaced, and cells sensitised to complement with 2.5% v/v COS-1 antiserum +/- MEM43 anti-CD59 antibody at doses between 0 and 37.5 µg/ml for 20 minutes at room temperature. Cell media was replaced, and PI added at 10 µg/ml. Plates were transported to the Clariostar plate reader and subsequently attacked with 10% NHS as a source of complement. PI fluorescence was measured over time with excitation at 480 nm, a dichroic setting of 568 nm and an emission of 615 nm respectively. Data was analysed in the MARS analysis software and plotted in GraphPad PRISM 5. In the absence of MEM43 or presence of the lowest dose (5 µg/ml), NLRP3-/- cells were resistant to lysis. At higher doses of MEM43, lysis of NLRP3-/- cells increased approaching that of WT cells. Lysis of WT cells was not affected by the presence of MEM43. F,G. Dose responses to MEM43 for WT and NLRP3-/- SW 982 synoviocytes respectively.

Although the data above demonstrate that the observed differences in cell death between WT and NLRP3-/- cells was predominantly CD59 dependent, there remains the possibility that downstream effects of MAC deposition, are also affected. To test this, Ca^{2+} influx, was investigated. It was hypothesised that the WT SW 982 cells would experience a MAC mediated spike in Ca^{2+} whereas the NLRP3 -/- cells would experience little or no change due to the increased CD59 expression. Cells were loaded with Fluo-3-AM as previously described for THP-1 cells (Chapter 3, section 7) and in materials and methods. Time 0 readings were taken, sensitised cells were stimulated with a titration of NHS or C5 depleted NHS and the changes in fluorescence from baseline measured. A positive control of maximal exposure of the dye to Ca^{2+} was performed with 1% Triton X and the change in intracellular Ca^{2+} concentration calculated. NLRP3 -/- SW 982 cells did not exhibit Ca^{2+} flux above baseline, whereas MAC treated WT cells demonstrated a rapid influx as previously described (Fig 5.14.A). To confirm that this was due to the higher expression of CD59 inhibiting MAC formation on the $NLRP3^{-/-}$ cell surface, cells were incubated with MEM 43 at a previously demonstrated inhibitory dose and Ca^{2+} flux measured. With CD59 function impaired, NLRP3 -/- SW 982 cells demonstrated a similar Ca^{2+} flux profile to WT cells (Fig 5.14.B).

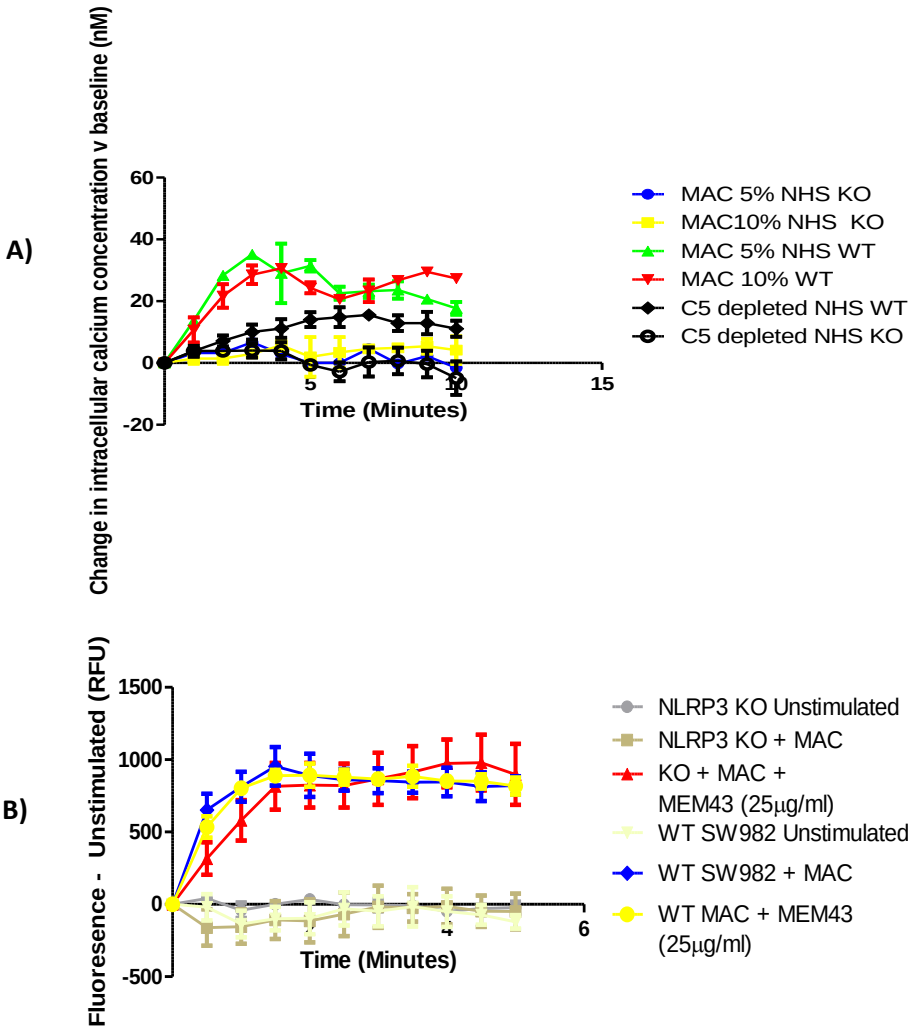

Figure 5.14.A. Calcium flux assay comparing WT and NLRP3 -/- (KO) SW 982 cells. 2x104 WT and NLRP3 KO cells were seeded at 2x104 cells per well in opaque white plates in complete RPMI media and allowed to adhere overnight. On the day of the experiment, media was replaced and both cell types were loaded with 2.5 µM Fluo-3-AM for 45 minutes at 37 °C in complete medium as previously described. Cells were subsequently washed twice with sterile PBS and sensitised to complement with 2.5 % v/v COS-1 antiserum for 20 minutes at room temperature. Cells media was then replaced, and cells transported to the Clariostar plate reader. The plate reader was configured with 505 nm / 525 nm excitation / emission respectively cells and exposed to 10 or 5% NHS or C5 depleted NHS as a source of complement and fluorescence measured. WT SW 982 cells exhibited a rapid influx of Ca^{2+}, whereas NLRP3 -/- cells did not exhibit a Ca^{2+} signal in the same manner, suggesting that MAC formation was inhibited on these cells, in agreement with the PI staining data. B. Cells were prepared as in A. However, upon sensitisation, WT and NLRP3 KO samples were treated +/- 25 µg/ml Mem43, which was permissive of PI uptake on NLRP3 KO cells from figure 5.13. Plate reader configuration and NHS stimulation conditions were performed as in A. and Ca^{2+} flux measured. After CD59 blockade, NLRP3-/- SW 982 cells showed a similar Ca^{2+} influx to the WT cells, suggesting the protection from Ca^{2+} flux and PI uptake is CD59 dependent.

5.5 -Conclusions of Chapter 5

In this series of experiments, the effects of NLRP3 deletion or inhibition in SW 982 synovial cells was investigated. It was demonstrated that commercially available gRNA's against NLRP3 exon 1 in a CRISPR/Cas9 system were effectively ablated NLRP3 expression at the mRNA and protein levels. Unexpectedly, loss of NLRP3 expression in these cells rendered them highly resistant to MAC mediated cell death, demonstrated using both LDH release and PI uptake assays, with cell death under the selected conditions less than 10% greater than controls, whereas WT cells demonstrated 50% cell death. This surprising finding is not without precedent; SiRNA knockdown of RIPK1, a central mediator of necroptosis, in a range of cell types was recently demonstrated to influence MAC mediated death, reducing killing measured by PI and Trypan blue uptake by 40-50% through RIPK1, RIPK3 and phospho-MLKL mediated necroptotic cell death (Lusthaus *et al* 2018).

To determine the mechanism by which NLRP3 deletion or inhibition protected SW 982 cells from MAC killing, complement deposition and regulator expression were measured; one purpose of these experiments was to ensure there were no off-target effects of the CRISPR process used to target NLRP3 on complement resistance mechanisms. CD55 expression and C3b deposition upon complement activation were comparable between the two cell types, indicating that there was no difference in capacity to activate the early stages of complement; however, CD59 expression on the cell surface was essentially absent in WT cells and markedly upregulated on the NLRP3 -/- cells, measured by both flow cytometry and confocal microscopy. Permeabilisation experiments showed that WT SW 982 cells retained a large proportion of CD59 within the cell, likely in granule stores. Remarkably, WT cells exposed to the specific NLRP3 inhibitor MCC950 showed a rapid, dose-dependent increase in surface expression of CD59 and increased resistance to MAC lysis. Cell surface expression of CD59 was demonstrated to be the major cause of MAC resistance in NLRP3-/- cells by blocking CD59 function with the monoclonal antibody MEM43; this treatment rendered the NLRP3 -/- cells sensitive to complement mediated death to a comparable degree to WT SW 982 cells. MAC-induced Ca^{2+} flux was also absent in NLRP3 -/- cells, confirming failure of MAC pore formation; MEM43 blocking restored MAC-induced Ca^{2+} flux to levels equivalent to WT cells.

The mechanism by which CD59 localisation is affected by NLRP3 expression is unclear. However, CD59 translocation to the membrane has been previously demonstrated following cell activation by FMLP, and CD59 has been implicated in the secretion pathways of insulin from β pancreatic cells, demonstrating that CD59 cellular localisation can undergo rapid alterations, impacting functional roles in cellular processes (Okada *et al* 1994; Krus *et al* 2014). Further, both CD59 translocation and NLRP3 activity have links to the trafficking and distribution of cholesterol within the cell. Previous studies have highlighted that CD59 translocation from the ER to the Golgi is cholesterol dependent, with cholesterol depletion using methyl-β-cyclodextrin inhibiting CD59 ER to Golgi transport (Bonnon *et al* 2010). This relates to NLRP3 activation because NLRP3 activation can be mediated not only by ER stress, but also by altered cholesterol homeostasis within the organelle (de la Roche *et al* 2018). It was shown that inhibition of effective trafficking of cholesterol to the ER, via both pharmacological and genetic deficiency, dampened inflammasome responses, whereas inhibition or modulation of sterol transport to the plasma membrane had no effect on NLRP3 activation. Yet more suggestions of an association between NLRP3 and CD59 come from a study linking MAC deposition, NLRP3 activation and IL-1β secretion in a Uveitis model, where MAC induced IL-1β production was demonstrated to be pathogenic (Kumar *et al* 2018). Interestingly, a disparity was observed between C9 -/- mice and WT mice treated with a soluble CD59 expression vector. C9 -/- mice lacking MAC still demonstrated histological retina damage which was consistent with the WT Uveitis mice, despite a reduction in inflammasome associated activation markers. In contrast to C9 -/- mice, WT mice which were treated with a soluble CD59 expression vector had statistically significantly reduced histological damage as well as NLRP3, IL-1β and Caspase activation levels which were further decreased relative to controls than in C9 -/- mice, suggesting an inflammasome related role for CD59 beyond MAC regulation (Kumar *et al* 2018).

Taken together, these data, alongside the observations made in this thesis, suggest a link between endosomal transport systems, CD59 cellular localisation and NLRP3 activity; however, further investigation is necessary to delineate specific mechanisms linking the two proteins.

Chapter 6 – Final discussion and conclusions

6.1 – Research aims

The complement system and NLRP3 inflammasome are both individually potent drivers of inflammation; however, they may act in synergy to drive inflammation in chronic and acute conditions. In this thesis, I have explored the molecular mechanisms linking sublytic MAC deposition and NLRP3 activation. By furthering the current understanding of the interplay between the two systems, the work may guide strategies for modulation of the signalling pathways involved, thus potentially mitigating complement induced inflammation in disease models in the future.

6.2 – Outline of study

The complement system is an evolutionarily conserved innate immune pathway which mediates inflammatory, opsonic and lytic responses upon activation by pathogens or altered cell surface epitope expressing cells (reviewed in Sarma and Ward 2011). The lytic and a portion of the inflammatory effects of complement activation are attributable to the MAC, with pore formation resulting in chemiosmotic lytic effects on bacterial and non-nucleated cells. MAC formation on nucleated cells, however, is generally tolerated due to cell surface regulation, active removal of MAC lesions from the membrane via endo- and exo-cytosis and active transport of ions to rectify the dysregulated ion balance (Morgan *et al* 2016).

Despite the reduced susceptibility of nucleated cells to MAC mediated lysis, sublytic MAC deposition is not without consequence. The induced signalling events have been demonstrated to mediate proliferation, adhesion, apoptosis and cytokine secretion (Morgan 2016), the last of which is the focus of this work. One of the inflammatory cytokines which has previously been demonstrated by our group to be induced by sublytic MAC is IL-1β, which was secreted in an NLRP3 inflammasome dependent manner (Triantafilou *et al* 2013). The activation of NLRP3 by sublytic MAC was demonstrated to require the complete complement terminal pathway and was Ca^{2+} flux dependent; further studies implicated ROS as a secondary messenger in macrophages, but more detail has not been resolved (Suresh *et al* 2016).

Furthermore, as MAC activates NLRP3 in a range of cell types and NLRP3 and Caspase-1 activation can mediate pyroptotic cell death, the ability of MAC to induce pyroptosis and the relevance of NLRP3 activation as a driver of MAC mediated cell death were also explored.

6.3 – Summary of main findings

In the first results chapter, methods of instigating complement activation to allow investigation of the effects of sublytic MAC were explored, with both early (C3b) and terminal pathway (C9) complement deposition on sensitised THP-1 cells demonstrated to verify activation and MAC formation. Interestingly, recent literature has suggested a role for CD59 in the modulation of C3 deposition (Thielen *et al* 2018). To investigate this, the levels of C3b deposition were measured by flow cytometry on MAC-attacked THP-1 monocytes +/- BRIC 229, a CD59 inhibiting antibody. Whilst BRIC 229 significantly modulated CD59 function and enhanced MAC mediated cell death, it failed to elicit any changes in C3b deposition (Figure 3.13 A/B). Whilst the method used to inhibit CD59 function (CRISPR/CAS9 deletion v antibody inhibition) and the cell types differed in the published study, my data did not support the surprising contention that CD59 regulated C3b deposition.

Following on from these experiments, it was observed that C5 depleted serum controls, which were permissive of C3b deposition but had no complement mediated cell death, deposited statistically significantly more C3b on the cell surface than the same dose of NHS (Figure 3.14 B). This finding was replicated by inhibiting C5 in NHS with Eculizumab, yielding a similar effect to C5 depletion and demonstrating that the observation was not an artefact of the protein purification process; however, inhibition of the terminal pathway at the C7 stage using 23D10, an in house inhibitory monoclonal antibody, did not generate higher levels of C3b deposition compared to NHS (Figure 3.15 and 3.16). A possible explanation for this may be that in the absence of available C5 ligand, the C5 convertase can continue to cleave C3, resulting in increased levels of C3b deposition on the cell surface. Whilst the literature on C5 convertase affinity for C3 is scarce, generation of the C5 convertase is dependent on C3b concentration; it is therefore possible that in the absence of C5 the convertase may bind and cleave more C3 (Rawal and Pangburn 2001).

After establishing mechanisms of sublytic MAC deposition, the capacity of sublytic MAC to induce NLRP3 activation was explored. Sublytic MAC induced IL-1β release and Caspase-1 activation in an NLRP3 dependent manner in LPS primed THP-1 cells, with C5 depleted controls failing to induce responses, demonstrating a dependence on MAC (Figures 4.1 and 4.2.D). Inhibitors of NLRP3, Caspase-1 and all Caspases dose-dependently inhibited sublytic MAC mediated IL-1β secretion without significantly affecting complement activity (Figure 4.2.A-C).

The mechanisms underlying MAC-induced NLRP3 activation where then investigated. K^+ efflux is a leading hypothesis for NLRP3 activation in inhibiting MAC mediated NLRP3 activation (Suresh *et al* 2016). In accordance with the literature, the addition of KCl to the extracellular medium inhibited IL-1β secretion in response to sublytic MAC; however, this inhibitory effect was also noted for NaCl titrations performed alongside KCl (Figure 4.4.A/B), suggesting that there was no specific role for K^+ in the activation mechanism but rather the effect was simply due to salt concentration (Figure 4.4.D). High extracellular salt concentrations were also protective in haemolytic assays, suggesting that the buffering of osmotic potential, independent of cell signalling pathways, has the potential to reduce MAC mediated damage, and therefore may indirectly influence NLRP3 activation. A possible explanation is that cell swelling, which is dependent on the osmotic potential across the cell membrane, is an important mediator of MAC mediated NLRP3 activation. Other studies in the absence of pore forming activators have highlighted that hypotonic solutions can induce NLRP3 activation in LPS primed cells; therefore, hypertonic extracellular conditions may prevent cell swelling in response to membrane damage, consequently reducing inflammasome activation.

The role for Ca^{2+} influx was then addressed and more clearly demonstrated in the current work. Both BAPTA-AM and Xestospongin C dose-dependently altered the Ca^{2+} flux profiles and inhibited IL-1β secretion from THP-1 monocytes (Figures 4.5 and 4.6). The direct modulation of Ca^{2+} concentrations, through chelation or the addition of excess extracellular calcium is problematic in the context of complement activation because Ca^{2+} has a direct role in classical pathway activation; chelation or addition of Ca^{2+} could ablate or enhance complement activation. It was hypothesised that inhibition of intracellular Ca^{2+} flux through BAPTA-AM treatment might affect secondary pathways such as ROS production and mitochondrial damage / depolarisation, which may align with published data that suggest a

Ca^{2+} flux / ROS / Mitochondrial dysfunction axis as a causative mechanism for NLRP3 activation in response to MAC (Keep, Galluzzi and Kroemer 2011). However, whilst pre-treatment of THP-1 cells with BAPTA-AM abrogated both IL-1β secretion and Ca^{2+} flux, it failed to inhibit MAC-induced Superoxide production and marginally decreased TMRE staining, indicative of elevated mitochondrial dysfunction. Subsequently BAPTA-AM chelation of intracellular Ca^{2+} was shown not to inhibit NLRP3 activation through ROS inhibition or mitochondrial protection (Figures 4.8 and 4.9). Interestingly, the ROS scavenger NAC inhibited IL-1β secretion and had marginal effects on Caspase-1 activity, suggesting a role for ROS in MAC induced NLRP3 activation that was not directly linked to Ca^{2+} influx (Figure 4.7).

To determine whether inhibition of any downstream, Ca^{2+} and MAC activated kinases impacted NLRP3 activation, several previously established sublytic MAC activated pathways were targeted using specific cell signalling inhibitors (Figure 4.10). Across an initial screen of MAC induced kinases, the inhibition of AKT using Perifosine, an alkylphospholipid which inhibits membrane associated AKT signalling, caused a significant increase in MAC induced IL-1β secretion and an increase in the Caspase-1 activity, albeit to a non-significant level via the Caspase-1 glo luminescence assay (Figure 4.11 A/B) . However, other AKT pathway inhibitors failed to induce the same effects (Figure 4.12.) This suggested that Perifosine may be inducing off-target effects on other pathways which mediate this effect. Some of the previously described effects of Perifosine include activation of FAS-L signalling and JNK activation, both associated with non-canonical IL-1β and IL-18 secretion in an NLRP3 independent manner (Latz *et al* 2012). The impact of these off-target effects were then investigated. Blockade of signalling through JNK and ERK 1/2, previously described as modulators of NLRP3 activation, MAC induced kinases, caused statistically significant decreases in both IL-1β secretion and Caspase-1 activity, suggesting that a broad MAPK inhibitory strategy was necessary to impact NLRP3 activation in response to MAC (Figure 4.14 A-C).

The reactive lysis system for the generation of MAC avoids some of the potential confounding factors often encountered in using NHS to study MAC mediated signalling events, including potential pleiotropic effects of using heterologous serum as a complement source and signalling induced by antibody binding on the cell surface. Sublytic MAC generated using reactive lysis mediated inflammasome activation and IL-1β secretion in THP-1 monocytes (Figure 4.15) and primary macrophages (Figure 4.16). The transcriptomic changes in response

to reactive lysis generated sublytic MAC were recorded using RNA-Seq; which has identified several target pathways although these have not yet been validated. Preliminary analysis of the integrated pathways correlates well with RNA profiles in a recently published study in experimental autoimmune encephalomyelitis (EAE) where disease progression is MAC mediated (Michailaidou *et al* 2018). Whilst the RNA-Seq performed in the published paper was from mouse spinal cord, the RNA-Seq Z-score pathway hits correlate with our reactive lysis data from THP-1 monocytes, suggesting that highly conserved pathways are activated in response to MAC. The pathways highlighted by the RNA-Seq analysis in the published study are shown in Figure 6.1. This work is currently being replicated and built upon by others in the lab, to attempt to generate a consensus as to underlying transcriptional changes in response to sublytic MAC. Many of the highlighted pathways from our reactive lysis model and that of the mouse EAE model have implications for this work. As investigated, PKA signalling may be a negative regulator of NLRP3 activation, whilst IL-1 signalling validates inflammasome activation occurring are of importance from our RNA-Seq experiment. Further pathways from the EAE model which have implications for inflammatory signalling, NLR activation or links to pathways investigated in this thesis include ROS/RNS production in macrophages, NF-κB signalling, p38 MAPK signalling, TLR signalling, Inflammasome pathway and IRF activation by cytosolic PRR's (Michailaidou *et al* 2018).

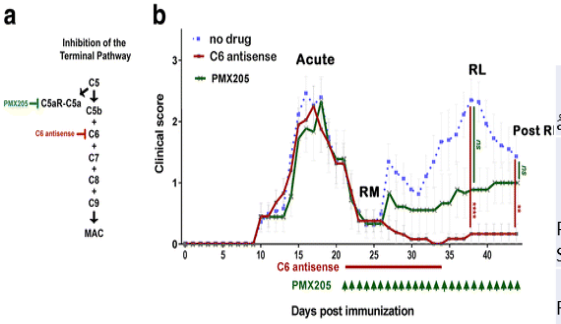

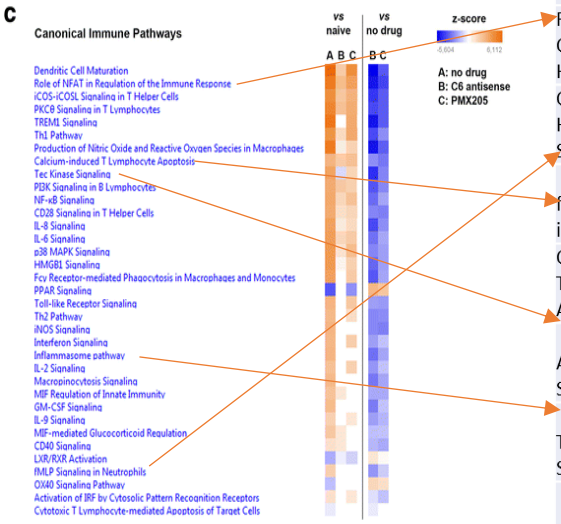

å	-log(B-H p-value)	Ratio	z-score	Molecules
Protein Kinase A Signaling	4.4	0.0553	-1.342	GNAS,PTPN23,YWHAE,YWHAB,PDE4A,GSK3A,PTP4A1,PTPN12,RAP1A,PTPRF,EP300,GNB1,PPP3CB,TGFB1,PPP3R1,PRKCD,PRKACA,GNB2,DUSP7,GNG5,SIRPA
RhoGDI Signaling	3.75	0.0756	1	GNB1,ACTR2,GNAS,WASF2,ACTB,GNA12,RHOT2,PAK2,GNB2,ARHGDIA,GNG5,ARHGAP1,EP300
Role of NFAT in Cardiac Hypertrophy	3.44	0.0684	#NUM!	GNAS,EP300,GNB1,PPP3CB,TGFB1,PRKCD,PPP3R1,MEF2D,PRKACA,GNB2,PIK3CB,MAP2K3,GNG5
Cardiac Hypertrophy Signaling	3.29	0.0601	-2.887	GNAS,GNA12,RHOT2,EP300,GNB1,PPP3CB,TGFB1,MEF2D,PPP3R1,PRKACA,GNB2,PIK3CB,MAP2K3,GNG5
fMLP Signaling in Neutrophils	3.21	0.082	-3	GNB1,ACTR2,GNAS,PPP3CB,WAS,PPP3R1,PRKCD,GNB2,PIK3CB,GNG5
Calcium-induced T Lymphocyte Apoptosis	2.93	0.117	2.449	PPP3CB,MEF2D,CD4,PPP3R1,PRKCD,ATP2A2,EP300
Androgen Signaling	2.93	0.0818	-2	GNB1,POLR2A,GNAS,GNA12,PRKCD,GNB2,PRKACA,GNG5,EP300
Tec Kinase Signaling	2.93	0.0655	-1.89	GNB1,GNAS,WAS,GNA12,ACTB,PRKCD,RHOT2,PAK2,GNB2,PIK3CB,GNG5
IL-1 Signaling	2.75	0.087	-2.236	GNB1,GNAS,GNA12,TAB2,GNB2,PRKACA,MAP2K3,GNG5

Figure 6.1. Comparison of RNA SEQ pathway analysis of reactive lysis stimulated THP-1 monocytes with Rat spinal cord RNA from an EAE model. Arrows highlight the same or similar pathways implicated in both experiments, suggesting even in diverse models of MAC mediated signalling conserved pathways are activated. Image adapted from Michailaidou et al 2018.

Finally, as PKA signalling was implicated as the most changed signalling pathway from the RNA-Seq data and has implications as a negative regulator of NLRP3, a PKA antagonist H89 dichloride was utilised. However, H89 had no significant effects on IL-1β secretion, suggesting that the upregulation of PKA-related mRNA in response to sub-lytic MAC, at least when observed 8 hours after MAC deposition, is not clear evidence of a role of PKA in inhibiting NLRP3 activity.

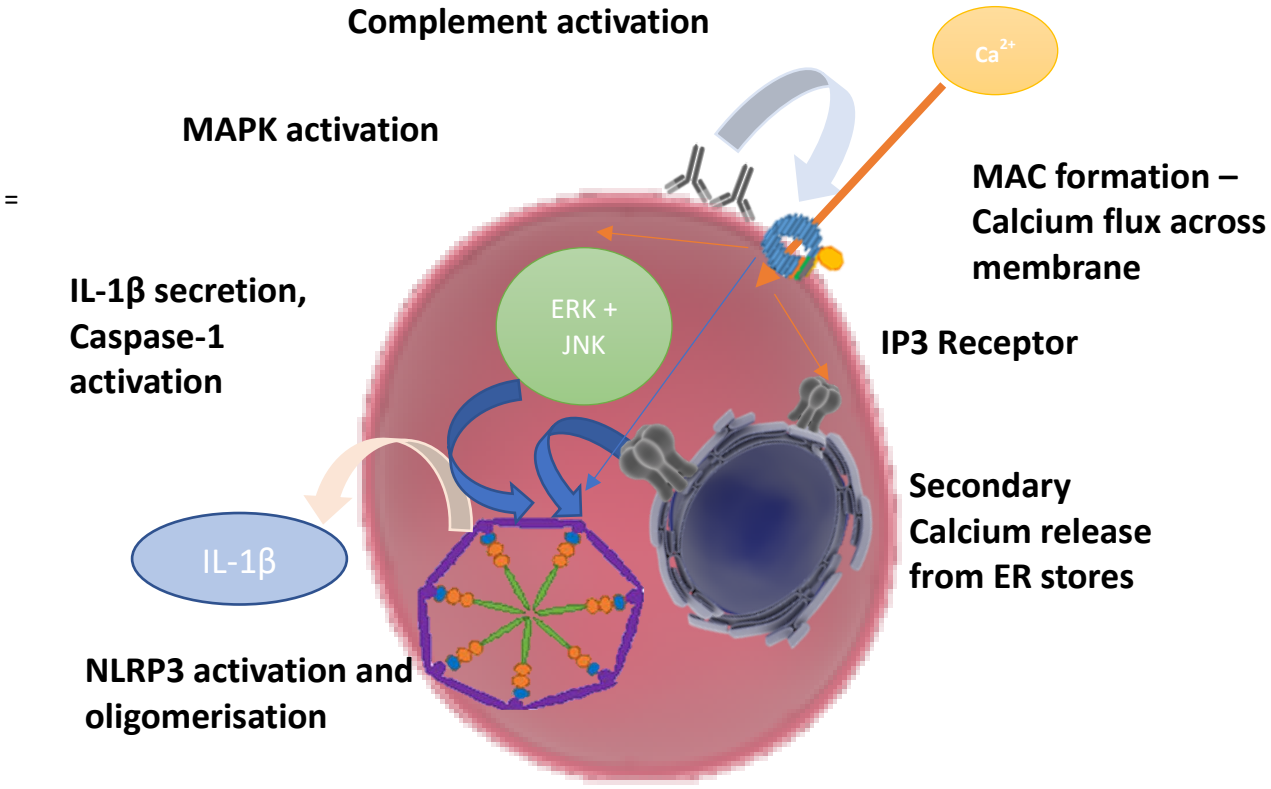

Figure 6.2. Schematic of working hypothesis of MAC mediated NLRP3 activation in THP-1 monocytes. Sublytic MAC deposition on the cell surface induces primary and secondary Calcium flux events across chemiosmotic gradient and from IP3R gated channels respectively. Chelation of calcium using BAPTA-AM and inhibition of IP3R channels using Xestospongin C statistically significantly inhibited MAC mediated IL-1β secretion. The influx of Calcium may directly activate signalling pathways or NLRP3 itself or may mediate the activation of secondary messengers such as ROS/RNS production, which when neutralised through antioxidant pre-treatment of the cells statistically significantly inhibited IL-1β secretion. Both Calcium influx and ROS/RNS production can mediate MAPK activation, with ERK1/2 and JNK inhibition being the most potent combination for inhibiting IL-1β secretion and Caspase-1 activation.

Because MAC deposition results in NLRP3 inflammasome activation and NLRP3 has been implicated in driving pyroptotic cell death, the links between MAC, inflammasomes and cell survival and death pathways were investigated (Fink and Cookson 2005; Triantafilou *et al* 2013). SW 982 synovial cells were subjected to CRISPR/CAS9 mediated deletion of NLRP3, verified by western blot and RT-PCR (Figure 5.1). These cells were then subjected to complement deposition and viability assays in a similar manner to THP-1 cells. Surprisingly, the NLRP3 -/- SW 982 cells demonstrated robust resistance to MAC mediated cell death in response to COS-1 antiserum + NHS in both LDH and PI cell death assays (Figures 5.2 and 5.3). To investigate the cause of this, complement regulator expression and complement activation

fragment deposition was compared between the knockout and WT control cells, demonstrating comparable C3b staining (Figure 5.8). I then demonstrated a marked increase in CD59 expression in the NLRP3 -/- cells relative to WT and antibody blockade of CD59 on NLRP3 -/- cells rendered them equally sensitive to MAC mediated cell death as WT cells (Figures 5.9 and 5.13). To investigate the cause of differential CD59 expression, WT SW 982 cells were treated with the NLRP3 inhibitor MCC950; this caused a marked increase in CD59 cell surface staining within 1 hour and partial protection from MAC mediated cell death (Figures 5.11 and 5.5). The rapid nature of this upregulation suggested that the changes observed were due to shuttling of CD59 from intracellular stores rather than changes in gene expression and de novo protein synthesis. This was supported through permeabilization and staining for CD59 of the WT and NLRP3 -/- SW 982 cells; WT and KO cells stained equally for CD59 upon permeabilization, suggesting the differences observed with MCC950 treatment and under normal conditions is due to differences in the cellular distribution of CD59 rather than overall expression (Figure 5.11). Immunofluorescence imaging supported this finding with the bulk of CD59 in WT cells present in intracellular stores, generating CD59 positive staining upon cell permeabilization (Figure 5.12).

The modulation of sensitivity to complement and MAC mediated cell death in synovial cells may have consequences in pathologies, including RA. Both pyroptotic and necroptotic forms of cell death have been implicated in RA pathogenesis; published studies and the data presented here suggest that these could be mediated by excessive complement activation (Van de Walle *et al* 2014; Wu *et al* 2018; Chen *et al* 2018). Furthermore, NLRP3 activation and Gasdermin D oligomerisation drive NET formation, heavily implicated in RA pathogenesis; this may also be partly attributable to MAC activation of NLRP3 in Neutrophils (Sollberger *et al* 2018; Kenny *et al* 2018). MAC deposition has also been shown to drive production of hypercitrullination patterns on neutrophils (Romero *et al* 2013). If the observed effects of MCC950 in this thesis in upregulating CD59 cell surface expression on SW 982 cells is reciprocated *in vivo*, this may prevent the Calcium influx responsible for activation of the citrullinating enzyme PAD4, which in turn induces citrullination, thus linking MAC, NLRP3 and CD59 in the disease. MCC950 has already been used in mouse CAIA models, with statistically significant decreases in inflammatory cytokine levels, joint histopathology and clinical score

(Guo *et al* 2018); whether these effects may in part be through regulation of the above described MAC mediated processes remains to be explored.

Therefore, the main conclusions of the work presented in this thesis are:

1) Sublytic MAC, generated through reactive lysis or classical activation, is capable of inducing NLRP3 activation in primed THP-1 monocytes and primary macrophages.
2) The induction of NLRP3 activation by sublytic MAC is Ca^{2+} dependent, K^{+} independent and may involve ROS.
3) Pharmacological manipulation of sublytic MAC induced NLRP3 activation is possible with inflammasome specific inhibitors, modulators of Calcium signalling or agents targeting MAPK associated pathways.
4) In SW982 synovial cells, NLRP3 activity determined CD59 surface expression. Consequently, NLRP3 -/- cells are highly resistant to MAC mediated cell death in comparison to WT counterparts. This can be partially reciprocated using MCC950 treatment of WT SW 982 cells and abrogated through the blocking of CD59 function using the CD59 functional blocking antibody MEM43.

6.4 – Future Directions

This work has identified and/or confirmed some of the signalling pathways associated with sublytic MAC mediated NLRP3 activation; however, a deeper investigation is still required in multiple cell types to establish any conserved roles and pathways by which MAC activates. The proliferative pathways initially investigated, such as PI3K, AKT and mTORC1, failed to elicit specific significant changes upon pharmacological inhibition, suggesting that the damage and cell death pathways implicated in response to sublytic MAC, such as MAPK and JNK activation, may be more relevant for MAC mediated NLRP3 activation. The recent observation that MAC induced cell death in K562 cells was necroptosis mediated (Lusthaus *et al* 2018), together with a significant literature linking necroptosis and NLRP3 activation, aligns MAC, necroptosis and NLRP3 in a cell damage / stress axis. However, in preliminary experiments, Necrostatin-1, a

RIPK1 inhibitor used to inhibit necroptosis in the literature, failed to elicit the same protective effects in terms of MAC mediated cell death in THP-1 cells.

The next steps to build on the current work might involve an investigation of the effects of MAC in primary macrophages using MAPK, JNK and Necroptosis inhibitors in the contexts of both cell death and NLRP3 activation; such a study would increase the relevance of the work by demonstrating that the mechanisms displayed are not unique to the immortalised cell line. Furthermore, the highlighted MAPK associated inhibitors, alongside canonical NLRP3 inhibitors such as MCC950, could be tested *in vivo* in models of complement-driven diseases, for example, RA, Alzheimer's or atherosclerosis. The value of inhibition of NLRP3 using MCC950 has already been demonstrated in models of various inflammatory diseases including Ischaemia reperfusion injury, atherosclerosis and Alzheimer's disease; a role for complement is also established in each of these model diseases. Whether the administration of MAPK inhibitors alongside or instead of MCC950 may be suppressive of inflammation in such conditions is unclear; however, the evidence presented here implicating these pathways and the potential for ERK and JNK to drive other inflammatory outputs such as IL-6 and IL-8 secretion, may which may allow further amelioration of complement associated inflammation (Wang *et al* 2012).

The association of NLRP3 expression and synovial cell susceptibility to MAC mediated cell death was a surprising outcome of this study, with the mechanism shown to be CD59 dependent and through translocation of the protein from intracellular stores to the cell surface as shown by flow cytometry and confocal microscopy. Taking this observation forward would require replication in primary synovial cells and further work to address the mechanism underpinning this NLRP3-dependent translocation of CD59. The working hypothesis proposed, involving ER stress and cholesterol translocation, would require further validation; nevertheless, the work would provide exciting and novel links between complement and NLRP3 activation in the context of inflammatory disease.

Bibliography:

Abais, J. M., Xia, M., Zhang, Y., Boini, K. M., & Li, P.-L. (2015). Redox Regulation of NLRP3 Inflammasomes: ROS as Trigger or Effector? *Antioxidants & Redox Signaling*, *22*(13), 1111–1129. https://doi.org/10.1089/ars.2014.5994

Abarrategui-Garrido, C., Martínez-Barricarte, R., López-Trascasa, M., Rodríguez De Córdoba, S., & Sánchez-Corral, P. (2009). Characterization of complement factor H-related (CFHR) proteins in plasma reveals novel genetic variations of CFHR1 associated with atypical hemolytic uremic syndrome. *Blood*, *114*(19), 4261–4271. https://doi.org/10.1182/blood-2009-05-223834

Abderrazak, A., Syrovets, T., Couchie, D., El Hadri, K., Friguet, B., Simmet, T., & Rouis, M. (2015). NLRP3 inflammasome: From a danger signal sensor to a regulatory node of oxidative stress and inflammatory diseases. *Redox Biology*, *4*, 296–307. https://doi.org/10.1016/j.redox.2015.01.008

Agarwal, S., Ferreira, V. P., Cortes, C., Pangburn, M. K., Rice, P. A., & Ram, S. (2010). An Evaluation of the Role of Properdin in Alternative Pathway Activation on Neisseria meningitidis and Neisseria gonorrhoeae. *The Journal of Immunology*, *185*(1), 507–516. https://doi.org/10.4049/jimmunol.0903598

Al-Ani, F., Chin-Yee, I., & Lazo-Langner, A. (2016). Eculizumab in the management of paroxysmal nocturnal hemoglobinuria: Patient selection and special considerations. *Therapeutics and Clinical Risk Management*, *12*, 1161–1170. https://doi.org/10.2147/TCRM.S96720

Alba-Domínguez, M., Lápez-Lera, A., Garrido, S., Nozal, P., González-Granado, I., Melero, J., Lápez-Trascasa, M. (2012). Complement factor i deficiency: A not so rare immune defect. Characterization of new mutations and the first large gene deletion. *Orphanet Journal of Rare Diseases*, *7*(1), 42. https://doi.org/10.1186/1750-1172-7-42

Alcorlo, M., Tortajada, A., Rodriguez de Cordoba, S., & Llorca, O. (2013). Structural basis for the stabilization of the complement alternative pathway C3 convertase by properdin. *Proceedings of the National Academy of Sciences*, *110*(33), 13504–13509. https://doi.org/10.1073/pnas.1309618110

Amara, U., Rittirsch, D., Flierl, M., Bruckner, U., Klos, A., Gebhard, F., Huber-Lang, M. (2008). Interaction Between the Coagulation and Complement System. *Advances in Experimental Medicine and Biology*, *632*, 68–76. https://doi.org/10.1007/978-0-387-78952-1_6

Apel, F., Zychlinsky, A., & Kenny, E. F. (2018). The role of neutrophil extracellular traps in rheumatic diseases. *Nature Reviews Rheumatology*, *14*(8), 467–475. https://doi.org/10.1038/s41584-018-0039-z

Arbore, G., & Kemper, C. (2016). A novel "complement–metabolism–inflammasome axis" as a key regulator of immune cell effector function. *European Journal of Immunology*, *46*(7), 1563–1573. https://doi.org/10.1002/eji.201546131

Arbore, G., Kemper, C., & Kolev, M. (2017). Intracellular complement − the complosome − in immune cell regulation. *Molecular Immunology*, *89*, 2–9. https://doi.org/10.1016/j.molimm.2017.05.012

Arlaud, G. J., Gaboriaud, C., Thielens, N. M., Budayova-Spano, M., Rossi, V., & Fontecilla-Camps, J. C. (2002). Structural biology of the C1 complex of complement unveils the mechanisms of its activation and proteolytic activity. *Molecular Immunology*, *39*(7–8), 383–394. https://doi.org/10.1016/S0161-5890(02)00143-8

Arnaout, R., Al Shorbaghi, S., Al Dhekri, H., Al-Mousa, H., Al Ghonaium, A., Al Saud, B., Hawwari, A. (2013). C5 complement deficiency in a saudi family, molecular characterization of mutation and literature review. *Journal of Clinical Immunology*, *33*(4), 871–875. https://doi.org/10.1007/s10875-013-9872-7

Asgari, E., Friec, G. Le, Yamamoto, H., Perucha, E., Sacks, S. S., Cook, H. T., & Kemper, C. (2017). C3a modulates IL-1 b secretion in human monocytes by regulating ATP ef fl ux and subsequent NLRP3 in fl ammasome activation. *Blood*, *122*(20), 3473–3482. https://doi.org/10.1182/blood-2013-05-502229.The

Babiychuk, E. B., Monastyrskaya, K., Potez, S., & Draeger, A. (2009). Intracellular Ca2+ operates a switch between repair and lysis of streptolysin O-perforated cells. *Cell Death and Differentiation*, *16*(8), 1126–1134. https://doi.org/10.1038/cdd.2009.30

Bajic, G., Yatime, L., Klos, A., & Andersen, G. R. (2013). Human C3a and C3a desArg anaphylatoxins have conserved structures, in contrast to C5a and C5a desArg. *Protein Science*, *22*(2), 204–212. https://doi.org/10.1002/pro.2200

Baker, P. J., Boucher, D., Bierschenk, D., Tebartz, C., Whitney, P. G., D'Silva, D. B., Masters, S. L. (2015). NLRP3 inflammasome activation downstream of cytoplasmic LPS recognition by both caspase-4 and caspase-5. *European Journal of Immunology*, *45*(10), 2918–2926. https://doi.org/10.1002/eji.201545655

Ballanti, E., Perricone, C., Di Muzio, G., Kroegler, B., Chimenti, M. S., Graceffa, D., & Perricone, R. (2011). Role of the complement system in rheumatoid arthritis and psoriatic arthritis: Relationship with anti-TNF inhibitors. *Autoimmunity Reviews*, *10*(10), 617–623. https://doi.org/10.1016/j.autrev.2011.04.012

Banda, N. K., Hyatt, S., Antonioli, A. H., White, J. T., Glogowska, M., Takahashi, K., Holers, V. M. (2011). Role of C3a Receptors, C5a Receptors, and Complement Protein C6 Deficiency in Collagen Antibody-Induced Arthritis in Mice. *The Journal of Immunology*, *188*(3), 1469–1478. https://doi.org/10.4049/jimmunol.1102310

Barbu, A., Hamad, O. A., Lind, L., Ekdahl, K. N., & Nilsson, B. (2015). The role of complement factor C3 in lipid metabolism. *Molecular Immunology*, *67*(1), 101–107. https://doi.org/10.1016/j.molimm.2015.02.027

Baroja-Mazo, A., Martín-Sánchez, F., Gomez, A. I., Martínez, C. M., Amores-Iniesta, J., Compan, V., Pelegrín, P. (2014). The NLRP3 inflammasome is released as a particulate danger signal that amplifies the inflammatory response. *Nature Immunology*, *15*(8), 738–748. https://doi.org/10.1038/ni.2919

Bauer, M. E., & Teixeira, A. L. (2019). Inflammation in psychiatric disorders: What comes first? *Annals of the New York Academy of Sciences*, *1437*(1), 57–67. https://doi.org/10.1111/nyas.13712

Bauernfeind, F. G., Horvath, G., Stutz, A., Alnemri, E. S., MacDonald, K., Speert, D., Latz, E. (2009). Cutting Edge: NF- B Activating Pattern Recognition and Cytokine Receptors License NLRP3 Inflammasome Activation by Regulating NLRP3 Expression. *The Journal of Immunology*, *183*(2), 787–791. https://doi.org/10.4049/jimmunol.0901363

Bayly-Jones, C., Bubeck, D., & Dunstone, M. A. (2017). The mystery behind membrane insertion: A review of the complement membrane attack complex. *Philosophical Transactions of the Royal Society B: Biological Sciences*, *372*(1726), 20160221. https://doi.org/10.1098/rstb.2016.0221

Beinrohr, L., Harmat, V., Dobó, J., Lörincz, Z., Gál, P., & Závodszky, P. (2007). C1 inhibitor serpin domain structure reveals the likely mechanism of heparin potentiation and conformational disease. *Journal of Biological Chemistry*, *282*(29), 21100–21109. https://doi.org/10.1074/jbc.M700841200

Benoit, M. E., Clarke, E. V., Morgado, P., Fraser, D. A., & Tenner, A. J. (2012). Complement Protein C1q Directs Macrophage Polarization and Limits Inflammasome Activity during the Uptake of Apoptotic Cells. *The Journal of Immunology*, *188*(11), 5682–5693. https://doi.org/10.4049/jimmunol.1103760

Bertero, E., & Maack, C. (2018). Calcium signaling and reactive oxygen species in Mitochondria. *Circulation Research*, *122*(10), 1460–1478. https://doi.org/10.1161/CIRCRESAHA.118.310082

Bessler, M., & Hiken, J. (2008). The pathophysiology of disease in patients with paroxysmal nocturnal hemoglobinuria. *Hematology / the Education Program of the American Society of Hematology. American Society of Hematology. Education Program*, 104–110. https://doi.org/10.1182/asheducation-2008.1.104

Bobak, D. A., Frank, M. M., & Tenner, A. J. (1988). Clq acts synergistically with phorbol dibutyrate to activate CR1-mediated phagocytosis by human mononuclear phagocytes. *European Journal of Immunology*, *18*(12), 2001–2007. https://doi.org/10.1002/eji.1830181220

Bohana-Kashtan, O., Ziporen, L., Donin, N., Kraus, S., & Fishelson, Z. (2004). Cell signals transduced by complement. *Molecular Immunology*, *41*(6–7), 583–597. https://doi.org/10.1016/j.molimm.2004.04.007

Bora, N. S., Kaliappan, S., Jha, P., Xu, Q., Sivasankar, B., Harris, C. L., Bora, P. S. (2007). CD59, a complement regulatory protein, controls choroidal neovascularization in a mouse model of wet-type age-related macular degeneration. *Journal of Immunology (Baltimore, Md. : 1950)*, *178*(3), 1783–90. Retrieved from http://www.ncbi.nlm.nih.gov/pubmed/17237428

Bordet J. Les leucocytes et les proprietes actives du serum chezles vaccines. Annales de L'Institut Pasteur 1895;9:462–506

Borkowska, S., Suszynska, M., Mierzejewska, K., Ismail, A., Budkowska, M., Salata, D., Ratajczak, M. Z. (2014). Novel evidence that crosstalk between the complement, coagulation and fibrinolysis proteolytic cascades is involved in mobilization of hematopoietic stem/progenitor cells (HSPCs). *Leukemia*, *28*(11), 2148–54. https://doi.org/10.1038/leu.2014.115

Bossaller, L., Chiang, P.-I., Schmidt-Lauber, C., Ganesan, S., Kaiser, W. J., Rathinam, V. A. K., Latz, E. (2012). Cutting edge: FAS (CD95) mediates noncanonical IL-1β and IL-18 maturation via caspase-8 in an RIP3-independent manner. *Journal of Immunology (Baltimore, Md. : 1950)*, *189*(12), 5508–12. https://doi.org/10.4049/jimmunol.1202121

Bosshart, H., & Heinzelmann, M. (2016). THP-1 cells as a model for human monocytes. *Annals of Translational Medicine*, *4*(21), 438. https://doi.org/10.21037/atm.2016.08.53

Brieger, K., Schiavone, S., Miller, J., & Krause, K. (2012). Reactive oxygen species: from health to disease. *Swiss Medical Weekly*. https://doi.org/10.4414/smw.2012.13659

Brodsky, R. A. (2014). Paroxysmal nocturnal hemoglobinuria. *Blood*, *124*(18), 2804–11. https://doi.org/10.1182/blood-2014-02-522128

Bruchard, M., Mignot, G., Derangère, V., Chalmin, F., Chevriaux, A., Végran, F., … Ghiringhelli, F. (2012). Chemotherapy-triggered cathepsin B release in myeloid-derived suppressor cells activates the Nlrp3 inflammasome and promotes tumor growth. *Nature Medicine*, *19*(1), 57–64. https://doi.org/10.1038/nm.2999

Bubeck, D. (2014). The making of a macromolecular machine: assembly of the membrane attack complex. *Biochemistry*, *53*(12), 1908–15. https://doi.org/10.1021/bi500157z

Buchner, H (1889). Über die bakterientödtende Wirkung des zellenfreien Blutserums (On the bacteriological effects of cell-free blood serum); (1889)

Burger, D., Dayer, J.-M., Palmer, G., & Gabay, C. (2006). Is IL-1 a good therapeutic target in the treatment of arthritis? *Best Practice & Research. Clinical Rheumatology*, *20*(5), 879–96. https://doi.org/10.1016/j.berh.2006.06.004

Butler, M. P., Hanly, J. A., & Moynagh, P. N. (2005). Pellino3 is a novel upstream regulator of p38 MAPK and activates CREB in a p38-dependent manner. *The Journal of Biological Chemistry*, *280*(30), 27759–68. https://doi.org/10.1074/jbc.M500756200

Byeon, H.-E., Jeon, J., Kim, H., Kim, D., Lee, K.-W., Kang, Y., & Han, S. (2017). MicroRNA-132 Negatively Regulates Palmitate-Induced NLRP3 Inflammasome Activation through FOXO3 Down-Regulation in THP-1 Cells. *Nutrients*, *9*(12), 1370. https://doi.org/10.3390/nu9121370

Camell, C., Goldberg, E., & Dixit, V. D. (2015). Regulation of Nlrp3 inflammasome by dietary metabolites. *Seminars in Immunology*, *27*(5), 334–342. https://doi.org/10.1016/j.smim.2015.10.004

Campbell, A. K., & Morgan, B. P. (1985). Monoclonal antibodies demonstrate protection of polymorphonuclear leukocytes against complement attack. *Nature*, *317*(6033), 164–166. https://doi.org/10.1038/317164a0

Campo, G. M., Avenoso, A., D'Ascola, A., Prestipino, V., Scuruchi, M., Nastasi, G., … Campo, S. (2012). Protein kinase a mediated anti-inflammatory effects exerted by adenosine treatment in mouse chondrocytes stimulated with IL-1β. *BioFactors*, *38*(6), 429–439. https://doi.org/10.1002/biof.1040

Cao, S., Wang, J. C. C., Gao, J., Wong, M., To, E., White, V. A., Matsubara, J. A. (2016). CFH Y402H polymorphism and the complement activation product C5a: effects on NF-κB activation and inflammasome gene regulation. *The British Journal of Ophthalmology*, *100*(5), 713–8. https://doi.org/10.1136/bjophthalmol-2015-307213

Cao, Y., Fei, D., Chen, M., Sun, M., Xu, J., Kang, K., Zhao, M. (2015). Role of the nucleotide-binding domain-like receptor protein 3 inflammasome in acute kidney injury. *FEBS Journal*, n/a-n/a. https://doi.org/10.1111/febs.13379

Carney, D. F., Koski, C. L., & Shin, M. L. (1985). Elimination of terminal complement intermediates from the plasma membrane of nucleated cells: the rate of disappearance differs for cells carrying C5b-7 or C5b-8 or a mixture of C5b-8 with a limited number of C5b-9. *Journal of Immunology (Baltimore, Md. : 1950)*, *134*(3), 1804–9. Retrieved from http://www.ncbi.nlm.nih.gov/pubmed/3968432

Carney, D. F., Lang, T. J., & Shin, M. L. (1990). Multiple signal messengers generated by terminal complement complexes and their role in terminal complement complex elimination. *Journal of Immunology (Baltimore, Md. : 1950)*, *145*(2), 623–9. Retrieved from http://www.ncbi.nlm.nih.gov/pubmed/2164064

Carpenter, S., & O'Neill, L. A. J. (2009). Recent insights into the structure of Toll-like receptors and post-translational modifications of their associated signalling proteins. *Biochemical Journal*, *422*(1), 1–10. https://doi.org/10.1042/BJ20090616

Carroll, M. V., & Sim, R. B. (2011). Complement in health and disease. *Advanced Drug Delivery Reviews*, *63*(12), 965–975. https://doi.org/10.1016/j.addr.2011.06.005

Chae, J. J., Park, Y. H., Park, C., Hwang, I.-Y., Hoffmann, P., Kehrl, J. H., Kastner, D. L. (2015). Brief Report: Connecting Two Pathways Through Ca^{2+} Signaling: NLRP3 Inflammasome Activation Induced by a Hypermorphic *PLCG2* Mutation. *Arthritis & Rheumatology*, *67*(2), 563–567. https://doi.org/10.1002/art.38961

Chang, J.-H., Lee, K.-J., Kim, S.-K., Yoo, D.-H., & Kang, T.-Y. (2014). Validity of SW982 synovial cell line for studying the drugs against rheumatoid arthritis in fluvastatin-induced apoptosis signaling model. *The Indian Journal of Medical Research*, *139*(1), 117–24. Retrieved from http://www.ncbi.nlm.nih.gov/pubmed/24604047

Chang, T.-H., Huang, J.-H., Lin, H.-C., Chen, W.-Y., Lee, Y.-H., Hsu, L.-C., Wu-Hsieh, B. A. (2017). Dectin-2 is a primary receptor for NLRP3 inflammasome activation in dendritic cell response to Histoplasma capsulatum. *PLOS Pathogens*, *13*(7), e1006485. https://doi.org/10.1371/journal.ppat.1006485

Chapman, H. A., Yang, X. L., Sailor, L. Z., Sugarbaker, D. J., Grover, M., Whoolery, K. L., Stahl, G. L. (1990). Developmental expression of plasminogen activator inhibitor type 1 by human alveolar macrophages. Possible role in lung injury. *Journal of Immunology (Baltimore, Md. : 1950)*, *145*(10), 3398–405. https://doi.org/10.4049/jimmunol.165.2.1059

Charles A Janeway, J., Travers, P., Walport, M., & Shlomchik, M. J. (2001). The complement system and innate immunity. Retrieved from https://www.ncbi.nlm.nih.gov/books/NBK27100/

Chatterjee, S., & Mayor, S. (2001). The GPI-anchor and protein sorting. *Cellular and Molecular Life Sciences*, *58*(14), 1969–1987. https://doi.org/10.1007/PL00000831

Chauhan, A. K., & Moore, T. L. (2006). Presence of plasma complement regulatory proteins clusterin (Apo J) and vitronectin (S40) on circulating immune complexes (CIC). *Clinical and Experimental Immunology*, *145*(3), 398–406. https://doi.org/10.1111/j.1365-2249.2006.03135.x

Chen, K. W., Boucher, D., & Broz, P. (2019). Divide to conquer: NLRP3 is activated on dispersed trans-Golgi network. *Cell Research*, 1. https://doi.org/10.1038/s41422-018-0138-z

Chen, M., Daha, M. R., & Kallenberg, C. G. M. (2010). The complement system in systemic autoimmune disease. *Journal of Autoimmunity*, *34*(3), J276–J286. https://doi.org/10.1016/J.JAUT.2009.11.014

Chen, Y., Zhu, C.-J., Zhu, F., Dai, B.-B., Song, S.-J., Wang, Z.-Q., Chen, F.-H. (2018). Necrostatin-1 ameliorates adjuvant arthritis rat articular chondrocyte injury via inhibiting ASIC1a-mediated necroptosis. *Biochemical and Biophysical Research Communications*, *504*(4), 843–850. https://doi.org/10.1016/j.bbrc.2018.09.031

Chimin, P., Andrade, M. L., Belchior, T., Paschoal, V. A., Magdalon, J., Yamashita, A. S., Festuccia, W. T. (2017). Adipocyte mTORC1 deficiency promotes adipose tissue inflammation and NLRP3 inflammasome activation via oxidative stress and de novo ceramide synthesis. *Journal of Lipid Research*, *58*(9), 1797–1807. https://doi.org/10.1194/jlr.M074518

Choi, N. H., Nakano, Y., Tobe, T., Mazda, T., & Tomita, M. (1990). Incorporation of SP-40,40 into the soluble membrane attack complex (SMAC, SC5b-9) of complement. *International Immunology*, *2*(5), 413–7. Retrieved from http://www.ncbi.nlm.nih.gov/pubmed/2150757

Chu, J., Thomas, L. M., Watkins, S. C., Franchi, L., Núñez, G., & Salter, R. D. (2009). Cholesterol-dependent cytolysins induce rapid release of mature IL-1beta from murine

macrophages in a NLRP3 inflammasome and cathepsin B-dependent manner. *Journal of Leukocyte Biology*, *86*(5), 1227–38. https://doi.org/10.1189/jlb.0309164

Clark, S. J., Ridge, L. A., Herbert, A. P., Hakobyan, S., Mulloy, B., Lennon, R., Day, A. J. (2013). Tissue-Specific Host Recognition by Complement Factor H Is Mediated by Differential Activities of Its Glycosaminoglycan-Binding Regions. *The Journal of Immunology*, *190*(5), 2049–2057. https://doi.org/10.4049/JIMMUNOL.1201751

Cole, D. S., & Morgan, B. P. (2003). Beyond lysis: how complement influences cell fate. *Clinical Science (London, England : 1979)*, *104*(5), 455–66. https://doi.org/10.1042/CS20020362

Coll, R. C., Robertson, A. A. B., Chae, J. J., Higgins, S. C., Muñoz-Planillo, R., Inserra, M. C., O'Neill, L. A. J. (2015). A small-molecule inhibitor of the NLRP3 inflammasome for the treatment of inflammatory diseases. *Nature Medicine*, *21*(3), 248–55. https://doi.org/10.1038/nm.3806

Compan, V., Baroja-Mazo, A., López-Castejón, G., Gomez, A. I., Martínez, C. M., Angosto, D., Pelegrín, P. (2012). Cell Volume Regulation Modulates NLRP3 Inflammasome Activation. *Immunity*, *37*(3), 487–500. https://doi.org/10.1016/j.immuni.2012.06.013

Conos, S. A., Chen, K. W., De Nardo, D., Hara, H., Whitehead, L., Núñez, G., Vince, J. E. (2017). Active MLKL triggers the NLRP3 inflammasome in a cell-intrinsic manner. *Proceedings of the National Academy of Sciences of the United States of America*, *114*(6), E961–E969. https://doi.org/10.1073/pnas.1613305114

Cooper, N. R., & Müller-Eberhard, H. J. (1970). The reaction mechanism of human C5 in immune hemolysis. *The Journal of Experimental Medicine*, *132*(4), 775–93. Retrieved from http://www.ncbi.nlm.nih.gov/pubmed/5508377

Cordero, M. D., Williams, M. R., & Ryffel, B. (2018). AMP-Activated Protein Kinase Regulation of the NLRP3 Inflammasome during Aging. *Trends in Endocrinology & Metabolism*, *29*(1), 8–17. https://doi.org/10.1016/J.TEM.2017.10.009

Cortes, C., Ohtola, J. A., Saggu, G., & Ferreira, V. P. (2012). Local release of properdin in the cellular microenvironment: role in pattern recognition and amplification of the alternative pathway of complement. *Frontiers in Immunology*, *3*, 412. https://doi.org/10.3389/fimmu.2012.00412

Cragg, M. S., Morgan, S. M., Chan, H. T. C., Morgan, B. P., Filatov, A. V, Johnson, P. W. M., Glennie, M. J. (2003). Complement-mediated lysis by anti-CD20 mAb correlates with segregation into lipid rafts. *Blood*, *101*(3), 1045–52. https://doi.org/10.1182/blood-2002-06-1761

Craven, R. R., Gao, X., Allen, I. C., Gris, D., Wardenburg, J. B., McElvania-TeKippe, E., Duncan, J. A. (2009). Staphylococcus aureus α-Hemolysin Activates the NLRP3-Inflammasome in Human and Mouse Monocytic Cells. *PLoS ONE*, *4*(10), e7446. https://doi.org/10.1371/journal.pone.0007446

Cugno, M., Zanichelli, A., Foieni, F., Caccia, S., & Cicardi, M. (2009). C1-inhibitor deficiency and angioedema: molecular mechanisms and clinical progress. *Trends in Molecular Medicine*, *15*(2), 69–78. https://doi.org/10.1016/j.molmed.2008.12.001

Cybulsky, A. V., Takano, T., Papillon, J., Khadir, A., Liu, J., & Peng, H. (2002). Complement C5b-9 Membrane Attack Complex Increases Expression of Endoplasmic Reticulum Stress Proteins in Glomerular Epithelial Cells. *Journal of Biological Chemistry*, *277*(44), 41342–41351. https://doi.org/10.1074/jbc.M204694200

Daha, M. R. (2013). Unexpected role for properdin in complement C3 glomerulopathies. *Journal of the American Society of Nephrology : JASN*, *24*(1), 5–7. https://doi.org/10.1681/ASN.2012111110

Das, D., Barnes, M. A., & Nagy, L. E. (2014). Anaphylatoxin C5a modulates hepatic stellate cell migration. *Fibrogenesis & Tissue Repair*, *7*(1), 9. https://doi.org/10.1186/1755-1536-7-9

Davis, B. K., Wen, H., & Ting, J. P.-Y. (2011). The inflammasome NLRs in immunity, inflammation, and associated diseases. *Annual Review of Immunology*, *29*, 707–735. https://doi.org/10.1146/annurev-immunol-031210-101405

de la Roche, M., Hamilton, C., Mortensen, R., Jeyaprakash, A. A., Ghosh, S., & Anand, P. K. (2018). Trafficking of cholesterol to the ER is required for NLRP3 inflammasome activation. *The Journal of Cell Biology*, *217*(10), 3560–3576. https://doi.org/10.1083/jcb.201709057

de Zoete, M. R., Palm, N. W., Zhu, S., & Flavell, R. A. (2014). Inflammasomes. *Cold Spring Harbor Perspectives in Biology*, *6*(12), a016287–a016287. https://doi.org/10.1101/cshperspect.a016287

Design, D. (2014). Genistein suppresses tumor necrosis factor α -induced inflammation via modulating reactive oxygen species / Akt / nuclear factor κ B and adenosine monophosphate-activated protein kinase signal pathways in human synoviocyte MH7A cells, 315–323.

Dessauer, A., & Rother, U. (1983). The fifth component of complement (C5): Purification without Activation. *Immunobiology*, *164*(5), 370–379. https://doi.org/10.1016/S0171-2985(83)80033-3

DESSAUER, A., ROTHER, U., ROTHER, K., & LUDWIG, H. (1985). FPLC for the Isolation of a New Intermediate in the Reaction of the Fifth (C5) and Sixth (C6) Component of Complement. *Protides of the Biological Fluids*, *32*, 1101–1104. https://doi.org/10.1016/B978-0-08-031739-7.50268-8

Deutz, N. E. P., Pereira, S. L., Hays, N. P., Oliver, J. S., Edens, N. K., Evans, C. M., & Wolfe, R. R. (2013). Effect of β-hydroxy-β-methylbutyrate (HMB) on lean body mass during 10 days of bed rest in older adults. *Clinical Nutrition*, *32*(5), 704–712. https://doi.org/10.1016/J.CLNU.2013.02.011

Di, A., Xiong, S., Ye, Z., Malireddi, R. K. S., Kometani, S., Zhong, M., … Malik, A. B. (2018). The TWIK2 Potassium Efflux Channel in Macrophages Mediates NLRP3 Inflammasome-Induced Inflammation. *Immunity*, *49*(1), 56–65.e4. https://doi.org/10.1016/j.immuni.2018.04.032

Diebolder, C. A., Beurskens, F. J., de Jong, R. N., Koning, R. I., Strumane, K., Lindorfer, M. A., … Parren, P. W. H. I. (2014). Complement is activated by IgG hexamers assembled at the cell surface. *Science (New York, N.Y.)*, *343*(6176), 1260–3. https://doi.org/10.1126/science.1248943

Dinarello, C. A. (2011). Interleukin-1 in the pathogenesis and treatment of inflammatory diseases. *Blood*, *117*(14), 3720–3732. https://doi.org/10.1182/blood-2010-07-273417

DiScipio, R. G., Smith, C. A., Muller-Eberhard, H. J., & Hugli, T. E. (1983). The activation of human complement component C5 by a fluid phase C5 convertase. *The Journal of Biological Chemistry*, *258*(17), 10629–36. Retrieved from http://www.ncbi.nlm.nih.gov/pubmed/6554279

Dommett, R. M., Klein, N., & Turner, M. W. (2006). Mannose-binding lectin in innate immunity: past, present and future. *Tissue Antigens*, *68*(3), 193–209. https://doi.org/10.1111/j.1399-0039.2006.00649.x

Dong, W., Zhou, M., Dong, M., Pan, B., Liu, Y., Shao, J., … Sun, H. (2016). Keto acid metabolites of branched-chain amino acids inhibit oxidative stress-induced necrosis and attenuate myocardial ischemia–reperfusion injury. *Journal of Molecular and Cellular Cardiology*, *101*, 90–98. https://doi.org/10.1016/j.yjmcc.2016.11.002

Doyle, S. L., Campbell, M., Ozaki, E., Salomon, R. G., Mori, A., Kenna, P. F., Humphries, P. (2012). NLRP3 has a protective role in age-related macular degeneration through the induction of IL-18 by drusen components. *Nature Medicine*, *18*(5), 791–8. https://doi.org/10.1038/nm.2717

Dragon-Durey, M.-A. (2004). Heterozygous and Homozygous Factor H Deficiencies Associated with Hemolytic Uremic Syndrome or Membranoproliferative Glomerulonephritis: Report and Genetic Analysis of 16 Cases. *Journal of the American Society of Nephrology*, *15*(3), 787–795. https://doi.org/10.1097/01.ASN.0000115702.28859.A7

Duncan, A. R., & Winter, G. (1988). The binding site for C1q on IgG. *Nature*, *332*(6166), 738–40. https://doi.org/10.1038/332738a0

Duncan, J. A., Bergstralh, D. T., Wang, Y., Willingham, S. B., Ye, Z., Zimmermann, A. G., & Ting, J. P.-Y. (2007). Cryopyrin/NALP3 binds ATP/dATP, is an ATPase, and requires ATP binding to mediate inflammatory signaling. *Proceedings of the National Academy of Sciences of the United States of America*, *104*(19), 8041–6. https://doi.org/10.1073/pnas.0611496104

Dunkelberger, J. R., & Song, W.-C. (2010). Complement and its role in innate and adaptive immune responses. *Cell Research*, *20*(1), 34–50. https://doi.org/10.1038/cr.2009.139

Dunne, A., & O'Neill, L. A. J. (2003). The Interleukin-1 Receptor/Toll-Like Receptor Superfamily: Signal Transduction During Inflammation and Host Defense. *Science Signaling*, *2003*(171), re3-re3. https://doi.org/10.1126/stke.2003.171.re3

Earl, F. B., Shelly, M. P., Stephanie, C., Sheena, B., S, ra, D., Yasmine, K. (2011). New mechanism for complement killing of Gram-negative bacteria. *African Journal of Microbiology Research*, *5*(23), 3936–3941. https://doi.org/10.5897/AJMR11.660

Ekman, S., Wynes, M. W., & Hirsch, F. R. (2012). The mTOR Pathway in Lung Cancer and Implications for Therapy and Biomarker Analysis. *Journal of Thoracic Oncology*, *7*(6), 947–953. https://doi.org/10.1097/JTO.0B013E31825581BD

Elimam, H., Papillon, J., Takano, T., & Cybulsky, A. V. (2013). Complement-mediated activation of calcium-independent phospholipase A2γ: role of protein kinases and phosphorylation. *The Journal of Biological Chemistry*, *288*(6), 3871–85. https://doi.org/10.1074/jbc.M112.396614

Elmore, S. (2007). Apoptosis: a review of programmed cell death. *Toxicologic Pathology*, *35*(4), 495–516. https://doi.org/10.1080/01926230701320337

Endo, Y., Matsushita, M., & Fujita, T. (2011). The role of ficolins in the lectin pathway of innate immunity. *The International Journal of Biochemistry & Cell Biology*, *43*(5), 705–12. https://doi.org/10.1016/j.biocel.2011.02.003

Escárcega, R. O., Lipinski, M. J., García-Carrasco, M., Mendoza-Pinto, C., Galvez-Romero, J. L., & Cervera, R. (2018). Inflammation and atherosclerosis: Cardiovascular evaluation in patients with autoimmune diseases. *Autoimmunity Reviews*. https://doi.org/10.1016/j.autrev.2018.01.021

Evans, J. B., & Syed, B. A. (2013). New hope for dry AMD? *Nature Reviews. Drug Discovery*, *12*(7), 501–2. https://doi.org/10.1038/nrd4038

Ezekowitz, R. A., Sim, R. B., MacPherson, G. G., & Gordon, S. (1985). Interaction of human monocytes, macrophages, and polymorphonuclear leukocytes with zymosan in vitro. Role of type 3 complement receptors and macrophage-derived complement. *Journal of Clinical Investigation*, *76*(6), 2368–2376. https://doi.org/10.1172/JCI112249

Fakhouri, F., Jorge, E. G. de, Brune, F., Azam, P., Cook, H. T., & Pickering, M. C. (2010). Treatment with human complement factor H rapidly reverses renal complement deposition in factor H-deficient mice. Kidney International, 78(3), 279. https://doi.org/10.1038/KI.2010.132

Farshidfar, F., Shulgina, V., & Myrie, S. B. (2016). Nutritional supplementations and administration considerations for sarcopenia in older adults. *Nutrition and Aging*, *3*(2–4), 147–170. https://doi.org/10.3233/NUA-150057

Ferreira, V. P., Pangburn, M. K., & Cortés, C. (2010). Complement control protein factor H: the good, the bad, and the inadequate. *Molecular Immunology*, *47*(13), 2187–97. https://doi.org/10.1016/j.molimm.2010.05.007

Fink, S. L., & Cookson, B. T. (2006). Caspase-1-dependent pore formation during pyroptosis leads to osmotic lysis of infected host macrophages. *Cellular Microbiology*, *8*(11), 1812–1825. https://doi.org/10.1111/j.1462-5822.2006.00751.x

Firestein, G. S. (2003). Evolving concepts of rheumatoid arthritis. *Nature*, *423*(6937), 356–361. Retrieved from http://dx.doi.org/10.1038/nature01661

Foltyn Zadura, A., Memon, A. A., Stojanovich, L., Perricone, C., Conti, F., Valesini, G., … Blom, A. M. (2015). Factor H Autoantibodies in Patients with Antiphospholipid Syndrome and Thrombosis. *The Journal of Rheumatology*, *42*(10), 1786–93. https://doi.org/10.3899/jrheum.150185

Forneris, F., Ricklin, D., Wu, J., Tzekou, A., Wallace, R. S., Lambris, J. D., & Gros, P. (2010). Structures of C3b in complex with factors B and D give insight into complement convertase formation. *Science (New York, N.Y.)*, *330*(6012), 1816–20. https://doi.org/10.1126/science.1195821

Forrester, S. J., Kikuchi, D. S., Hernandes, M. S., Xu, Q., & Griendling, K. K. (2018). Reactive Oxygen Species in Metabolic and Inflammatory Signaling. *Circulation Research*, *122*(6), 877–902. https://doi.org/10.1161/CIRCRESAHA.117.311401

Fosbrink, M., Niculescu, F., Rus, V., Shin, M. L., & Rus, H. (2006). C5b-9-induced endothelial cell proliferation and migration are dependent on Akt inactivation of forkhead transcription factor FOXO1. *The Journal of Biological Chemistry*, *281*(28), 19009–18. https://doi.org/10.1074/jbc.M602055200

Fossati-Jimack, L., Ling, G. S., Cortini, A., Szajna, M., Malik, T. H., McDonald, J. U., Botto, M. (2013). Phagocytosis is the main CR3-mediated function affected by the lupus-associated variant of CD11b in human myeloid cells. *PloS One*, *8*(2), e57082. https://doi.org/10.1371/journal.pone.0057082

Franchi, L., Eigenbrod, T., Muñoz-Planillo, R., & Nuñez, G. (2009). The inflammasome: a caspase-1-activation platform that regulates immune responses and disease pathogenesis. *Nature Immunology*, *10*(3), 241–247. https://doi.org/10.1038/ni.1703

Frank, M. G., Weber, M. D., Watkins, L. R., & Maier, S. F. (2015). Stress sounds the alarmin: The role of the danger-associated molecular pattern HMGB1 in stress-induced neuroinflammatory priming. *Brain, Behavior, and Immunity*, *48*, 1–7. https://doi.org/10.1016/j.bbi.2015.03.010

Franklin, B. S., Bossaller, L., De Nardo, D., Ratter, J. M., Stutz, A., Engels, G., … Latz, E. (2014). The adaptor ASC has extracellular and “prionoid” activities that propagate inflammation. *Nature Immunology*, *15*(8), 727–737. https://doi.org/10.1038/ni.2913

Franklin, B. S., Latz, E., & Schmidt, F. I. (2018). The intra- and extracellular functions of ASC specks. *Immunological Reviews*, *281*(1), 74–87. https://doi.org/10.1111/imr.12611

Fujita, T. (2002). Evolution of the lectin-complement pathway and its role in innate immunity. *Nature Reviews. Immunology*, *2*(5), 346–53. https://doi.org/10.1038/nri800

Fukuzawa, T., Sampei, Z., Haraya, K., Ruike, Y., Shida-Kawazoe, M., Shimizu, Y., Nezu, J. (2017). Long lasting neutralization of C5 by SKY59, a novel recycling antibody, is a potential therapy for complement-mediated diseases. *Scientific Reports*, *7*(1), 1080. https://doi.org/10.1038/s41598-017-01087-7

Gaboriaud, C., Frachet, P., Thielens, N. M., & Arlaud, G. J. (2011). The human c1q globular domain: structure and recognition of non-immune self ligands. *Frontiers in Immunology*, *2*, 92. https://doi.org/10.3389/fimmu.2011.00092

Gaboriaud, C., Ling, W. L., Thielens, N. M., Bally, I., & Rossi, V. (2014). Deciphering the fine details of c1 assembly and activation mechanisms: "mission impossible"? *Frontiers in Immunology*, *5*, 565. https://doi.org/10.3389/fimmu.2014.00565

Gaboriaud, C., Thielens, N. M., Gregory, L. A., Rossi, V., Fontecilla-Camps, J. C., & Arlaud, G. J. (2004). Structure and activation of the C1 complex of complement: unraveling the puzzle. *Trends in Immunology*, *25*(7), 368–73. https://doi.org/10.1016/j.it.2004.04.008

Gál, P., Dobó, J., Závodszky, P., & Sim, R. B. M. (2009). Early complement proteases: C1r, C1s and MASPs. A structural insight into activation and functions. *Molecular Immunology*, *46*(14), 2745–2752. https://doi.org/10.1016/j.molimm.2009.04.026

Gao, J., Choe, H., Bota, D., Wright, P. L., Gerard, C., & Gerard, N. P. (2003). Sulfation of Tyrosine 174 in the Human C3a Receptor Is Essential for Binding of C3a Anaphylatoxin. *Journal of Biological Chemistry*, *278*(39), 37902–37908. https://doi.org/10.1074/jbc.M306061200

Gao, L., Qiu, W., Wang, Y., Xu, W., Xu, J., & Tong, J. (2006). Sublytic complement C5b-9 complexes induce thrombospondin-1 production in rat glomerular mesangial cells via PI3-k/Akt: association with activation of latent transforming growth factor-beta1. *Clinical and Experimental Immunology*, *144*(2), 326–34. https://doi.org/10.1111/j.1365-2249.2006.03069.x

García, M. A., Gil, J., Ventoso, I., Guerra, S., Domingo, E., Rivas, C., & Esteban, M. (2006). Impact of protein kinase PKR in cell biology: from antiviral to antiproliferative action. *Microbiology and Molecular Biology Reviews : MMBR*, *70*(4), 1032–60. https://doi.org/10.1128/MMBR.00027-06

Garcia-Ortega, M., Lopez, G., Jimenez, G., Garcia-Garcia, J., Conde, V., Boulaiz, H., Garcia, M. (2017). Clinical and therapeutic potential of protein kinase PKR in cancer and metabolism. *Expert Reviews in Molecular Medicine*, *19*, e9. https://doi.org/10.1017/erm.2017.11

Garlanda, C., Dinarello, C. A., & Mantovani, A. (2013). The interleukin-1 family: back to the future. *Immunity*, *39*(6), 1003–18. https://doi.org/10.1016/j.immuni.2013.11.010

Gauvreau, D., Roy, C., Tom, F.-Q., Lu, H., Miegueu, P., Richard, D., Cianflone, K. (2012). A new effector of lipid metabolism: Complement factor properdin. *Molecular Immunology*, *51*(1), 73–81. https://doi.org/10.1016/J.MOLIMM.2012.02.110

Genetical Society (Great Britain), B., Pan, H., Najafov, A., & Yuan, J. (1987). *Genes & development.* Cold Spring Harbor Laboratory in association with the Genetical Society of Great Britain. Retrieved from http://genesdev.cshlp.org/content/32/5-6/327/F2.expansion.html

Ghebrehiwet, B., Hosszu, K. K., Valentino, A., & Peerschke, E. I. B. (2012). The C1q family of proteins: insights into the emerging non-traditional functions. *Frontiers in Immunology*, *3*. https://doi.org/10.3389/fimmu.2012.00052

Ghonime, M. G., Shamaa, O. R., Das, S., Eldomany, R. A., Fernandes-Alnemri, T., Alnemri, E. S., … Wewers, M. D. (2014). Inflammasome Priming by Lipopolysaccharide Is Dependent upon ERK Signaling and Proteasome Function. *The Journal of Immunology*, *192*(8), 3881–3888. https://doi.org/10.4049/jimmunol.1301974

Goicoechea de Jorge, E., Caesar, J. J. E., Malik, T. H., Patel, M., Colledge, M., Johnson, S., Lea, S. M. (2013). Dimerization of complement factor H-related proteins modulates complement activation in vivo. *Proceedings of the National Academy of Sciences of the United States of America*, *110*(12), 4685–90. https://doi.org/10.1073/pnas.1219260110

Gordon, D., Papazaharoudakis, H., Sadlon, T., Arellano, A., & Okada, N. (1994). Upregulation of human neutrophil CD59, a regulator of the membrane attack complex of complement, following cell activation. *Immunology & Cell Biology*, *72*(3), 222–229. https://doi.org/10.1038/icb.1994.33

Görlach, A., Bertram, K., Hudecova, S., & Krizanova, O. (2015). Calcium and ROS: A mutual interplay. *Redox Biology*, *6*, 260–71. https://doi.org/10.1016/j.redox.2015.08.010

Gottlieb, Y., Topaz, O., Cohen, L. A., Yakov, L. D., Haber, T., Morgenstern, A., Meyron-Holtz, E. G. (2012). Physiologically aged red blood cells undergo erythrophagocytosis in vivo but not in vitro. *Haematologica*, *97*(7), 994–1002. https://doi.org/10.3324/haematol.2011.057620

Gower, R. G., Busse, P. J., Aygören-Pürsün, E., Barakat, A. J., Caballero, T., Davis-Lorton, M., Maurer, M. (2011). Hereditary Angioedema Caused By C1-Esterase Inhibitor Deficiency: A Literature-Based Analysis and Clinical Commentary on Prophylaxis Treatment Strategies. *World Allergy Organization Journal*, *4*(2), S9–S21. https://doi.org/10.1097/WOX.0b013e31821359a2

Groslambert, M., & Py, B. (2018). Spotlight on the NLRP3 inflammasome pathway. *Journal of Inflammation Research*, *Volume 11*, 359–374. https://doi.org/10.2147/JIR.S141220

Groß, C. J., & Groß, O. (2016). PKA Has the Gall to Oppose NLRP3. *Immunity*, *45*(4), 707–709. https://doi.org/10.1016/J.IMMUNI.2016.09.019

Gross, O., Thomas, C. J., Guarda, G., & Tschopp, J. (2011). The inflammasome: an integrated view. *Immunological Reviews*, *243*(1), 136–151. https://doi.org/10.1111/j.1600-065X.2011.01046.x

Guo, C., Fu, R., Wang, S., Huang, Y., Li, X., Zhou, M., Yang, N. (2018). NLRP3 inflammasome activation contributes to the pathogenesis of rheumatoid arthritis.

Clinical and Experimental Immunology, *194*(2), 231–243. https://doi.org/10.1111/cei.13167

Guo, R.-F., & Ward, P. A. (2005). Role of C5a in inflammatory responses. *Annual Review of Immunology*, *23*, 821–52. https://doi.org/10.1146/annurev.immunol.23.021704.115835

Gurung, P., Lukens, J. R., & Kanneganti, T.-D. (2015). Mitochondria: diversity in the regulation of the NLRP3 inflammasome. *Trends in Molecular Medicine*, *21*(3), 193–201. https://doi.org/10.1016/j.molmed.2014.11.008

Hadders, M. A., Bubeck, D., Roversi, P., Hakobyan, S., Forneris, F., Morgan, B. P., … Gros, P. (2012). Assembly and Regulation of the Membrane Attack Complex Based on Structures of C5b6 and sC5b9. *Cell Reports*, *1*(3), 200–207. https://doi.org/10.1016/j.celrep.2012.02.003

Hageman, G. S., Anderson, D. H., Johnson, L. V, Hancox, L. S., Taiber, A. J., Hardisty, L. I., Allikmets, R. (2005). A common haplotype in the complement regulatory gene factor H (HF1/CFH) predisposes individuals to age-related macular degeneration. *Proceedings of the National Academy of Sciences of the United States of America*, *102*(20), 7227–32. https://doi.org/10.1073/pnas.0501536102

Haggadone, M. D., Grailer, J. J., Fattahi, F., Zetoune, F. S., & Ward, P. A. (2016). Bidirectional Crosstalk between C5a Receptors and the NLRP3 Inflammasome in Macrophages and Monocytes. *Mediators of Inflammation*, *2016*, 1340156. https://doi.org/10.1155/2016/1340156

Hamidinia, S. A., Tan, B., Erdahl, W. L., Chapman, C. J., Taylor, R. W., & Pfeiffer, D. R. (2004). The Ionophore Nigericin Transports Pb 2+ with High Activity and Selectivity: A Comparison to Monensin and Ionomycin †. https://doi.org/10.1021/bi048175z

Haneklaus, M., & O'Neill, L. A. J. (2015). NLRP3 at the interface of metabolism and inflammation. *Immunological Reviews*, *265*(1), 53–62. https://doi.org/10.1111/imr.12285

Hara, K., Yonezawa, K., Weng, Q. P., Kozlowski, M. T., Belham, C., & Avruch, J. (1998). Amino acid sufficiency and mTOR regulate p70 S6 kinase and eIF-4E BP1 through a common effector mechanism. *The Journal of Biological Chemistry*, *273*(23), 14484–94. https://doi.org/10.1074/JBC.273.23.14484

Harris, C. L., Heurich, M., Cordoba, S. R. de, & Morgan, B. P. (2012). The complotype: dictating risk for inflammation and infection. *Trends in Immunology*, *33*(10), 513–521. https://doi.org/10.1016/j.it.2012.06.001

Harris, C. L., Pettigrew, D. M., Lea, S. M., & Morgan, B. P. (2007). Decay-accelerating factor must bind both components of the complement alternative pathway C3 convertase to mediate efficient decay. *Journal of Immunology (Baltimore, Md. : 1950)*, *178*(1), 352–9. Retrieved from http://www.ncbi.nlm.nih.gov/pubmed/17182573

Haseloff, J. (1999). Methods in Molecualr Biology: Protocols in confocal microscopy, 18. https://doi.org/10.1385/1-59259-722

He, Y., Hara, H., & Núñez, G. (2016). Mechanism and Regulation of NLRP3 Inflammasome Activation. *Trends in Biochemical Sciences*, *41*(12), 1012–1021. https://doi.org/10.1016/j.tibs.2016.09.002

He, Y., Zeng, M. Y., Yang, D., Motro, B., & Núñez, G. (2016). NEK7 is an essential mediator of NLRP3 activation downstream of potassium efflux. *Nature*, *530*(7590), 354–357. https://doi.org/10.1038/nature16959

Heid, M. E., Keyel, P. A., Kamga, C., Shiva, S., Watkins, S. C., & Salter, R. D. (2013). Mitochondrial reactive oxygen species induces NLRP3-dependent lysosomal damage and inflammasome activation. *Journal of Immunology (Baltimore, Md. : 1950)*, *191*(10), 5230–8. https://doi.org/10.4049/jimmunol.1301490

Heinen, S., Hartmann, A., Lauer, N., Wiehl, U., Dahse, H.-M., Schirmer, S., Skerka, C. (2009). Factor H-related protein 1 (CFHR-1) inhibits complement C5 convertase activity and terminal complex formation. *Blood*, *114*(12), 2439–47. https://doi.org/10.1182/blood-2009-02-205641

Helmy, K. Y., Katschke, K. J., Gorgani, N. N., Kljavin, N. M., Elliott, J. M., Diehl, L., van Lookeren Campagne, M. (2006). CRIg: A Macrophage Complement Receptor Required for Phagocytosis of Circulating Pathogens. *Cell*, *124*(5), 915–927. https://doi.org/10.1016/j.cell.2005.12.039

Hila, S., Soane, L., & Koski, C. L. (2001). Sublytic C5b-9-stimulated Schwann cell survival through PI 3-kinase-mediated phosphorylation of BAD. *Glia*, *36*(1), 58–67. Retrieved from http://www.ncbi.nlm.nih.gov/pubmed/11571784

Hill, A., Ridley, S. H., Esser, D., Oldroyd, R. G., Cullen, M. J., Kareclas, P., Hillmen, P. (2006). Protection of erythrocytes from human complement-mediated lysis by membrane-targeted recombinant soluble CD59: a new approach to PNH therapy. *Blood*, *107*(5), 2131–7. https://doi.org/10.1182/blood-2005-02-0782

Hill, A., Rother, R. P., Arnold, L., Kelly, R., Cullen, M. J., Richards, S. J., & Hillmen, P. (2010). Eculizumab prevents intravascular hemolysis in patients with paroxysmal nocturnal hemoglobinuria and unmasks low-level extravascular hemolysis occurring through C3 opsonization. *Haematologica*, *95*(4), 567–73. https://doi.org/10.3324/haematol.2009.007229

Hillmen, P., Young, N. S., Schubert, J., Brodsky, R. A., Socié, G., Muus, P., Luzzatto, L. (2006). The Complement Inhibitor Eculizumab in Paroxysmal Nocturnal Hemoglobinuria. *New England Journal of Medicine*, *355*(12), 1233–1243. https://doi.org/10.1056/NEJMoa061648

Hoesel, B., & Schmid, J. A. (2013). The complexity of NF-κB signaling in inflammation and cancer. *Molecular Cancer*, *12*(1), 86. https://doi.org/10.1186/1476-4598-12-86

Holers, V. M., & Banda, N. K. (2018). Complement in the Initiation and Evolution of Rheumatoid Arthritis. *Frontiers in Immunology*, *9*, 1057. https://doi.org/10.3389/fimmu.2018.01057

Hornung, V., & Latz, E. (2010). Critical functions of priming and lysosomal damage for NLRP3 activation. *European Journal of Immunology*, *40*(3), 620–623. https://doi.org/10.1002/eji.200940185

Hornung, V., Bauernfeind, F., Halle, A., Samstad, E. O., Kono, H., Rock, K. L., Latz, E. (2008). Silica crystals and aluminum salts activate the NALP3 inflammasome through phagosomal destabilization. *Nature Immunology*, *9*(8), 847–856. https://doi.org/10.1038/ni.1631

Howard, C., Noe, A., Skerjanec, A., Holzhauer, B., Wernsing, M., Ligueros-Saylan, M., & Thuren, T. (2014). Safety and tolerability of canakinumab, an IL-1β inhibitor, in type 2 diabetes mellitus patients: a pooled analysis of three randomised double-blind studies. *Cardiovascular Diabetology*, *13*(1), 94. https://doi.org/10.1186/1475-2840-13-94

Hu, R., Chen, Z.-F., Yan, J., Li, Q.-F., Huang, Y., Xu, H., Jiang, H. (2014). Complement C5a exacerbates acute lung injury induced through autophagy-mediated alveolar macrophage apoptosis. *Cell Death & Disease*, *5*, e1330. https://doi.org/10.1038/cddis.2014.274

Hu, V. W., Esser, A. F., Podack, E. R., & Wisnieski, B. J. (1981). The membrane attack mechanism of complement: photolabeling reveals insertion of terminal proteins into target membrane. *Journal of Immunology (Baltimore, Md. : 1950)*, *127*(1), 380–6. Retrieved from http://www.ncbi.nlm.nih.gov/pubmed/7240749

Hu, Z., Yan, C., Liu, P., Huang, Z., Ma, R., Zhang, C., Chai, J. (2013). Crystal Structure of NLRC4 Reveals Its Autoinhibition Mechanism. *Science*, *341*(6142), 172–175. https://doi.org/10.1126/science.1236381

Huang, M. T.-H., Taxman, D. J., Holley-Guthrie, E. A., Moore, C. B., Willingham, S. B., Madden, V., Ting, J. P.-Y. (2009). Critical Role of Apoptotic Speck Protein Containing a Caspase Recruitment Domain (ASC) and NLRP3 in Causing Necrosis and ASC Speck Formation Induced by Porphyromonas gingivalis in Human Cells. *The Journal of Immunology*, *182*(4), 2395–2404. https://doi.org/10.4049/jimmunol.0800909

Huang, Y., Qiao, F., Abagyan, R., Hazard, S., & Tomlinson, S. (2006). Defining the CD59-C9 Binding Interaction. *Journal of Biological Chemistry*, *281*(37), 27398–27404. https://doi.org/10.1074/jbc.M603690200

Huber-Lang, M., Younkin, E. M., Sarma, J. V., Riedemann, N., McGuire, S. R., Lu, K. T., … Ward, P. A. (2002). Generation of C5a by phagocytic cells. *The American Journal of Pathology*, *161*(5), 1849–59. https://doi.org/10.1016/S0002-9440(10)64461-6

Ip, W. K., Lau, Y. L., Chan, S. Y., Mok, C. C., Chan, D., Tong, K. K., & Lau, C. S. (2000). Mannose-binding lectin and rheumatoid arthritis in Southern Chinese. *Arthritis & Rheumatism*, *43*(8), 1679–1687. https://doi.org/10.1002/1529-0131(200008)43:8<1679::AID-ANR3>3.0.CO;2-D

Iyer, S. S., He, Q., Janczy, J. R., Elliott, E. I., Zhong, Z., Olivier, A. K., Sutterwala, F. S. (2013). Mitochondrial Cardiolipin Is Required for Nlrp3 Inflammasome Activation. *Immunity*, *39*(2), 311–323. https://doi.org/10.1016/j.immuni.2013.08.001

Jane-wit, D., Surovtseva, Y. V, Qin, L., Li, G., Liu, R., Clark, P., Pober, J. S. (2015). Complement membrane attack complexes activate noncanonical NF-κB by forming an Akt+ NIK+ signalosome on Rab5+ endosomes. *Proceedings of the National Academy of Sciences of the United States of America*, *112*(31), 9686–91. https://doi.org/10.1073/pnas.1503535112

Java, A., Liszewski, M. K., Hourcade, D. E., Zhang, F., & Atkinson, J. P. (2015). Role of complement receptor 1 (CR1; CD35) on epithelial cells: A model for understanding complement-mediated damage in the kidney. *Molecular Immunology*, *67*(2 Pt B), 584–95. https://doi.org/10.1016/j.molimm.2015.07.016

Jéru, I., Marlin, S., Le Borgne, G., Cochet, E., Normand, S., Duquesnoy, P., Amselem, S. (2010). Functional consequences of a germline mutation in the leucine-rich repeat domain of NLRP3 identified in an atypical autoinflammatory disorder. *Arthritis & Rheumatism*, *62*(4), 1176–1185. https://doi.org/10.1002/art.27326

Jo, E.-K., Kim, J. K., Shin, D.-M., & Sasakawa, C. (2016). Molecular mechanisms regulating NLRP3 inflammasome activation. *Cellular and Molecular Immunology*, *13*(2), 148–159. https://doi.org/10.1038/cmi.2015.95

Juliana, C., Fernandes-Alnemri, T., Wu, J., Datta, P., Solorzano, L., Yu, J.-W., … Alnemri, E. S. (2010). Anti-inflammatory compounds parthenolide and Bay 11-7082 are direct inhibitors of the inflammasome. *The Journal of Biological Chemistry*, *285*(13), 9792–802. https://doi.org/10.1074/jbc.M109.082305

Kadota, Y., Shirasu, K., & Guerois, R. (2010). NLR sensors meet at the SGT1–HSP90 crossroad. *Trends in Biochemical Sciences*, *35*(4), 199–207. https://doi.org/10.1016/j.tibs.2009.12.005

Kahle, P., Saal, J. G., Schaudt, K., Zacher, J., Fritz, P., & Pawelec, G. (1992). Determination of cytokines in synovial fluids: correlation with diagnosis and histomorphological characteristics of synovial tissue. *Annals of the Rheumatic Diseases*, *51*(6), 731–4. Retrieved from http://www.ncbi.nlm.nih.gov/pubmed/1616355

Kalogeropoulou, D., LaFave, L., Schweim, K., Gannon, M. C., & Nuttall, F. Q. (2008). Leucine, when ingested with glucose, synergistically stimulates insulin secretion and lowers blood glucose. *Metabolism*, *57*(12), 1747–1752. https://doi.org/10.1016/J.METABOL.2008.09.001

Katschke, K. J., Wu, P., Ganesan, R., Kelley, R. F., Mathieu, M. A., Hass, P. E., van Lookeren Campagne, M. (2012). Inhibiting Alternative Pathway Complement Activation by Targeting the Factor D Exosite. *Journal of Biological Chemistry*, *287*(16), 12886–12892. https://doi.org/10.1074/jbc.M112.345082

Katschke, K. J., Wu, P., Ganesan, R., Kelley, R. F., Mathieu, M. A., Hass, P. E., van Lookeren Campagne, M. (2012). Inhibiting alternative pathway complement activation by targeting the factor D exosite. *The Journal of Biological Chemistry*, *287*(16), 12886–92. https://doi.org/10.1074/jbc.M112.345082

Katsnelson, M. A., Rucker, L. G., Russo, H. M., & Dubyak, G. R. (2015). K^+ Efflux Agonists Induce NLRP3 Inflammasome Activation Independently of Ca^{2+} Signaling. *The Journal of Immunology*, *194*(8), 3937–3952. https://doi.org/10.4049/jimmunol.1402658

Kawai, T., & Akira, S. (2007). Signaling to NF-κB by Toll-like receptors. *Trends in Molecular Medicine*, *13*(11), 460–469. https://doi.org/10.1016/j.molmed.2007.09.002

Kay, J., & Calabrese, L. (2004). The role of interleukin-1 in the pathogenesis of rheumatoid arthritis. *Rheumatology*, *43*(suppl_3), iii2-iii9. https://doi.org/10.1093/rheumatology/keh201

Kazatchkine, M. D., Fearon, D. T., & Austen, K. F. (1979). Human alternative complement pathway: membrane-associated sialic acid regulates the competition between B and beta1 H for cell-bound C3b. *Journal of Immunology (Baltimore, Md. : 1950)*, *122*(1), 75–81. https://doi.org/10.4049/jimmunol.169.9.4702

Kepp, O., Galluzzi, L., & Kroemer, G. (2011). Mitochondrial control of the NLRP3 inflammasome. *Nature Immunology*, *12*(3), 199–200. https://doi.org/10.1038/ni0311-199

Kerjaschki, D., Schulze, M., Binder, S., Kain, R., Ojha, P. P., Susani, M., Couser, W. G. (1989). Transcellular transport and membrane insertion of the C5b-9 membrane attack complex of complement by glomerular epithelial cells in experimental membranous nephropathy. *Journal of Immunology (Baltimore, Md. : 1950)*, *143*(2), 546–52. Retrieved from http://www.ncbi.nlm.nih.gov/pubmed/2738403

Khamesipour, F., & Doosti, A. (2013). *Molecular Detection of Brucella spp. in the Semen, Testis and Blood Samples of Cattle and Sheep MYH7, MYBPC3 and TNNT2 Genes Mutations from 200 Patients with HCM in Iran View project*. *Article in Journal of Pure and Applied Microbiology*. Retrieved from https://www.researchgate.net/publication/262337318

Kienhöfer, D., Boeltz, S., & Hoffmann, M. H. (2016). Reactive oxygen homeostasis – the balance for preventing autoimmunity. *Lupus*, *25*(8), 943–954. https://doi.org/10.1177/0961203316640919

Kilgore, K. S., Schmid, E., Shanley, T. P., Flory, C. M., Maheswari, V., Tramontini, N. L., Warren, J. S. (1997). Sublytic concentrations of the membrane attack complex of complement induce endothelial interleukin-8 and monocyte chemoattractant protein-1 through nuclear factor-kappa B activation. *The American Journal of Pathology*, *150*(6), 2019–31.

Killick, J., Morisse, G., Sieger, D., & Astier, A. L. (n.d.). Complement as a regulator of adaptive immunity. *Seminars in Immunopathology*, 1–12. https://doi.org/10.1007/s00281-017-0644-y

Kim, J.-J., & Jo, E.-K. (2013). NLRP3 Inflammasome and Host Protection against Bacterial Infection. *Journal of Korean Medical Science*, *28*(10), 1415. https://doi.org/10.3346/jkms.2013.28.10.1415

Kim, S. H., Carney, D. F., Hammer, C. H., & Shin, M. L. (1987). Nucleated cell killing by complement: effects of C5b-9 channel size and extracellular Ca2+ on the lytic process. *Journal of Immunology (Baltimore, Md. : 1950)*, *138*(5), 1530–6. Retrieved from http://www.ncbi.nlm.nih.gov/pubmed/2433349

Kimberley, F. C., Sivasankar, B., & Paul Morgan, B. (2007). Alternative roles for CD59. *Molecular Immunology*, *44*(1–3), 73–81. https://doi.org/10.1016/j.molimm.2006.06.019

King, B. C., & Blom, A. M. (2017). Non-traditional roles of complement in type 2 diabetes: Metabolism, insulin secretion and homeostasis. *Molecular Immunology*, *84*, 34–42. https://doi.org/10.1016/j.molimm.2016.12.009

Kishore, U., Kojouharova, M. S., & Reid, K. B. M. (2002). Recent progress in the understanding of the structure-function relationships of the globular head regions of C1q. *Immunobiology*, *205*(4–5), 355–64. https://doi.org/10.1078/0171-2985-00138

Klein, R. J., Zeiss, C., Chew, E. Y., Tsai, J.-Y., Sackler, R. S., Haynes, C., Hoh, J. (2005). Complement factor H polymorphism in age-related macular degeneration. *Science (New York, N.Y.)*, *308*(5720), 385–9. https://doi.org/10.1126/science.1109557

Klein, T., Shephard, P., Kleinert, H., & Kömhoff, M. (2007). Regulation of cyclooxygenase-2 expression by cyclic AMP. *Biochimica et Biophysica Acta (BBA) - Molecular Cell Research*, *1773*(11), 1605–1618. https://doi.org/10.1016/J.BBAMCR.2007.09.001

Kobe, B., & Kajava, A. V. (2001). The leucine-rich repeat as a protein recognition motif. *Current Opinion in Structural Biology*, *11*(6), 725–32. Retrieved from http://www.ncbi.nlm.nih.gov/pubmed/11751054

Kolev, M., & Kemper, C. (2017). Keeping It All Going-Complement Meets Metabolism. *Frontiers in Immunology*, *8*, 1. https://doi.org/10.3389/fimmu.2017.00001

Korbecki, J., Baranowska-Bosiacka, I., Gutowska, I., & Chlubek, D. (2013). The effect of reactive oxygen species on the synthesis of prostanoids from arachidonic acid. *Journal of Physiology and Pharmacology : An Official Journal of the Polish Physiological Society*, *64*(4), 409–21. Retrieved from http://www.ncbi.nlm.nih.gov/pubmed/24101387

Kotas, M. E., Jurczak, M. J., Annicelli, C., Gillum, M. P., Cline, G. W., Shulman, G. I., & Medzhitov, R. (2013). Role of caspase-1 in regulation of triglyceride metabolism. *Proceedings of the National Academy of Sciences of the United States of America*, *110*(12), 4810–5. https://doi.org/10.1073/pnas.1301996110

Krus, U., King, B. C., Nagaraj, V., Gandasi, N. R., Sjölander, J., Buda, P., Renström, E. (2014). The complement inhibitor CD59 regulates insulin secretion by modulating exocytotic events. *Cell Metabolism*, *19*(5), 883–90. https://doi.org/10.1016/j.cmet.2014.03.001

Krych-Goldberg, M., & Atkinson, J. P. (2001). Structure-function relationships of complement receptor type 1. *Immunological Reviews*, *180*, 112–22. Retrieved from http://www.ncbi.nlm.nih.gov/pubmed/11414353

Kumar, B., Cashman, S. M., & Kumar-Singh, R. (2018). Complement-Mediated Activation of the NLRP3 Inflammasome and Its Inhibition by AAV-Mediated Delivery of CD59 in a Model of Uveitis. *Molecular Therapy*, *26*(6), 1568–1580. https://doi.org/10.1016/J.YMTHE.2018.03.012

Lachmann, P. J. (2009). The amplification loop of the complement pathways. *Advances in Immunology*, *104*, 115–49. https://doi.org/10.1016/S0065-2776(08)04004-2

Lachmann, P. J., & Halbwachs, L. (1975). The influence of C3b inactivator (KAF) concentration on the ability of serum to support complement activation. *Clinical and Experimental Immunology*, *21*(1), 109–14. Retrieved from http://www.ncbi.nlm.nih.gov/pubmed/52423

Lachmann, P. J., & Nicol, P. (1973). Reaction mechanism of the alternative pathway of complement fixation. *Lancet (London, England)*, *1*(7801), 465–7. Retrieved from http://www.ncbi.nlm.nih.gov/pubmed/4120372

Lagouge, M., Argmann, C., Gerhart-Hines, Z., Meziane, H., Lerin, C., Daussin, F., … Auwerx, J. (2006). Resveratrol Improves Mitochondrial Function and Protects against Metabolic Disease by Activating SIRT1 and PGC-1α. *Cell*, *127*(6), 1109–1122. https://doi.org/10.1016/J.CELL.2006.11.013

Lakkaraju, A., Toops, K. A., & Xu, J. (2014). Should I Stay or Should I Go? Trafficking of Sub-Lytic MAC in the Retinal Pigment Epithelium. In *Advances in experimental medicine and biology* (Vol. 801, pp. 267–274). https://doi.org/10.1007/978-1-4614-3209-8_34

Lamkanfi, M., Mueller, J. L., Vitari, A. C., Misaghi, S., Fedorova, A., Deshayes, K., Dixit, V. M. (2009). Glyburide inhibits the Cryopyrin/Nalp3 inflammasome. *The Journal of Cell Biology*, *187*(1), 61–70. https://doi.org/10.1083/jcb.200903124

Lane, P. J., Ledbetter, J. A., McConnell, F. M., Draves, K., Deans, J., Schieven, G. L., & Clark, E. A. (1991). The role of tyrosine phosphorylation in signal transduction through surface Ig in human B cells. Inhibition of tyrosine phosphorylation prevents intracellular calcium release. *Journal of Immunology (Baltimore, Md. : 1950)*, *146*(2), 715–22. Retrieved from http://www.ncbi.nlm.nih.gov/pubmed/1702814

Lange, C., Hemmrich, G., Klostermeier, U. C., López-Quintero, J. A., Miller, D. J., Rahn, T., Rosenstiel, P. (2011). Defining the origins of the NOD-like receptor system at the base of animal evolution. *Molecular Biology and Evolution*, *28*(5), 1687–702. https://doi.org/10.1093/molbev/msq349

LaRocca, T. J., Stivison, E. A., Mal-Sarkar, T., Hooven, T. A., Hod, E. A., Spitalnik, S. L., & Ratner, A. J. (2015). CD59 signaling and membrane pores drive Syk-dependent erythrocyte necroptosis. *Cell Death & Disease*, *6*(5), e1773–e1773. https://doi.org/10.1038/cddis.2015.135

Latz, E. (2010). The inflammasomes: mechanisms of activation and function. *Current Opinion in Immunology*, *22*(1), 28–33. https://doi.org/10.1016/j.coi.2009.12.004

Latz, E., Xiao, T. S., & Stutz, A. (2013). Activation and regulation of the inflammasomes. *Nature Reviews. Immunology*, *13*(June), 397–411. https://doi.org/10.1038/nri3452

Laudisi, F., Spreafico, R., Evrard, M., Hughes, T. R., Mandriani, B., Kandasamy, M., … Mortellaro, A. (2013). Cutting edge: the NLRP3 inflammasome links complement-mediated inflammation and IL-1β release. *Journal of Immunology (Baltimore, Md. : 1950)*, *191*(3), 1006–10. https://doi.org/10.4049/jimmunol.1300489

Laursen, I. A., Thielens, N. M., Christiansen, M., & Houen, G. (2012). MASP interactions with plasma-derived MBL. *Molecular Immunology*, *52*(2), 79–87. https://doi.org/10.1016/j.molimm.2012.04.014

Lawlor, K. E., Khan, N., Mildenhall, A., Gerlic, M., Croker, B. A., D'Cruz, A. A., … Vince, J. E. (2015). RIPK3 promotes cell death and NLRP3 inflammasome activation in the absence of MLKL. *Nature Communications*, *6*(1), 6282. https://doi.org/10.1038/ncomms7282

Lechtenberg, B. C., Mace, P. D., & Riedl, S. J. (2014). Structural mechanisms in NLR inflammasome signaling. *Current Opinion in Structural Biology*, *29*, 17–25. https://doi.org/10.1016/j.sbi.2014.08.011

Lee, G.-S., Subramanian, N., Kim, A. I., Aksentijevich, I., Goldbach-Mansky, R., Sacks, D. B., Chae, J. J. (2012). The calcium-sensing receptor regulates the NLRP3 inflammasome through Ca2+ and cAMP. *Nature*, *492*(7427), 123–127. https://doi.org/10.1038/nature11588

Lee, H., Whitfeld, P. L., & Mackay, C. R. (2008). Receptors for complement C5a. The importance of C5aR and the enigmatic role of C5L2. *Immunology and Cell Biology*, *86*(2), 153–60. https://doi.org/10.1038/sj.icb.7100166

Legendre, C. M., Licht, C., Muus, P., Greenbaum, L. A., Babu, S., Bedrosian, C., Loirat, C. (2013). Terminal Complement Inhibitor Eculizumab in Atypical Hemolytic–Uremic Syndrome. *New England Journal of Medicine*, *368*(23), 2169–2181. https://doi.org/10.1056/NEJMoa1208981

Lewis, R. D., Jackson, C. L., Morgan, B. P., & Hughes, T. R. (2010). The membrane attack complex of complement drives the progression of atherosclerosis in apolipoprotein E knockout mice. *Molecular Immunology*, *47*(5), 1098–1105. https://doi.org/10.1016/j.molimm.2009.10.035

Li, G., Scull, C., Ozcan, L., & Tabas, I. (2010). NADPH oxidase links endoplasmic reticulum stress, oxidative stress, and PKR activation to induce apoptosis. *The Journal of Cell Biology*, *191*(6), 1113–25. https://doi.org/10.1083/jcb.201006121

Li, R., Coulthard, L. G., Wu, M. C. L., Taylor, S. M., & Woodruff, T. M. (2013). C5L2: a controversial receptor of complement anaphylatoxin, C5a. *The FASEB Journal*, *27*(3), 855–864. https://doi.org/10.1096/fj.12-220509

Li, X.-F., Shen, W.-W., Sun, Y.-Y., Li, W.-X., Sun, Z.-H., Liu, Y.-H., … Li, J. (2016). MicroRNA-20a negatively regulates expression of NLRP3-inflammasome by targeting

TXNIP in adjuvant-induced arthritis fibroblast-like synoviocytes. *Joint, Bone, Spine : Revue Du Rhumatisme*. https://doi.org/10.1016/j.jbspin.2015.10.007

Liepinsh, E., Barbals, R., Dahl, E., Sharipo, A., Staub, E., & Otting, G. (2003). The death-domain fold of the ASC PYRIN domain, presenting a basis for PYRIN/PYRIN recognition. *Journal of Molecular Biology*, *332*(5), 1155–63. Retrieved from http://www.ncbi.nlm.nih.gov/pubmed/14499617

Lim, K.-H., & Staudt, L. M. (2013). Toll-like receptor signaling. *Cold Spring Harbor Perspectives in Biology*, *5*(1), a011247. https://doi.org/10.1101/cshperspect.a011247

Lin, K.-M., Hu, W., Troutman, T. D., Jennings, M., Brewer, T., Li, X., … Pasare, C. (2014). IRAK-1 bypasses priming and directly links TLRs to rapid NLRP3 inflammasome activation. *Proceedings of the National Academy of Sciences*, *111*(2), 775–780. https://doi.org/10.1073/pnas.1320294111

Liu, J., Miwa, T., Hilliard, B., Chen, Y., Lambris, J. D., Wells, A. D., & Song, W.-C. (2005). The complement inhibitory protein DAF (CD55) suppresses T cell immunity in vivo. *Journal of Experimental Medicine*, *201*(4). Retrieved from http://jem.rupress.org/content/201/4/567

Liu, L., Qiu, W., Wang, H., Li, Y., Zhou, J., Xia, M., Wang, Y. (2012). Sublytic C5b-9 complexes induce apoptosis of glomerular mesangial cells in rats with Thy-1 nephritis through role of interferon regulatory factor-1-dependent caspase 8 activation. *The Journal of Biological Chemistry*, *287*(20), 16410–23. https://doi.org/10.1074/jbc.M111.319566

Liu, Q., Zhang, D., Hu, D., Zhou, X., & Zhou, Y. (2018). The role of mitochondria in NLRP3 inflammasome activation. *Molecular Immunology*, *103*, 115–124. https://doi.org/10.1016/J.MOLIMM.2018.09.010

Liu, W., Luo, Y., Dunn, J. H., Norris, D. A., Dinarello, C. A., & Fujita, M. (2013). Dual role of apoptosis-associated speck-like protein containing a CARD (ASC) in tumorigenesis of human melanoma. *The Journal of Investigative Dermatology*, *133*(2), 518–27. https://doi.org/10.1038/jid.2012.317

Low, J. M., & Moore, T. L. (2005). A role for the complement system in rheumatoid arthritis. *Current Pharmaceutical Design*, *11*(5), 655–70. Retrieved from http://www.ncbi.nlm.nih.gov/pubmed/15720280

Lu, A., & Wu, H. (2015). Structural mechanisms of inflammasome assembly. *FEBS Journal*, *282*(3), 435–444. https://doi.org/10.1111/febs.13133

Lubbers, R., van Essen, M. F., van Kooten, C., & Trouw, L. A. (2017). Production of complement components by cells of the immune system. *Clinical & Experimental Immunology*, *188*(2), 183–194. https://doi.org/10.1111/cei.12952

Luheshi, N. M., Giles, J. A., Lopez-Castejon, G., & Brough, D. (2012). Sphingosine regulates the NLRP3-inflammasome and IL-1β release from macrophages. *European Journal of Immunology*, *42*(3), 716–725. https://doi.org/10.1002/eji.201142079

Luo, B., Li, B., Wang, W., Liu, X., Xia, Y., Zhang, C., An, F. (2014). NLRP3 gene silencing ameliorates diabetic cardiomyopathy in a type 2 diabetes rat model. *PloS One*, *9*(8), e104771. https://doi.org/10.1371/journal.pone.0104771

Lusthaus, M., Mazkereth, N., Donin, N., & Fishelson, Z. (2018). Receptor-Interacting Protein Kinases 1 and 3, and Mixed Lineage Kinase Domain-Like Protein Are Activated by Sublytic Complement and Participate in Complement-Dependent Cytotoxicity. *Frontiers in Immunology*, *9*. https://doi.org/10.3389/fimmu.2018.00306

M, P., & N, R. (2001). Structure and function of complement C5 convertase enzymes. Retrieved from http://www.biochemsoctrans.org/bst/030/1006/bst0301006.htm

Major, B., Kardos, J., Kékesi, K. A., Lőrincz, Z., Závodszky, P., & Gál, P. (2010). Calcium-dependent Conformational Flexibility of a CUB Domain Controls Activation of the Complement Serine Protease C1r. *Journal of Biological Chemistry*, *285*(16), 11863–11869. https://doi.org/10.1074/jbc.M109.098541

Makrides, S. C., Wuillemin, W. A., Zeerleder, S., Redondo, M., Eisele, B., & Hack, C. E. (1998). Therapeutic inhibition of the complement system. *Pharmacological Reviews*, *50*(1), 59–87. Retrieved from http://www.ncbi.nlm.nih.gov/pubmed/9549758

Malireddi, R. K. S., Gurung, P., Mavuluri, J., Dasari, T. K., Klco, J. M., Chi, H., & Kanneganti, T.-D. (2018). TAK1 restricts spontaneous NLRP3 activation and cell death to control myeloid proliferation. *The Journal of Experimental Medicine*, *215*(4), 1023–1034. https://doi.org/10.1084/jem.20171922

Man, S. M., Karki, R., & Kanneganti, T.-D. (2017). Molecular mechanisms and functions of pyroptosis, inflammatory caspases and inflammasomes in infectious diseases. *Immunological Reviews*, *277*(1), 61–75. https://doi.org/10.1111/imr.12534

Manthey, H. D., Woodruff, T. M., Taylor, S. M., & Monk, P. N. (2009). Complement component 5a (C5a). *The International Journal of Biochemistry & Cell Biology*, *41*(11), 2114–7. https://doi.org/10.1016/j.biocel.2009.04.005

Mariathasan, S., Weiss, D. S., Newton, K., McBride, J., O'Rourke, K., Roose-Girma, M., … Dixit, V. M. (2006). Cryopyrin activates the inflammasome in response to toxins and ATP. *Nature*, *440*(7081), 228–232. https://doi.org/10.1038/nature04515

Markiewski, M. M., & Lambris, J. D. (2007). The Role of Complement in Inflammatory Diseases From Behind the Scenes into the Spotlight. *The American Journal of Pathology*, *171*(3), 715–727. https://doi.org/10.2353/ajpath.2007.070166

Mastellos, D. C., Ricklin, D., Yancopoulou, D., Risitano, A., & Lambris, J. D. (2014). Complement in paroxysmal nocturnal hemoglobinuria: exploiting our current knowledge to improve the treatment landscape. *Expert Review of Hematology*, *7*(5), 583–98. https://doi.org/10.1586/17474086.2014.953926

Mastellos, D., & Lambris, J. D. (2002). Complement: More than a "guard" against invading pathogens? *Trends in Immunology*. https://doi.org/10.1016/S1471-4906(02)02287-1

Masumoto, J., Taniguchi, S., Ayukawa, K., Sarvotham, H., Kishino, T., Niikawa, N., … Sagara, J. (1999). ASC, a novel 22-kDa protein, aggregates during apoptosis of human promyelocytic leukemia HL-60 cells. *The Journal of Biological Chemistry*, *274*(48), 33835–8. https://doi.org/10.1074/JBC.274.48.33835

Mathern, D. R., & Heeger, P. S. (2015). Molecules Great and Small: The Complement System. *Clinical Journal of the American Society of Nephrology*, CJN.06230614-. https://doi.org/10.2215/CJN.06230614

Matsushita, M. (2013). Ficolins in complement activation. *Molecular Immunology*, *55*(1), 22–6. https://doi.org/10.1016/j.molimm.2012.08.017

MATSUSHITA, M., & Fujita, T. (2002). The Role of Ficolins in Innate Immunity. *Immunobiology*, *205*(4–5), 490–497. https://doi.org/10.1078/0171-2985-00149

Mayer, M. M. (1972). Mechanism of cytolysis by complement. *Proceedings of the National Academy of Sciences of the United States of America*, *69*(10), 2954–8. Retrieved from http://www.pubmedcentral.nih.gov/articlerender.fcgi?artid=389682&tool=pmcentrez&rendertype=abstract

Mayor, A., Martinon, F., De Smedt, T., Pétrilli, V., & Tschopp, J. (2007). A crucial function of SGT1 and HSP90 in inflammasome activity links mammalian and plant innate immune responses. *Nature Immunology*, *8*(5), 497–503. https://doi.org/10.1038/ni1459

Mbengue, M., Bourdais, G., Gervasi, F., Beck, M., Zhou, J., Spallek, T., Robatzek, S. (2016). Clathrin-dependent endocytosis is required for immunity mediated by pattern recognition receptor kinases. *Proceedings of the National Academy of Sciences*, *113*(39), 11034–11039. https://doi.org/10.1073/pnas.1606004113

McNeil, L. K., Zagursky, R. J., Lin, S. L., Murphy, E., Zlotnick, G. W., Hoiseth, S. K., Anderson, A. S. (2013). Role of factor H binding protein in Neisseria meningitidis virulence and its potential as a vaccine candidate to broadly protect against meningococcal disease. *Microbiology and Molecular Biology Reviews : MMBR*, *77*(2), 234–52. https://doi.org/10.1128/MMBR.00056-12

Menny, A., Serna, M., Boyd, C. M., Gardner, S., Joseph, A. P., Morgan, B. P., Bubeck, D. (2018). CryoEM reveals how the complement membrane attack complex ruptures lipid bilayers. *Nature Communications*, *9*(1), 5316. https://doi.org/10.1038/s41467-018-07653-5

Meri, S., Morgan, B. P., Davies, A., Daniels, R. H., Olavesen, M. G., Waldmann, H., & Lachmann, P. J. (1990). Human protectin (CD59), an 18,000-20,000 MW complement lysis restricting factor, inhibits C5b-8 catalysed insertion of C9 into lipid bilayers. *Immunology*, *71*(1), 1–9. Retrieved from http://www.ncbi.nlm.nih.gov/pubmed/1698710

MERTENS, M., & SINGH, J. A. (2009). Anakinra for Rheumatoid Arthritis: A Systematic Review. *The Journal of Rheumatology*, *36*(6), 1118–1125. https://doi.org/10.3899/jrheum.090074

Mertens, M., & Singh, J. A. (2018). The Journal of Rheumatology Anakinra for Rheumatoid Arthritis: A Systematic Review. *The Journal of Rheumatology of Rheumatology The Journal on August*, *14*. https://doi.org/10.3899/jrheum.090074

Mevorach, D. (2015). Paroxysmal nocturnal hemoglobinuria (PNH) and primary p.Cys89Tyr mutation in CD59: Differences and similarities. *Molecular Immunology*, *67*(1), 51–55. https://doi.org/10.1016/j.molimm.2015.03.005

Miao, E. A., Rajan, J. V, & Aderem, A. (2011). Caspase-1-induced pyroptotic cell death. *Immunological Reviews*, *243*(1), 206–14. https://doi.org/10.1111/j.1600-065X.2011.01044.x

Michailidou, I., Jongejan, A., Vreijling, J. P., Georgakopoulou, T., de Wissel, M. B., Wolterman, R. A., Baas, F. (2018). Systemic inhibition of the membrane attack complex impedes neuroinflammation in chronic relapsing experimental autoimmune encephalomyelitis. *Acta Neuropathologica Communications*, *6*(1), 36. https://doi.org/10.1186/s40478-018-0536-y

Ming Man, S., Karki, R., Briard, B., Burton, A., Gingras, S., Pelletier, S., & Kanneganti, T.-D. (2017). Differential roles of caspase-1 and caspase-11 in infection and inflammation. *Scientific Reports*, *7*, 45126. https://doi.org/10.1038/srep45126

Monk, P. N., Scola, A.-M., Madala, P., & Fairlie, D. P. (2007). Function, structure and therapeutic potential of complement C5a receptors. *British Journal of Pharmacology*, *152*(4), 429–448. https://doi.org/10.1038/sj.bjp.0707332

MONSINJON, T., GASQUE, P., CHAN, P., ISCHENKO, A., BRADY, J. J., & FONTAINE, M. (2003). Regulation by complement C3a and C5a anaphylatoxins of cytokine production in human umbilical vein endothelial cells. *The FASEB Journal*, *17*(9), 1003–1014. https://doi.org/10.1096/fj.02-0737com

Morgan, B. P. (1989). Complement membrane attack on nucleated cells: resistance, recovery and non-lethal effects. *The Biochemical Journal*, *264*(1), 1–14. Retrieved from http://www.pubmedcentral.nih.gov/articlerender.fcgi?artid=1133540&tool=pmcentrez&rendertype=abstract

Morgan, B. P. (1992). Effects of the membrane attack complex of complement on nucleated cells. *Current Topics in Microbiology and Immunology*, *178*, 115–40. Retrieved from http://www.ncbi.nlm.nih.gov/pubmed/1424771

Morgan, B. P. (2000). The Complement System: An Overview. In *Complement Methods and Protocols* (pp. 1–13). New Jersey: Humana Press. https://doi.org/10.1385/1-59259-056-X:1

Morgan, B. P. (2015). The membrane attack complex as an inflammatory trigger. *Immunobiology*. https://doi.org/10.1016/j.imbio.2015.04.006

Morgan, B. P., Dankert, J. R., & Esser, A. F. (1987). Recovery of human neutrophils from complement attack: removal of the membrane attack complex by endocytosis and

exocytosis. *Journal of Immunology (Baltimore, Md. : 1950)*, *138*(1), 246–53. Retrieved from http://www.ncbi.nlm.nih.gov/pubmed/3782799

Morgan, B. P., Luzio, J. P., & Campbell, A. K. (1986). Intracellular Ca2+ and cell injury: A paradoxical role of Ca2+ in complement membrane attack. *Cell Calcium*, *7*(5–6), 399–411. https://doi.org/10.1016/0143-4160(86)90042-4

Morgan, B. P., van den Berg, C. W., Davies, E. V., Hallett, M. B., & Horejsi, V. (1993). Cross-linking of CD59 and of other glycosyl phosphatidylinositol-anchored molecules on neutrophils triggers cell activation via tyrosine kinase. *European Journal of Immunology*, *23*(11), 2841–2850. https://doi.org/10.1002/eji.1830231118

Morgan, B. P., Walters, D., Serna, M., & Bubeck, D. (2016). Terminal complexes of the complement system: new structural insights and their relevance to function. *Immunological Reviews*, *274*(1), 141–151. https://doi.org/10.1111/imr.12461

Morgan, H. P., Schmidt, C. Q., Guariento, M., Blaum, B. S., Gillespie, D., Herbert, A. P., … Hannan, J. P. (2011). Structural basis for engagement by complement factor H of C3b on a self surface. *Nature Structural & Molecular Biology*, *18*(4), 463–470. https://doi.org/10.1038/nsmb.2018

Moriwaki, K., & Chan, F. K.-M. (2013). RIP3: a molecular switch for necrosis and inflammation. *Genes & Development*, *27*(15), 1640–9. https://doi.org/10.1101/gad.223321.113

Mortimer, L., Moreau, F., MacDonald, J. A., & Chadee, K. (2016). NLRP3 inflammasome inhibition is disrupted in a group of auto-inflammatory disease CAPS mutations. *Nature Immunology*, *17*(10), 1176–1186. https://doi.org/10.1038/ni.3538

Mosca, R., Ceol, A., & Aloy, P. (2013). Interactome3D: adding structural details to protein networks. *Nat Meth*, *10*(1), 47–53. Retrieved from http://dx.doi.org/10.1038/nmeth.2289

Moskovich, O., Herzog, L. O., Ehrlich, M., & Fishelson, Z. (2012). Caveolin-1 and dynamin-2 are essential for removal of the complement C5b-9 complex via endocytosis. *Journal of Biological Chemistry*, *287*(24), 19904–19915. https://doi.org/10.1074/jbc.M111.333039

Motta, V., Soares, F., Sun, T., & Philpott, D. J. (2015). NOD-like receptors: versatile cytosolic sentinels. *Physiological Reviews*, *95*(1), 149–78. https://doi.org/10.1152/physrev.00009.2014

Muñoz-Planillo, R., Franchi, L., Miller, L. S., & Núñez, G. (2009). A Critical Role for Hemolysins and Bacterial Lipoproteins in Staphylococcus aureus-Induced Activation of the Nlrp3 Inflammasome. *The Journal of Immunology*, *183*(6), 3942–3948. https://doi.org/10.4049/JIMMUNOL.0900729

Murakami, T., Ockinger, J., Yu, J., Byles, V., McColl, A., Hofer, A. M., & Horng, T. (2012). Critical role for calcium mobilization in activation of the NLRP3 inflammasome. *Proceedings of the National Academy of Sciences of the United States of America*, *109*(28), 11282–7. https://doi.org/10.1073/pnas.1117765109

Murphy, K. M. (2011). *Janeway's Immunobiology*. Garland Science. Retrieved from https://books.google.com/books?id=WDMmAgAAQBAJ&pgis=1

Nauta, A. J., Daha, M. R., Tijsma, O., van de Water, B., Tedesco, F., & Roos, A. (2002). The membrane attack complex of complement induces caspase activation and apoptosis. *European Journal of Immunology*, *32*(3), 783–92. https://doi.org/10.1002/1521-4141(200203)32:3<783::AID-IMMU783>3.0.CO;2-Q

Nelson, G., Kucheryavenko, O., Wordsworth, J., & von Zglinicki, T. (2018). The senescent bystander effect is caused by ROS-activated NF-κB signalling. *Mechanisms of Ageing and Development*, *170*, 30–36. https://doi.org/10.1016/J.MAD.2017.08.005

Nemerow, G. R., Yamamoto, K. I., & Lint, T. F. (1979). Restriction of complement-mediated membrane damage by the eighth component of complement: a dual role for C8 in the complement attack sequence. *Journal of Immunology (Baltimore, Md. : 1950)*, *123*(3), 1245–52. Retrieved from http://www.ncbi.nlm.nih.gov/pubmed/469249

Nettesheim, D. G., Edalji, R. P., Mollison, K. W., Greer, J., & Zuiderweg, E. R. (1988). Secondary structure of complement component C3a anaphylatoxin in solution as determined by NMR spectroscopy: differences between crystal and solution conformations. *Proceedings of the National Academy of Sciences of the United States of America*, *85*(14), 5036–40. Retrieved from http://www.ncbi.nlm.nih.gov/pubmed/3260670

Nevo, Y., Ben-Zeev, B., Tabib, A., Straussberg, R., Anikster, Y., Shorer, Z., … Elpeleg, O. (2013). CD59 deficiency is associated with chronic hemolysis and childhood relapsing immune-mediated polyneuropathy. Blood, 121(1), 129–135. https://doi.org/10.1182/blood-2012-07-441857

Newsholme, P., Cruzat, V. F., Keane, K. N., Carlessi, R., & de Bittencourt, P. I. H. (2016). Molecular mechanisms of ROS production and oxidative stress in diabetes. *The Biochemical Journal*, *473*(24), 4527–4550. https://doi.org/10.1042/BCJ20160503C

Nicholson-Weller Jose Halperin, A. A. (1993). Membrane Signaling by Complement C5b-9, the Membrane Attack Complex. *Immunol Res*, *12*, 244–257. Retrieved from https://link.springer.com/content/pdf/10.1007/BF02918256.pdf

Nicholson-Weller, A., & Wang, C. E. (1994). Structure and function of decay accelerating factor CD55. *The Journal of Laboratory and Clinical Medicine*, *123*(4), 485–91. Retrieved from http://www.ncbi.nlm.nih.gov/pubmed/7511675

Nicolas, A., Lucchetti-Miganeh, C., Yaou, R. Ben, Kaplan, J.-C., Chelly, J., Leturcq, F., … Le Rumeur, E. (2012). Assessment of the structural and functional impact of in-frame mutations of the DMD gene, using the tools included in the eDystrophin online database. *Orphanet Journal of Rare Diseases*, *7*(1), 45. https://doi.org/10.1186/1750-1172-7-45

Niculescu, F., Rus, H., Shin, S., Lang, T., & Shin, M. L. (1993). Generation of diacylglycerol and ceramide during homologous complement activation. *Journal of Immunology*

(Baltimore, Md. : 1950), *150*(1), 214–24. Retrieved from http://www.ncbi.nlm.nih.gov/pubmed/8417124

Nilsson, B., & Nilsson Ekdahl, K. (2012). The tick-over theory revisited: is C3 a contact-activated protein? *Immunobiology*, *217*(11), 1106–10. https://doi.org/10.1016/j.imbio.2012.07.008

Nilsson, B., Hamad, O. A., Ahlström, H., Kullberg, J., Johansson, L., Lindhagen, L., Lind, L. (2014). C3 and C4 are strongly related to adipose tissue variables and cardiovascular risk factors. *European Journal of Clinical Investigation*, *44*(6), 587–96. https://doi.org/10.1111/eci.12275

Nilsson, U. R., & Nilsson, B. (1984). Simplified assays of hemolytic activity of the classical and alternative complement pathways. *Journal of Immunological Methods*, *72*(1), 49–59. Retrieved from http://www.ncbi.nlm.nih.gov/pubmed/6747305

Noris, M., & Remuzzi, G. (2013). Overview of complement activation and regulation. *Seminars in Nephrology*, *33*(6), 479–92. https://doi.org/10.1016/j.semnephrol.2013.08.001

Novak, I., & Solini, A. (2018). P2X receptor-ion channels in the inflammatory response in adipose tissue and pancreas — potential triggers in onset of type 2 diabetes? *Current Opinion in Immunology*, *52*, 1–7. https://doi.org/10.1016/j.coi.2018.02.002

Nowak, W. N., Deng, J., Ruan, X. Z., & Xu, Q. (2017). Reactive Oxygen Species Generation and Atherosclerosis. *Arteriosclerosis, Thrombosis, and Vascular Biology*, *37*(5), e41–e52. https://doi.org/10.1161/ATVBAHA.117.309228

Nymo, S., Niyonzima, N., Espevik, T., & Mollnes, T. E. (2014). Cholesterol crystal-induced endothelial cell activation is complement-dependent and mediated by TNF. *Immunobiology*, *219*(10), 786–92. https://doi.org/10.1016/j.imbio.2014.06.006

O'Barr, S., Cooper, N. R., Arend, W. P., Massoni, R. J., Niemann, M. A., Giclas, P. C., … Colton, C. A. (2000). The C5a complement activation peptide increases IL-1beta and IL-6 release from amyloid-beta primed human monocytes: implications for Alzheimer's disease. *Journal of Neuroimmunology*, *109*(2), 87–94. https://doi.org/10.1016/S0165-5728(00)00291-5

O'Hanlon, G. M., Humphreys, P. D., Goldman, R. S., Halstead, S. K., Bullens, R. W. M., Plomp, J. J., … Willison, H. J. (2003). Calpain inhibitors protect against axonal degeneration in a model of anti-ganglioside antibody-mediated motor nerve terminal injury. *Brain : A Journal of Neurology*, *126*(Pt 11), 2497–509. https://doi.org/10.1093/brain/awg254

O'Neill, L. A., & Greene, C. (1998). Signal transduction pathways activated by the IL-1 receptor family: ancient signaling machinery in mammals, insects, and plants. *Journal of Leukocyte Biology*, *63*(6), 650–7. Retrieved from http://www.ncbi.nlm.nih.gov/pubmed/9620655

Ogundele, M. (2001). Role and significance of the complement system in mucosal immunity: particular reference to the human breast milk complement. *Immunology and Cell Biology*, *79*(1), 1–10. https://doi.org/10.1046/j.1440-1711.2001.00976.x

Oikawa, D., Tokuda, M., & Iwawaki, T. (2007). Site-specific cleavage of CD59 mRNA by endoplasmic reticulum-localized ribonuclease, IRE1. *Biochemical and Biophysical Research Communications*, *360*(1), 122–127. https://doi.org/10.1016/j.bbrc.2007.06.020

Okada, M., Matsuzawa, A., Yoshimura, A., & Ichijo, H. (2014). The lysosome rupture-activated TAK1-JNK pathway regulates NLRP3 inflammasome activation. *The Journal of Biological Chemistry*, *289*(47), 32926–36. https://doi.org/10.1074/jbc.M114.579961

Orlowski, G. M., Colbert, J. D., Sharma, S., Bogyo, M., Robertson, S. A., & Rock, K. L. (2015). Multiple Cathepsins Promote Pro–IL-1β Synthesis and NLRP3-Mediated IL-1β Activation. *The Journal of Immunology*, *195*(4). Retrieved from http://www.jimmunol.org/content/195/4/1685.long#ref-7

Ospelt, C. (2017). Synovial fibroblasts in 2017. *RMD Open*, *3*(2), e000471. https://doi.org/10.1136/rmdopen-2017-000471

Panagiotou, A., Trendelenburg, M., & Osthoff, M. (2018). The Lectin Pathway of Complement in Myocardial Ischemia/Reperfusion Injury—Review of Its Significance and the Potential Impact of Therapeutic Interference by C1 Esterase Inhibitor. *Frontiers in Immunology*, *9*, 1151. https://doi.org/10.3389/fimmu.2018.01151

Panesar, M., Papillon, J., McTavish, A. J., & Cybulsky, A. V. (1997). Activation of phospholipase A2 by complement C5b-9 in glomerular epithelial cells. *Journal of Immunology (Baltimore, Md. : 1950)*, *159*(7), 3584–94. Retrieved from http://www.ncbi.nlm.nih.gov/pubmed/9317158

Pangburn, M. K., & Rawal, N. (2002). Structure and function of complement C5 convertase enzymes. *Biochemical Society Transactions*, *30*(Pt 6), 1006–10. https://doi.org/10.1042/

Pangburn, M. K., Schreiber, R. D., & Müller-Eberhard, H. J. (1981). Formation of the initial C3 convertase of the alternative complement pathway. Acquisition of C3b-like activities by spontaneous hydrolysis of the putative thioester in native C3. *The Journal of Experimental Medicine*, *154*(3), 856–67. Retrieved from http://www.ncbi.nlm.nih.gov/pubmed/6912277

Pani, B., & Singh, B. B. (2009). Lipid rafts/caveolae as microdomains of calcium signaling. *Cell Calcium*, *45*(6), 625–33. https://doi.org/10.1016/j.ceca.2009.02.009

Papadimitriou, J. C., Ramm, L. E., Drachenberg, C. B., Trump, B. F., & Shin, M. L. (1991). Quantitative analysis of adenine nucleotides during the prelytic phase of cell death mediated by C5b-9. *Journal of Immunology (Baltimore, Md. : 1950)*, *147*(1), 212–7. Retrieved from http://www.ncbi.nlm.nih.gov/pubmed/1904901

Parajuli, B., Sonobe, Y., Horiuchi, H., Takeuchi, H., Mizuno, T., & Suzumura, A. (2013). Oligomeric amyloid β induces IL-1β processing via production of ROS: implication in

Alzheimer's disease. *Cell Death & Disease*, *4*, e975. https://doi.org/10.1038/cddis.2013.503

Park, B.-S., Henning, P. C., Grant, S. C., Lee, W. J., Lee, S.-R., Arjmandi, B. H., & Kim, J.-S. (2013). HMB attenuates muscle loss during sustained energy deficit induced by calorie restriction and endurance exercise. *Metabolism*, *62*(12), 1718–1729. https://doi.org/10.1016/j.metabol.2013.06.005

Park, J.-E., Kim, Y.-I., & Yi, A.-K. (2009). Protein Kinase D1 Is Essential for MyD88-Dependent TLR Signaling Pathway. *The Journal of Immunology*, *182*(10), 6316–6327. https://doi.org/10.4049/jimmunol.0804239

Patel, D., Gaikwad, S., Challagundla, N., Nivsarkar, M., & Agrawal-Rajput, R. (2018). Spleen tyrosine kinase inhibition ameliorates airway inflammation through modulation of NLRP3 inflammosome and Th17/Treg axis. *International Immunopharmacology*, *54*, 375–384. https://doi.org/10.1016/j.intimp.2017.11.026

Patel, S. N., Berghout, J., Lovegrove, F. E., Ayi, K., Conroy, A., Serghides, L., Kain, K. C. (2008). C5 deficiency and C5a or C5aR blockade protects against cerebral malaria. *The Journal of Experimental Medicine*, *205*(5), 1133–43. https://doi.org/10.1084/jem.20072248

Patston, P. A., Gettins, P., Beechem, J., & Schapira, M. (1991). Mechanism of serpin action: evidence that C1 inhibitor functions as a suicide substrate. *Biochemistry*, *30*(36), 8876–82. Retrieved from http://www.ncbi.nlm.nih.gov/pubmed/1888745

Pellegrini, C., Antonioli, L., Lopez-Castejon, G., Blandizzi, C., & Fornai, M. (2017). Canonical and Non-Canonical Activation of NLRP3 Inflammasome at the Crossroad between Immune Tolerance and Intestinal Inflammation. *Frontiers in Immunology*, *8*, 36. https://doi.org/10.3389/fimmu.2017.00036

Peng, Q., Li, K., Wang, N., Li, Q., Asgari, E., Lu, B., Zhou, W. (2009). Dendritic Cell Function in Allostimulation Is Modulated by C5aR Signaling. *The Journal of Immunology*, *183*(10), 6058–6068. https://doi.org/10.4049/jimmunol.0804186

Petersen, S. V, Thiel, S., & Jensenius, J. C. (2001). The mannan-binding lectin pathway of complement activation: biology and disease association. *Molecular Immunology*, *38*(2–3), 133–49. Retrieved from http://www.ncbi.nlm.nih.gov/pubmed/11532276

Phieler, J., Garcia-Martin, R., Lambris, J. D., & Chavakis, T. (2013). The role of the complement system in metabolic organs and metabolic diseases. *Seminars in Immunology*, *25*(1), 47–53. https://doi.org/10.1016/j.smim.2013.04.003

Pilzer, D., Gasser, O., Moskovich, O., Schifferli, J. A., & Fishelson, Z. (2005). Emission of membrane vesicles: roles in complement resistance, immunity and cancer. *Springer Seminars in Immunopathology*, *27*(3), 375–387. https://doi.org/10.1007/s00281-005-0004-1

Pio, R., Ajona, D., & Lambris, J. D. (2013). Complement inhibition in cancer therapy. *Seminars in Immunology*, *25*(1), 54–64. https://doi.org/10.1016/j.smim.2013.04.001

Prabhananda, B. S., & Ugrankar, M. M. (1991). Nigericin-mediated H+, K+ and Na+ transports across vesicular membrane: T-jump studies. *Biochimica et Biophysica Acta (BBA) - Biomembranes*, *1070*(2), 481–491. https://doi.org/10.1016/0005-2736(91)90090-U

Próchnicki, T., & Latz, E. (2017). Inflammasomes on the Crossroads of Innate Immune Recognition and Metabolic Control. *Cell Metabolism*, *26*(1), 71–93. https://doi.org/10.1016/j.cmet.2017.06.018

Py, B. F., Kim, M.-S., Vakifahmetoglu-Norberg, H., & Yuan, J. (2013). Deubiquitination of NLRP3 by BRCC3 Critically Regulates Inflammasome Activity. *Molecular Cell*, *49*(2), 331–338. https://doi.org/10.1016/j.molcel.2012.11.009

Qiu, W., Zhang, Y., Liu, X., Zhou, J., Li, Y., Zhou, Y., Wang, Y. (2012). Sublytic C5b-9 complexes induce proliferative changes of glomerular mesangial cells in rat Thy-1 nephritis through TRAF6-mediated PI3K-dependent Akt1 activation. *The Journal of Pathology*, *226*(4), 619–32. https://doi.org/10.1002/path.3011

Qiu, Y., Huang, X., Huang, L., Tang, L., Jiang, J., Chen, L., & Li, S. (2016). 5-HT(1A) receptor antagonist improves behavior performance of delirium rats through inhibiting PI3K/Akt/mTOR activation-induced NLRP3 activity. *IUBMB Life*, *68*(4), 311–9. https://doi.org/10.1002/iub.1491

Qiu, Z., Lei, S., Zhao, B., Wu, Y., Su, W., Liu, M., Xia, Z.-Y. (2017). NLRP3 Inflammasome Activation-Mediated Pyroptosis Aggravates Myocardial Ischemia/Reperfusion Injury in Diabetic Rats. *Oxidative Medicine and Cellular Longevity*, *2017*, 9743280. https://doi.org/10.1155/2017/9743280

Ramm, L. E., Whitlow, M. B., & Mayer, M. M. (1982). Size of the transmembrane channels produced by complement proteins C5b-8. *Journal of Immunology (Baltimore, Md. : 1950)*, *129*(3), 1143–6. Retrieved from http://www.ncbi.nlm.nih.gov/pubmed/6286757

Rawal, N., & Pangburn, M. (2001). Formation of high-affinity C5 convertases of the alternative pathway of complement. *Journal of Immunology (Baltimore, Md. : 1950)*, *166*(4), 2635–42. https://doi.org/10.4049/JIMMUNOL.166.4.2635

Razani, B., Woodman, S. E., & Lisanti, M. P. (2002). Caveolae: from cell biology to animal physiology. *Pharmacological Reviews*, *54*(3), 431–67. Retrieved from http://www.ncbi.nlm.nih.gov/pubmed/12223531

Reis, E. S., Mastellos, D. C., Ricklin, D., Mantovani, A., & Lambris, J. D. (2017). Complement in cancer: untangling an intricate relationship. *Nature Reviews Immunology*, *18*(1), 5–18. https://doi.org/10.1038/nri.2017.97

Reuter, M., Caswell, C. C., Lukomski, S., & Zipfel, P. F. (2010). Binding of the human complement regulators CFHR1 and factor H by streptococcal collagen-like protein 1 (Scl1) via their conserved C termini allows control of the complement cascade at multiple levels. The Journal of Biological Chemistry, 285(49), 38473–85. https://doi.org/10.1074/jbc.M110.143727

Rheinheimer, J., de Souza, B. M., Cardoso, N. S., Bauer, A. C., & Crispim, D. (2017). Current role of the NLRP3 inflammasome on obesity and insulin resistance: A systematic review. *Metabolism*, *74*, 1–9. https://doi.org/10.1016/j.metabol.2017.06.002

Ribeiro, C. B., Christofoletti, D. C., Pezolato, V. A., de Cássia Marqueti Durigan, R., Prestes, J., Tibana, R. A., … da Silva, C. A. (2015). Leucine minimizes denervation-induced skeletal muscle atrophy of rats through akt/mtor signaling pathways. *Frontiers in Physiology*, *6*, 73. https://doi.org/10.3389/fphys.2015.00073

Richardson, P. G., Eng, C., Kolesar, J., Hideshima, T., & Anderson, K. C. (2012). Perifosine , an oral, anti-cancer agent and inhibitor of the Akt pathway: mechanistic actions, pharmacodynamics, pharmacokinetics, and clinical activity. *Expert Opinion on Drug Metabolism & Toxicology*, *8*(5), 623–33. https://doi.org/10.1517/17425255.2012.681376

Ricklin, D., & Lambris, J. D. (2016). Therapeutic control of complement activation at the level of the central component C3. *Immunobiology*, *221*(6), 740–746. https://doi.org/10.1016/J.IMBIO.2015.06.012

Ricklin, D., Hajishengallis, G., Yang, K., & Lambris, J. D. (2010). Complement: a key system for immune surveillance and homeostasis. *Nature Immunology*, *11*(9), 785–97. https://doi.org/10.1038/ni.1923

Riedemann, N. C., Guo, R.-F., Gao, H., Sun, L., Hoesel, M., Hollmann, T. J., Ward, P. A. (2004). Regulatory Role of C5a on Macrophage Migration Inhibitory Factor Release from Neutrophils. *The Journal of Immunology*, *173*(2), 1355–1359. https://doi.org/10.4049/jimmunol.173.2.1355

Rittig, M. G., Burmester, G.-R., & Krause, A. (1998). Coiling phagocytosis: when the zipper jams, the cup is deformed. *Trends in Microbiology*, *6*(10), 384–388. https://doi.org/10.1016/S0966-842X(98)01343-2

Rittirsch, D., Flierl, M. A., & Ward, P. A. (2008). Harmful molecular mechanisms in sepsis. *Nature Reviews. Immunology*, *8*(10), 776–87. https://doi.org/10.1038/nri2402

Rivers-Auty, J., & Brough, D. (2015). Potassium efflux fires the canon: Potassium efflux as a common trigger for canonical and noncanonical NLRP3 pathways. *European Journal of Immunology*, *45*(10), 2758–2761. https://doi.org/10.1002/eji.201545958

Rizzi, F., & Bettuzzi, S. (2010). The clusterin paradigm in prostate and breast carcinogenesis. *Endocrine-Related Cancer*, *17*(1), R1-17. https://doi.org/10.1677/ERC-09-0140

Romero, V., Fert-Bober, J., Nigrovic, P. A., Darrah, E., Haque, U. J., Lee, D. M., … Andrade, F. (2013). Immune-Mediated Pore-Forming Pathways Induce Cellular Hypercitrullination and Generate Citrullinated Autoantigens in Rheumatoid Arthritis. *Science Translational Medicine*, *5*(209), 209ra150-209ra150. https://doi.org/10.1126/scitranslmed.3006869

Romero, V., Fert-Bober, J., Nigrovic, P. A., Darrah, E., Haque, U. J., Lee, D. M., Andrade, F. (2013). Immune-Mediated Pore-Forming Pathways Induce Cellular Hypercitrullination

and Generate Citrullinated Autoantigens in Rheumatoid Arthritis. *Science Translational Medicine*, *5*(209), 209ra150-209ra150. https://doi.org/10.1126/scitranslmed.3006869

Rosenstiel, P., Till, A., & Schreiber, S. (2007). NOD-like receptors and human diseases. *Microbes and Infection / Institut Pasteur*, *9*(5), 648–57. https://doi.org/10.1016/j.micinf.2007.01.015

Roversi, P., Johnson, S., Caesar, J. J. E., McLean, F., Leath, K. J., Tsiftsoglou, S. A., Lea, S. M. (2011). Structural basis for complement factor I control and its disease-associated sequence polymorphisms. *Proceedings of the National Academy of Sciences*, *108*(31), 12839–12844. https://doi.org/10.1073/pnas.1102167108

Rubartelli, A. (2012). Redox control of NLRP3 inflammasome activation in health and disease. *Journal of Leukocyte Biology*, *92*(5), 951–958. https://doi.org/10.1189/jlb.0512265

Ruiz-Delgado, G. J., Vázquez-Garza, E., Méndez-Ramírez, N., & Gómez-Almaguer, D. (2009). Abnormalities in the expression of CD55 and CD59 surface molecules on peripheral blood cells are not specific to paroxysmal nocturnal hemoglobinuria. *Hematology*, *14*(1), 33–37. https://doi.org/10.1179/102453309X385089

Rus, H. G., Niculescu, F. I., & Shin, M. L. (2001). Role of the C5b-9 complement complex in cell cycle and apoptosis. *Immunological Reviews*, *180*, 49–55. Retrieved from http://www.ncbi.nlm.nih.gov/pubmed/11414362

Rus, H. G., Niculescu, F., & Shin, M. L. (1996). Sublytic complement attack induces cell cycle in oligodendrocytes. *Journal of Immunology (Baltimore, Md. : 1950)*, *156*(12), 4892–900. Retrieved from http://www.ncbi.nlm.nih.gov/pubmed/8648139

Rus, H., Cudrici, C., Niculescu, F., & Shin, M. L. (2006). Complement activation in autoimmune demyelination: Dual role in neuroinflammation and neuroprotection. *Journal of Neuroimmunology*. https://doi.org/10.1016/j.jneuroim.2006.07.009

Rutkowski, M. J., Sughrue, M. E., Kane, A. J., Ahn, B. J., Fang, S., & Parsa, A. T. (2010). The complement cascade as a mediator of tissue growth and regeneration. *Inflammation Research*, *59*(11), 897–905. https://doi.org/10.1007/s00011-010-0220-6

Sahu, A., & Lambris, J. D. (2001). Structure and biology of complement protein C3, a connecting link between innate and acquired immunity. *Immunological Reviews*, *180*(1), 35–48. https://doi.org/10.1034/j.1600-065X.2001.1800103.x

Santos, A. L., Sinha, S., & Lindner, A. B. (2018). The Good, the Bad, and the Ugly of ROS: New Insights on Aging and Aging-Related Diseases from Eukaryotic and Prokaryotic Model Organisms. *Oxidative Medicine and Cellular Longevity*, *2018*, 1–23. https://doi.org/10.1155/2018/1941285

Saresella, M., La Rosa, F., Piancone, F., Zoppis, M., Marventano, I., Calabrese, E., … Clerici, M. (2016). The NLRP3 and NLRP1 inflammasomes are activated in Alzheimer's disease. *Molecular Neurodegeneration*, *11*(1), 23. https://doi.org/10.1186/s13024-016-0088-1

Sarma, J. V., & Ward, P. A. (2011). The complement system. *Cell and Tissue Research*, *343*(1), 227–35. https://doi.org/10.1007/s00441-010-1034-0

Schaloske, R., Schlatterer, C., & Malchow, D. (2000). A Xestospongin C-sensitive Ca(2+) store is required for cAMP-induced Ca(2+) influx and cAMP oscillations in Dictyostelium. *The Journal of Biological Chemistry*, *275*(12), 8404–8. https://doi.org/10.1074/JBC.275.12.8404

Schmid-Burgk, J. L., Gaidt, M. M., Schmidt, T., Ebert, T. S., Bartok, E., & Hornung, V. (2015). Caspase-4 mediates non-canonical activation of the NLRP3 inflammasome in human myeloid cells. *European Journal of Immunology*, *45*(10), 2911–2917. https://doi.org/10.1002/eji.201545523

Schraufstatter, I. U., Trieu, K., Sikora, L., Sriramarao, P., & DiScipio, R. (2002). Complement c3a and c5a induce different signal transduction cascades in endothelial cells. *Journal of Immunology (Baltimore, Md. : 1950)*, *169*(4), 2102–10. Retrieved from http://www.ncbi.nlm.nih.gov/pubmed/12165538

Schreiber, R. D., Pangburn, M. K., Lesavre, P. H., & Müller-Eberhard, H. J. (1978). Initiation of the alternative pathway of complement: recognition of activators by bound C3b and assembly of the entire pathway from six isolated proteins. *Proceedings of the National Academy of Sciences of the United States of America*, *75*(8), 3948–52. Retrieved from http://www.ncbi.nlm.nih.gov/pubmed/279011

Seow, V., Lim, J., Iyer, A., Suen, J. Y., Ariffin, J. K., Hohenhaus, D. M., Fairlie, D. P. (2013). Inflammatory Responses Induced by Lipopolysaccharide Are Amplified in Primary Human Monocytes but Suppressed in Macrophages by Complement Protein C5a. *The Journal of Immunology*, *191*(8), 4308–4316. https://doi.org/10.4049/jimmunol.1301355

Shahzad, K., Bock, F., Dong, W., Wang, H., Kopf, S., Kohli, S., Isermann, B. (2015). Nlrp3-inflammasome activation in non-myeloid-derived cells aggravates diabetic nephropathy. *Kidney International*, *87*(1), 74–84. https://doi.org/10.1038/ki.2014.271

Shen, J., Wang, L., Jiang, N., Mou, S., Zhang, M., Gu, L., Ni, Z. (2016). NLRP3 inflammasome mediates contrast media-induced acute kidney injury by regulating cell apoptosis. *Scientific Reports*, *6*, 34682. https://doi.org/10.1038/srep34682

Shi, H., Williams, J. A. E., Guo, L., Stampoulis, D., Francesca Cordeiro, M., & Moss, S. E. (2015). Exposure to the complement C5b-9 complex sensitizes 661W photoreceptor cells to both apoptosis and necroptosis. *Apoptosis : An International Journal on Programmed Cell Death*, *20*(4), 433–43. https://doi.org/10.1007/s10495-015-1091-7

Shin, H. J., Lee, H., Park, J. D., Hyun, H. C., Sohn, H. O., Lee, D. W., & Kim, Y. S. (2007). Kinetics of binding of LPS to recombinant CD14, TLR4, and MD-2 proteins. *Molecules and Cells*, *24*(1), 119–24. Retrieved from http://www.ncbi.nlm.nih.gov/pubmed/17846506

Shuster, D. E., Kehrli, M. E., Rainard, P., & Paape, M. (1997). Complement fragment C5a and inflammatory cytokines in neutrophil recruitment during intramammary infection

with Escherichia coli. *Infection and Immunity*, *65*(8), 3286–92. Retrieved from http://www.ncbi.nlm.nih.gov/pubmed/9234788

Sica, M., Rondelli, T., Ricci, P., De Angioletti, M., Risitano, A. M., & Notaro, R. (2017). Eculizumab treatment: stochastic occurrence of C3 binding to individual PNH erythrocytes. *Journal of Hematology & Oncology*, *10*(1), 126. https://doi.org/10.1186/s13045-017-0496-x

Skerka, C., Chen, Q., Fremeaux-Bacchi, V., & Roumenina, L. T. (2013). Complement factor H related proteins (CFHRs). *Molecular Immunology*, *56*(3), 170–80. https://doi.org/10.1016/j.molimm.2013.06.001

Smeets, R. L., Joosten, L. A. B., Arntz, O. J., Bennink, M. B., Takahashi, N., Carlsen, H., van de Loo, F. A. J. (2005). Soluble interleukin-1 receptor accessory protein ameliorates collagen-induced arthritis by a different mode of action from that of interleukin-1 receptor antagonist. *Arthritis & Rheumatism*, *52*(7), 2202–2211. https://doi.org/10.1002/art.21108

Soane, L., Rus, H., Niculescu, F., & Shin, M. L. (1999). Inhibition of oligodendrocyte apoptosis by sublytic C5b-9 is associated with enhanced synthesis of bcl-2 and mediated by inhibition of caspase-3 activation. *Journal of Immunology (Baltimore, Md. : 1950)*, *163*(11), 6132–8. Retrieved from http://www.ncbi.nlm.nih.gov/pubmed/10570303

Sollberger, G., Choidas, A., Burn, G. L., Habenberger, P., Di Lucrezia, R., Kordes, S., … Zychlinsky, A. (2018). Gasdermin D plays a vital role in the generation of neutrophil extracellular traps. *Science Immunology*, *3*(26), eaar6689. https://doi.org/10.1126/sciimmunol.aar6689

Sollberger, G., Strittmatter, G. E., Kistowska, M., French, L. E., & Beer, H.-D. (2012). Caspase-4 Is Required for Activation of Inflammasomes. *The Journal of Immunology*, *188*(4), 1992–2000. https://doi.org/10.4049/jimmunol.1101620

Sollberger, G., Strittmatter, G. E., Kistowska, M., French, L. E., & Beer, H.-D. (2012). Caspase-4 is required for activation of inflammasomes. *Journal of Immunology (Baltimore, Md. : 1950)*, *188*(4), 1992–2000. https://doi.org/10.4049/jimmunol.1101620

Son, G.-Y., Son, A., Yang, Y.-M., Park, W., Chang, I., Lee, J.-H., & Shin, D. M. (2016). Airborne allergens induce protease activated receptor-2-mediated production of inflammatory cytokines in human gingival epithelium. *Archives of Oral Biology*, *61*, 138–43. https://doi.org/10.1016/j.archoralbio.2015.10.015

Spel, L., & Martinon, F. (2018). Gasdermin D opens the way for NETs. *Nature Reviews Rheumatology*, 1. https://doi.org/10.1038/s41584-018-0124-3

Spicer, B. A., Law, R. H. P., Caradoc-Davies, T. T., Ekkel, S. M., Bayly-Jones, C., Pang, S.-S., Dunstone, M. A. (2018). The first transmembrane region of complement component-9 acts as a brake on its self-assembly. *Nature Communications*, *9*(1), 3266. https://doi.org/10.1038/s41467-018-05717-0

Srirangan, S., & Choy, E. H. (2010). The role of Interleukin 6 in the pathophysiology of rheumatoid arthritis. *Therapeutic Advances in Musculoskeletal Disease* , *2*(5), 247–256. https://doi.org/10.1177/1759720X10378372

Stephan, A. H., Barres, B. A., & Stevens, B. (2012). The Complement System: An Unexpected Role in Synaptic Pruning During Development and Disease. *Annual Review of Neuroscience*, *35*(1), 369–389. https://doi.org/10.1146/annurev-neuro-061010-113810

Stephan, A. H., Barres, B. A., & Stevens, B. (2012). The Complement System: An Unexpected Role in Synaptic Pruning During Development and Disease. *Annual Review of Neuroscience*, *35*(1), 369–389. https://doi.org/10.1146/annurev-neuro-061010-113810

Stutz, A., Golenbock, D. T., & Latz, E. (2009). Inflammasomes: too big to miss. *Journal of Clinical Investigation*, *119*(12), 3502–3511. https://doi.org/10.1172/JCI40599

Stutz, A., Kolbe, C.-C., Stahl, R., Horvath, G. L., Franklin, B. S., van Ray, O., Latz, E. (2017). NLRP3 inflammasome assembly is regulated by phosphorylation of the pyrin domain. *The Journal of Experimental Medicine*, *214*(6), 1725–1736. https://doi.org/10.1084/jem.20160933

Sugita, Y., Ito, K., Shiozuka, K., Suzuki, H., Gushima, H., Tomita, M., & Masuho, Y. (1994). Recombinant soluble CD59 inhibits reactive haemolysis with complement. *Immunology*, *82*(1), 34–41. Retrieved from http://www.ncbi.nlm.nih.gov/pubmed/7519172

Sugiyama, R., Agematsu, K., Migita, K., Nakayama, J., Mokuda, S., Ogura, F., … Masumoto, J. (2014). Defect of suppression of inflammasome-independent interleukin-8 secretion from SW982 synovial sarcoma cells by familial Mediterranean fever-derived pyrin mutations. *Molecular Biology Reports*, *41*(1), 545–553. https://doi.org/10.1007/s11033-013-2890-y

Sugiyama, R., Agematsu, K., Migita, K., Nakayama, J., Mokuda, S., Ogura, F., … Masumoto, J. (2014). Defect of suppression of inflammasome-independent interleukin-8 secretion from SW982 synovial sarcoma cells by familial Mediterranean fever-derived pyrin mutations. *Molecular Biology Reports*, *41*(1), 545–53. https://doi.org/10.1007/s11033-013-2890-y

Suresh, R., Chandrasekaran, P., Sutterwala, F. S., & Mosser, D. M. (2016). Complement-mediated “bystander” damage initiates host NLRP3 inflammasome activation. *Journal of Cell Science*, *129*(9), 1928–39. https://doi.org/10.1242/jcs.179291

Sutterwala, F. S., Cassel Iyer, S. L., Stotland, A., Weiss, J. P., Eric I Elliott, R. A., Miller, A. N., Cassel, S. L. (2018). Cutting Edge: Mitochondrial Assembly of the Cutting Edge: Mitochondrial Assembly of the NLRP3 Inflammasome Complex Is Initiated at Priming. *J Immunol Material SupplementaryDCSupplemental The Journal of Immunology by Guest on April*, *3*(4). Retrieved from http://www.jimmunol.org/content/early/2018/03/29/jimmun

Sutterwala, F. S., Haasken, S., & Cassel, S. L. (2014). Mechanism of NLRP3 inflammasome activation. *Annals of the New York Academy of Sciences*, *1319*, 82–95. https://doi.org/10.1111/nyas.12458

Sutterwala, F. S., Haasken, S., & Cassel, S. L. (2014). Mechanism of NLRP3 inflammasome activation. *Annals of the New York Academy of Sciences*, *1319*(1), 82–95. https://doi.org/10.1111/nyas.12458

Suzuki, H., Yamaji, N., Egashira, A., Yasunaga, K., Sugita, Y., & Masuho, Y. (1996). Effect of the sugar chain of soluble recombinant CD59 on complement inhibitory activity. *FEBS Letters*, *399*(3), 272–6. Retrieved from http://www.ncbi.nlm.nih.gov/pubmed/8985161

Symmons, D., Turner, G., Webb, R., Asten, P., Barrett, E., Lunt, M., Silman, A. (2002). The prevalence of rheumatoid arthritis in the United Kingdom: new estimates for a new century. *Rheumatology , 41*(7), 793–800. https://doi.org/10.1093/rheumatology/41.7.793

Takahashi, K., & Ezekowitz, R. A. B. (2005). The role of the mannose-binding lectin in innate immunity. *Clinical Infectious Diseases : An Official Publication of the Infectious Diseases Society of America*, *41 Suppl 7*(Supplement_7), S440-4. https://doi.org/10.1086/431987

Takahashi, M., Iwaki, D., Kanno, K., Ishida, Y., Xiong, J., Matsushita, M., Fujita, T. (2008). Mannose-Binding Lectin (MBL)-Associated Serine Protease (MASP)-1 Contributes to Activation of the Lectin Complement Pathway. *The Journal of Immunology*, *180*(9), 6132–6138. https://doi.org/10.4049/jimmunol.180.9.6132

Tashima, Y., Taguchi, R., Murata, C., Ashida, H., Kinoshita, T., & Maeda, Y. (2006). PGAP2 Is Essential for Correct Processing and Stable Expression of GPI-anchored Proteins. *Molecular Biology of the Cell*, *17*(3), 1410–1420. https://doi.org/10.1091/mbc.e05-11-1005

Tegla, C. A., Cudrici, C., Patel, S., Trippe, R., Rus, V., Niculescu, F., & Rus, H. (2011). Membrane attack by complement: the assembly and biology of terminal complement complexes. *Immunologic Research*, *51*(1), 45–60. https://doi.org/10.1007/s12026-011-8239-5

Teixeira, G. R., Gobbo, L. A., Dos Santos, N. J., De Araújo, R. G., Dos Santos, C. C., De Mello Malheiro, O. C., Papoti, M. (2016). The effect of β-hydroxy-β-methylbutyrate (HMB) on the morphology of skeletal muscle after concurrent training. *Motriz. Revista de Educacao Fisica*. https://doi.org/10.1590/S1980-6574201600030010

Thielen, A. J. F., van Baarsen, I. M., Jongsma, M. L., Zeerleder, S., Spaapen, R. M., & Wouters, D. (2018). CRISPR/Cas9 generated human CD46, CD55 and CD59 knockout cell lines as a tool for complement research. *Journal of Immunological Methods*, *456*, 15–22. https://doi.org/10.1016/j.jim.2018.02.004

Thurman, J. M., & Holers, V. M. (2006). The Central Role of the Alternative Complement Pathway in Human Disease. *The Journal of Immunology*, *176*(3), 1305–1310. https://doi.org/10.4049/jimmunol.176.3.1305

Togo, T. (2017). Cell membrane disruption stimulates cAMP and Ca2+ signaling to potentiate cell membrane resealing in neighboring cells. *Biology Open*, *6*(12), 1814–1819. https://doi.org/10.1242/bio.028977

Tong, Y., Ding, Z.-H., Zhan, F.-X., Cai, L., Yin, X., Ling, J.-L., Liu, J.-F. (2015). The NLRP3 inflammasome and stroke. *International Journal of Clinical and Experimental Medicine*, *8*(4), 4787–4794. Retrieved from http://www.ncbi.nlm.nih.gov/pmc/articles/PMC4483817/

Topham, P. S., Haydar, S. A., Kuphal, R., Lightfoot, J. D., & Salant, D. J. (1999). Complement-mediated injury reversibly disrupts glomerular epithelial cell actin microfilaments and focal adhesions. *Kidney International*, *55*(5), 1763–75. https://doi.org/10.1046/j.1523-1755.1999.00407.x

Tornatore, L., Thotakura, A. K., Bennett, J., Moretti, M., & Franzoso, G. (2012). The nuclear factor kappa B signaling pathway: integrating metabolism with inflammation. *Trends in Cell Biology*, *22*(11), 557–566. https://doi.org/10.1016/j.tcb.2012.08.001

Towner, L. D., Wheat, R. A., Hughes, T. R., & Morgan, B. P. (2016). Complement Membrane Attack and Tumorigenesis: A SYSTEMS BIOLOGY APPROACH. *The Journal of Biological Chemistry*, *291*(29), 14927–38. https://doi.org/10.1074/jbc.M115.708446

Triantafilou, K., Hughes, T. R., Triantafilou, M., & Morgan, B. P. (2013). The complement membrane attack complex triggers intracellular Ca2+ fluxes leading to NLRP3 inflammasome activation. *Journal of Cell Science*, *126*(Pt 13), 2903–13. https://doi.org/10.1242/jcs.124388

Triantafilou, M., Hughes, T. R., Morgan, B. P., & Triantafilou, K. (2016). Complementing the inflammasome. *Immunology*, *147*(2), 152–164. https://doi.org/10.1111/imm.12556

Trouw, L. A., Bengtsson, A. A., Gelderman, K. A., Dahlbäck, B., Sturfelt, G., & Blom, A. M. (2007). C4b-binding Protein and Factor H Compensate for the Loss of Membrane-bound Complement Inhibitors to Protect Apoptotic Cells against Excessive Complement Attack. *Journal of Biological Chemistry*, *282*(39), 28540–28548. https://doi.org/10.1074/jbc.M704354200

Tschopp, J., Podack, E. R., & Müller-Eberhard, H. J. (1982). Ultrastructure of the membrane attack complex of complement: detection of the tetramolecular C9-polymerizing complex C5b-8. *Proceedings of the National Academy of Sciences of the United States of America*, *79*(23), 7474–8. Retrieved from http://www.ncbi.nlm.nih.gov/pubmed/6961424

Turner, M. W. (1998). Mannose-Binding Lectin (MBL) in Health and Disease. *Immunobiology*, *199*(2), 327–339. https://doi.org/10.1016/S0171-2985(98)80037-5

van den Berg, C. W. (2000). Purification of complement components, regulators, and receptors by classical methods. *Methods in Molecular Biology (Clifton, N.J.)*, *150*, 15–52. https://doi.org/10.1385/1-59259-056-X:15

van den Berg, C. W. (2000). Purification of Complement Components, Regulators, and Receptors by Classical Methods. In *Complement Methods and Protocols* (Vol. 150, pp. 15–52). New Jersey: Humana Press. https://doi.org/10.1385/1-59259-056-X:15

van den Berg, C. W., Cinek, T., Hallett, M. B., Horejsi, V., & Morgan, B. P. (1995). Exogenous glycosyl phosphatidylinositol-anchored CD59 associates with kinases in membrane clusters on U937 cells and becomes Ca(2+)-signaling competent. *The Journal of Cell Biology*, *131*(3), 669–77. Retrieved from http://www.pubmedcentral.nih.gov/articlerender.fcgi?artid=2120624&tool=pmcentrez&rendertype=abstract

van Lookeren Campagne, M., Wiesmann, C., & Brown, E. J. (2007). Macrophage complement receptors and pathogen clearance. *Cellular Microbiology*, *9*(9), 2095–102. https://doi.org/10.1111/j.1462-5822.2007.00981.x

VENKATESHA, R., THANGAM, E., ZAIDI, A., & ALI, H. (2005). Distinct regulation of C3a-induced MCP-1/CCL2 and RANTES/CCL5 production in human mast cells by extracellular signal regulated kinase and PI3 kinase. *Molecular Immunology*, *42*(5), 581–587. https://doi.org/10.1016/j.molimm.2004.09.009

Venkatraman Girija, U., Gingras, A. R., Marshall, J. E., Panchal, R., Sheikh, M. A., Gál, P., Wallis, R. (2013). Structural basis of the C1q/C1s interaction and its central role in assembly of the C1 complex of complement activation. *Proceedings of the National Academy of Sciences of the United States of America*, *110*(34), 13916–20. https://doi.org/10.1073/pnas.1311113110

Verschoor, A., Karsten, C. M., Broadley, S. P., Laumonnier, Y., & Köhl, J. (2016). Old dogs-new tricks: immunoregulatory properties of C3 and C5 cleavage fragments. *Immunological Reviews*, *274*(1), 112–126. https://doi.org/10.1111/imr.12473

Vicencio, J. M., Yellon, D. M., Sivaraman, V., Das, D., Boi-Doku, C., Arjun, S., Davidson, S. M. (2015). Plasma Exosomes Protect the Myocardium From Ischemia-Reperfusion Injury. *Journal of the American College of Cardiology*, *65*(15), 1525–1536. https://doi.org/10.1016/j.jacc.2015.02.026

Vogel, C. W., & Müller-Eberhard, H. J. (1984). Cobra venom factor: improved method for purification and biochemical characterization. *Journal of Immunological Methods*, *73*(1), 203–20. Retrieved from http://www.ncbi.nlm.nih.gov/pubmed/6491300

Vogel, C.-W., & Fritzinger, D. C. (2010). Cobra venom factor: Structure, function, and humanization for therapeutic complement depletion. *Toxicon*, *56*(7), 1198–1222. https://doi.org/10.1016/J.TOXICON.2010.04.007

Walle, L. Vande, Van Opdenbosch, N., Jacques, P., Fossoul, A., Verheugen, E., Vogel, P., … Lamkanfi, M. (2014). Negative regulation of the NLRP3 inflammasome by A20 protects against arthritis. *Nature*, *advance on*. Retrieved from http://dx.doi.org/10.1038/nature13322

Wallis, R., Mitchell, D. A., Schmid, R., Schwaeble, W. J., & Keeble, A. H. (2010). Paths reunited: Initiation of the classical and lectin pathways of complement activation. *Immunobiology*, *215*(1), 1–11. https://doi.org/10.1016/j.imbio.2009.08.006

Wan, J., Chen, D., Yu, B., Luo, Y., Mao, X., Zheng, P., He, J. (2017). Leucine Protects Against Skeletal Muscle Atrophy in Lipopolysaccharide-Challenged Rats. *Journal of Medicinal Food*, *20*(1), 93–101. https://doi.org/10.1089/jmf.2016.3759

Wang, H., Ricklin, D., & Lambris, J. D. (2017). Complement-activation fragment C4a mediates effector functions by binding as untethered agonist to protease-activated receptors 1 and 4. *Proceedings of the National Academy of Sciences of the United States of America*, *114*(41), 10948–10953. https://doi.org/10.1073/pnas.1707364114

Wang, L. F., Ding, Y. J., Zhao, Q., & Zhang, X. L. (2015). Investigation on the association between NLRP3 gene polymorphisms and susceptibility to primary gout. *Genetics and Molecular Research*, *14*(4), 16410–16414. https://doi.org/10.4238/2015.December.9.10

Wang, Y., Han, Z., Fan, Y., Zhang, J., Chen, K., Gao, L., Wang, C. (2017). MicroRNA-9 Inhibits NLRP3 Inflammasome Activation in Human Atherosclerosis Inflammation Cell Models through the JAK1/STAT Signaling Pathway. *Cellular Physiology and Biochemistry*, *41*(4), 1555–1571. https://doi.org/10.1159/000470822

Ward, P. A. (2004). The dark side of C5a in sepsis. *Nature Reviews Immunology*, *4*(2), 133–142. https://doi.org/10.1038/nri1269

Wassermann-Dozorets, R., & Rubinstein, M. (2017). C/EBPβ LIP augments cell death by inducing osteoglycin. *Cell Death & Disease*, *8*(4), e2733–e2733. https://doi.org/10.1038/cddis.2017.155

Winters, M. S., Spellman, D. S., & Lambris, J. D. (2005). Solvent Accessibility of Native and Hydrolyzed Human Complement Protein 3 Analyzed by Hydrogen/Deuterium Exchange and Mass Spectrometry. *The Journal of Immunology*, *174*(6), 3469–3474. https://doi.org/10.4049/jimmunol.174.6.3469

Wintrobe, Maxwell Myer; Lee, G. R. (1993). *Wintrobe's Clinical Hematology*. *Journal of Clinical Pathology* (Vol. 46). Lippincott Williams & Wilkins. https://doi.org/10.1136/jcp.46.12.1142-c

Wouters, D., Voskuyl, A. E., Molenaar, E. T. H., Dijkmans, B. A. C., & Hack, C. E. (2006). Evaluation of classical complement pathway activation in rheumatoid arthritis: measurement of C1q-C4 complexes as novel activation products. *Arthritis and Rheumatism*, *54*(4), 1143–50. https://doi.org/10.1002/art.21729

Wu, X., Ren, G., Zhou, R., Ge, J., & Chen, F.-H. (2018). The role of Ca2+ in acid-sensing ion channel 1a-mediated chondrocyte pyroptosis in rat adjuvant arthritis. *Laboratory Investigation*. https://doi.org/10.1038/s41374-018-0135-3

Xie, Q., Wei, M., Zhang, B., Kang, X., Liu, D., Zheng, W., Shen, J. (2018). *Molecular medicine reports. Molecular Medicine Reports* (Vol. 17). D.A. Spandidos. Retrieved from https://www.spandidos-publications.com/mmr/17/2/3318

Yamamoto, H., Fara, A. F., Dasgupta, P., & Kemper, C. (2013). CD46: The "multitasker" of complement proteins. *The International Journal of Biochemistry & Cell Biology*, *45*(12), 2808–2820. https://doi.org/10.1016/j.biocel.2013.09.016

Yamamoto, H., Fara, A. F., Dasgupta, P., & Kemper, C. (2013). CD46: The "multitasker" of complement proteins. *The International Journal of Biochemistry & Cell Biology*, *45*(12), 2808–2820. https://doi.org/10.1016/j.biocel.2013.09.016

Yang, H., Rudge, D. G., Koos, J. D., Vaidialingam, B., Yang, H. J., & Pavletich, N. P. (2013). mTOR kinase structure, mechanism and regulation. *Nature*, *497*(7448), 217–223. https://doi.org/10.1038/nature12122

Yang, J., Chi, Y., Burkhardt, B. R., Guan, Y., & Wolf, B. A. (2010). Leucine metabolism in regulation of insulin secretion from pancreatic beta cells. *Nutrition Reviews*, *68*(5), 270–9. https://doi.org/10.1111/j.1753-4887.2010.00282.x

Yao, Y., Chen, S., Cao, M., Fan, X., Yang, T., Huang, Y., Qian, Y. (2017). Antigen-specific CD8+ T cell feedback activates NLRP3 inflammasome in antigen-presenting cells through perforin. *Nature Communications*, *8*, 15402. https://doi.org/10.1038/ncomms15402

Yaron, J. R., Gangaraju, S., Rao, M. Y., Kong, X., Zhang, L., Su, F., Meldrum, D. R. (2015). K+ regulates Ca2+ to drive inflammasome signaling: dynamic visualization of ion flux in live cells. *Cell Death and Disease*, *6*(10), e1954. https://doi.org/10.1038/cddis.2015.277

Ye, X., Zuo, D., Yu, L., Zhang, L., Tang, J., Cui, C., Cui, G. (2017). ROS/TXNIP pathway contributes to thrombin induced NLRP3 inflammasome activation and cell apoptosis in microglia. *Biochemical and Biophysical Research Communications*, *485*(2), 499–505. https://doi.org/10.1016/j.bbrc.2017.02.019

Yu, J., Abagyan, R., Dong, S., Gilbert, A., Nussenzweig, V., & Tomlinson, S. (1997). Mapping the active site of CD59. *The Journal of Experimental Medicine*, *185*(4), 745–53. Retrieved from http://www.ncbi.nlm.nih.gov/pubmed/9034152

Yuan, B., Fu, F., Huang, S., Lin, C., Yang, G., Ma, K., Yang, Z. (2017). C5a/C5aR Pathway Plays a Vital Role in Brain Inflammatory Injury via Initiating Fgl-2 in Intracerebral Hemorrhage. *Molecular Neurobiology*, *54*(8), 6187–6197. https://doi.org/10.1007/s12035-016-0141-7

Yuan, G., Wei, J., Zhou, J., Hu, H., Tang, Z., & Zhang, G. (2003). Expression of C5aR (CD88) of synoviocytes isolated from patients with rheumatoid arthritis and osteoarthritis. *Chinese Medical Journal*, *116*(9), 1408–12. Retrieved from http://www.ncbi.nlm.nih.gov/pubmed/14527377

Zelek, W. M., Stott, M., Walters, D., Harris, C. L., & Morgan, B. P. (2018). Characterising a pH-switch anti-C5 antibody as a tool for human and mouse complement C5 purification and cross-species inhibition of classical and reactive lysis. *Immunology*. https://doi.org/10.1111/imm.12982

Zhang, J., Li, Y., Shan, K., Wang, L., Qiu, W., Lu, Y., Wang, Y. (2014). Sublytic C5b-9 induces IL-6 and TGF-β1 production by glomerular mesangial cells in rat Thy-1 nephritis through p300-mediated C/EBPβ acetylation. *FASEB Journal : Official*

Publication of the Federation of American Societies for Experimental Biology, *28*(3), 1511–25. https://doi.org/10.1096/fj.13-242693

Zhang, L., Chen, S., Ruan, J., Wu, J., Tong, A. B., Yin, Q., Wu, H. (2015). Cryo-EM structure of the activated NAIP2-NLRC4 inflammasome reveals nucleated polymerization. *Science (New York, N.Y.)*, *350*(6259), 404–9. https://doi.org/10.1126/science.aac5789

Zhang, L., Zhang, L., Huang, Z., Xing, R., Li, X., Yin, S., Wang, P. (2019). Increased HIF-1 *α* in Knee Osteoarthritis Aggravate Synovial Fibrosis via Fibroblast-Like Synoviocyte Pyroptosis. *Oxidative Medicine and Cellular Longevity*, *2019*, 1–11. https://doi.org/10.1155/2019/6326517

Zhang, M.-H., Fan, J., Xie, X., Deng, Y., Chen, Y., Zhen, R., Wen, J. (2011). Ginsenoside-Rg1 protects podocytes from complement mediated injury. *Journal of Ethnopharmacology*, *137*(1), 99–107. https://doi.org/10.1016/J.JEP.2011.04.045

Zhang, Y., Rong, H., Zhang, F.-X., Wu, K., Mu, L., Meng, J., Shi, Y. (2018). A Membrane Potential- and Calpain-Dependent Reversal of Caspase-1 Inhibition Regulates Canonical NLRP3 Inflammasome. *Cell Reports*, *24*(9), 2356–2369.e5. https://doi.org/10.1016/j.celrep.2018.07.098

Zhao, G., & Xie, Z. (2014). Pyroptosis and neurological diseases. *Neuroimmunology and Neuroinflammation*, *1*(2), 60. https://doi.org/10.4103/2347-8659.139716

Zhao, Y., Xu, H., Yu, W., & Xie, B.-D. (2014). Complement anaphylatoxin C4a inhibits C5a-induced neointima formation following arterial injury. *Molecular Medicine Reports*, *10*(1), 45–52. Retrieved from http://www.spandidos-publications.com/mmr/10/1/45/abstract

Zhong, L., Li, H., Li, Z., Shi, B., Wang, P., Wang, C., Peng, Z. (2016). C7 genotype of the donor may predict early bacterial infection after liver transplantation. *Scientific Reports*, *6*, 24121. https://doi.org/10.1038/srep24121

Zhou, W., Chen, C., Chen, Z., Liu, L., Jiang, J., Wu, Z., Chen, Y. (2018). NLRP3: A Novel Mediator in Cardiovascular Disease. *Journal of Immunology Research*, *2018*, 1–8. https://doi.org/10.1155/2018/5702103

Zhu, G., Qiu, W., Li, Y., Zhao, C., He, F., Zhou, M., Wang, Y. (2017). Sublytic C5b-9 Induces Glomerular Mesangial Cell Apoptosis through the Cascade Pathway of MEKK2–p38 MAPK–IRF-1–TRADD–Caspase 8 in Rat Thy-1 Nephritis. *The Journal of Immunology*, *198*(3), 1104–1118. https://doi.org/10.4049/jimmunol.1600403